Isothermal Martensite Formation

Villa, Matteo

Publication date:
2014

Document Version
Publisher's PDF, also known as Version of record

Isothermal Martensite Formation

PhD Thesis

$$(EIv'')''=q-\rho A\ddot{v}$$

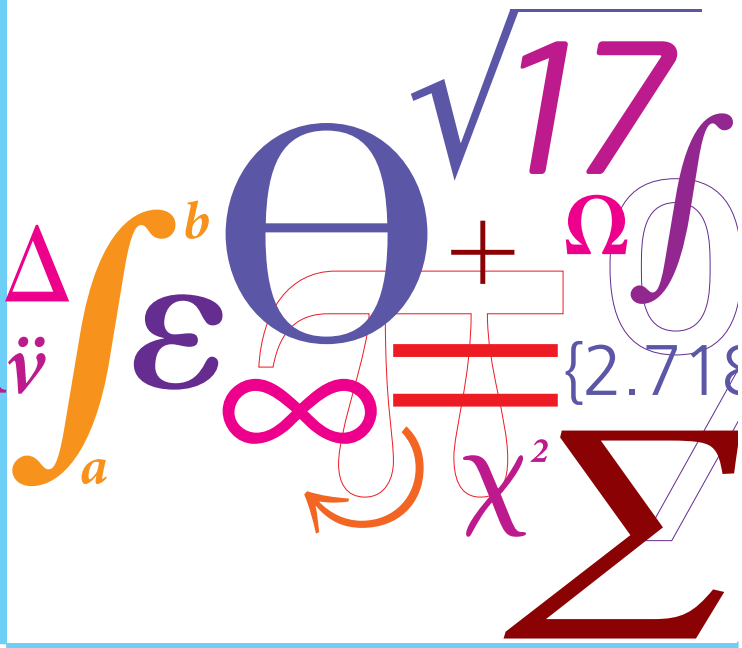

Matteo Villa
September 2013

DTU Mechanical Engineering
Department of Mechanical Engineering

Isothermal Martensite Formation

Ph.D Thesis

September 2013

By

Matteo Villa

Department of Mechanical Engineering

Technical University of Denmark (DTU)

DK-2800 Kgs. Lyngby, Denmark

Preface

The present thesis is submitted in candidacy for a Ph.D. degree from the technical University of Denmark (DTU).

The work presented in this thesis has been carried out at the department of Mechanical Engineering (MEK) under the supervision of Professor Marcel A.J. Somers and Associate Professor Karen Pantleon during the period August 2010 to September 2013.

Kgs Lyngby, September 2013

Matteo Villa

Acknowledgements

Firstly, I would like to particularly thank my main supervisor, Marcel A.J. Somers, who significantly contributed to the development of this project though his continuous and outstanding support.

A special thank you also to Karen Pantleon for her valuable constructive criticism and her fruitful assistance.

Mikkel F. Hansen is gratefully acknowledged for his continuous, prompt and precise support with magnetometry activity.

Olaf Kessler, Michael Reich, Christoph Schweigel and Kristin Aurich are acknowledged for their support with the dilatometry activities at Rostock University.

Thanks are given to Christoph Genzel and Manuela Klaus for their enthusiasm and support during my stays at the HZB-BESSY II synchrotron facility.

Ralf Feyerherm, Esther Dudzik, Flemming B. Grumsen and Ole West are acknowledged for their support with the experimental activities at the HZB-BESSY II.

A necessary thank you to all my colleagues who contributed actively to build a nice working environment.

A special final thanks to my relatives who always represent a fundamental reference point for my life and supported me during this experience.

Abstract

Isothermal (i.e. time dependent) martensite formation in steel was first observed in the 40ies of the XXth century and is still treated as an anomaly in the description of martensite formation which is considered as a-thermal (i.e. independent of time). Recently, the clarification of the mechanism leading to isothermal kinetics acquired new practical relevance because of the identification of isothermal martensite formation as the most likely process responsible for enhanced performances of sub-zero Celsius treated high carbon steel products.

In the present work, different iron based alloys are chosen to investigate time dependent martensite formation. Among them, a Fe-11wt%Ni-0.6wt%C model alloy and Fe-1.6wt%Cr-1wt%C (AISI 52100), Fe-17wt%Cr-7wt%Ni (AISI 631) and Fe-16wt%Cr-5wt%Ni (AISI 630) commercial steels.

The investigation was performed with in situ magnetometry, dilatometry, synchrotron X-Ray diffraction and ex situ electron backscatter diffraction. Magnetometry and dilatometry were applied to investigate the kinetics of the transformation. Synchrotron X-Ray diffraction was applied for the determination of lattice strains in austenite. Electron backscatter diffraction was applied to characterize the microstructure of the material and the morphology of martensite.

The investigation of the kinetics yielded information on the mechanism responsible for time dependent martensite formation, which was indicated as thermally activated growth of a-thermally nucleated martensite. The investigation of lattice strains provided fundamental information on the state of stress in the material and clarified the role of the strain energy on martensite formation. Electron backscatter diffraction revealed that the microstructure of the material and the morphology of martensite were independent on the cooling conditions during sub-zero Celsius treatment.

Irrespective of the morphology of martensite (lath or lenticular), it was observed that decelerations and accelerations of the transformation occur. This characteristic of the transformation was explained as a consequence of a partially athermal, partially thermally activated character of the transformation.

Resumé

Isoterm, dvs. tidsafhængig, martensitdannelse i stål blev iagttaget for første gang i fyrrene af det forrige århundrede og bliver til stadighed behandlet som en undtagelse i beskrivlesen af martensitdannelse, som i almindelighed betragtes som atermisk, dvs. uafhængig af tid. For nylig har forståelsen af isoterm martensitdannelse fået en ny praktisk anvendelse, idet denne mekanisme anses for at give anledning til en markant forbedring af stålprodukter med højt kulstofindhold efter kryogen behandling.

I denne afhandling blev adskellige jernbaserede legeringer valgt for at undersøge tidsafhængig martensitdannelse. Blandt disse legeringer er en Fe-11wt%Ni-0.6wt%C modellegering og følgende kommercielle ståltyper Fe-1.6wt%Cr-1wt%C (AISI 52100), Fe-17wt%Cr-7wt%Ni (AISI 631) and Fe-16wt%Cr-5wt%Ni (AISI 630).

Undersøgelserne blev gennemført med in situ magnetometri, dilatometri og synkrotron røntgen diffraktion, samt ex situ elektron backscatter diffraktion. Magnetometri og dilatometri anvendedes for at kvantificere transformationskinetikken, Synkrotron røntgen diffraktion tillod at bestemme gittertøjninger i austenit. Elektron backscatter diffraktion anvendedes for at karakterisere mikrostrukturen.

Kinetikundersøgelserne resulterede i oplysninger om de bagliggende mekanismer ved tidsafhængig martensitdannelse og kunne idnetificeres som termisk aktiveret vækst af atermisk kimdannet martensit. Analysen af gittertøjninger gav grundlæggende oplysninger om spændingstilstanden i stålet og tøjningsenergiens rolle ved martensitdannelsen. Elektron backscatter diffraktion viste at martensitens morfologi er uafhængig af kølebetingelserne ved kryogen behandling.

Uafhængig af om martensitens morfolgi kan betegnes som koloni- eller som plademartensit, viste det sig at transformationshastigheden viste opbremsninger og accelerationer ved omdannelsen. Denne karakterstik kunne forklares som et resultat af den delvis atermale og delvis termisk aktiverede mekansime af omdannelsen.

Guidelines for the reader

The present text, starts with an introduction to sub-zero Celsius treatment and on the motivation for the investigation of isothermal martensite formation (chapter 1).

Chapter 2 presents an overview of the relevant literature on martensite. The general description of the characteristics of martensitic transformations is reported in sections 2.1, 2.2 and 2.3, which can easily be skipped by a reader familiar with this topic. The following sections, in particular 2.4, 2.6, 2.7 and 2.8 present details of martensitic transformations which have not received the same attention as those in sections 2.1, 2.2 and 2.3.

Similarly to chapter 2, the first part of chapter 3, specifically sections 3.1, 3.2 and 3.3 are general descriptions which a reader experienced in solid state transformations in steels is likely to be most familiar with, whereas less well-known concepts are introduced in sections 3.4 and 3.5.

In relation to the results section, it is emphasized that results reported obtained with the Fe-Ni-C model alloy (APPENDIX A and APPENDIX B) should be considered as the chronological starting point of the investigations of this thesis. After these experiments were finished, model alloys were abandoned and commercial steels were chosen instead.

Main attention should be given to the results presented in the manuscripts reported in APPENDIX D, APPENDIX E, APPENDIX G, APPENDIX I and APPENDIX J.

Table of contents

1. Introduction

Steels are alloys containing at least 50wt% iron (1) together with other chemical elements, among which carbon in a content below 2.1wt% (2). According to (2), steels are classified as *high carbon steels* when the carbon content in the material is in the range of 0.6wt% to 1wt%; in the present work, the terminology *high carbon steel* refers to a steel with a carbon content in the range 0.6wt% to 2.1wt%. High carbon steels are used for tools, dies, gears and bearings (3), applications where dimensional stability and wear resistance are paramount. In order to meet material requirements, steel parts are subjected to a *hardening* heat treatment followed by a *tempering* heat treatment (3) (4).

Heat treating consist in the use of a thermal process to alter the physical and mechanical properties of a material in order to adapt its characteristic to the requirements of a specific application. Among conventional heat treatments of steels, *hardening* consists of a heating step to high temperatures to obtain a face centered cubic, f.c.c., crystal structure, followed by fast cooling to room temperature to transform the crystal structure in body centered cubic/tetragonal, b.c.c. / b.c.t., by a *diffusionless transformation* (4). The microstructural component organized in a f.c.c. crystal structure is called *austenite* and is indicated as γ-phase. *Martensite* is the hard constituent that results from such transformation. Martensite is indicated as α′ (5) to emphasize the close relationship of its crystal structure with the equilibrium b.c.c. α-phase of pure iron at room temperature, called *ferrite*. The temperature region where it is possible to obtain the f.c.c. crystal structure is reported in the phase diagram of the system (Figure 1, as an example for the Fe-C binary system), while martensite is not the thermodynamically stable phase and therefore cannot be represented in the Fe-C phase diagram.

The crystal structure of martensite is b.c.c. when neither nitrogen or carbon atoms are dissolved in the martensite. With carbon or nitrogen in solid solution, the b.c.c. crystal structure is elongated in one direction, the *c* direction, while shrinking occurs in the other directions, the *a* directions (5) (6) (7). The resulting crystal structure is b.c.t.. The *tetragonality* of martensite is defined as the ratio of *a* and *c* lattice parameters, the *c/a ratio*, which is proportional to the carbon and nitrogen contents (5) (7).

For the majority of the commercial steels, the transformation of austenite into martensite is completed after cooling to room temperature. However, carbon is a chemical element which thermodynamically stabilizes the austenite, and consequently the material, against complete martensite formation and retained austenite remains. The higher the carbon content, the lower the temperature where the transformation goes to completion. Consequently, a part of the austenite is retained on reaching room temperature and further cooling is necessary (8) (9).

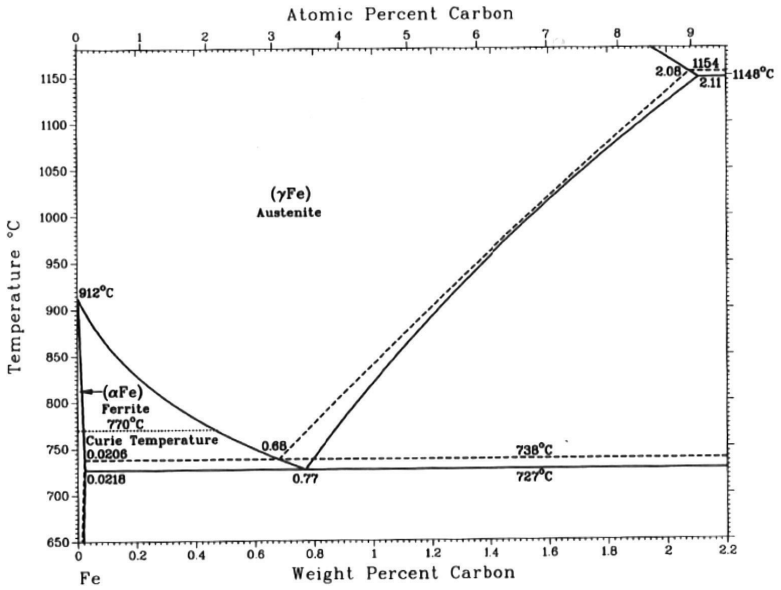

Figure 1. Selected portion of the iron-carbon binary phase diagram. The region where f.c.c. is the most stable crystal structure corresponds to the region indicated as γ and is function of both temperature and carbon content (10).

After hardening, steel is heated above room temperature to temper the material and optimize its mechanical properties through the formation of precipitates, i.e. (mainly) carbides, and the contemporary relaxation of internal stresses. Generally, *tempering* results in progressive softening and toughening of the material the higher the treating temperature and the longer the tempering time (4).

Tempering of steels occurs into the following four stages as a function of temperature (11): the precipitation of transition iron carbides; the decomposition of retained austenite into

ferrite and *cementite* (i.e. the most stable form of iron carbide); the formation of *cementite* within the martensite phase and dissolution of transition carbides; the precipitation of alloy carbides.

The precipitation of transition iron carbides in the first stage of tempering starts upon heating at temperatures above 353 K – 373 K (12) and is associated with a complete relaxation of the b.c.t structure to b.c.c. (13) (14) (15). In the case of plain carbon steels and low alloyed steels the best combination of mechanical properties is obtained after the first stage of tempering. However, in the presence of a large amount of retained austenite, tempering is performed in the second stage where retained austenite decomposes. Retained austenite is a soft constituent that degrades the performances of hard parts during service. The decomposition of retained austenite into ferrite and cementite starts at temperatures above 513 K – 523 K (12) (16) and takes place simultaneously to the formation of cementite within martensite. The formation of cementite within martensite represents the third stage of tempering and reduces the beneficial effect of the transition carbide precipitates on the properties of the material, specifically hardness. The fourth stage is associated with the presence of carbide forming alloy elements and takes place at temperatures above 773 K (17) (18). The precipitation of alloy carbides results in optimal properties for parts made of alloyed steels, as tool steels.

As an additional step in the heat treatment of steel parts, sub-zero Celsius treatment, which subjects the material to a sub-zero Celsius thermal cycle, may improve the performance of high carbon steels, for example reducing the fraction of retained austenite in the material prior or after low temperature tempering (i.e. up to the first stage). In particular, a noteworthy improvement is observed with regard to wear resistance and geometrical stability when the sub-zero Celsius treatment is performed prior to tempering (19) (20) (21) (22) (23) (24) (25). This improvement is of particular technological interest, since it may drive to relevant economical savings enhancing life service of steel products.

Despite large scale application, particularly in U.S.A., a metallurgical mechanism responsible for enhanced wear resistance of sub-zero Celsius treated high Carbon steel parts is not understood yet. Reviews on the topic (26) (27) (28) (29), put forward as possible interpretations other than the reduction of the content of retained austenite, an enhanced and more uniform formation of precipitates during tempering, a modification of the substructure of martensite and a more favorable macro-stress state.

Among the diverging interpretations, an enhanced and more uniform formation of transition carbide precipitates appears most plausible (23) (24) (30) (31) (32). For example, in (24), a positive correlation between enhanced precipitation of transition carbides and increased wear resistance was reported. A 1.4%Cr-1%C steel was subjected to two sub-zero Celsius treatments at173 K and 77 K. Both treatments resulted in reducing the content of retained austenite in the material, but only the treatment to 77 K promoted a finer precipitation of carbides and a significant increase in wear resistance.[1] The mechanism that controls the enhanced and refined precipitation is still unrevealed.

Specifically, it is documented that both wear resistance and precipitation phenomena are promoted by an isothermal process occurring at a temperature lower than 194 K (i.e. sublimation temperature of carbon dioxide at one atmosphere) and as low as 77 K (i.e. boiling point of liquid nitrogen at one atmosphere) (21) (32) (33) (34) (35) (36), but the nature of the isothermal process remains unrecognized. In the present work, temperatures below 194 K are designated *cryogenic*. According to (23) (26) (27) (28) (29), where prior works are reviewed, there are four different interpretations as to why isothermal holding at a cryogenic temperature would promote (transition) carbide precipitation.

As a first interpretation, the diffusion of Carbon atoms to lattice defects during isothermal sub-zero Celsius holding may result in the formation of carbon clusters. According to this interpretation, these clusters act as nucleation sites for the precipitation of carbides during tempering. To the author´s knowledge, this interpretations remains purely speculative and no evidence of this supposed clustering has been provided. Moreover, this interpretation is inconsistent with the availability of thermal energy, which is insufficient for carbon redistribution at temperatures below about 230 K (38) (39) (40).

As a second interpretation, the internal structure of the martensite (further on *substructure*) and the stress state are modified during isothermal holding at cryogenic temperatures. As a consequence, the driving force for the formation of precipitates during tempering would be enhanced. This interpretation remains phenomenological as it does not

[1] In (37), it was also suggested that the formation of finer precipitates may be associated with a change in the crystal structure of transition Iron Carbides from hexagonal to orthorhombic.

propose a mechanism that would promote either a modification of the stress state in the material or a change in the martensite substructure. To the author´s knowledge, this interpretations is also speculative.

According to a third phenomenological interpretation, a modification of the tetragonality of martensite upon sub-zero Celsius treating (41) (42), which drives to an increased instability of its crystal structure, promotes enhanced precipitation of carbides in association with relaxation of b.c.t. into b.c.c.. For example, in (42), a positive correlation between enhanced tetragonality of martensite and enhanced precipitation was reported. In (42), the tempering reaction of an alloyed steel subjected to 12 h isothermal holding at 77 K after quenching was compared with the tempering reaction in the as quenched material. The detectable differences in the samples prior to tempering were a reduced content of retained austenite and a larger tetragonality of martensite in the sub-zero Celsius treated condition. The first stage of tempering was observed to be more pronounced for the sub-zero Celsius treated specimen. It was concluded that enhanced precipitation was promoted by a change in the tetragonality of martensite during sub-zero Celsius treatment.

The fourth interpretation indicates the formation of martensite isothermally, i.e. at a constant cryogenic temperature, as the reason for enhanced precipitation. According to (26) (27) (28) (29), isothermal martensite formation at cryogenic temperature may either modify the structure of the material by the activation of processes not occurring during standard heat treating, or may be connected with the generation of a different type of martensite,[2] which is more prone to form precipitates.

To the author´s understanding, isothermal martensite formation appears the most likely explanation, because the process occurs in association with the generation of a large amount of strain energy (43), which is (partially) stored in the material and may act as a driving force for a modification of its microstructure and / or stress state. For this reason, the main focus of the present project, which was initially addressed to the investigation of sub-zero Celsius treatments, is isothermal martensite formation.

[2] i.e. a *not* specified type of martensite which can form only during long isothermal holding at cryogenic temperature.

Recent observations in (38) (44) reported experimental evidence for the role of isothermal martensite formation at cryogenic temperature. In (38) (44), the effect of isothermal martensite formation at cryogenic temperature on tempering was investigated in a 1.55%C-11.9%Cr-0.7%V-0.86%Mo steel.

According to (38) (44), the formation of martensite at cryogenic temperature is accompanied by plastic deformation of the pre-existing martensite and results in the following observable effects. Firstly, martensite formation at cryogenic temperature promotes a refinement of the *substructure* of pre-existing martensite, in association with an increase of nucleation sites for the formation of precipitates (38). Secondly, the tetragonality of martensite is reduced. According to (38) (44), a reduction in tetragonality is promoted by gliding dislocations in pre-existing martensite which capture a part of the carbon atoms dissolved within the b.c.t. structure. This process is speculated to take place in association with the formation of new nucleation sites for carbide precipitation.

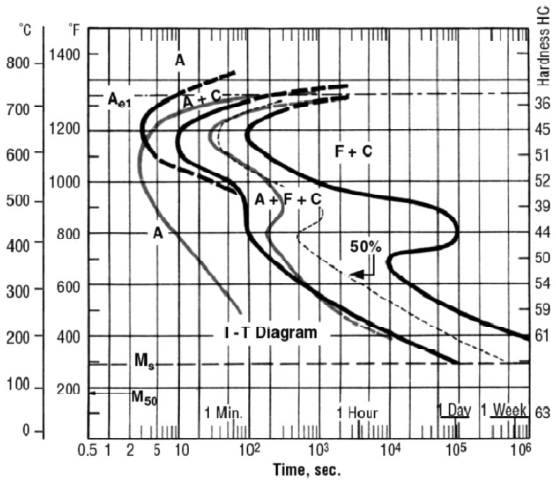

Figure 2. Iso-transformation curves in time-temperature space (TTT diagram) for martensite formation in a Fe-1%C-1.5%Cr steel: martensite formation is expressed in terms of horizontal lines. M_S indicates the temperature martensite is first detected; M_{50} the temperature where 50% transformation has taken place on cooling (45).

Note that the definition of martensite as *isothermal,* indicates that the martensitic transformation is *time dependent*. Nevertheless, apart from a few exceptions (46), in textbooks

martensite formation is described as *in*dependent of time (18) (47) (48) and modeled consistently (49). This approach is clearly visible in *Continuous-Cooling-Transformation*, CCT (50), and *Time-Temperature-Transformation*, TTT (45), diagrams (51), which represent the temperature where martensite is first observed on cooling, the martensite start temperature, M_S, by a horizontal line, implying an a-thermal mechanism (Figure 2).

Time dependent martensite formation, appears less known phenomenon in industrial practice, in spite its first observation reported as early as 1948 (52). Several observations followed and are listed in (53). Impressively, time dependent martensite formation can result in so called *C-shape* (referring to their aspect) transformation curves in TTT diagrams (Figure 3).

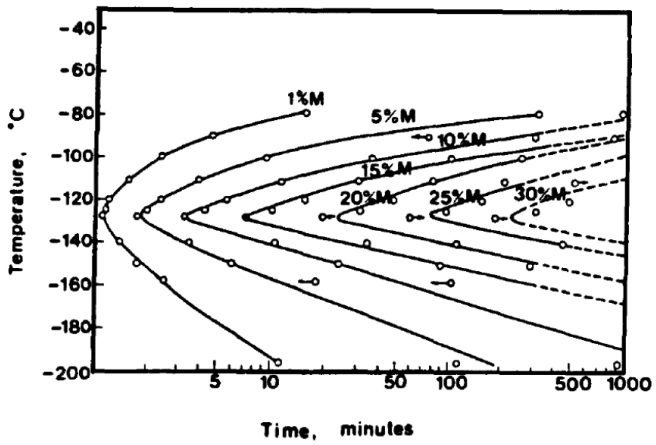

Figure 3. Iso-transformation curves in time-temperature space (TTT diagram) for martensite formation in a Fe-23.2%Ni-3.6%Mn alloy: martensite formed isothermally shows a C-shaped curve (54).

Time dependent martensite formation has been reported for several iron based systems. Time dependent martensite formation has been reported for iron-nickel-manganese (52), iron-nickel-chromium (55) (56) (57) (58) and iron-aluminum (59) systems. Time dependent martensite formation has been rationalized as an intrinsic characteristic of steels (51).

Among iron-based systems, steels are of large industrial relevance. In commercial steel, time dependent martensite formation was documented for high carbon steels (60), low alloyed steels (61) (62) and stainless steels (57) (58). Industrially, time dependent martensite formation is

exploited during sub-zero Celsius treatment of high carbon steels (63), maraging steels (64) and precipitation hardenable stainless steels (65).

Moreover, in addition to the possibilities given by sub-zero Celsius treating, time dependent martensite formation may result in extensive opportunities to tailor the characteristics of steel products through engineering their thermal treatments. For example, time dependent martensite formation in steel was shown to influence the mechanical properties of the material (61) (see also prior work in (66)).

Finally, martensite formation in steel shows two distinct transformation paths (48) (58): the formation of hexagonal close-packed, h.c.p. (defined ε), martensite, may precede the formation of body centered cubic/tetragonal martensite (67) (i.e. $\gamma \rightarrow \varepsilon \rightarrow \alpha'$); the formation of body centered cubic/tetragonal martensite, may occur directly (i.e. $\gamma \rightarrow \alpha'$). The first path is limited to a few systems with a very low stacking fault energy in austenite, as for example in certain stainless steels (68). The second path is more widely observed.

In conclusion, time dependent martensite formation may be of noteworthy technological importance, both in relation to the development of *ad-hoc* sub-zero Celsius treatments to tailor the performance of high carbon steels, and in connection to the optimization of mechanical properties of products heat treated according to *conventional* (i.e. not involving sub-zero Celsius steps) heat treatments. However, the mechanism controlling time dependent martensite formation has been debated for more than half a century now, but remains obscured.

The present work aims to contribute to the understanding of isothermal martensite formation in steel and deals with the direct formation of cubic/tetragonal martensite only. The focus has been addressed to commercial materials rather than model alloys. The influence of sub-zero Celsius martensite formation on the tempering response of high carbon steel is also (partially) addressed.

2. Overview of the literature on martensite

This chapter presents the theory of martensite formation described (mainly) on the basis of two reviews available in the literature (5) (69)[3]. Several additional references are given either because of historical importance or with the purpose to report observations and details considered of particular interest. The focus has been addressed to iron-based alloys and time dependent transformation mechanisms.

In this text, the terminology *iron-based* alloy is used to refer indistinctly to alloys *not* containing carbon and to steel, where a certain amount of carbon is intentionally alloyed into the material. Martensite that forms in iron-based system is referred to as *ferrous* martensite (69). Finally, the terminology *time dependent* kinetics is used to refer to a time scale that may be of engineering relevance for heat treatment practice, indicatively in the range from several seconds to a few hours.

The final purpose of this chapter is to indicate which mechanisms are responsible for a macroscopically observed time dependent kinetics, in order to develop a solid basis for the following kinetics analysis. It is not the purpose of this chapter to describe martensite formation in terms of fraction of material transformed versus time and temperature.

2.1. Martensite as the product of a transformation

Originally, *martensite* referred to the hard micro-constituent found in quenched steels. Nowadays, materials other than steels, are known to exhibit a solid state transformation that is *martensitic* (70) and the final product of the transformation is called *martensite* (70). A martensitic transformation is defined as a "*diffusionless, lattice-distortive, shear dominant transformation occurring by nucleation and growth*" (74). According to (70), the origins of this definition are appointed to (75).

[3] Further on given as references (68) (70) (71) (72) (73) to the book´s chapters.

Diffusionless indicates that atoms can be displaced by the transformation over a distance shorter than the interatomic spacing,[4] but any movement involving their redistribution, along the crystal or across the austenite to martensite interface, is forbidden.

Lattice-distortive describes the type of atomic displacements governing the transformation process. Specifically, relative movement of atoms may occur within the existing lattice unit cell, or may distort the initial lattice unit cell into a new one. In a martensitic transformation, the process is dominated by the lattice distortive displacements.

The lattice strain can be described in terms of a dilatational component, associated with a volume change, and a shear component, describing the shape change (Figure 4). *Shear dominant* indicates that the dilatational component represents only a minor part of the transformation strain (70).

Finally the definition describes the formation of martensite as occurring by the initial formation of a nucleus that progressively extends to its final dimension by growth.

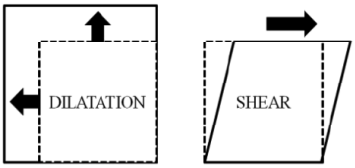

Figure 4. Description of the lattice strain according to (76): a) dilatation, further on δ; b) shear, further on s.

2.2. Experimental evidence and related theoretical aspects

2.2.1. Diffusionless nature

There are three main proofs for the diffusionless character of the martensitic transformation. Firstly, martensite can form at very low temperatures[5] (77), where atomic mobility is so low that diffusion within the time scale of the process is effectively *im*possible.

[4] Divided in *shuffles* and lattice distortive after (75).
[5] According to (5), the observation of martensite formation at temperatures near 0 K was made on 18%Cr-8%Ni stainless steel, 1% C steel and different Fe-20%Ni alloys.

The second proof is the possibility for the austenite-martensite interface to move at a velocity approaching the speed of sound in the material (78), that is orders of magnitude too fast for a mechanism involving diffusion. The third proof is that the composition of the transformed area is identical to the composition of the parent phase, suggesting, but not actually proving a diffusionless mechanism[6].

As a consequence of the diffusionless character, there is a direct correspondence between the positions of atoms in the martensite and the austenite phase. A direct correspondence means that every atom can be associated with its initial position and that the transformation happens by a coordinated movement of atoms. For this reason, martensitic transformation are also called *military* (69). In a military transformation neighbor atoms move together and remain neighbors after the process has occurred, exactly like soldiers marching together do not change their relative positions when they change direction.

The diffusionless character implies that diffusion phenomena cannot be the rate-controlling mechanism for time dependent martensite formation.

2.2.2. Shape change

The martensitic transformation is related to a macroscopic shape change in the material as a consequence of the transformation strain (Figure 5). This characteristic is so fundamental that in (79) the transformation process itself was defined as a sort of deformation. This deformation is *plane-invariant* meaning that the interface between the generating phase and the product phase is macroscopically undistorted and un-rotated. The invariant plane is referred to as *habit plane* and characterizes a martensite structure.

The transformation strain is readily observable under *un*constrained conditions of transformation (compare Figure 5a, top and Figure 4). Under *un*constrained conditions, the coordinate movement of atoms leads to a macroscopic shape change of the sample which corresponds to the transformation strain. Under *un*constrained conditions, the shear results in a

[6] For example, re-crystallization processes involve atomic diffusion but do not modify the composition of the re-crystallized areas (i.e. are compositionally invariant).

displacement of the material parallel to the invariant plane while the dilatation takes place in the direction normal to this plane.

Under *constrained* conditions, the transformation strain is counteracted by the presence of the surrounding material. As the transformation strain is too large for elastic accommodation, deformation mechanisms in martensite (i.e. slip, twinning) are activated reducing the elastic strain energy in the system. Consequently, under *constrained* conditions, the transformation strain is not macroscopically visible (i.e. the shape strain and the strain of the sample do *not* correspond). Under *constrained* conditions martensite forms either in the shape of narrow strips, the so called *laths* (80), or in the form of *plates* (Figure 5a, bottom right). In both cases, the transformation maintains its invariant plane character but loses the parallelism between the habit plane and the shear direction. The habit plane is defined either as the middle plane of the martensite unit or as the interface between product and parent phases (81).

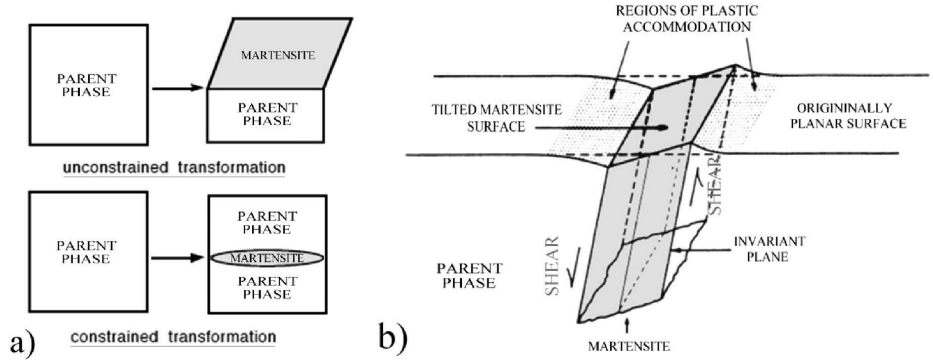

Figure 5. Description of the shape change. (a) Martensite formation in unconstrained and constrained conditions (according to (76)); the shape of martensite in uncostrained condition is represented for plate like morphology as it appears on the plate cross section. (b) Surface relief (after (74)).

On a flat surface, the macroscopic deformation appears in the form of *surface relief* (Figure 5b). The transformation strain is accommodated as follows: the shear is parallel to the undistorted and un-rotated plane as for the *un*constrained conditions and results in surface tilting; the dilatational component of the transformation strain is accommodated in the untransformed matrix. Martensite forming in the proximity of a free surface is sometimes referred to as *surface martensite* (81) to point out that its nature differs from the martensite formed in the bulk of the material (i.e. under *constrained* conditions) (5).

2.2.3. The interface between martensite and parent phase

According to (76) (82) (71), the characteristics of the martensite / austenite interface can be inferred from the possibility for martensite to form without relying on thermal activation. The following two experimental observations indicate that martensite formation does *not* rely on thermal activation: martensite formation at temperatures approaching absolute zero (77); an interface velocity *in*dependent of temperature (78). According to (5), the second observation is a sufficient evidence by itself.

The condition that the martensite forms athermally, indicates that the interface between the martensite and austenite must be able to move conservatively (i.e. athermally) during the transformation, i.e. the interface must be glissile, and must be coherent or at least semi-coherent.

According to (76), in order for the interface to be able to move conservatively, there must exist at least one invariant line in the interface that remains undistorted and un-rotated by the transformation process (76). Fully coherent planar interfaces require at least two unparallel invariant lines (forming a plane) to move conservatively. This is the case for a face centered cubic, f.c.c., to hexagonal close-packed, h.c.p., transformation (83). For f.c.c. to body centered cubic/tetragonal, b.c.c. / b.c.t., transformations, fully coherent interfaces are not possible; in this case the interface consists of coherent patches separated by (almost (71)) periodically spaced dislocations that *may* be able to move conservatively (76).

Athermal conservative movement of the interface implies that the mobility of the interface is not rate-controlling for time dependent martensite formation.

2.2.4. Orientation relationship, O.R.

The crystal structure of a product phase possesses an O.R. with the crystal structure of the parent phase if a unique relation exists between their crystallographic orientations. An O.R. limits growth of the product phase to a region where the crystal lattice of the parent phase remains oriented in a specific direction. Martensite has an O.R. with austenite. Consequently, growth of a martensite unit is limited to a single grain of the parent phase. Similarly, plastically deformed areas, associated with large changes in the orientation of the crystal lattice of austenite can limit the dimensions of a martensite unit (5).

An O.R. is expressed by parallel crystal planes and parallel crystal directions within these planes. Historically, for the face centered cubic, f.c.c., to body centered cubic/tetragonal, b.c.c. / b.c.t. transformation, the O.R. has been described by the approximate O.R.s reported in Table 1[7].

Table 1. Main approximate O.R.s for the f.c.c. to b.c.c. / b.c.t. martensitic transformation that have been reported in the literature.

Kurdjumov- Sachs (K-S) (86)	$(1\,1\,1)\gamma \,//\, (0\,1\,1)\alpha'$, $[\bar{1}\,0\,1]\gamma \,//\, [\bar{1}\,\bar{1}\,1]\alpha'$
Nishiyama-Wasserman (N-W) (87) (88)	$(1\,1\,1)\gamma \,//\, (0\,1\,1)\alpha'$, $[\bar{1}\,\bar{1}\,2]\gamma \,//\, [0\,\bar{1}\,1]\alpha$

The O.R.s in Table 1 correspond to parallel close-packet planes and directions within the planes of the parent and product phases. Specifically, the N-W O.R. can also be expressed as $(1\,1\,1)\gamma \,//\, (0\,1\,1)\alpha'$ and $[\bar{1}\,0\,1]\gamma$ about 5.3° from $[\bar{1}\,\bar{1}\,1]\alpha'$, towards $[\bar{1}\,1\,\bar{1}]\alpha'$ (i.e. 5.3° from K-S O.R.). A third O.R., the Greininger-Troiano (G-T) (89), was also proposed and represents an intermediate case between N-W and K-S O.R.s with $(1\,1\,1)\gamma$ about 0.2° from $(0\,1\,1)\alpha'$, $[\bar{1}\,0\,1]\gamma$ about 2.5° from $[\bar{1}\,\bar{1}\,1]\alpha'$ towards $[\bar{1}\,1\,\bar{1}]\alpha'$.

However, the approximate O.R.s in Table 1 do not satisfy the condition of a line invariant transformation (76) and are rational, while the O.R. of martensite with austenite was found to be irrational (76) (68).[8] Irrational O.R. means that the parallelism between planes and directions in the two crystals can no longer be expressed in terms of integer numbers. The habit plane of martensite was found to be irrational as well (76) (68).

In spite of being approximations, the O.R.s are relevant for the investigation of the transformation because the O.R. determines the number of equivalent orientations[9] in the austenite crystal where martensite forms. The equivalent orientations are *variants* of martensite. For example, for the N-W O.R., martensite forms in twelve variants. On the other hand, for the K-S O.R, twenty-four variants coupled in twelve pairs exist (5).

Historically, the different O.R. were identified by investigating the relative orientation between austenite and martensite crystals. This method requires the presence of a certain amount

[7] The crystal planes and directions are hereby described according to (84) (85).
[8] Actually, it is not possible to express an irrational O.R. with the notation introduced in (84).
[9] Equivalent directions result from the symmetries of the crystal lattices of the parent and product phases.

of retained austenite and is *not* straightforward experimentally because the approximate O.R.s differ only by a few degrees.

Nowadays, with Electron backscatter Diffraction, EBSD (see section 4.4), it is possible to determine the type of O.R. in a fully martensitic sample from the distribution of misorientation angles for the martensite variants present in a sample. Figure 6 shows the calculated frequency of misorientation angles for the three O.R.s. These new possibilities for the investigation of the O.R.s, provided new impetus for understanding the transformation mechanisms (see (90) (91)).

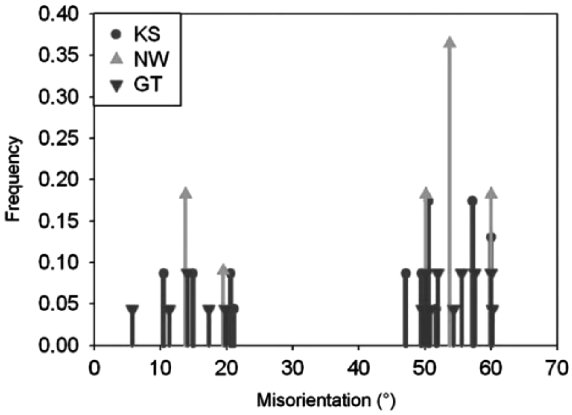

Figure 6. Misorientation angle distribution for the three approximate O.R.s. The frequency relates to the number of possible combinations of variants leading to a specific misorientation angle (90).

2.3. The crystallography of martensite

2.3.1. General introduction to the Phenomenological Theory of the Martensite Crystallography, PTMC

The basic idea of the PTMC (92)[10] is to describe the atomic displacements involved in the transformation in terms of basic matrix algebra[11]. Three distinct mathematical operations are considered in the PTMC.

[10] Also referred to as Phenomenological Theory of the Martensitic Transformation, PTMT. Equivalent theories have been reported in (93) (94).

The first mathematical operation describes a displacement of the atoms, which produces the correct observed shape of the martensite unit, but does *not* change the crystal structure of the parent phase into the crystal structure of martensite. The second operation distorts, i.e. transforms, the crystal lattice to the correct one, but modifies the correct shape. The third operation maintains the correct crystal lattice and compensates the shape change introduced by the crystal distortion, restoring the correct shape of the martensite unit.

According to (92), the third operation must arise from localized displacements, which compensate the shear originated from the transformation, but leave the crystal lattice continuous and undistorted. This is possible either by a relative movement of adjacent atomic rows, i.e. slip, or by the formation of twins. The classical graphical description of the PTMC is presented in Figure 7.

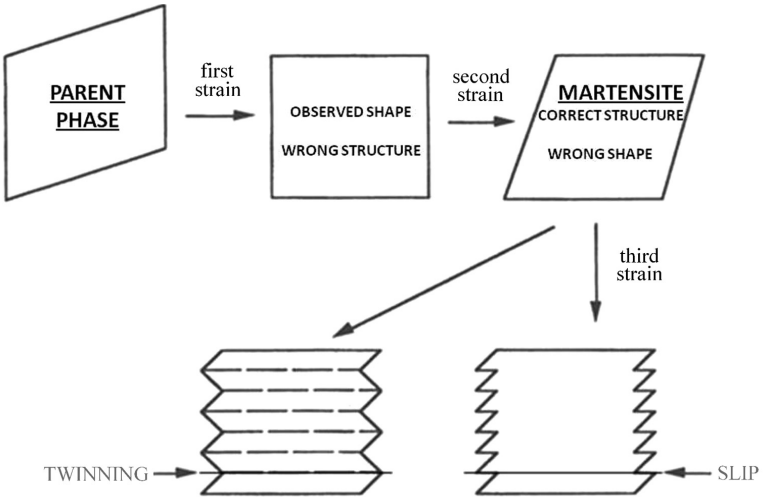

Figure 7. Schematic representation of the three mathematical operation considered in the PTMC (according to(95))

The PTMC does *not* describe the mechanisms that generate martensite but only the correspondence in atoms positions in the crystal structures of the parent and product phases (92).

---

[11] The mathematical description is reported pedagogically in (76).

The PTMC considers an ideal situation in which local imperfections are absent, so that the determination of the structural characteristics can be treated as a purely geometrical problem. The PTMC appears allowed because of the diffusionless nature of the transformation (see paragraph 2.2.1).

From a computational point of view, the output of the PTMC is the amount of displacement introduced by the third operation, the macroscopic shape change and the O.R. between parent and product phase (96). As input the lattice correspondence between martensite and austenite and the type of lattice invariant strain, i.e. the slip or twinning system, are required. More practically, the PTMC predicts the direction of the habit plane and the direction of the shape strain; these directions generally do not correspond.[12]

In the following, the PTMC is described according to (76) (95).

2.3.2. The PTMC of the f.c.c. to b.c.c. transformation

An essential work for the comprehension of the crystallography of b.c.c. / b.c.t. martensite was reported in (97). This work defines a lattice distortive strain, called the *Bain strain*, which essentially is able to transform the f.c.c. crystal lattice into b.c.c. / b.c.t.. The Bain description is represented schematically in Figure 8.

The success of the mechanism described in (97) is related to the fact that it requires the minimal displacement of the atoms to accomplish the f.c.c. to b.c.c. / b.c.t. lattice distortion and it shows a direct comparison between the f.c.c. and b.c.c. / b.c.t. lattices in the form of simple dilatations (Figure 8). Moreover, the mechanism shows that the carbon and nitrogen atoms must align along the c axis, hence predicting the tetragonality of the martensite structure. However, the mechanism fails to predict the correct O.R. and does not leave any line invariant (the $\overline{\overline{B}}$ matrix in Figure 8 does not present any invariant direction, which would correspond to a 1 on its diagonal).

[12] Reconsider Figure 5 and the difference between bulk and surface martensites

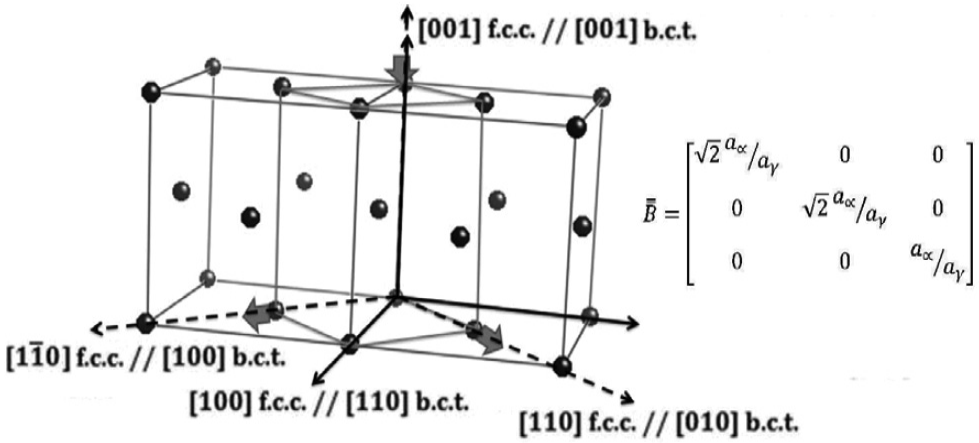

Figure 8. The face centered cubic, f.c.c., to body centered cubic, b.c.c., transformation according to (97) and the corresponding strain in matrix notation (according to (48) (76)). According to (97), the f.c.c. crystal structure can be described as b.c.t. from a different perspective. The f.c.c./b.c.t. structure is transformed into b.c.c. though a compression along $[0\ 0\ 1]_{f.c.c.}$ // $[0\ 0\ 1]_{b.c.t.}$ *and two dilatations along* $[1\ \bar{1}\ 0]_{f.c.c.}$ // $[1\ 0\ 0]_{b.c.t.}$ *and* $[1\ 0\ 0]_{f.c.c.}$ // $[0\ 1\ 0]_{b.c.t.}$ *, respectively. The matrix* $\bar{\bar{B}}$ *describes the atomic displacement according to basic algebra notation, with* a_α *and* a_γ *lattice parameters of the b.c.c. and f.c.c. unit cells, respectively.*

The second step in the comprehension of the crystallography of b.c.c. / b.c.t. martensites is reported in (98), where it was proposed that martensite formation results from the lattice distortive Bain mechanism coupled with a rotation of the crystal lattice. In the presented description, the rotation of the lattice is a necessary mathematical operation to obtain an invariant line (see paragraph 2.2.3). This concept is described with a sphere subjected to two mathematical operations: dilatation of a sphere to an ellipsoid of revolution followed by a rotation of the ellipsoid (Figure 9). The sphere represent the f.c.c. crystal, while the ellipsoid of revolution represents the b.c.t. crystal.

These two mathematical operations are sufficient to predict the correct O.R of martensite in respect to the austenite (76), but do not describe correctly the crystallography of martensite. As a matter of fact, in real systems, the transformation presents an *invariant plane* while, from Figure 9, it is not visible how to reconcile the transformation with an invariant plane strain, i.e. to leave two unparallel lines invariant.

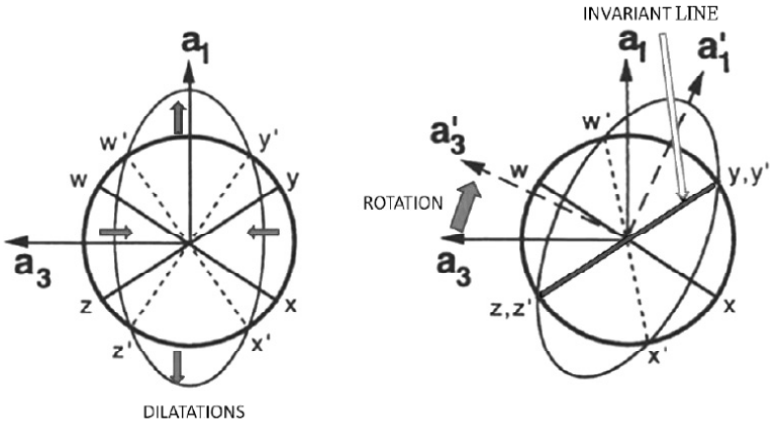

Figure 9. Graphical representation of the habit plane after the second mathematical operation: the dilatation transforms the sphere into an ellipsoid of revolution but does not leave any line invariant. The rotation reports to its original position; the invariant line condition is satisfied. The plane invariant condition cannot be satisfied (i.e. two unparallel lines cannot be driven to the initial position simultaneously). Description according to (48) (76).

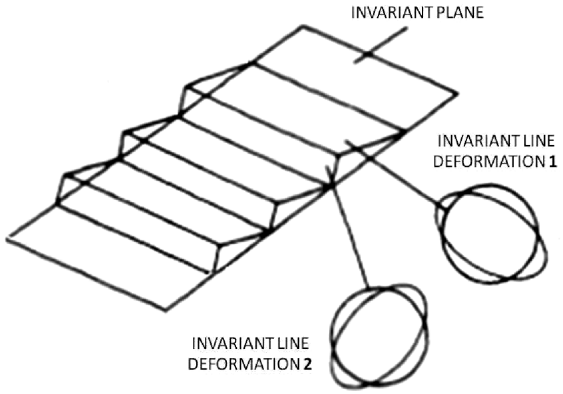

Figure 10. A series of (equally spaced) local line invariant deformations can result in a macroscopically invariant plane. Description according to (48) (76).

As elegantly pointed out in (99), the dilemma is resolved by the PTMC (92), recognizing that the Bain strain that distorts the f.c.c. lattice into the b.c.t., and the macroscopic shape change of the material, as experimentally observed from the investigation of surface relief, do *not* correspond (Figure 5). The theory in (92) introduces a series of localized additional displacements as a necessary condition for the transformation to occur. In the presented

description these displacements correspond to opposite line invariant operations (Figure 9), which are graphically described as opposite twins in Figure 10.[13]

2.4. Ferrous b.c.c. / b.c.t. martensites: habit planes, morphologies and substructures

2.4.1. Definitions and classification of ferrous martensites

The purpose of this section is to give a general overview of the characteristics of ferrous martensites and to point out the connections existing between different ferrous systems. The characteristics of b.c.c. / b.c.t. martensites in iron-based alloys are described in terms of *habit plane*, *morphology* and *substructure*. The characteristics that may be connected to time dependent kinetics are emphasized.

The *morphology* of martensite describes the shape of the martensite units. The morphology can be plate like or lath like. Plate morphology indicates a structure that extends along the habit plane to the first encountered discontinuity in the crystal lattice, i.e an austenite grain boundary, twin boundary or another martensite unit, while being very thin[14] in the direction perpendicular to the habit plane (Figure 11, plate cross section). Lath morphology refers to a structure in which one direction is dominant and the martensite units assume the shape of a rod, a needle, a band, a strip (Figure 12).

The *substructure* of martensite refers to the type of inhomogeneous deformation mechanism that is resolved inside a martensite unit: groups of parallel twins (Figure 13a); arrays of dislocation (i.e. slip) (Figure 13b).

[13] Note that the Bain strain and the rotation do not correspond directly to the first two operations in Figure 7, but their combination lead to the same result: correct structure, wrong shape.
[14] According to (100), the thickness of a martensite plate is in the order of 0.05 times the length of the plate along its principal direction.

Figure 11. Optical micrograph showing examples of plate martensite (light grey) grown in a Fe-7%Al-2%C alloy. Specifically the micrograph refers to plate martensite defined as thin plate (see paragraph 2.4.2) (101).

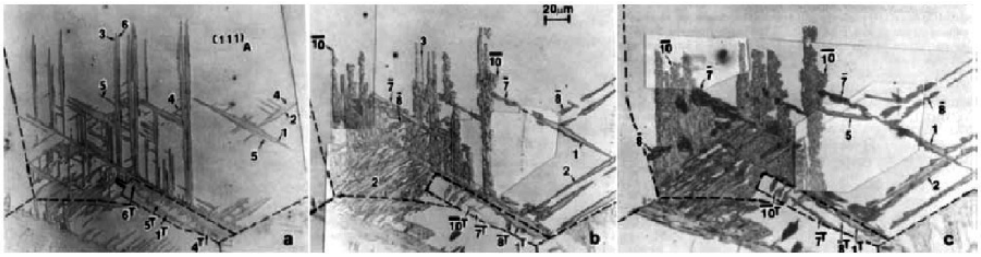

Figure 12. Optical micrographs showing examples of lath martensite(dark grey) grown in a Fe-20%Ni-5%Mn alloy: a, b and c refer to micrograph taken from progressive removal of material (102).

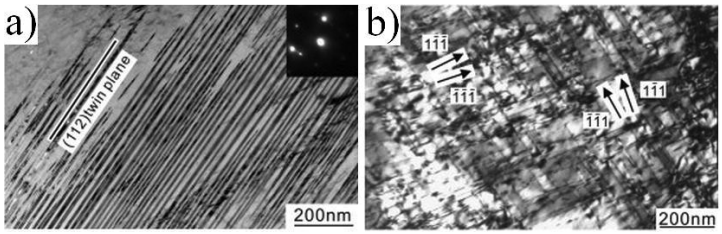

Figure 13. TEM micrographs showing the substructure of martensite. a) twinning on $\{1\,1\,2\}\alpha'$, visualized in cross section as parallel lines; b) slip on $<1\,1\,1>\alpha'$, i.e. dislocation rich areas (103).

Ferrous martensite shows different features, i.e. morphology and substructure, which are always associated with a specific habit plane (68). The indication of the martensite habit plane unequivocally defines the type of martensite. The irrational habit planes observed in ferrous systems are classified according to the approximate crystallographic planes in the f.c.c. crystal as

$\{5\ 5\ 7\}\gamma$, $\{2\ 2\ 5\}\gamma$, $\{2\ 5\ 9\}\gamma$ and $\{3\ 10\ 15\}\gamma$[15]. The habit plane is generally reported in a stereographic triangle (Figure 14).

The (approximate) habit plane evolves in the following order $\{5\ 5\ 7\}\gamma \rightarrow \{2\ 2\ 5\}\gamma \rightarrow \{2\ 5\ 9\}\gamma \rightarrow \{3\ 10\ 15\}\gamma$ on decreasing the transformation temperature and increasing the yield strength of the austenite or increasing its stacking fault energy (68).

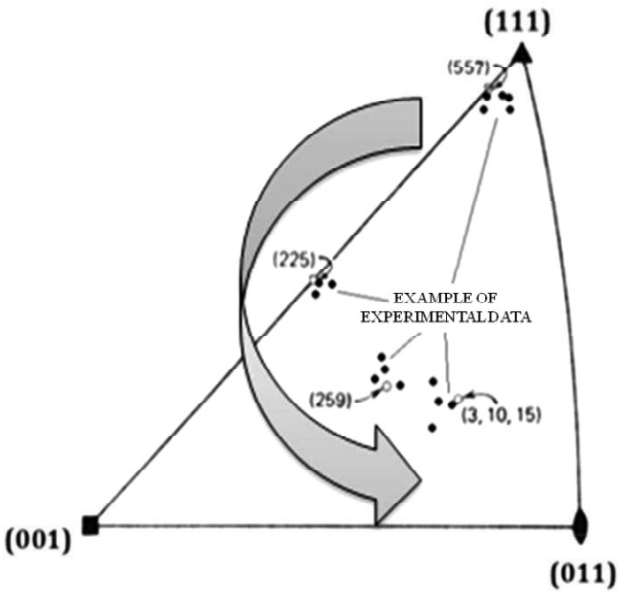

Figure 14. Representation of a texture analysis in a cubic crystal: the "triangle" is a quadrant of the stereographic projection used to represent reciprocal orientation between different components of a system (after (74)). The arrow indicates the evolution of habit planes.

According to (68), the reasons for the occurrence of various habit planes are unclear. In (68), the temperature where martensite formation is first observed, M_S, the relative yield strength of the phases (see also (104)) and the stacking fault energy of austenite, characteristics (mainly) determined by the chemical composition were pointed out as indicative criteria to predict the features of martensite (68). An example of the use of chemical composition (specifically the

[15] Hexagonal close packed martensite has a $\{1\ 1\ 1\}\gamma$ habit plane.

carbon content) and M_S temperature to predict the characteristic (specifically the morphology) of the obtained martensite is given in Figure 15.

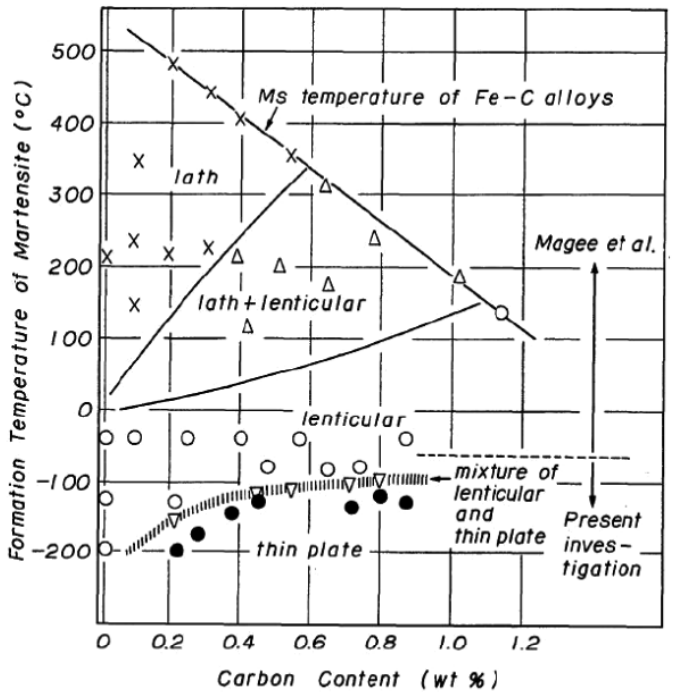

Figure 15. Example of prediction of martensite morphology on the bases of M_S (formation temperature of martensite) and the Carbon content. (graph reported in (105), to which the label "present investigation" refers, including prior results from (106)). Lenticular morphology refers to a type of plate martensite (see paragraph 2.4.2).

In the author´s understanding, among the proposed criteria, the stacking fault energy criterion appears the most consistent with experimental observations. For example, manganese is known to decrease the stacking fault energy of austenite (107) and to promote a transition towards a $\{5\ 5\ 7\}\gamma$ habit plane (further described as a rotation towards $\{1\ 1\ 1\}\gamma$, see Figure 14) in spite of lowering M_S (see Fig. 17 in (51), after (108)). The same applies for chromium.

From a theoretical point of view, a few descriptions (80) (109) indicated the substructure of martensite as the key factor to understand the presence of a specific habit plane (see next paragraph). According to (109), the habit plane is determined by the mechanism that introduces

the lowest plastic work into the system to accommodate the shape strain: slip or twinning. Alternatively, the habit plane is determined by the lowest shear stress to promote slip or twinning in martensite (80).

2.4.2. (3 10 15)γ and (2 5 9) γ plate martensites: the successes of the PTMC

{3 10 15}γ thin plate martensites

In {3 10 15}γ systems, martensite forms with plate morphology. The {3 10 15}γ martensite plates present an internal substructure consisting of twins on {1 1 2}α', which extend over the thickness of the plate (68) (Figure 16). {3 10 15} plate martensite is generally referred to as *thin plate martensite* (68). A typical appearance of thin plate martensite in the microstructure is shown in Figure 11. Ferrous thin plate martensite has been extensively studied in iron-nickel-carbon alloys (68).

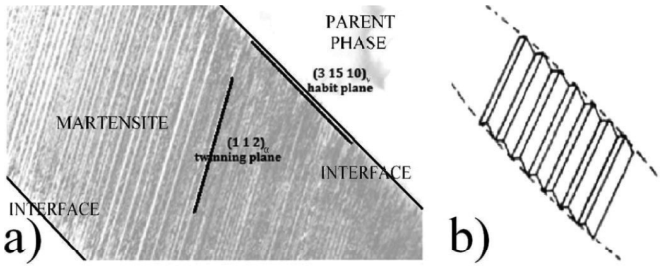

Figure 16. Martensite substructure in a (3 10 15)γ system. a) Example of TEM picture for a Fe-30wt%Ni-0.4wt%C steel: indication of habit plane and twinning plane (after (110)). b) Schematic representation of the observed features according to the description in paragraph 2.3.2.

The PTMC is able to exactly predict the characteristics of these systems: the O.R. between α´ and γ and the habit plane are both calculated within an interval compatible within experimental accuracy and the presence of the observed twinned substructure is predicted. The O.R. of these systems is close to G-T (see paragraph 2.2.4) (68). As a consequence of the fact that the twinning plane is fixed, the relative dimension of the opposite twins (Figure 16b) is determined by the requirement concerning the direction of the habit plane. Finally, the absolute dimensions of the twins is related to the mechanical strength of the austenitic matrix: the stronger austenite, the smaller the twins (110), as less transformation strain can be accommodated by austenite.

To the author´s understanding, there are no elements in the crystallography, morphology and substructure of $\{3\ 10\ 15\}\gamma$ martensite that may be connected with time dependent kinetics (see below).

$\{2\ 5\ 9\}\gamma$ *lenticular martensite*

The $\{2\ 5\ 9\}\gamma$ systems, are strictly related to the $\{3\ 10\ 15\}\gamma$ systems (105). In $\{2\ 5\ 9\}\gamma$ martensites, the martensitic plates have lost their near flat interface typical of $\{3\ 10\ 15\}\gamma$ systems and have developed a lenticular shape. Lenticular martensite forms as $\{3\ 10\ 15\}\gamma$ thin plates that evolve towards a $\{2\ 5\ 9\}\gamma$ lenticular morphology (111) (112). Typical systems showing lenticular morphology are iron-nickel alloys with nickel contents higher than 29wt% and iron-carbon alloys with carbon contents higher than 1.4wt% (68). Lenticular martensite is reported also in iron-carbon-chromium systems (112).

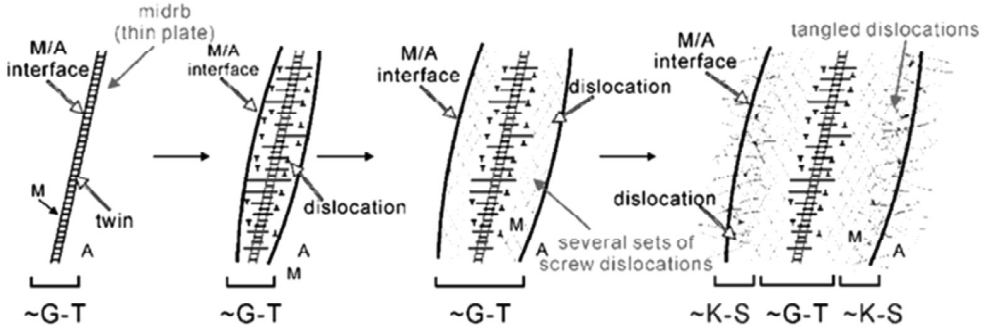

Figure 17. Schematic illustration of the substructure of lenticular martensite (113), based on the description in (103). K-S and G-T refers to Kurdjumov-Sachs and Greininger-Troiano O.R.s.

Lenticular martensites present a central region of $\{1\ 1\ 2\}\alpha'$ transformation twins surrounded by regions which contain arrays of $< 1\ 1\ 1 > \alpha'$ screw dislocations (68). The central region is called *midrib* and appears in the form of a thin plate (Figure 17). The O.R. is close to G-T at the midrib and evolves into K-S towards the interface with austenite (114) (Figure 17).

According to (68) (115), martensite formation in $\{2\ 5\ 9\}\gamma$ systems often occurs in the form of multiple bursts. In a burst, a large part of the material is transformed in a unique instantaneous event. Bursts result in a zigzag morphology (Figure 18a) ($\{2\ 5\ 9\}\gamma$ systems) and in coupled martensite variants in the form of Chevron plates, often referred to as butterfly

martensite (Figure 18b) ({2 2 5}γ systems) (68). Moreover, bursts are associated with a marked (in the range of several degrees) local temperature increase (68). When the transformation starts with a burst, the martensite start temperature, M_S is indicated as *martensite burst temperature* M_b (69).

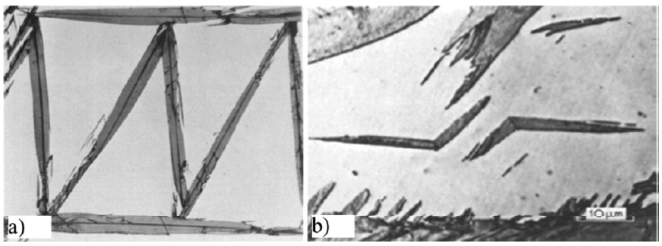

Figure 18. Optical micrographs of coupled variant morphologies arising from autocatalysis: (a) zigzag morphology (80); (b) Chevron plates (116).

For higher transformation temperature of the material, a continuous transition from systems forming fully internally twinned plates, to systems evolving into internally slipped lenses is promoted (117) (Figure 19). The transition between twin and slip in the internal substructure may be related to the feasibility of thermally activated processes at higher temperatures. Thermal activation is discussed in the following.

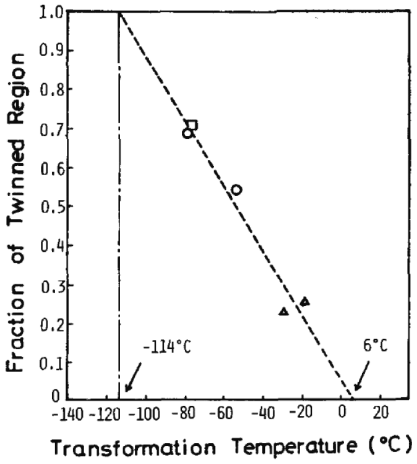

Figure 19. Fraction of twinned region as a function of M_S for Fe-Ni-C lenticular martensites (117). According to (117), no twins should be observed as martensite substructure for alloys having M_S above $6°C$; in alloys having M_S below $-114°C$ only fully dislocated plate would form.

In (118), it is reported that the interface between martensite and the parent phase is *not* glissile for lenticular martensite. Moreover, according to (119), the strain associated with the formation of lenticular martensite is plastically accommodated in the austenite (Figure 20) while accommodation occurs elastically for thin plate $\{3\ 10\ 15\}\gamma$ martensites. The movement of the sessile interface and the plastic accommodation are likely to proceed by thermally activated mechanisms.

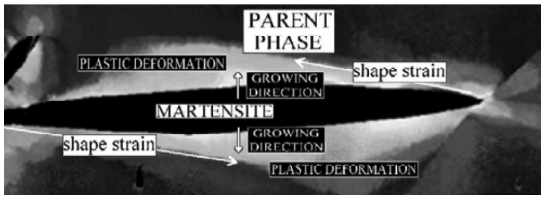

Figure 20. Illustration of the plastic deformation (inferred from crystal misorientation). a) Lenticular martensite: plastic deformation is reported in austenite on both side of the lens (after (119)).

Evidence of thermal activated formation of lenticular martensite was reported in (111), where austenite was transformed into martensite at sub-zero Celsius temperature under the combined effect of undercooling and stress fields. First, thin plate martensite was formed athermally during an initial cooling cycle; thereafter, the material was partially reheated and transformation was continued isothermally at various temperatures while martensite growth was promoted by applying an uniaxial tension[16] (Figure 21). It was observed that thin plate martensite evolves towards a lenticular morphology when the tension was applied above 160 K, while the martensite plates maintain thin plate morphology when the tension was applied below 110 K. A combination of the two morphologies is observed for temperatures in the range 110 K to 160 K.

The evolution of thin plates into lenses for the addition of thermal energy is a very strong indication that the formation of lenticular martensite requires thermal activation. Thermally

[16] The reason why a uniaxial tension promote thickening of the martensite plate are described in section 2.5, paragraph 2.5.3. It is hereby anticipated that the uniaxial tension increases the driving force for martensite formation and consequently the maximum lateral dimension that can be reached by a martensite plate.

activated growth of thin plate martensite into lenticular morphology may be connected with time dependent kinetics. This point is discussed in the following.

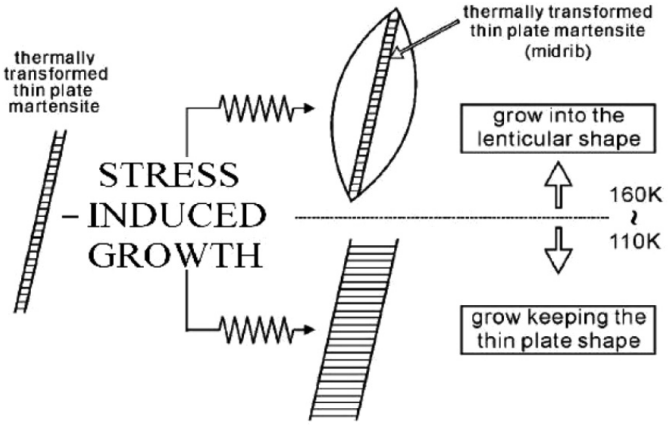

Figure 21. Summary description of the different stress induced thickening mechanisms ((111). Martensite growth leads to different morphologies as a function of the temperature: for temperature above 160 K the lenticular morphology develops from a thin plate nucleus formed on cooling; martensite growth remains fully internally twinned plate at temperatures below 110 K; at temperatures between 110 K and 160 K a progressive transition from thin plate to lenticular martensite is observed.

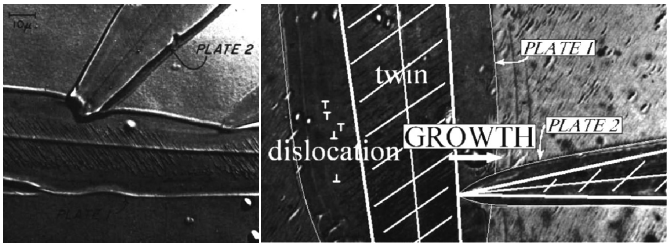

Figure 22. Junctions of two martensite plates formed in a single transformation event. a) Plate 2 extents to the twinned region of plate 1 (i.e. the midrib of plate 1) (after (120)). This implies that the midrib of plate 2 formed prior to the dislocated regions of plate 1. The work in (120) proved that thickening is slower than growth of the midrib in the principal direction of the plate. b) Schematic representation of the concept (micrograph after (120)).

It was demonstrated in (120), that thickening of lenses occurs more slowly than growth along the direction of the habit plane (i.e. the formation of the midrib) (Figure 22). Nevertheless, in (120), thickening of lenticular martensite is considered to proceed extremely fast: the change in martensite substructure is considered promoted by a local temperature rise as a consequence of the heat released by exothermal martensite formation. The description in (120) is generally

accepted (68) (117) (118) and implies that thermal activation does *not* result in time dependent kinetics. On the other hand, thickening of lenticular martensite on a timescale not compatible with the description in (120) was observed in situ in (121) and can be inferred indirectly from (112).

In (121), a Fe-28.8%Ni alloy was transformed into martensite at room temperature. It was reported that thickening of lenticular martensite may continue on a time scale of a few weeks. The work in (121) was afterwards discarded from the discussion on time dependent formation of lenticular martensite because it refers to martensite formation on a free surface, which was appointed as *surface martensite* (122).

In (112), martensite was formed at sub-zero Celsius temperature in a Fe-17%Cr-1%C steel quenching the material in boiling nitrogen and held isothermally in boiling nitrogen for different times. Martensite formation was investigated ex situ in the bulk of the material with microscopy. It was reported that the formation of lenses requires isothermal holding at 77 K for several seconds (Figure 23) and growth continued on a time scale of dozen of minutes. This behavior is inconsistent with the work in (120) and support time dependent kinetics of lenticular martensite as a general characteristic.

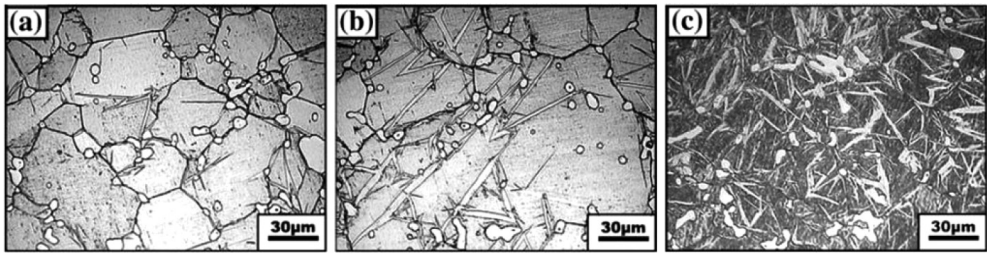

Figure 23. Optical micrographs showing the formation of lenticular martensite upon isothermal holding of Fe-17%Cr-1%C stainless steel at 77K. a) 8s isothermal holding: a few thin plates are visible. b) 10s:the number of plates was increased; the plates appear thicker. c) 12s: plate martensite starts to assume the shape of lenses. Lenticular morphology is thermally activated and develops as continuous growth of thin plate martensite (112).[17]

[17] Note that the work in (112) indicated also time dependent nucleation of martensite (consider Figure 23a and Figure 23b). Time dependent martensite nucleation is discussed in the next section.

In conclusion, several observations indicate that growth of thin plate martensite into lenses may be time dependent. In spite of these observations, the currently accepted opinion indicate that growth of $\{2\ 5\ 9\}\gamma$ lenticular martensites is *in*dependent of time.

Independently of the time scale of lens thickening, it is established that thickening of lenticular martensite takes place on both sides of the plate (Figure 17, Figure 20). The works in (121) (123), where the martensite plate was observed to grow in situ on a free surface either on both sides or unidirectionally, are exceptional. According to (5), unidirectional growth may occur for *surface martensite* with lenticular morphology.

2.4.3. $\{2\ 2\ 5\}\gamma$ plate martensites

The $\{2\ 2\ 5\}\gamma$ systems form martensite in the shape of plates (68). The substructure of the martensite plates has not been completely resolved yet and the habit plane was reported to spread over a certain angular interval (68). The systems showing $\{2\ 2\ 5\}\gamma$ martensite are iron-carbon, iron-carbon-chromium and iron-carbon-chromium-manganese steels with a carbon content ranging from 0.5wt% to 1.4%wt (68) and iron-nickel-manganese alloys. The transformation generally starts above room temperature. The transformation can start at sub-zero Celsius temperature in case of an increased content of the alloying elements (68).

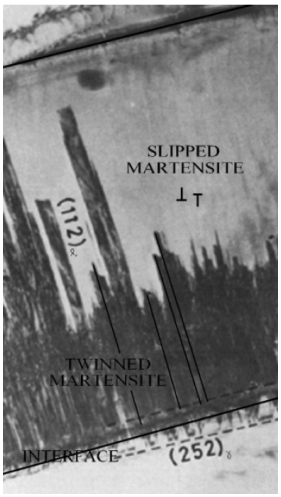

Figure 24. TEM micrograph showing the substructure of {2 2 5}γ martensite: twins are visible on one side of the martensitic plate (the picture refers to a the {2 5 2}γ variant); after (124).

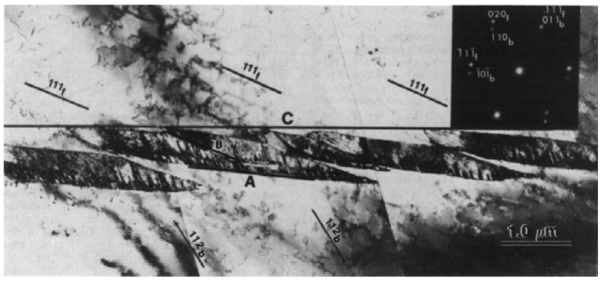

Figure 25. TEM micrograph showing the initial stage of plate martensite formation in $\{2\ 2\ 5\}\gamma$ systems (125). The plate is oriented along the direction C, but is formed by a series of small palettes oriented along A. The direction C represents the habit plane of the macroscopically observed plate after complete impingement of the palettes.

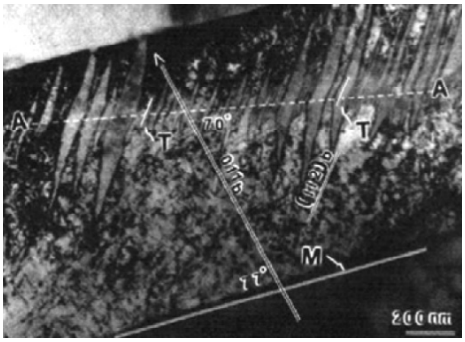

Figure 26. TEM micrograph showing the rotation of the habit plane during growth. The initial direction of the habit plane is inferred from the presence of the twins, T, to be $\overline{AA}$. During growth, the habit plane evolves towards the observed interface, M, which lies much closer to $\{1\ 1\ 1\}\gamma$, i.e. perpendicular to $(0\ 1\ 1)b$ (the big arrow), where b stands for b.c.c. structure. (125)

Both twinning and slip deformation mechanisms have been observed in $\{2\ 2\ 5\}\gamma$ martensites (99) (124) (126) (127): twins along $\{1\ 1\ 2\}\alpha'$, when present, are visible on one side of the plate (Figure 24); dislocations are observed in the rest of the martensitic plate. Thin plates (<0.3 μm thick) may be fully twinned (125).

Martensite plates may result from either the coalescence of smaller internally twinned plates resulting from autocatalytic nucleation (Figure 25), which are defined *palettes* (125) and possess $\{1\ 2\ 1\}\gamma$ habit plane, or from the progressive growth of a single plate (125) (128) (127). According to (125) (127), growth is thermally activated and promotes a rotation of the habit

plane towards $\{1\ 1\ 1\}\gamma$ (Figure 26). On the other hand, the rotation of the habit plane is not observed in (128).

Regarding the crystallography of $\{2\ 2\ 5\}\gamma$ martensites, it is reported that the PTMC does not apply. The failure of the PTMC has been debated extensively (68) (92) (99) (129) (130) (131) (132) (133). Special emphasis has been directed to the observation of crystal defects. The PTMC assumes that martensite forms in a perfect crystal (see paragraph 2.3.1). In the case of $\{2\ 2\ 5\}\gamma$ systems, different crystal defects were reported on both inside the martensite units and in the surrounding matrix and it is unknown which of these defects plays a role during the transformation and which results from the accommodation of the shape strain (see (5) (68) (134)). The debate is shortly reviewed in the following.

The first attempt to reconcile the PTMC with the $\{2\ 2\ 5\}\gamma$ transformation was reported in (92) and introduces the opportunity for the *invariant* plane to undergo a small dilatation, $< 2\%$. The theoretical implication of the small dilatation is that the *invariant plane* is no longer invariant, implying a certain amount of strain in the material surrounding the martensite units (i.e. in the austenite). According to (129), the dilatation parameter is physically *not* reasonable when a macroscopic event is considered.[18] However, the theory may be consistent within the nucleation stage. As explained in (130), conditions can arise when the gaining in terms of interfacial energy as a consequence of complete matching of close-packed atomic rows, can overcome the strain energy associated with the deformation of the matrix. The dilatation parameter theory has so far not been rejected (131) (133).

The plastic accommodation theories are another attempt to deal with the problem and assume the accommodation strains in the austenite throughout the activation of proper shear systems. Of particular relevance according to (68), is the theory in (132), which assumes complete matching of close-packed atomic rows in the two crystal lattices, obtained allowing a small bending angle [≈1°] between close-packed planes (98). The interface (i.e. the habit plane)

[18] To the author´s understanding this claim is based on the fact that martensite formation is assumed time-independent (see paragraph 2.4.4).

is maintained invariant through the activation of proper slips systems in austenite. However, this description is *in*consistent with the observation of an irrational O.R. (see paragraph 2.2.4).[19]

According to (68), the activation of multiple complex shear systems in martensite was proposed in a third group of interpretations, referred to as *multiple shear theories* (135). These theories are extensively reviewed in (5). This interpretation lack of experimental evidence because particular shear systems homogeneously distributed in the martensite are generally not observed.

In conclusion, time dependent formation of $\{2\ 2\ 5\}\gamma$ martensites is reported and accepted. It is however not clarified which characteristic in the crystallography, morphology and substructure is connected with time dependent kinetics.

2.4.4. $\{5\ 5\ 7\}\gamma$ lath martensites

The $\{5\ 5\ 7\}\gamma$ martensite is associated with lath morphology. In lath martensites the plate aspect is abandoned in favor of a thin narrow strip / needle like shape (80). Lath martensite is reported in low alloyed steels with carbon content below 0.4%wt, forming martensite above room temperature (68) and in iron-nickel-manganese alloys, transforming isothermally at sub-zero Celsius temperature (68). Most of the information about lath martensites originates from the investigation of iron-nickel-manganese alloys (136) due to the possibility to study individually transformed laths. The lath martensite formation in these systems occurs at sub-zero Celsius temperature and is time dependent (53).

The crystallography of lath martensite cannot be described by the PTMC. Also, according to the review in (68), a large scattering in the habit plane is reported. Concerning the substructure, the laths are not internally twinned, but contain a high dislocation density (68). Dislocations in martensite are of screw type and are in-homogeneously distributed. Moreover, different sets of dislocations were reported to coexist in a single martensite unit (137). More specifically, the substructure of martensite appears organized, i.e. dislocations are *not* randomly

[19] Note that, even if the exact determination of the O.R. is difficult to obtain, the experimental errors are sufficiently small to conclude about the irrationality.

oriented, but this organization is not connected with the transformation process since the pattern is not uniform within a single lath (68).

Concerning the microstructure, lath martensite formation in a prior austenite grain lead to microstructure features at four length scales (Figure 27). The prior austenite grains is divided into packets, which are defined as groups of laths with the same habit plane (138). Each packet contains several parallel blocks, which are a group of laths with similar crystal orientation (139); blocks are separated by high-angle boundaries and may be twin related (140). Blocks are formed by sub-blocks of two coupled variants according to K-S O.R.. The single laths represent the smallest level of subdivision.

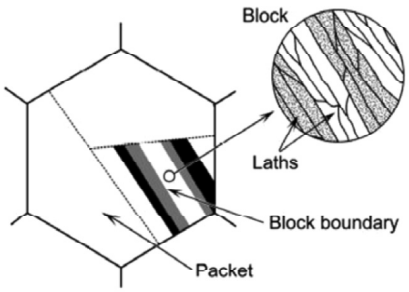

Figure 27. Schematic illustration of lath martensite (139) (141). A prior austenite grain is subdivided in packets; packets contains blocks, which are formed by sub-blocks of coupled variants of martensite.

The classification of the microstructure at four different scales was further investigated in (142). Essentially, there appears to be three types of microstructures (Figure 28): (A) packets are subdivided directly in sub-blocks and two different lath variants exist in each sub-block; (B) packets are divided in blocks formed by sub-blocks of two variants; (C) packets are divided in blocks, formed by sub-blocks containing one variant only. The types of microstructure are a characteristic shared between martensite and *bainitic ferrite* (see paragraph 3.3.1). This indication is in agreement with prior study in (143) andsuggests a reconciliation of the different transformations in steel, which was already investigated in (143) (144) and emphasised in (51).

Several factors were observed to influence the microstructure of lath martensite. The influence of the carbon content in the material was investigated in (142). According to (142) (as referred to in (145)), in carbon low alloyed steels, the dimension of the martensite structures depends on the carbon content: a single lath and a block are smaller the higher the carbon

content. The influence of the pre-strain (i.e. straining of the material prior to martensite formation) was investigated in (146). In was reported that the dimension of the block is reduced on pre-straining the material, while the dimension of the packet is increased. The influence of the applied thermal cycle (i.e. applied cooling rate and presence of isothermal steps) was reported in (59) (61) (62) (139) (147) (148).

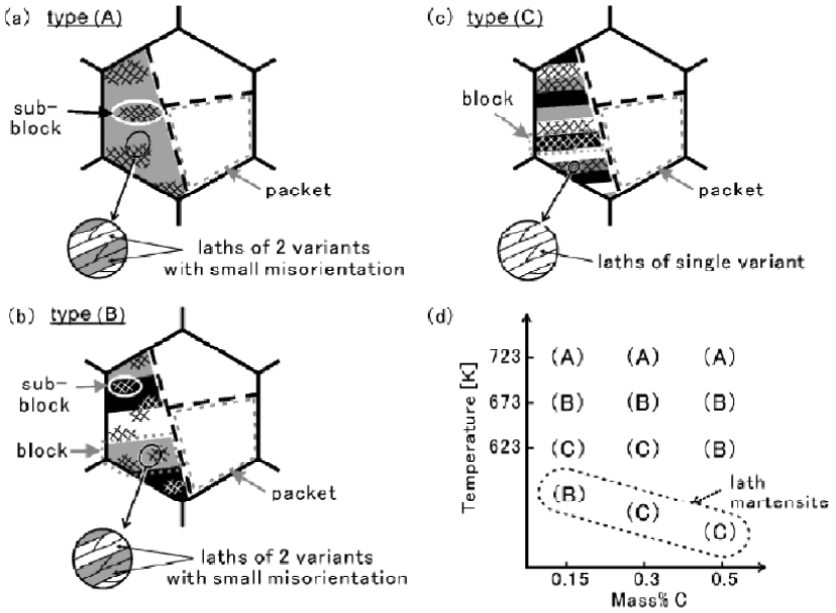

Figure 28. Schematic illustration of lath martensite and bainitic ferrite. In general terms, an austenite grain is divided in packets; packets contain blocks, which are formed by sub-blocks of laths. However, these subdivisions do not always exist and the microstructure of the material may be of different types. The type of microstructure is determined by the transformation temperature and the carbon content in the material (142).

The cooling rate was observed to affect martensite formation in (59) (139) (147) (148). In (59) martensite formation was followed recording the elongation of the sample versus temperature,[20] while the microstructure was observed ex situ. Martensite becomes finer the slower the cooling. On the other hand, in (139) (147) (148) martensite was reported to become

[20] See paragraph 3.3.2.

finer the faster the cooling (Figure 29), with the dimension of the lath that was observed to be independent on the cooling rate, while the dimension of blocks and packets was reported to be reduced the faster the cooling.[21]

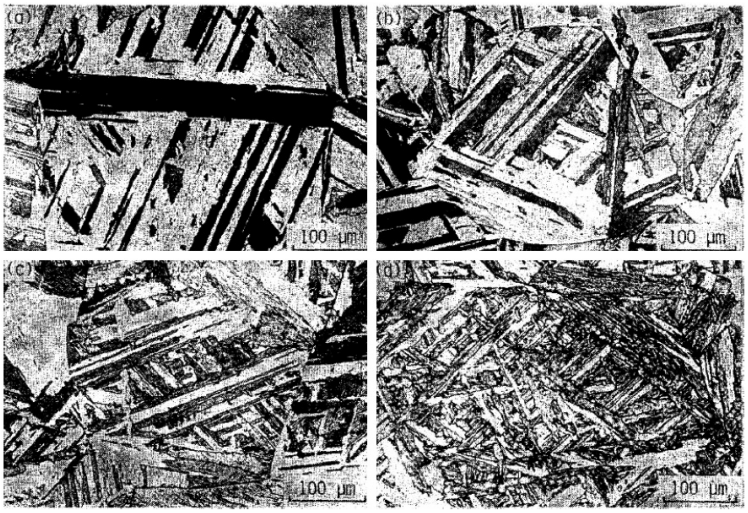

Figure 29. Optical micrographs showing a progressive refinement of lath martensite in a Fe-18.5%Ni-8.95%Co-0.7%Ti maraging steel: a) furnace cooling; b) air quench; c) water quench; d) Iced-brine quench. (147).

In (61) (62), continuous cooling at 150 K/s from the austenitization temperature of 1223 K was interrupted at 663 K after 10% transformation and the transformation was completed isothermally. The isothermal product was compared with the product formed during continuous cooling. It was reported that the isothermal product is coarser, but contrary to (139) (147), coarsening is observed at the lath scale only (Figure 30).

In conclusion, the applied thermal cycle influences the features of the final product. This indicates time dependent transformation. Consequently, the works in (59) (61) (62) (139) (147) all indicate that the formation of lath martensite is time dependent. On the other hand, according

[21] It is noted that the works in (138) (146) did not followed martensite formation in situ. Consequently, the occurrence of a different type of shear transformation (i.e. bainitic ferrite) cannot be excluded.

to (140), lath martensite formation may occur athermally. The work in (140) is further discussed in the end of the present chapter.

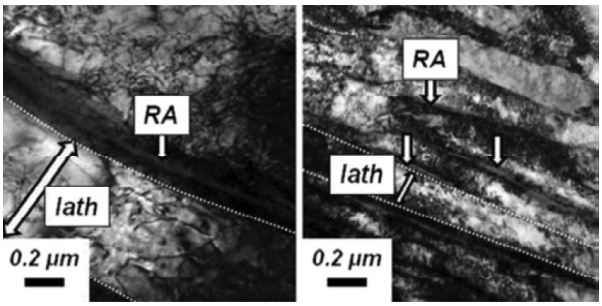

Figure 30. TEM micrographs showing the lateral dimension of single laths. On the left: isothermal martensite. on the right: martensite formed during continuous cooling (62). RA stands for Retained Austenite, which is observed in between the laths of martensite.

In agreement with time dependent description, in (149) (150) a fast cooling rate was observed to suppress lath morphology. When lath martensite formation is suppressed, martensite assumes plate morphology at temperatures which may be significantly lower than M_S for lath martensite. This observation suggests time dependent nucleation and / or growth of lath martensite (150). According to (51), consistent observations are reported in (151) (152) (153). More generally, the observation in (149) should be considered as a general characteristic of steels (51).

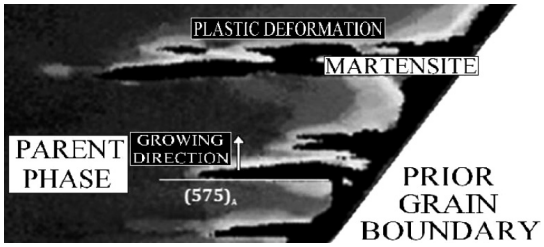

Figure 31. Illustration of the plastic deformation (inferred from crystal misorientation). Plastic deformation is reported in austenite on one side of the lath only (after (119)).

As opposed to the case of lenticular martensite, where thickening generally takes place on both sides of the plate (Figure 17), growth of each lath occurs on one side of the structure only (119), as observed in situ in (154). Growth is accomplished with large plastic deformation in the

adjacent austenitic matrix (Figure 31) (119). The work in (137), which showed that the dislocations in austenite are concentrated on one side of the lath also support the notion of unidirectional growth. According to (119) (154), the interface between martensite and the parent phase is wavy on the thickened side of the lath, while it is planar on the opposite side.

The O.R. of lath martensite is historically described as approximatively K-S (68). However, large scatter is reported for the determinated O.R.. In recent studies both O.R.s close to K-S (61) (62) (139) and to G-T (155) (156) are reported. The misorientation angle distribution among different areas of martensite recently indicated an O.R. of G-T type in several systems (138) ((90) referring to prior works). Moreover, in (157) it was reported that the O.R. may differ for the two sides of a single lath, being close to N-W on the planar side and to K-S on the wavy side. This observation, reconnected with the work in (119) (154), may indicate a progressive rotation of the martensite lath during thickening.

2.4.5. Rationalization of the observations in connection with time dependent kinetics

A transition between internal twinning and slip in martensite can be promoted by two phenomena (128) (127): a local temperature rise due to the heat evolved during the transformation; the generation of dislocations in austenite that are inherited during the transformation. The first interpretation is considered generally valid for the case of lenticular martensite (120). The growth of lenticular plates is consequently modeled as *in*dependent of time.

However, a rationalization of the observation in different systems is possible if the second hypothesis is considered to stand instead. This concept is discussed in the following.

Here, it is emphasized that indications of possible rotations of the habit plane towards $\{1\ 1\ 1\}\gamma$ and a K-S O.R. during growth of martensite are reported for $\{2\ 5\ 9\}\gamma$, $\{2\ 2\ 5\}\gamma$ and $\{5\ 5\ 7\}\gamma$ systems. The rotation of the habit plane during growth may be associated with time dependent kinetics as discussed below.

According to (5), growth should occur along rational directions in the parent crystal, for example $< 1\ 1\ 1 > \gamma$. However, growth along a rational direction is not consistent with plane invariant transformations (see paragraph 2.4.3), but requires a certain plastic accommodation in

the matrix surrounding the martensite units. If this mechanism is active, growth is thermally activated and is likely to be time dependent.

For example, according to (5), in (158), martensite in a Fe-29wt%Ni alloy was observed in situ and it was reported that martensite initially formed away from $\{1\ 1\ 1\}\gamma$, but thereafter slowly grew along the $\{1\ 1\ 1\}\gamma$ plane. Also, according to a theory for martensite formation reported in (159), lath martensite grows along $< 1\ 1\ 1 > \gamma$ and thickened by a ledge mechanism (Figure 32).

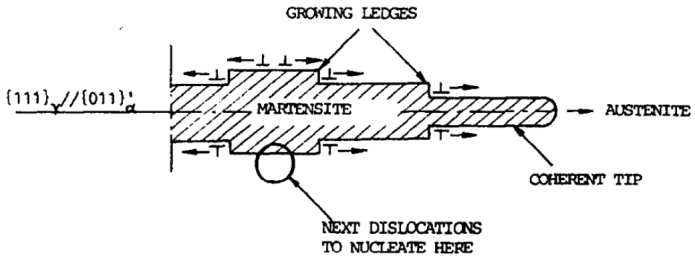

Figure 32. Schematic representation of the thickening by a ledge mechanism and growth of lath martensite in steel (159).

The theory in (159) is supported by recent in situ observations reported in (160) where discontinuous reverse martensite to austenite transformation by a ledge mechanism is reported, suggesting that the mechanism may be active also in the direct process.

Moreover, under this description, the failure of the PTMC to predict $\{2\ 2\ 5\}\gamma$ and $\{5\ 5\ 7\}\gamma$ systems can be interpreted in terms of plastic accommodation of the shape strain in the austenite that results from progressive thermally activated, time dependent, growth of martensite along a rational direction. This interpretation suggests that the dislocations visible inside a martensite unit are likely to be connected with plastic deformation of the austenite prior to transformation.

The concept was investigated in (110) for the $\{2\ 2\ 5\}\gamma$ system. In (110), dislocations were introduced in virginal austenite by plastic deformation; thereafter martensite was formed through cooling the material. It was shown that the dislocations are inherited by martensite without modifications. Similarly, it was suggested in (113) that the tangled dislocations reported for the general description of lenticular martensite (Figure 17, $\{2\ 5\ 9\}\gamma$ systems) result from the

dislocations introduced in austenite by martensite formation and are inherited by the growing martensite. In the following, a series of works that support plastic accommodation in the austenite are briefly discussed.

In (161) (162), the effect of martensite formation in the surrounding austenite was studied ex situ in bulk and surface areas. According to (161) (162), martensite formation is always accompanied with plastic deformation in the adjacent austenite. This deformation was defined spontaneous and it was claimed to precede martensite formation (161).

In (163), it was reported that the habit plane of a $\{2\ 2\ 5\}\gamma$ martensite formed in single crystals of austenite depends on the geometry of the crystal and it was concluded that austenite spontaneously deformed prior to martensite formation along specific directions that depend on the crystal geometry. In (5), referring to (164), this deformation was claimed to depend on the crystallographic direction in the austenite: martensite formation was observed in association with compressive strain along $< 1\ 1\ 1 > \gamma$ and tensile strain along $< 0\ 0\ 2 > \gamma$.

Finally, in (165), time dependent growth of lath martensite in the longitudinal direction was observed in situ. It was reported that growth occurs discontinuously and was preceded by the movement of $(a/2) < 1\ 1\ 1 > \gamma$ screw dislocations along $\{1\ 1\ 1\}\gamma$ just in front of the martensite to austenite interface. As described in (165), this observation was consistent with a model developed in (166) and with prior observations in (167) (168). According to (128), the model in (166) applies also in the case of $\{2\ 2\ 5\}\gamma$ martensites. The model in (166) was described in detail in (5).

A $(a/2) < 0\ 1\ 1 > \gamma$ type screw dislocation dissociates into two partials of type $(a/6) < 1\ 1\ 2 > \gamma$ (166). This dissociation is considered in association with the Bain strain that converts $(a/2) < 1\ 1\ 1 > \gamma$ into $(a/2) < 0\ 1\ \bar{1} > \alpha'$ and allows the interface to move along $\{1\ 1\ 1\}\gamma$, providing that $\{1\ 1\ 1\}\gamma\ //\ \{1\ 1\ 0\}\alpha'$.[22] Consequently, the model forces the system to follow K-S O.R. As mentioned in paragraph 2.4.3, this assumption requires to relax the invariant

[22] This mechanism appears equivalent to assume an $\gamma \rightarrow \varepsilon \rightarrow \alpha'$ transformation path, hence reconnecting the different transformation mechanism reported for Iron based alloys (see chapter 1).

habit plane condition. Moreover, according to (5) it requires an anisotropic deformation of the austenite (like observed in (164)) in front of the martensite interface.

In conclusion, plastic accommodation of the shape strain in the austenite appears consistent with several observations reported in the literature and may be the reason why the PTMC fails for $\{2\ 2\ 5\}\gamma$ and $\{5\ 5\ 7\}\gamma$ systems. Moreover, it leads to the notion of time dependent martensite formation in terms of time dependent growth of martensite. If this is the case, time dependent kinetics is an intrinsic characteristic of $\{2\ 5\ 9\}\gamma$, $\{2\ 2\ 5\}\gamma$ and $\{5\ 5\ 7\}\gamma$ martensites, which are all characterized by the presence of slip at the substructure level. This implies that the description in (120), which indicate instantaneous formation of lenticular martensite, is unlikely.

2.5. Thermodynamics of the martensitic transformation in steel

2.5.1. Introduction on the thermodynamics of the transformation

Thermodynamics deals with the possible energy configurations of a system and indicates the direction a system would like to evolve spontaneously (169). Whether a system actually does evolve in this direction depends on the availability of a sustainable kinetics path.

To generate martensite, it is required that the parent phase is not the most stable energy configuration of the system: the presence of a driving force, *i.e.* an excess of Gibbs energy in the system, for a phase transition is a necessary condition.

Generally, martensite in ferrous systems is a *non* equilibrium structure, as it is *not* the energetically most favorable configuration of the system. The main reason for martensite formation despite its metastability is that the attainment of a state of equilibrium would involve partitioning of atoms which cannot be obtained rapidly enough under the given conditions. Development of martensite is associated with the introduction of a large strain energy and numerous new interfaces and associated interfacial energy. The energy contribution of the interfaces is generally neglected for iron-based systems, while the strain energy contribution is *not* negligible (96) (170).

The definition of the thermodynamics of the martensitic transformation is mainly directed to the determination of the temperature where martensite formation is first observed on cooling, defined M_S, which is in good approximation *in*dependent of the cooling rate (51).

2.5.2. Temperature as the only state variable

As mentioned in chapter 1, ferrous martensites are b.c.c. in absence of Nitrogen and Carbon atoms, while being b.c.t. otherwise. However, in a first approximation, it can be assumed that martensite possesses the b.c.c. crystal structure of supersaturated (i.e. containing a carbon or nitrogen content above the equilibrium content) ferrite (72).[23]

The temperature at which austenite and supersaturated ferrite with the same composition have identical (chemical) Gibbs energy, while ignoring strain and interfacial energy contributions, is generally defined T_0 (72) (171). At T_0, $\Delta G_{chem} = 0$, where ΔG_{chem} is the difference in the chemical contribution to Gibbs energy between the supersaturated ferrite and the austenite. At T_0, neglecting the interfacial energies, an infinitively thin nucleus of martensite would be in thermodynamic equilibrium as austenite and martensite co-exist. A real nucleus of martensite is instead associated with strain and interfacial energy terms that have to be taken into account.

The strain energy due to martensite formation, ΔG_ε, is added directly to the Gibbs energy curve ΔG of the phases to define a new "equilibrium" (172) (see also (96)) and is partitioned over both martensite and austenite. The partitioning of strain energy is determined by the configuration that yields the lowest energy for the system. The lowest energy configuration is *not* identical to the most stable configuration of the system, since it exclude a redistribution of atoms over the phases present. The temperature where strained austenite and martensite are in equilibrium and below which a driving force build up for martensite formation is M_S.

[23] It is not the purpose of this text to deepen further the description of the b.c.c. versus b.c.t. structures from a thermodynamic point of view.

At M_S, neglecting the interfacial energy term, $\Delta G_{chem} = -\Delta G_\varepsilon$. T_0 is theoretically equal to M_S when martensite is fully self-accommodated[24] or unconstrained conditions exist. In real cases M_S is always lower than T_0 (Figure 33).

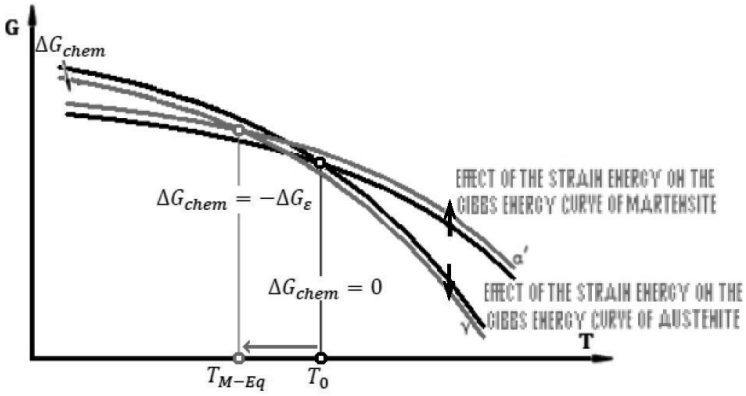

Figure 33. Schematic representation of the chemical driving force for the transformation and the effect of the strain energy on the equilibrium temperature.

In the following, to convey the state of the art in a simple way, the definition of $\Delta G_{chem} = -\Delta G_\varepsilon$ as the energy condition at M_S is abandoned and a new definition is introduced. The condition will be expressed as "meta-equilibrium" and the temperature where it is satisfied "meta-equilibrium temperature", T_{M-Eq}.

Assuming elastic accommodation, the contribution of the strain energy is calculated according to the approximate formula:

$$\Delta G_\varepsilon = \frac{t}{l}\mu(s^2 + \delta^2) \qquad [1]$$

where $\frac{t}{l}$ is the thickness to length ratio for the martensite unit (approximated by an ellipsoid of revolution), μ the shear modulus of the phase that accommodates the strain elastically and s and δ are the shear and dilatational components of the shape strain, respectively (133) (173). It follows that the energy configuration of the system depends on the lateral

[24] *Self-accommodation* indicates the contemporary formation of different martensite variants that reduce the total strain energy term.

dimension of the martensite unit $\Delta G_{\varepsilon}\left(\frac{t}{l}\right)$ and progressively increases for continuous thickening of the ellipsoid, i.e. the plate / lath.

Accordingly, $T_{M-Eq}\left(\frac{t}{l}\right)$ is the temperature at which a martensitic unit with its specific geometry and dimension, can form. $T_{M-Eq}\left(\frac{t}{l}\right)$ is also the temperature at which the reverse transformation can occur, assuming that no irreversible phenomena, *i.e.* energy dissipative processes (see (174)), have occurred during martensite formation.

Irreversible phenomena result in a temperature hysteresis for the transformation (96) and are always present. Irreversible phenomena are of two types: the energy which is stored in the material (175) in the form of crystal defects, $\Delta G_{\varepsilon_{irr.}}$, and the heat that is released during the transformation (i.e. an enthalpy effect), $\Delta H_{\gamma\rightarrow\alpha'}$. Because of irreversible phenomena, the transformation process starts when $\Delta G_{chem} = -\Delta G_{\varepsilon}\left(\frac{t}{l}\right) - \Delta G_{\varepsilon_{irr.}} - \Delta H_{\gamma\rightarrow\alpha'}$.

2.5.3. The effect of magnetic and mechanical forces

The influence of stress fields

A stress field acting on the system changes the meta-equilibrium condition. The reasons are: the isotropic volume change on transformation; the anisotropic volume change of the transformation that can lead to anisotropic transformation in directions complying with the imposed stress field (5).

The energy component generated by the presence of a stress field can be added algebraically to the Gibbs function as mechanical work exerted onto the system, W_{σ} (176). Accordingly, the resulting Gibbs energy function becomes $\Delta G^{*} = \Delta G_{chem} + W_{\sigma}$. Following (176), $W_{\sigma} = -\tau \cdot \gamma_0 - \varepsilon_0 \cdot \sigma$, where $\tau \cdot \gamma_0$ is the shear stress, τ, resolved along a potential habit plane times the transformation shear strain, γ_0, and $\varepsilon_0 \cdot \sigma(f)$ is the normal stress, $\sigma(f)$, resolved perpendicular to the habit plane times the normal component of the transformation strain, ε_0. In the presence of a hydrostatic pressure, P, on the austenite, the last term become $-\varepsilon_0 \cdot P$ (177), or $-\varepsilon_0 \cdot P \cdot V_m$ with V_m molar volume (178), depending on how ΔG^{*} is defined. The sign is defined as negative for hydrostatic pressure and positive for hydrostatic tension.

An applied stress field can influence the texture of the developing martensite. The influence is determined by the ratio between the mechanical contribution and the driving force for the transformation. The formation of martensite along preferential directions, defined as *variant* (see paragraph 2.2.4) *selection,* is *un*likely when $W_\sigma \ll \Delta G^*$, (179) (see also (115) (180)).

According to (5), the presence of a stress fields affects martensite formation significantly. The application of a hydrostatic pressure shifts the equilibrium temperature in the order of 100 K / GPa.

The effect of hydrostatic pressure is particularly relevant in connection with the interaction of different phases in the material. In (6) (178) (181), it was suggested that martensite formation generates a macroscopic state of compression in austenite. On the other hand, no macroscopic effect was reported in (182), while a mechanical interaction between different grains was reported; specifically, the austenite retained in transforming austenite grains experiences compression, while not transforming austenite grains experience a general state of tension (182).

The interaction among different phases in terms of deviatoric component is discussed in the section 2.7..

The influence of magnetic fields

A magnetic field influences the martensitic transformation. The reasons are mainly twofold: the different magnetic properties of austenite (paramagnetic) and b.c.c. / b.c.t. martensite (ferromagnetic) (see (63) (58)); the possibility for a magnetic field to favor energetically specific variants in anisotropic phases.

The effect of the magnetic field on the Gibbs free energy of the system is described and quantified in (177) and can also be included as an energy term W_m. In good approximation W_m is proportional to the intensity of the magnetic field.

Magnetic fields in the order of a few Tesla or larger are necessary to affect martensite formation significantly (183) (184). For example, a magnetic field of 1.6 T shifts the equilibrium temperature by about 4 K ((5) based on prior work in (185)).

2.6. The kinetics of martensite formation in terms of nucleation and growth

The martensitic transformation in steel is historically defined as *nucleation controlled* and classified in *athermal* and *isothermal*. *Athermal* refers to transformations that depend only on temperature and are *in*dependent of time. *Isothermal* indicates time dependent transformations (53).

2.6.1. Nucleation controlled description

In a *nucleation controlled* description, time dependent martensite formation is interpreted in terms of time dependent nucleation, while growth is presumed infinitely rapid and instantaneous upon nucleation. According to (53), the model in (186) is the most accurate description of time dependent martensite formation so far reported in the literature. This model considers nucleation controlled kinetics. Nucleation controlled descriptions are still extensively applied nowadays (see for example (182) (183) (187) (188) (189)).

According to (53), the assumption of nucleation controlled kinetics is based on the pioneering work in (78) (190) and is consistent with recent works in (191) (192), which showed martensite formation events of the duration in the order of fractions of seconds. The work in (191) and (192) deals with plate morphology and lath morphology, respectively.

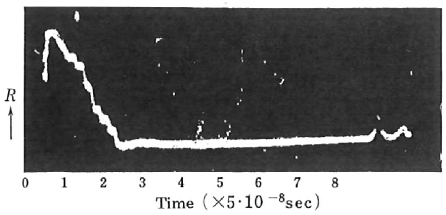

Figure 34. Electrical resistance plotted versus time, describing martensite formation in a Fe-29.5%Ni alloy ((5) after (193)). Martensite formation appears as a sudden reduction in resistivity; the duration of the event is about 100 ns.

A series of works consistent with the nucleation controlled description are listed in (5). In these investigations, martensite formation is generally determined from a change in electrical

resistance of the sample versus time. The technique allows to measure the duration of a single transformation event (Figure 34).

The thermally activated motion of dislocations is accepted as rate controlling mechanism for time dependent nucleation (53). Following (79) (194), the rate controlling mechanism is the motion of interfacial dislocations (which were introduced in the nucleation theory to describe the f.c.c. to b.c.c. lattice distortion (194)), while the work in (128) (195) supports the motion of lattice dislocations in austenite as the rate-controlling mechanism.

2.6.2. Athermal versus isothermal

The distinction between *athermal* and *isothermal* kinetics was introduced in (196). This distinction met opposition in (100) (165), where the athermal transformation was defined as a rapid isothermal reaction and the distinction between athermal and isothermal kinetics was considered purely empirical. Several years later, the model in (197) explained both the athermal and the isothermal behavior in a unified theory.

According to (197), martensite nucleates either instantaneously, when a *critical* driving force for the martensitic transformation is reached upon cooling, or after an incubation time defined by the presence of an energy barrier, when the critical driving force for the transformation is *not* reached. Only the first nucleation event is considered. One of the major assets is that the model allows the possibility to switch between isothermal and athermal kinetics by applying external forces (177) (198). Specifically, the theory in (197) is able to describe quantitatively the effect of magnetic fields and hydrostatic pressure on the spontaneous nucleation of martensite.

As for as the author´s is aware, no other unifying theories have been proposed yet to reconcile the effects of different forces on the nucleation kinetics. The model in (197), does not account for thermally activated motion of dislocations as rate-controlling mechanism for time dependent nucleation.

2.6.3. Time dependent growth

Nowadays, the notion of nucleation controlled kinetics is under debate. According to (59) (61) (62) nucleation is athermal while growth is thermally activated. The notion of athermal

nucleation is put forward to explain the independence of M_S on the cooling rate. This interpretation implies that the final microstructure of the material depends on the applied thermal cycle, as is the case for a few works on lath martensite reported in the literature (59) (139) (147).

Time dependent growth was generally accepted in the Japanese literature in the ´70ies (see (5)) but appears to have been forgotten. In particular, (5) follows (199) and classifies martensitic transformations in *Umklapp* transformations and *Schiebung* transformations: *Umklapp* refers to systems characterized by athermal fast growth and the presence of twins in the martensite substructure; *Schiebung* to slow growth of martensites characterized by the presence of dislocations in the internal substructure.

In the end of this section, it will be shown that the work in (192), which supported athermal formation of lath martensite, is compatible with *Schiebung* transformations. Similar conclusions stand for (140), where athermal lath martensite formation was claimed.

2.7. Theory of martensite nucleation

2.7.1. General aspects

The general aspects to be considered in relation to nucleation of martensite are (73): the degree of coherency of the interface between product and parent phases, homogeneous versus heterogeneous nucleation and so called *lattice instability*.

Degree of coherency of the interface

Following (48), a nucleus of martensite is initially coherent with the austenite matrix. An increase of electrical resistance at the beginning of the process (see Figure 34) is taken as the experimental evidence for initially coherent interfaces (193).[25] On the other hand, according to (5) (after (200) (201)), the initial increase in resistivity is either an artifact due to incorrect sample preparation or an effect of sample magnetization during martensite formation.

[25] As explained in (200), martensite formation is associated with a decrease in resistivity and the same applies for break of coherency at the martensite-austenite interface. The interpretation in (48) arises from the reasoning that an initial increment in resistivity followed by a subsequent decrease may result only from increased lattice strains at the coherent interface followed by the combined effect of strain relaxation and martensitic transformation.

For an initially coherent nucleus, coherency is lost when its dimension no longer energetically favor full coherency (159); then coherency is lost with the activation of internal deformation mechanisms in martensite. At this stage, instantaneous growth of the nucleus takes place. In (73) (202) it is claimed that the internal deformation mechanisms can be slip or twinning, hence determining the substructure of the martensite.

The coherency at the austenite-martensite interface was claimed to influence martensite tetragonality (202) (203). It was also discussed that coherency loss requires thermal activation (203). The work in (203) deserves further attention because it is particularly relevant in relation to the state of the art of cryogenic treatment of steels.

Martensite forming at cryogenic temperatures in a series of iron-nickel, iron-nickel-carbon and iron-manganese-carbon alloys was investigated in (203). In Fe-33.5%Ni martensite was tetragonal (it should not in absence of carbon atoms) and the tetragonality was lost during heating to room temperature. In Fe-30%Ni-0.37%C, Fe-25%Ni-0.7%C and Fe-20%Ni-0.7%C, the tetragonality of martensite was observed to be abnormally large and the abnormal characteristic was lost during heating to room temperature. In a Fe-1.5%C-3%Mn steel, the tetragonality was abnormally low and it is mentioned that no change in tetragonality are observed up to 170 K.

The abnormal tetragonality of martensite in iron-nickel, iron-nickel-carbon alloys was explained from the presence of coherent interfaces between austenite and thin plate martensite, which resulted from insufficient dislocation mobility in the austenite to plastically accommodate the shape strain. Thereafter, the presence of an observable phenomenon centered at 145 K (specifically an unusual *Internal Friction*, IF, peak), occurring in association with magnetic ordering / disordering transition (204), was associated with coherency loss. The abnormally low tetragonality in Fe-1.5%C-3%Mn remained unexplained.

The Fe-33.5%Ni and Fe-25%Ni-0.7%C alloys were also subjected to plastic deformation at cryogenic temperatures. It was possible to completely transform the b.c.t. structure into b.c.c. by plastic deformation. This observation was interpreted as follows. For the Fe-25%Ni-0.7%C material, no anomalies at 145 K were observed, and it was concluded that gliding dislocations in martensite, which trapped carbon atoms, reduced the tetragonality of martensite. For the Fe-33.5%Ni alloy plastic deformation induced coherency loss.

The same group of authors considered a Fe-1%C-1.5%Mn which was transformed at cryogenic temperature (44). The martensite was shown to present an abnormally low tetragonality. This phenomenon was applied to interpret an observed enhanced precipitation of carbides during tempering of cryogenically treated 1.55%C-11.9%Cr-0.7%V-0.86%Mo steel in terms of trapping of Carbon atoms by gliding dislocation in the martensite leading to the formation of nucleation sites form the formation of precipitates.

This interpretation appears *not* acceptable. Firstly, the Fe-1%C-1.5%Mn does *not* require any pre-existing martensite to show abnormally low tetragonality. Moreover, the formation of precipitates at Carbon clusters generated by gliding dislocations is *not* likely because the binding energy of Carbon to dislocations is larger than the energy gain in the carbide formation (63) (after (18)). Furthermore, an extensive study on all the possible phenomena leading to abnormally low tetragonality of martensite was presented in (205), where the mechanism presented in (44) was *not* reported.

In particular, according to (206), abnormally low tetragonality in iron-manganese-carbon results from ordering / disordering of carbon atoms along the different crystal axis of martensite unit cell. This is in agreement with the original work on iron-nickel-manganese martensites in (207), where ordering / disordering was reported to lead to different crystal structures. The mechanism responsible for ordering / disordering phenomena is strain interactions among carbon atoms (208) (209) (210) and is dependent of the chemical composition of the steel.

In conclusion, the initial stages of martensite formation in terms of coherent or incoherent interfaces are far from being clarified and the effects of cryogenic treatments on the tetragonality of martensite should be carefully considered prior to emphasize it as the metallurgical explanation to enhanced precipitation of iron carbides during tempering of high carbon steels.

Homogeneous versus heterogeneous nucleation

Homogeneous versus heterogeneous nucleation deals with the degree of interaction of a martensite nucleus with pre-existing imperfections in the material: if no such interaction occurs, nucleation is homogeneous. It can be demonstrated (96) that the energy barrier for homogeneous nucleation of martensite is unrealistically high. Consequently, nucleation of martensite proceeds

heterogeneously, on specific pre-existing nucleation sites. According to (5) (53) (211), the work in (212) is considered to be the most solid experimental evidence for heterogeneous nucleation.

It was shown in (212) that isolated particles with equal chemical composition do *not* nucleate martensite all at the same temperature, but certain particles are more prone to form martensite than others. Specifically, the larger the particles, the higher the probability that martensite starts to form at a lower degree of undercooling (i.e. at a higher temperature). Accordingly, it was concluded that the particles contain nucleation sites that are more or less effective for the formation of martensite (according to (53) (212) sites distributed in potency) and that the probability to encounter a potent nucleation site is the larger the larger the particle. The same conclusion was attained in (211).

Further experimental evidence of heterogeneous nucleation was reported in (213), where it was shown that in multiple thermal cycling of thermoelastic materials, martensite nucleates always at the same positions. Several consistent observations are listed in (5).

Nevertheless, the nature of the pre-existing nucleation sites, where martensite nucleate heterogeneously is *not* clarified. According to (96) (referring to prior work in (213)), it was recognized that martensite nucleates at stress concentrations. Accordingly, the role of the stress field surrounding a general defect in promoting martensite nucleation was modeled in (214). However, local stress fields arise in the presence of in-homogeneities, vacancies, solute atoms, dislocations, stacking faults, twin boundaries, grain boundaries, particles, etc.... The discussion on the type of defect promoting heterogeneous nucleation of martensite is shortly reviewed in the following.

According to (53), dislocations are accepted as the most important defect for martensite nucleation. Dislocations possess a strain / stress field around their core (215) that may be effective in promoting nucleation (216). No direct proof is reported in the literature. In disagreement with the review in (53), in (217) it is claimed on the basis of microscopy observations that dislocations do *not* act as nucleation sites, while grain boundaries do.

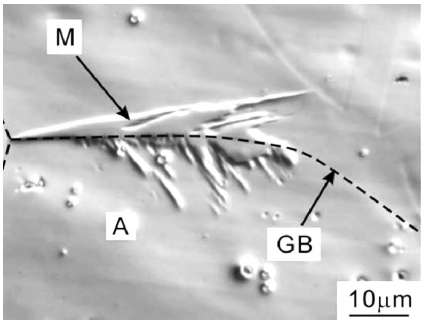

Figure 35. Nucleation of lath martensite on a austenite grain boundary in Fe-20%Ni-5%Mn alloy (119)(see also Figure 12)

The role of grain boundaries in the nucleation of lath martensite is recognized in several articles. For example, in (189) it is suggested on the bases of *in*direct investigations that lath martensite nucleates on grain boundaries. In (218), lath martensite is observed in ultra-fine grained 1.4% carbon steel, generally presenting plate morphology, and it is claimed that the presence of a large number of grain boundaries favor lath morphology over plate morphology. The work in (142) claimed that grain boundary nucleation of lath martensite is established. Evidence of nucleation of lath martensite at grain boundaries is reported in (142) (Figure 35, after (119)).

On the other hand, according to (5), nucleation occurs at austenite stacking faults, like it is the case for the f.c.c. to h.c.p. to b.c.c. / b.c.t. transformation (67)) and may be promoted at the interface boundaries in presence of a third phase ((5), after (219)), while the presence of grain boundaries is *un*favorable for martensite formation. As a further possibility, in (121) (154), martensite formation is observed in situ at twin boundaries.

Finally, free surfaces are known to favor martensite formation thermodynamically because the shape strain can be accommodated more easily close to the surface than in the bulk of the material (5) (after (220)) (221).

In conclusion, the nature of the defects which promote nucleation of martensite is *not* clarified, but several types of defects appear to apply.

Instability phenomena

Instability phenomena appear when nucleation takes place in absence of an energy barrier (73) and the martensite interface is free to propagate in the material resembling a mechanical wave. Nucleation in absence of a energy barrier is defined *barrierless nucleation* (73). Following (73), barrierless nucleation is promoted by the presence of strong defects (i.e. potent nucleation sites).

Instability phenomena in the austenite generate the martensite in *non classic* way, because nucleation cannot be treated with the classical approach. The so called *instability* of the austenite crystal lattice coincides with athermal nucleation and growth of martensite.

2.7.2. Spontaneous nucleation of martensite

The small particles experiments

In a small particles experiment, a large number of particles homogeneous in both composition and dimensions, are progressively transformed into martensite either by cooling or during isothermal holding. The martensite nucleation is investigated by magnetic separation: the particles which encountered a nucleation event become (partially) ferromagnetic and can be removed from the paramagnetic austenitic particles with a magnet. The fraction of transformed particles is evaluated measuring the mass fraction of the remaining paramagnetic particles.

Since a nucleation event in a single particle does *not* influence the stability of the surrounding particles, each nucleation event that is able to partially or fully transform a particle can be treated separately. For this reason, small particle experiments are fundamental for the investigation of spontaneous martensite nucleation. In the following, two small particles experiments are discussed in detail (211) (212).

The work in (212) was performed by progressively cooling a large number of particles with equal chemical composition (Fe-30.2wt%Ni) and size. The experiment was repeated for particles of different size (i.e. different batches). It was shown that, for an homogeneous population, the particles nucleated martensite athermally at different temperatures. Moreover, the larger the particles, the lower the degree of undercooling that is required for the transformation

of a certain fraction of particles. The result allowed to estimate the number of spontaneous nucleation events per unit volume of material versus ΔG^* (222) (Figure 36).

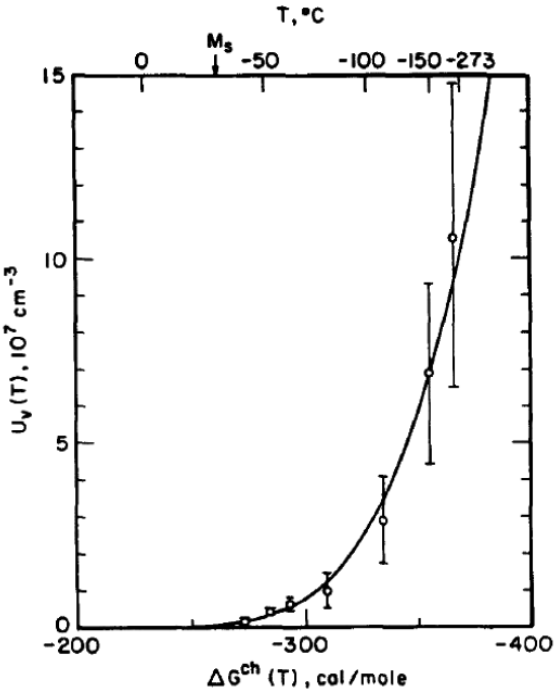

Figure 36. Number of nucleation event per cubic centimeter of virginal austenite plotted versus temperature and chemical driving force $\Delta G^{ch}(T)$ (i.e. ΔG_{chem} in the present work) for martensite formation (211).Since no external filed were applied in (212) it stands $\Delta G_{chem} = \Delta G^*$. Note that the analysis considers all the data in (212) and the obtained curve is independent on particle size.

The work in (211), was performed holding a large number of Fe-22%Ni-0.49%C and 24.2%Ni-3.6%Mn particles isothermally at different temperatures. It was observed that the number of particles which transformed during isothermal holding increases with time. It was concluded[26] that the potency of the nucleation sites is not uniquely determined, but there exists a distribution of potency among the nucleation sites in the material (i.e. heterogeneous nucleation

[26] The conclusion is actually based on the observation that a single activation energy cannot describe the process, but that a distribution of activation energies among different particles has to be assumed.

on more or less favorable positions); highly potent embryos (i.e. nucleation sites) develop martensite first (or at a lower undercooling as observed in (212)).

Interestingly, the work in (211) shows comparable results for the Fe-22%Ni-0.49%C alloy, which is an alloy characterized by athermal behavior and plate morphology when transformed in bulk material and the Fe-24.2%Ni-3.6%Mn alloy, material characterized by *purely isothermal* kinetics[27] and lath morphology. It was concluded that the isothermal and the athermal kinetics are intrinsically equivalent from the nucleation point of view. Moreover, in (211) it was claimed that there is no incubation time for the beginning of the transformation neither in case of athermal nor for isothermal kinetics.

The thermodynamic approach

In this paragraph, the theory in (197) is described. This theory consistently describes *quantitatively* the effect of magnetic fields and hydrostatic pressure on the spontaneous nucleation of martensite and reconciles both the athermal and the isothermal kinetics in a unified description.

The theory in (197) can be consistently described in terms of thermodynamics of the transformation only. However, the theory in (197) is developed on the assumption that nucleation occurs "*when some particles make a cluster and are simultaneously excited*" (i.e. dislocations do not play any role in the nucleation of martensite according to (197)), being consequently connected with a transformation mechanism.

According to (177) (197) (198), in absence of previously formed martensite, nucleation can occur athermally when the driving force for the transformation ΔG^* ($\Delta G(T)$ in (197), initially neglecting the effect of external fields) reaches a certain value ($\Delta G(M_S)$), hereby defined critical value $\Delta G_{critical}$, or can be thermally activated when the ΔG^* for the transformation is not sufficient to reach $\Delta G_{critical}$ (Figure 37).

[27] Purely isothermal behavior is defined in (53) as a behavior that results in a C-type curve in a TTT diagram.

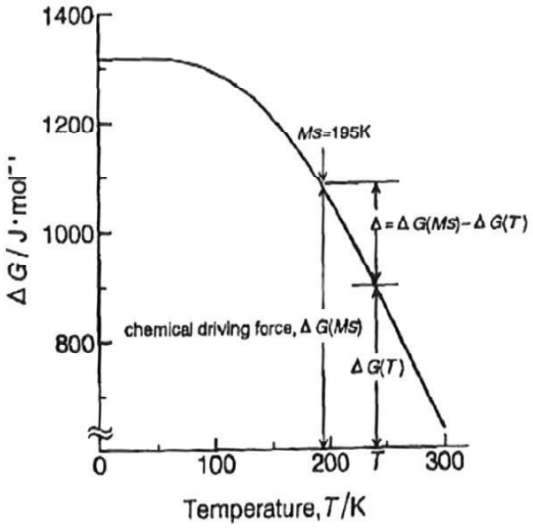

Figure 37. Schematic representation of the nucleation theory (197). According to the description in (197): at 195 K, the chemical driving force $\Delta G(T)$(curved line on the top and on the right, hereby defined ΔG^*) equals the critical one for athermal martensite formation $\Delta G(M_S)$ (upper horizontal line, hereby defined $\Delta G_{critical}$). At higher temperature, an energy gap equal to $\Delta = \Delta G(M_S) - \Delta G(T) = \Delta G_{critical} - \Delta G^*$ is observed.

When the critical driving force is not reached, i.e. when $-\Delta G_{critical} > -\Delta G^*$, martensite forms after an incubation time $t \propto exp\left(\frac{m^*\Delta}{kT}\right)$ determined by the presence of the energy barrier $\Delta = \Delta G_{critical} - \Delta G^*$, with m^* a proportional factor related to the critical dimensions of the martensite embryo (197) (T is temperature, k is Boltzmann constant).[28] According to (197), there is a direct relationship between the energy gap, Δ, and the activation energy for the transformation ΔE, which equals $\Delta = \frac{\Delta E}{m^*}$. It follows $\Delta E = -m^* \cdot (\Delta G_{critical} - \Delta G^*)$. Consequently, the activation energy for the transformation is treated in the form $\Delta E = A + B \cdot \Delta G^*$, which is in agreement with accepted experimental evidence ((53) after (122) (223) (224) (225)) (Figure 38).

[28] According to (197), and more generally to nucleation controlled descriptions, an embryo is defined critical when it leads to instantaneous growth of the martensite nucleus to its final dimension.

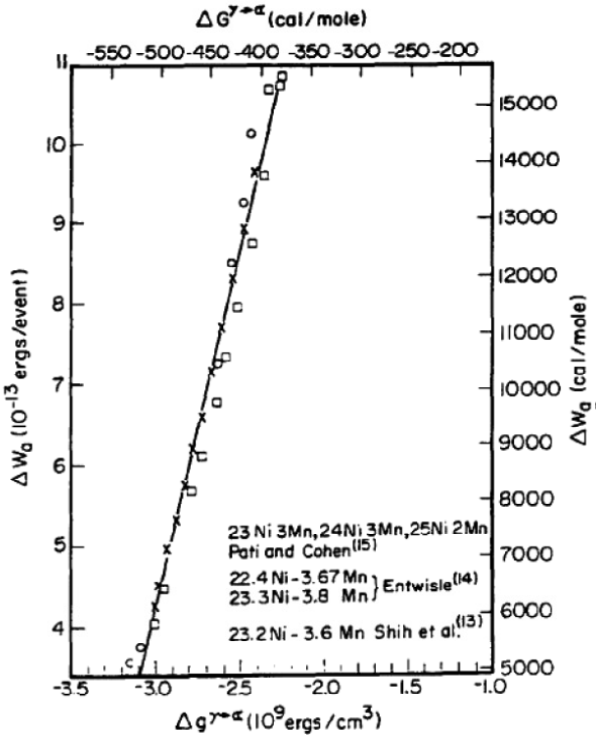

Figure 38. Activation energy for martensite formation ΔW_a (hereby defined ΔE) plotted versus driving force $\Delta G^{\gamma\rightarrow\alpha}$ (hereby defined ΔG^*). Clearly, ΔW_a is linearly related to ΔE ((224) after on prior work in(54)(226)).

Two cases for the spontaneous nucleation of martensite can be distinguished thermodynamically (197): in the first case, representing alloys typically showing athermal behavior, the critical driving force is reached during cooling (Figure 37); in the second case, the critical driving force cannot be reached on cooling (Figure 39) and spontaneous *athermal* nucleation is not possible.

Moreover, as pointed out in (197), in the second case, assuming that $\Delta G_{chem} = a + b \cdot T + c \cdot T^2$ (a good approximation in the temperature range where C-type curves are generally reported) the model predicts a minimum incubation time for nucleation at a specific temperature. This is described in (197) mentioning that the model can describe a C-type curve in a TTT diagram.

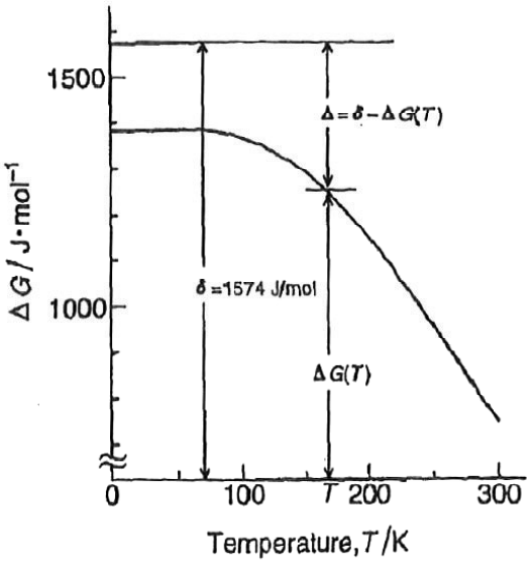

Figure 39. Schematic representation of the nucleation theory according to (197). The critical driving force for athermal nucleation is represented as δ. In the case of purely isothermal kinetics, the energy gap cannot be closed on cooling because the driving force $\Delta G(T) < \delta, \forall\, T$ and athermal nucleation is spontaneously not possible. Athermal nucleation can however be induced by the application of an external field that is effective in promoting an increment in driving force sufficient to close the gap Δ.

Finally, the model in (197) describes the effect of hydrostatic pressure and magnetic fields on the transformation kinetics. For example, in (58) (177) (198) (227) it was shown that athermal kinetics can be modified to purely isothermal kinetics under an applied hydrostatic pressure and vice versa, purely isothermal kinetics can be modified into athermal applying a magnetic field. Obviously, the driving force for the transformation is modified by the application of external fields (see paragraph 2.5.3) and this modification shifts $\Delta G(T)$ on the vertical scale in Figure 37 and Figure 39. The shift in $\Delta G(T)$ can result in the following: with respect to Figure 37, if $\Delta G(T)$ is decreased below $\Delta G(M_S)$, athermal nucleation is suppressed in alloys generally behaving athermally; on the other hand, in respect to Figure 39, if $\Delta G(T)$ exceeds $\Delta G(M_S)$ (indicated as δ in Figure 39), the application of external fields results into athermal nucleation of alloys generally presenting purely isothermal behavior (i.e. C-type curve). The reunification of athermal and isothermal martensite formation is a fundamental aspect of the work in (197) and is in agreement with (211).

To summarize, the theory in (197) describes *quantitatively* the effect of external fields on the martensitic transformation, unifies the isothermal and the athermal behavior, predicts C-type curve behavior at sub-zero Celsius temperature and describes the linear relation between ΔG^* and ΔE.

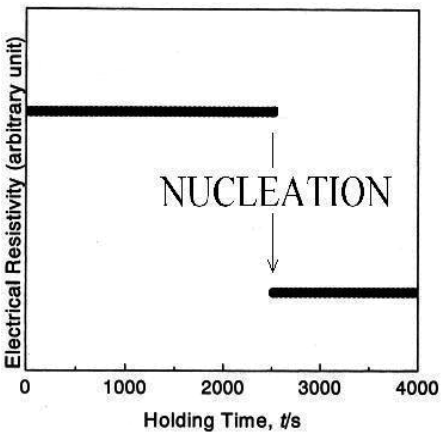

Figure 40. Electrical resistivity as a function of isothermal holding (after Fig. 29 in (177)). Data reports a sudden variation of the signal representative of the formation of a martensite thin plate that immediately reaches its final dimension.[29]

On the other hand, the theory in (197) appears *not* consistent with the absence of an incubation time for nucleation as claimed in (211). The presence of such an incubation time for nucleation was unequivocally demonstrated in (177) (198) (227), where the first martensite nucleation event is observed in a sudden change in electrical resistivity (Figure 40). Analyzing the work in (211), it is clear that the claim is based on the first data point at about $10^3\ s$. Specifically, Fig. 11 in (211) (Figure 41) reports extrapolations of the data to zero particles transformed: the linear extrapolation indicates the presence of an incubation time, which would be consistent with the theory in (197). The intercept of the linear extrapolation was interpreted in (211) in terms of a minimum activation energy for martensite nucleation Q_{MIN}. Hence, the work in (211) is consistent with the theory in (197) when $\Delta E = Q_{MIN}$.

[29] Figure 40 indicate that martensite forms instantaneously. The works in (177) (198) deal with plate martensite only. The validity of the theory for lath martensite is demonstrated in (57) (227) (228).

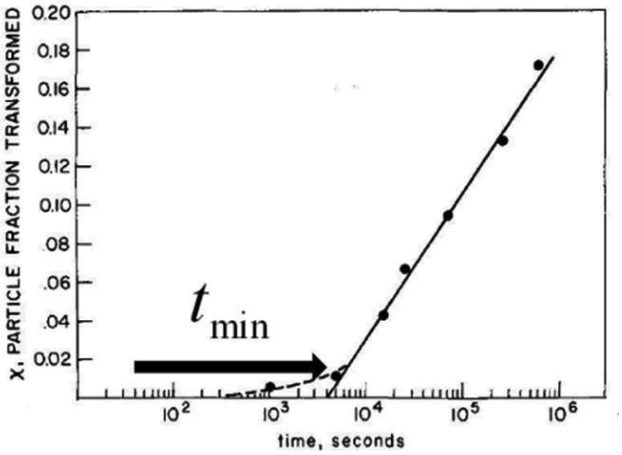

Figure 41. Fraction of ferromagnetic particles (particles that experienced at least one nucleation event) versus time for different temperatures of isothermal holding (after (211)) The label t_{min} in the graph refers to the incubation time for martensite formation.

The work in (211) also reports Q_{MIN} versus isothermal holding temperature (Figure 42). It was shown that the activation energy decreases with a decrease in temperature and goes towards zero for the alloy showing athermal behavior, i.e. Fe-22%Ni-0.49%C. This trend can be compared qualitatively with the description in (197).

In respect to (197), assuming $\Delta E = Q_{MIN}$, it would result $\Delta E = Q_{MIN} = m^*\Delta$. The value for Δ versus temperature that can qualitatively be obtained from Figure 37 and Figure 39: it is readily observed that Δ decreases with a decrease in temperature and may, or may not get to zero (Figure 37 and Figure 39, respectively). Clearly, this trend is compatible with the description in Figure 42, where the curves for Fe-22.3%Ni-0.49%C and Fe-24.2%Ni-3.6%Mn are representative of the cases in Figure 37 and Figure 39, respectively. Extrapolation of the line though the data for Fe-22%Ni-0.49%C yields athermal transformation below about 130 K.

In conclusion, apart from the first data point, no inconsistency exists between (197) and (211). However, in addition to the discrepancy regarding the incubation time, the model in (197) is incompatible with the concept that the nucleation of martensite is rate controlled by the movement of dislocation (53). An indisputable evidence of the role of dislocation in the kinetics of martensite formation is reported in (195). To accept the theory in (197), the work in (195) has to be similarly reconciled.

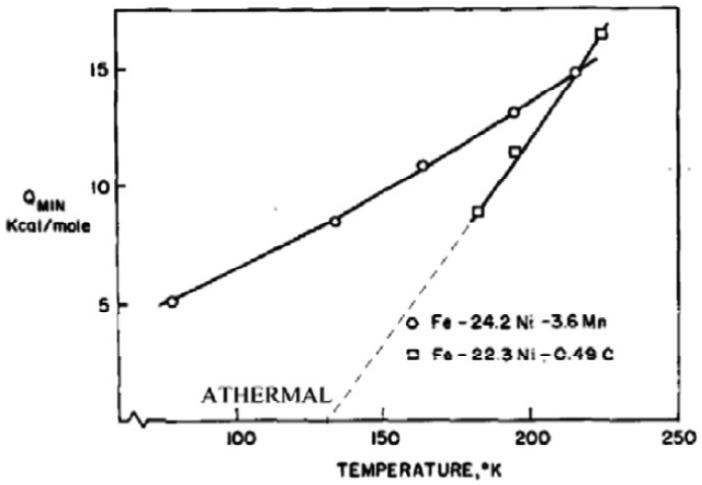

Figure 42. Minimum activation energy Q_{min} versus temperature of isothermal holding for a Fe-24.2%Ni-3.6%Mn alloy forming lath martensite and Fe-22%Ni-0.49%C material forming martensite with thin plate morphology after (211).

Motion of dislocations in austenite as rate-controlling mechanism

In (195), a series of Fe-Ni-Mn based alloys with Nickel content in the range 21.9% to 25.9% and Manganese content in the range 3.2% to 4.2%, were cooled to 77 K and thereafter subjected to uniaxial stress at 77 K. Martensite formation at 77 K was followed in situ by measuring the change in electrical resistance and magnetization of the samples.[30]

According to (195), the nucleation rate of isothermal martensite is controlled by thermally activated motion of dislocations in austenite which accommodate the shape strain of nucleating martensite. The following two experimental observations are pointed out to claim that the motion of dislocation in austenite controls time dependent martensite nucleation.

Firstly, a sudden increase of the transformation rate was observed when the stress exceeded the yield point (Figure 43). This indicates that martensite formation is favored by the presence of mobile dislocations in the austenite.

Secondly, bulk material can remain austenite on cooling to 77 K, but transforms into martensite, while thin foils transforms into martensite. This is interpreted as an indication that

[30] See paragraph 3.3.2.

constrained conditions are a prerequisite for time dependent transformation (note that in *un*constrained condition, i.e. for example in the case of surface martensite, the shape strain is easily relaxed, see paragraph 2.2.2).

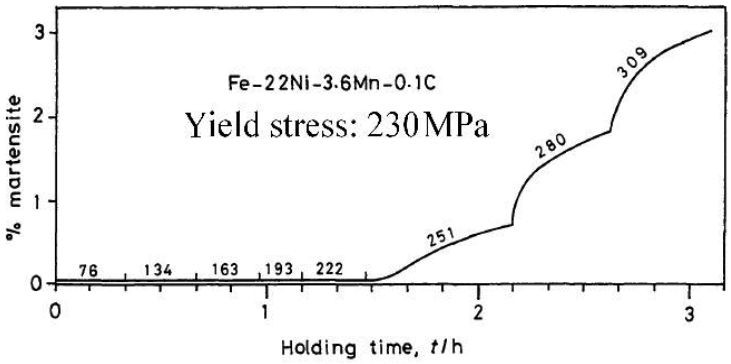

Figure 43. Martensite formation versus time. The numbers above in the graphs indicates the level of applied uniaxial stress (after (195)). It is reported that the effect of applied stress has a relevant effect on the martensite formation rate only when it exceeds the yield strength of austenite.

The first point is considered the most relevant in (195). This point was argued in (53), and it was suggested that the generation of new nuclei in the austenite (i.e. strain-induced nucleation, see below) due to the applied strain cannot be excluded. However, this point was addressed and excluded in (195). [31]

Apparently, the only limitation of the work in (195) is that it assumed *a priori* nucleation controlled kinetics, rather than considering the possibility of time dependent growth to be favored by the introduction of mobile dislocation in austenite after exceeding the yield strength.

Time dependent growth of martensite during isothermal holding at sub-zero Celsius temperature was reported for Fe-Ni-Mn alloys (Figure 44) (125) (127) (154) (228) (Figure 45). In particular, the work in (154) presented a transformation process which is comparable to the one reported by prior in situ investigation (229) performed on the same alloy used in (195) (compare Figure 45 with Figure 46).

[31] The reader is referred to (195) for further details on the reason why strain induced nucleation is not responsible for the observed behavior.

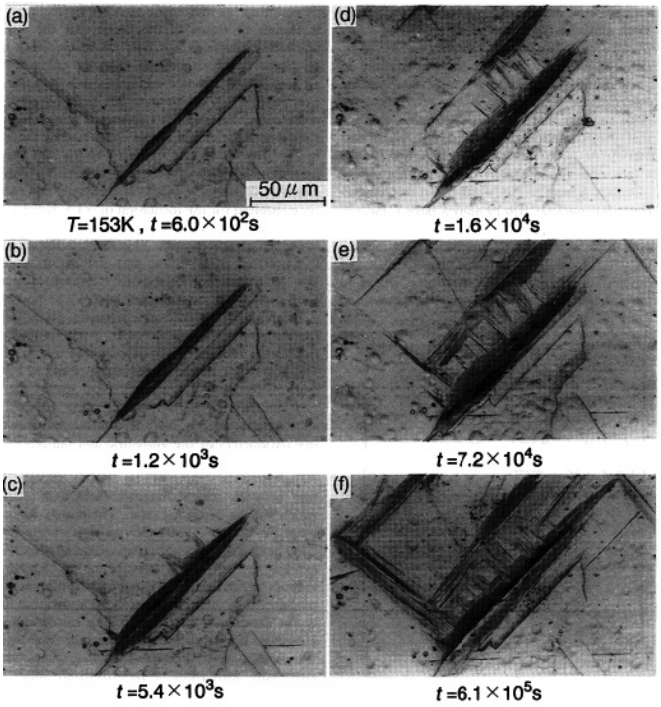

Figure 44. Optical micrographs showing isothermal martensite formation at 153 K in Fe-24.9%Ni-3.9%Mn alloy. The isothermal transformation was interrupted multiple times to record the progress of the transformation at room temperature. The isothermal holding time indicated below each micrograph indicates the cumulated holding time at 153 K (228).

Following the description in paragraph 2.4.4, where it was suggested that growth of martensite may be time dependent and rate controlled by the accommodation of the shape strain in the austenite, the above reported observations suggest a new interpretation of the work in (195). A few reports in the literature support the interpretation that a higher dislocation mobility in austenite facilitates growth of martensite, possibly leading to an enhanced transformation rate. For example, in (230) (231) (232), the mobility of dislocation in virginal austenite was reduced applying a pre-strain before martensite formation. It was observed that the aspect ratio for plate martensite is reduced when the pre-strain is applied (230), while a reduced mobility of dislocations in the austenite is reflected in a morphology change from lenticular (that requires plastic accommodation in the austenite) to thin plate martensite (associated with elastic accommodation) (231) (232).

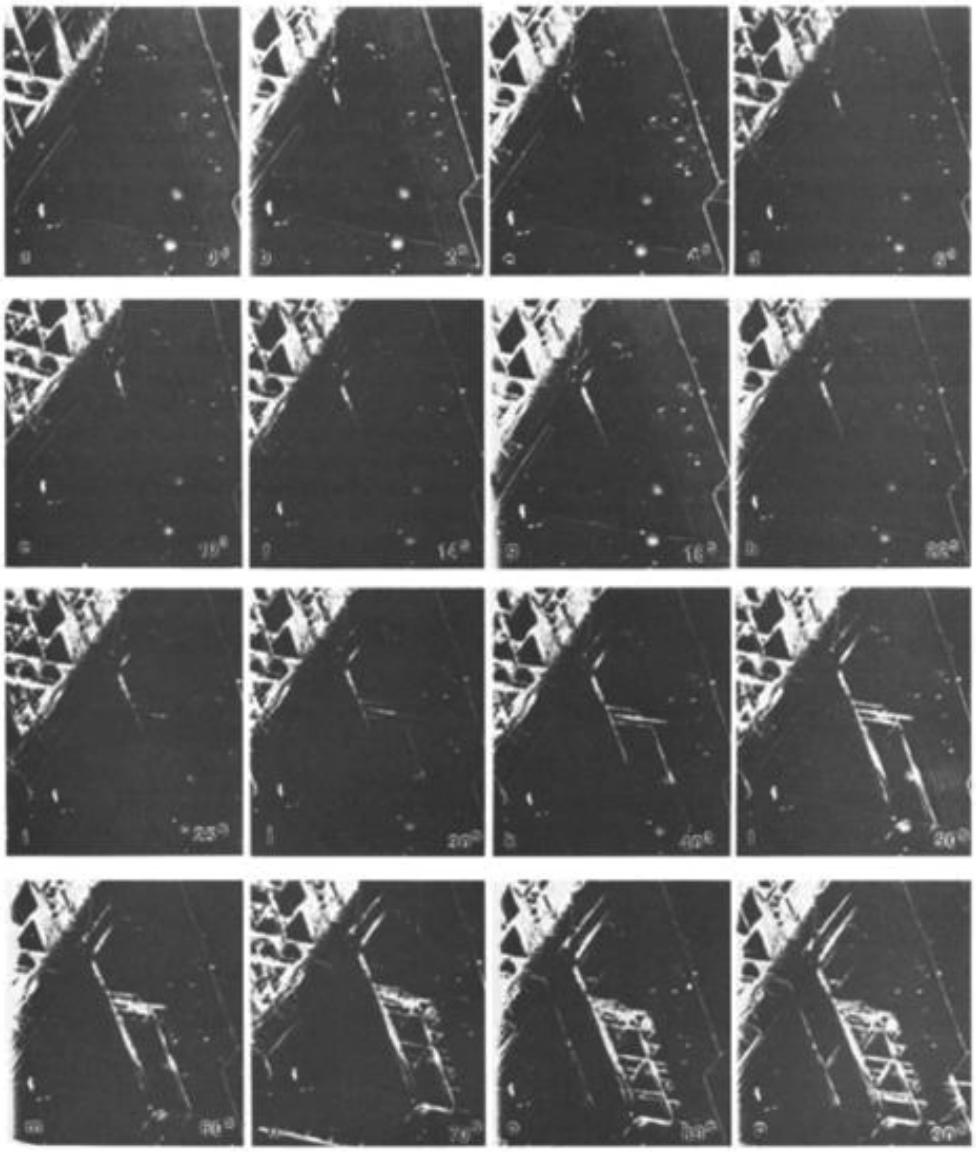

Figure 45. Light optical micrographs of in situ investigation of time dependent martensite formation during isothermal holding of Fe-21%Ni-4%Mn alloy at 193 K (154). Martensite formation started from a single nucleation site and propagates into the material. Time dependent nucleation of martensite is promoted by progressive growth of laths. According to (154), nucleation is promoted when the lath reaches a certain dimension and always takes place in front of the growing side of the lath.

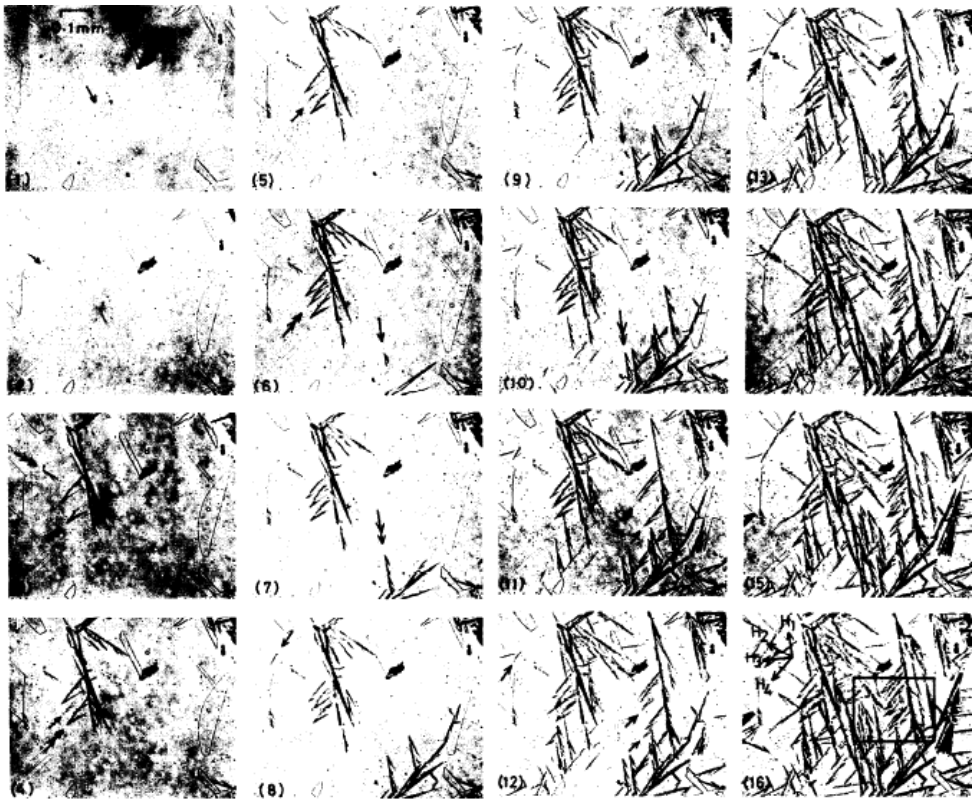

Figure 46. Optical micrographs of in situ observation of time dependent martensite formation in Fe-23%Ni-3.9%Mn alloy transformed holding the material in the temperature range 143 K to 163 K (229). The numbers on the micrograph refers to different holding time rather than temperatures. Martensite formation started from a single nucleation site and propagates into the material. In the interpretation given in the present text after (154), progressive thickening of the martensite units triggers the nucleation of martensite in the surrounding areas.

In conclusion, the observation in (195) that the generation of dislocation enhances martensite formation may be indicative of the mechanism responsible for thermally activated growth through dislocation movement rather than enhanced nucleation.

The observation of athermal transformation in thin foils versus time dependent transformation in bulk material is addressed in the following.

As described in paragraph 2.2.2, the transformation strain is relaxed in the presence of a free surface. The relaxation implies that the presence of a free surface affects the thermodynamic

equilibrium reducing the contribution of the strain energy term ΔG_ε (see paragraph 2.5.2). Consequently, the driving force for the transformation ΔG^* is increased. This is clearly demonstrated in (221) where martensite formation on the close surface region was observed in situ up to 120 K higher temperature than in the bulk. Referring to the theory in (197), evidently when the Fe-Ni-Mn alloys used in (195) are produced in form of thin films, the condition $-\Delta G^* < -\Delta G_{critical}$ is reversed to $-\Delta G^* \geq -\Delta G_{critical}$ and athermal nucleation occurs on cooling. The description is equally valid for the first data point in the small particle isothermal experiments, that remained unexplained in the previous paragraph. It is here interpreted as indicative of surface martensite formation in a few particles in which potent embryos are located particularly close to the particle surface.

In conclusion, it appears that the theory in (197) is fully consistent with available experimental data. Prior work where the effect of different parameters on the nucleation of martensite is interpreted presuming nucleation-controlled transformation should be carefully reconsidered, because thermally activated growth may have been overlooked.

2.7.3. General description of autocatalytic nucleation

After the first nucleation event has occurred, martensite formation experiences a strong autocatalytic behavior which consists in the stimulation of additional nucleation events and arises due to elastic and plastic strains set up in the surrounding austenite by the forming martensite (53) (186). Autocatalytic nucleation is problematic for the investigation of spontaneous nucleation of martensite in bulk materials since spontaneous events cannot be distinguished from autocatalytic events. Moreover, the number of spontaneous nucleation events is far too small to be compatible to macroscopic transformation in bulk materials (i.e. in the order of 10^5 (222), 10^7 (233) per cm^3. It is concluded that autocatalytic nucleation dominates over spontaneous nucleation and spontaneous nucleation has to be investigated in small particles experiments.

Autocatalytic nucleation can occur in a single grain of austenite or over neighboring grains (234) (Figure 47). A distribution over neighboring grains results in a large contribution to the transformation and is a necessary condition for a macroscopically observable transformation. Such a distribution implies that the strains are transferred to adjacent austenite grains, also implying the mechanical interaction between neighboring grains.

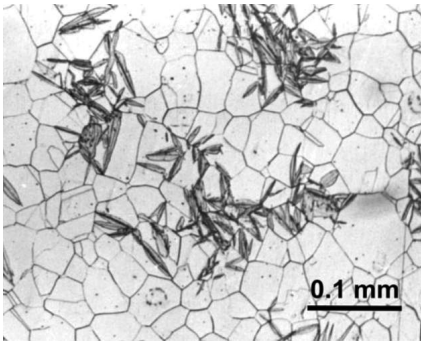

Figure 47. Optical micrographs of a 31%Ni-0.01%C steel partially transformed to martensite. Each nucleation event has catalyzed the formation of martensite in a portion of material extending across different grains (188).

It has been proposed that the martensitic transformation can induce the activation of new nuclei according to three mechanisms (232): interfacial autocatalysis; strain induced nucleation; stress assisted nucleation. All three mechanisms are connected to the number of martensite units and their distribution and orientation in the austenite. Consistently with this concept, autocatalysis has been described introducing a parameter called the *extent of plate association*, EPA (235). More commonly, autocatalysis is modeled introducing an autocatalytic term, either proportional to the fraction transformed (236) or to the number of nucleation events (187). This proportionality factor is the so called *autocatalytic factor* (53). The autocatalytic factor p and the extent of plate dissociation *EPA* are directly related: *EPA* increases logarithmically with p (235). The three mechanisms for autocatalytic nucleation of martensite are described separately in the following.

Interfacial autocatalysis

Interfacial autocatalysis deals with the nucleation of new martensite units by dislocation-dissociation process from existing martensitic interfacial structure (232) and is only relevant in respect to the nucleation model presented in (194). Generally, only strain-induced nucleation and stress-assisted nucleation are considered nowadays (53) (237) (238).

Strain-induced nucleation

According to (237), the nucleation of martensite in steel is driven by plastic deformation. The as formed martensite is termed *strain induced martensite*. Strain induced nucleation occurs

when plastic deformation creates and activates new embryos for the transformation. When martensite formation generates plastic strains in the surrounding austenite the process becomes autocatalytic. Consistently, the kinetics of martensite formation can be modified applying a pre-strain to virginal austenite. The effect is positive for small strain and negative for higher strain. This is generally described as a dependence of the autocatalytic parameter p on the pre-strain. The non monotonic effect of the pre-strain on p is discussed as follows: on the one hand, plastic deformation in austenite generates new embryos for martensite formation; on the other hand, the generation of defects in austenite, like entangled dislocations, enhance the flow stress (work hardening), and consequently $\Delta G_{critical}$ increases. This is a consequence of the proportionality between strain energy term associated with martensite formation (see paragraph 2.5.2) and the flow stress.[32] For the same reason, a pre-strain reduces the ability of a martensite plate to growth in the thickening direction and may induce morphology changes (see paragraph 2.7.2).

Finally, when an external strain is applied during martensite formation, the strain rate influences the yield strength of austenite (240) and affects martensite formation. The effect of the strain rate on martensite formation was investigated in (241) only, where it was observed that an increase in strain rate initially favors martensite formation while a further increase in the strain rate results in suppressing the transformation.

Stress-assisted nucleation

Stress-assisted nucleation is the result of the interaction of a stress field with the transformation strain (242). Following (176), the additional energy term added to ΔG^* is (elastic) mechanical work. The origin of the stress field can be external or internal. The effect of externally applied deviatoric stress components, σ_{ij}, on the autocatalytic factor, p, was determined to follow a linear relationship in the form of $p = a + b \cdot \sigma_{ij}$,[33] with a and b material parameters (235) (243). On the other hand, martensite formation itself generates deviatoric stress components in austenite. The stress fields that are generated by martensite formation are able to interact with the stress field of pre-existing embryos, and assists their nucleation process by

[32] Specifically, there is a linear relationship between the austenite yield resistance and M_S (239).
[33] Note that this relationship may indicate a direct correspondence between p and ΔG^* (see paragraph 2.5.3)

increasing the ΔG^* for the transformation. When this process occurs, martensite formation becomes autocatalytic. The stress distribution varies spatially all around a martensite unit (244) and is a function of the aspect ratio of martensite (i.e. $\frac{t}{l}$): the stress value increases with the plate thickness. [34]

The phenomenon differs fundamentally from strain-induced nucleation: in stress-assisted martensite formation, nucleation occurs "*on the same sites which trigger the spontaneous transformation on cooling, but assisted by the thermodynamic effect of applied stress, while strain induced* (martensite formation) *involves the production of new nucleation sites by plastic deformation*" (245).

Stress-assisted nucleation is generally described in association with the observation of bursts in $\{2\ 5\ 9\}\gamma$ lenticular martensite (68) (115). In the following, burst behavior is illustrated and autocatalysis discussed in relation to the different ferrous systems.

2.7.4. Autocatalysis in plate martensite

Bursts originate as a consequence of a cascade of nucleation events triggered by the stress field surrounding a martensite plate in a chain like reaction (68) (180) (246). A cascade of nucleation events results in a zig-zag microstructure to comply with the stress field (Figure 18). Under this description, bursts are a strong form of autocatalytic stress-assisted nucleation.

In (247) (also referring to (248)), it was shown that bursts in systems with lenticular morphology lead to *ir*reproducible transformation curves (Figure 48), as an indication of a strong influence of local stress interactions on the macroscopic process.

Burst behavior is described slightly differently in (115). Following (115), bursts originate from the reduction of the total strain energy for martensite formation obtained as a consequence of *simultaneous* formation of coupled, not parallel martensite variants.[35] This description sets in the reduction of the strain energy in the system and not in the stress field the point characterizing

[34] This point indicates that time dependent plate thickening (i.e. growth) can lead to time dependent nucleation.
[35] With coupled it is hereby intended variants with a relative orientation that minimizes the strain energy introduced in the system (i.e. variants which partially self-accommodate).

stress-assisted autocatalysis. Both descriptions for burst phenomenon, are compatible with experimental observations related to plate martensite. The first is straightforward in describing zig-zag morphology observed in $\{2\ 5\ 9\}\gamma$ systems, while the second applies better to Chevron plates with a $\{2\ 2\ 5\}\gamma$ habit plane (see Figure 18).

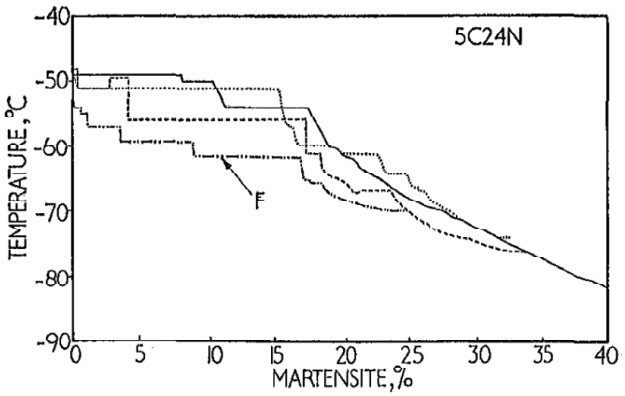

Figure 48. A series of martensite transformation curves in Fe-24%Ni-0.5%C steels subjected to continuous cooling at sub-zero Celsius temperature. In spite of following a unique curve after about 30% transformation, the transformation behavior is not reproducible among different samples at the earlier stages of the transformation (F stays for a fine grained sample).The multi-step behavior observed is indicative of burst (247).[36]

Finally, burst behavior can be reduced or suppressed by forcing the transformation into specific spatial directions through an applied stress field (115) or a pre-strain of the austenite (249) (246). In particular, it was shown that bursts are suppressed applying a uniaxial stress that results in conditions where the formation of coupled variants is no longer energetically favored (115).

2.7.5. Autocatalysis in lath martensite

According to (250) *(*after (251)), each martensite packet (see paragraph 2.4.4) either grows by formation of nonadjacent but parallel variants (grouped in blocks) or is formed by nucleation and growth of parallel laths adjacent to one another (similarly grouped in blocks).

[36] When a burst occurs, it is visualized in a fraction transformed versus temperature or time plot as instantaneous formation of a large amount of martensite (i.e. a horizontal straight line in Figure 48).

According to (137) (252), these adjacent laths would nucleate independently. Alternatively it was proposed that laths are generated autocatalytically (140) (142).

In (142), it is explained that the formation of lath martensite can trigger new nucleation events (i.e. autocatalytic nucleation) according to two mechanisms (Figure 49): (a) the transformation strain of a martensite lath may stimulate the generation of a new unit of the same variant in front of the growing block (after (124)); (b) the nucleation of a new block parallel to the previous one, is promoted autocatalytically by the reduction of the strain energy in the system (253).[37]

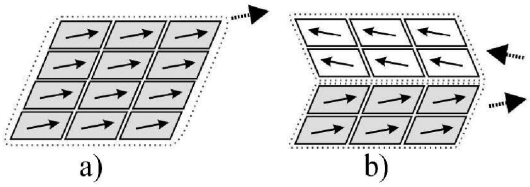

Figure 49. Autocatalytic nucleation of laths: a) the strain / stress field associated with the transformation generate a new nucleus (lath) in front of the transformation front; b) self-accommodation of the shape strain favor the formation of a new block (142).

If the first mechanism applies, autocatalysis is active on the lath scale and is of the strain-induced type. The reason is twofold: new nucleation sites are generated during the process; parallel laths of the same variant are *not* energetically favored, consequently ruling out stress-assisted nucleation. On the other hand, the second mechanism is active on the block scale and is (mainly, because new nuclei are likely to be generated) of stress-assisted type (i.e. it leads to a reduction of the strain energy). The mechanism which was observed to be active in different systems is discussed in the following.

It was claimed in (142) (after (124)), that blocks are formed from repetitive autocatalytic nucleation of laths of the same variant (mechanism (a)). This interpretation is consistent with (140), where it was shown that martensite formation occurs discontinuously by a series of bursts (Figure 50) and it is concluded that each burst results from autocatalytic formation of laths

[37] The laths of different variants are presented grouped in a parallel plate like structure, to comply with the description in (253), but the same concept is similarly valid for a non parallel groups (generation of a new packet instead of a new block).

within single blocks, as an indication that autocatalysis is active on the lath scale. Note that the mechanism resulting in bursts for systems forming lath martensite is not compatible with the descriptions presented in the previous section, where bursts are treated in terms of stress-assisted nucleation.

According to (142), lath martensite formation occurs as follows. First, the most favorite variant of martensite nucleates at a grain boundary. Continuous autocatalytic nucleation of parallel laths forms a block that grows as long as there is enough driving force to compensate for the strain energy associated with its formation. Here after, growth stops and the continuation of the transformation requires either the reduction of the strain energy though the formation of a new martensite variant (i.e. the nucleation of a new block) or an increase of the driving force (i.e. for example obtainable with increased undercooling). When a new block nucleates or the driving force is increased, the transformation continues. This mechanism is shared with bainitic ferrite (142).

This transformation mechanism would lead to reproducible transformation curves, which deviates from the kinetics of plate / lenticular martensite formation (see Figure 48). Moreover, this transformation mechanism is *not* necessarily *in*dependent of time. In (254) (255) it was shown that both the number of parallel laths and the number of non parallel variants can increase during isothermal holding. This behavior may result either from spontaneous time dependent nucleation of new laths or from time dependent growth of existing laths that catalyze the formation of new laths in the surrounding austenite.

Time-depenent nucleation promoted by time dependent growth was observed in situ in (154) (Figure 45). Specifically, in (154), the autocatalytis is of stress-assisted type, since the generation of new laths at sixty degrees misorientation drives to a reduction of the strain energy in the system (139).[38] Time-dependent stress-assisted autocatalysis does *not* result in bursts because progressive growth of the martensite structure requires time (154).

[38] As discussed previously, a necessary condition for stress-assisted nucleation is a reduction of the strain energy in the system because of mutual accommodation.

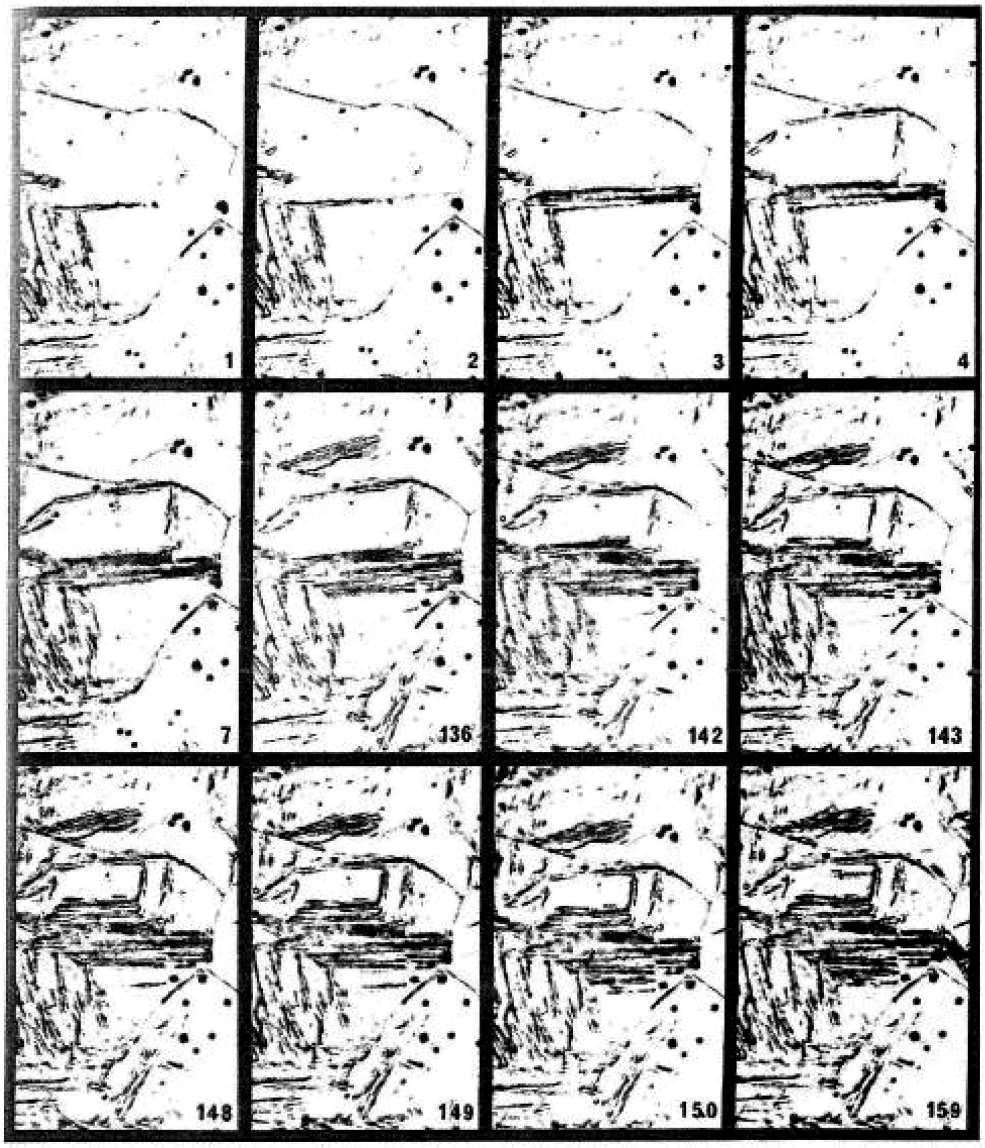

Figure 50. Light optical micrographs of in situ investigation of martensite formation during continuous cooling of Fe-24.5%Ni alloy (140). The numbers in the frames refer to their position in the acquired sequence; acquisition time was 48 frames per second. The micrographs show that the single blocks of martensite form one by one and progressively fill-in the austenite grains.

To summarize, the works in (124) (140) (142) indicate that bursts in lath martensite are controlled at the lath level and are of strain-induced type. On the other hand, the formation of new blocks and packets is stress-assisted and may require a relevant amount of time when autocatalytic martensite nucleation is promoted by time dependent growth in front of the growing interface.

As a final remark on the characteristics of martensite formation in different systems, from the point of view of autocatalysis, plates correspond to blocks (stress assisted formation), while laths correspond to palettes (see Figure 25) (strain induced formation). Hence, a new general classification of martensite as either plate versus blocks or lath versus palettes is suggested.

2.8. Martensite growth and interfacial mobility

This section presents growth of martensite and the classification of different growth regimes. The purpose of this section is to summarize and clarify concepts mainly presented fragmented in the previous paragraphs.

2.8.1. Dimension and equilibrium condition for a martensite unit

In order for the transformation to proceed, martensite nuclei needs to grow. The growth of martensite proceeds until the martensite units have reached their final dimension, which is determined by the thermodynamics of the transformation. According to the description in paragraph 2.5, growth is allowed as long as $\Delta G_{chem} = -\Delta G_{\varepsilon}\left(\frac{t}{l}\right) - \Delta G_{\varepsilon_{irr.}} - \Delta H_{\gamma \to \alpha'}$, where the sum $-\Delta G_{\varepsilon}\left(\frac{t}{l}\right) - \Delta G_{\varepsilon_{irr.}}$ account for the frictional work associated with the movement of the interface, plus the mechanical work necessary to accommodate the shape strain (231) (256).

Consistently, in (105) (111), an increase in driving force was shown to lead to plate thickening (Figure 51) (i.e. a larger driving force allows a larger aspect ratio of the martensite units). For lath martensite this concept applies to blocks, not to a single lath. Consequently, plates should be assimilated to blocks also with respect to the equilibrium dimension of a single martensite unit.

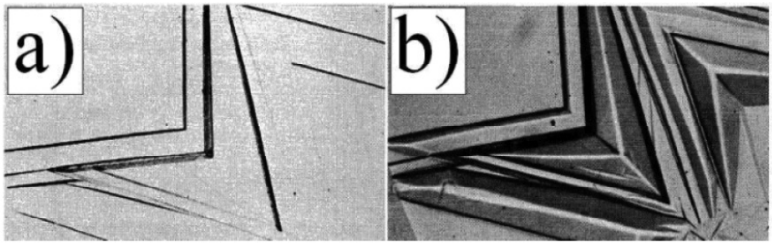

Figure 51. Optical micrographs taken after cooling a Fe-30%Ni-0.45%C alloy to a) 135 K and b) 116 K, respectively. The material starts to form martensite at 150 K (105). An increment in the driving force for martensite formation promotes thickening of the martensite plates that is reported after reheating to room temperature. Note that, contrary to thermoelastic transformations, for non thermoelastic cases the transformation process is not reversed on reheating.

Independent of the prior discussion, for a nucleus to be able to thicken, the martensite-austenite interface must be able to move. The interface may be able to move conservatively, *i.e.* be glissile, or may require thermal activation, i.e. be sessile. The mobility of the interface distinguishes the thermoelastic cases from the non thermoelastic transformation. The mechanism controlling the mobility of the interface determines its velocity and its characteristics. According to (5), the rate of martensite growth is classified into three velocity regimes that are described in the following.

2.8.2. Rate of martensite growth

Umklapp transformation velocity

The velocity in the fast regime, named *Umklapp* transformation, is in the same order as mechanical twinning and is associated with athermal martensitic transformation, i.e. it requires a glissile interface. According to the review in (80), *Umklapp* refers to plate morphology, which is characterized by the presence of twinned substructure. The presence of twins may be connected with the glissile nature of the interface. The mobility of a glissile interface in a non perfect crystal is determined by the ability of the interfacial dislocations to overcome the crystal defects that are encountered along the path (215) and the interface / obstacle interaction would be much weaker if the martensite is internally twinned (256). Hence the substructure and the morphology of plate martensite may be determined by the relatively fast kinetics of internal twinning as compared to the generation of dislocations. According to (191), in this regime, the velocity of the

interface ranges from 0.25 to 0.65 times the speed of sound in the material (it is in the order of 10^3 m/s (see (5))).

Schiebung transformation velocity

The velocity in the intermediate regime, named *Schiebung* transformation, is in the same order as dislocation velocities in slip deformation and is proportional to the driving force for the transformation. In this regime, growth in the principal direction of the martensite units is in the order of 10^{-6} m/s to 10^{-1} m/s, while progressive thickening may proceed more sluggishly. According to the review in (80), *Schiebung* refers to lath morphology. The movement of the interface in the intermediate regime is thermally activated.

The mechanism rate-controlling the interface velocity in the intermediate regime is *not* clarified yet. A first interpretation may deal with the movement of interfacial dislocation as the rate-controlling mechanism (194). This interpretation appears relevant in presence of sessile interfaces (118). However, in (118), it is suggested that the sessile interface may be able to move conservatively, inheriting sessile jogs in the microstructure or with the generation of vacancies at jogs. The work in (257) established that the interpretation in (194) is *not* correct. In (257), the structure of the interface for two alloys showing typical athermal and thermally activated behavior, was compared at the atomic level. It was concluded that the interfacial structure *per se* is *not* the controlling factor. According to (257), the rate-controlling mechanism is the movement of dislocations in austenite that accommodate the shape strain, in alignment with prior work in (128) (195) (217). Finally, the rate-controlling mechanism for growth was also suggested to be stress relaxation, either by the rearrangement of dislocations in martensite or in austenite (124) (166) (167), or driven by the diffusion of vacancies (60).

Thermoelastic transformation velocity

The slow velocity regime is associated with thermoelastic growth, where thickening of the martensite unit is rate-determined by the driving force for the transformation only. In the slow regime, the temperature in front of the martensite to austenite interface determines the condition for growth. A general temperature decrease is promoted by continuous cooling of the sample and is counteracted locally by the heat released during the transformation. The temperature balance determines the possibility for growth. Consequently, in the slow regime, the

velocity of the interface is rate-controlled either by the ability of the material to remove the heat released during martensite formation in front of the growing front or by the cooling rate. The slow regime appears to be a special case of the *Umklapp* and the *Schiebung* transformations.

Solute drag transformation velocity

A fourth velocity regime is not listed in (5) and is represented by the solute drag phenomenon. This regime is associated with extremely slow martensite growth (258). The phenomenon is explained by an elastic interaction between the interface and the crystal distorted by the presence of carbon atoms, which results in long range diffusion of carbon away from the moving interface as rate controlling mechanism (258).

2.8.3. Final remarks on the growth of martensite

On the basis of the discussion in section 2.3, in the present work the classification of transformation as *Umklapp* and *Schiebung* (5) is interpreted in connection with the observation of twin versus dislocation in the martensites substructure. On the other hand, the work in (80) refers to the plate versus lath morphology referring to *Umklapp* and *Schiebung* transformations. The different interpretations of (5) are relevant for $\{2\ 5\ 9\}\gamma$ and $\{2\ 2\ 5\}\gamma$ martensites, which possess plate morphology but are characterized by the presence of dislocations in part of the substructure.

Nowadays, time dependent growth of plate martensite with $\{2\ 2\ 5\}\gamma$ approximate habit plane is recognized after the works in (125) (128) (127). Growth of $\{2\ 5\ 9\}\gamma$ plate martensite with lenticular shape is instead considered extremely rapid (120). A reconciliation is attempted in paragraph 2.4.5 on the basis of (112) (121). A definitive proof of the interpretation given appears missing, but time dependent growth of lenticular martensite is strongly suggested.

Finally, with respect to lath martensite, independently on the interpretation given, a few descriptions (140) (192) are in apparent contradiction with the work in (5). Following (5), growth of lath martensite is always time dependent. On the other hand, the work in (140) claims athermal martensite formation while, the work in (192) supports nucleation controlled kinetics (i.e. time *in*dependent growth). Analyzing the work in (140) (192), the velocity of the interface

was estimated in the order of 10^{-4} m/s and 10^{-3} m/s, respectively. These values are compatible with *Schiebung* transformation velocities (10^{-6} m/s to 10^{-1} m/s, see above).

In conclusion, the case of lath martensite is fully clarified and growth must be considered time dependent for systems characterized by lath morphology. This implies that nucleation-controlled descriptions are generally inapt to describe the kinetics of lath martensite formation.

3. Transformation curves and kinetics analysis

The present chapter deals with the evolution of transformations described versus time and temperature. This description represents a *kinetics analysis* of transformations. Kinetic analyses have the purpose to determine the transformation mechanisms and their dependence of time and temperature, in order to predict the evolution of the transformation process in different conditions and to tailor the properties of heat treated parts.

Consistent with chapter 2, the terminology *time dependent* kinetics is used to refer to a time scale of engineering relevance for heat treatment practice, implying that thermally activated processes, which actually are time dependent, may be effectively described as *in*dependent of time.

3.1. Solid state transformations and kinetics analysis

3.1.1. Principles and classification

In materials science, the term *transformation* refers to *phase transitions* (259), where a phase indicates a region of matter homogeneous in terms of state aggregation, internal structure and composition (260). Transformations are distinguished in *thermally activated* transformations and *athermal* transformations.

Thermally activated transformations are characterized by the presence of an activation energy, i.e. an energy barrier, ΔE, which is determined by the mechanism rate-controlling the transformation and governs the temperature dependence of the transformation process. The temperature dependence of thermally activated processes is generally described with an *Arrhenius-type* equation, $k = k_0 \cdot exp\left(-\frac{\Delta E}{RT}\right)$, with k being the rate of the process, k_0 being a transformation dependent constant defined *pre-exponential factor* and R the gas constant (259).

Solid state transformations are phase transitions in condensed matter. According to (260), solid state transformations are classified as *diffusive* transformations, also defined *civilian* or *reconstructive* (259), and *diffusionless* transformations, also defined *military* or *displacive* (259).

Diffusive transformation are thermally activated and can be rate-controlled by the redistribution of atoms along the material (i.e. diffusion) or across the interface between product and parent phases. In the first case the transformation is defined *diffusion-controlled*, while in the second case is defined *interface-controlled*. On the other hand, *diffusionless transformation* are generally described as athermal.

In order to investigate solid-state transformations, the evolution of the transformation has to be recorded versus temperature and time (261). This implies monitoring a physical property, p_i, connected with the different states, i (i.e. austenite and martensite in the case of martensitic transformations). Examples of properties that are monitored to investigate transformations are: hardness, specific length, electrical resistivity, enthalpy (i.e. heat released / absorbed), magnetization,….

Different investigation techniques allow to monitor the different physical properties. The change in a specific physical property can be more or less pronounced depending on the singular solid state transformation. Consequently, decision about the investigation technique to be used requires the assessment of its *sensitivity*[39] in relation to the specific phenomenon of interest. On the other hand, various complementary techniques can be combined resulting in a more detailed picture of the transformation.

In order to perform a quantitative analysis, the physical properties have to be converted into the fraction transformed. When the fraction transformed is plotted versus temperature or time, a transformation curve is obtained and it can be analyzed in order to extract information about the transformation mechanisms (see below).

[39] In the present work, with *sensitivity* it is indicated the ability of a technique to distinguish among the two physical states, consequently (i) the ratio between the value of the physical property in the two state and (ii) the selectivity as compared to concurrent processes.

Two types of kinetics analysis are of particular interest: *isothermal* analysis and *isochronal* analysis. Isothermal and isochronal kinetics analyses are described in the following according to (261) (after (259)(262)(263)).

3.1.2. Isothermal kinetics

In *isothermal* analysis the sample is heated or cooled to the temperature of investigation. Thereafter, the physical property of interest is recorded at a constant temperature, T, as a function of time, t (Figure 52). The molar fraction of atoms that constitute the transformed part of the material, f_1, is calculated from the recorded physical property, p_i, generally assuming a linear relationship of the type:

$$f_1 = \frac{p(t) - p_0}{p_0 - p_1} \qquad [2]$$

with $p(t)$ recorded value of the physical property of interest and p_0, p_1 the values of the physical property in the initial and final state, 0 and 1, respectively. The linear relationship is based on the assumption that p_0 and p_1 are intrinsic properties of the material, i.e. are properties which depend on the moles of atoms only.

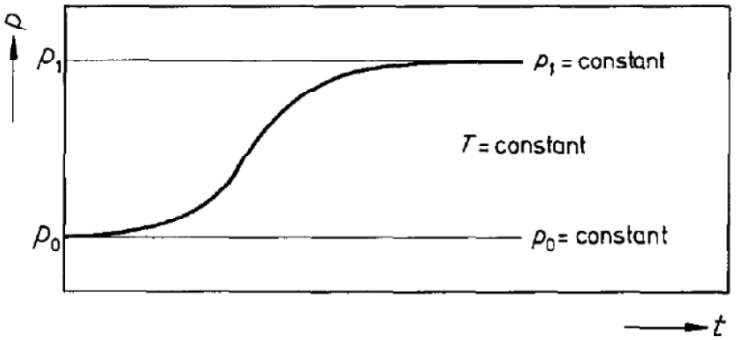

Figure 52. Schematic representation of the behavior of a general physical property, p_i, sensitive to the stage of transformation plotted versus time, t (261). Specifically, the property p_i, referred to as p in the axis,) equals p_0 at the beginning of the transformation process and p_1 when the process is completed.

According to (261), isothermal analysis allows to determine ΔE. In a isothermal test, the transformation rate is a function of temperature: for thermally activated processes the

transformation is the faster the higher the temperature. The temperature dependence of the transformation rate is determined by ΔE.

The measurement of ΔE requires to perform a set of isothermal tests at different temperatures. Thereafter, ΔE is calculated from the slope of the straight line obtained by plotting $ln(\Delta t)$ versus $\frac{1}{T}$ for fixed fractions transformed, f_{1_j} (261). The procedure is described graphically in Figure 53.

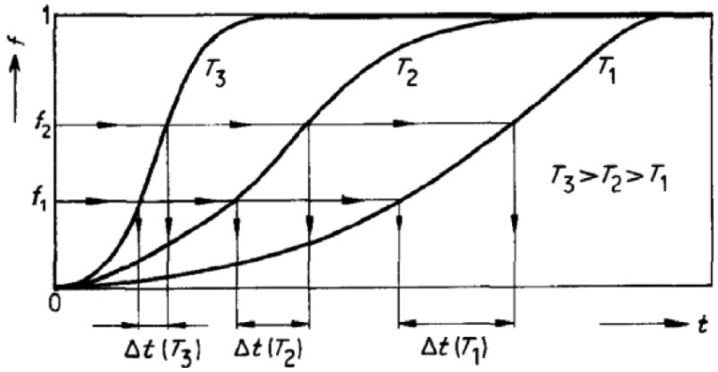

Figure 53. Schematic description of the procedure for the calculation of the activation energy for the transformation applying an isothermal analysis (261). The time to form $f = f_2 - f_1$ (specifically $f = (f_{1_2} - f_{1_1})$ in the notation used in the present text) is Δt and is a function of temperature, T. The higher the temperature, the faster the process. The temperature dependence is determined by ΔE. The procedure can be repeated for different fractions transformed f_{1_j}.

In particular, the fraction transformed at the maximal transformation rate is *in*dependent of the temperature of investigation, being a favorable choice for the calculation of ΔE in case of *isokinetic* reactions (261). *Isokinetic* reactions are reactions that are rate-determined by a single mechanism from their incipience to their completion (i.e. ΔE is constant during the process). On the other hand, if different processes act, or are dominant, at different stages of the transformation, the analysis taking into account different stages of the transformation, i.e. different f_{1_j} values, results in different values of ΔE.

Finally, for the calculation of ΔE to be consistent, the initial and final states of the material must be known and equal for the different holding temperatures. This means that the

transformation must be suppressed during cooling / heating to the temperature of interest and the level of saturation for the transformation must be *in*dependent of holding temperatures.

3.1.3. Isochronal analysis

In *isochronal* analysis, the sample is heated / cooled at a constant rate, $\emptyset$, and the physical property of interest is recorded as a function of temperature, T (Figure 54). When an isochronal analysis is performed, the dependence of temperature for $p_0(\mathrm{T})$ and $p_1(\mathrm{T})$ has to be considered in the calculation of the fraction transformed. Assuming $p_0(\mathrm{T})$ and $p_1(\mathrm{T})$ intrinsic properties of the material, it follows:

$$f_1 = \frac{p(T) - p_0(T)}{p_0(T) - p_1(T)} \qquad [3]$$

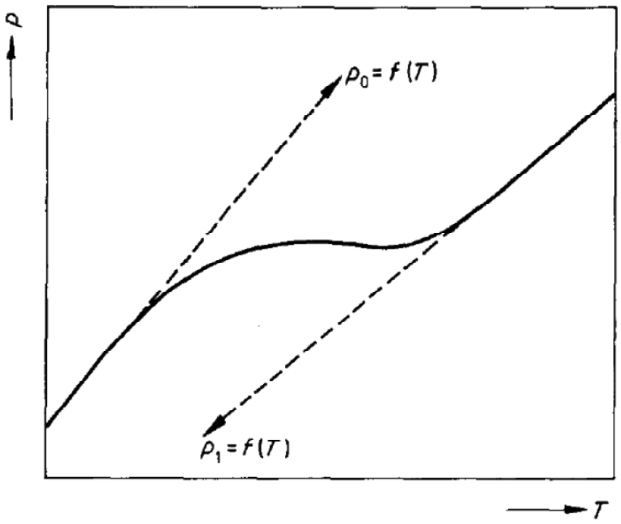

Figure 54. Schematic representation of the behavior of the physical property, p_i, sensitive to the stage of transformation plotted versus temperature, T. Specifically, the property $p_i = p_0$ at the beginning of the transformation process and $p_i = p_1$ when the process is completed. (261).

According to (261), isochronal analyses also allow to determine ΔE. In an isochronal analysis, the temperature interval where the transformation is observed is a function of the heating / cooling rate. The transformation progressively shifts on the temperature scale away

from equilibrium temperature the higher the applied temperature ramping rate. The temperature shift is determined by ΔE.

The measurement of ΔE requires to perform a set of isochronal tests at different cooling / heating rate. Thereafter, ΔE is calculated from the slope of the straight line obtained by plotting $\ln\left(\frac{T_{f_{1j}}^{\ 2}}{\emptyset}\right)$ versus $\frac{1}{T_{f_{1j}}}$, with $T_{f_{1j}}$ the temperature corresponding to a specific fixed fraction transformed, f_{1j} (261).[40] The procedure is described graphically in Figure 55.

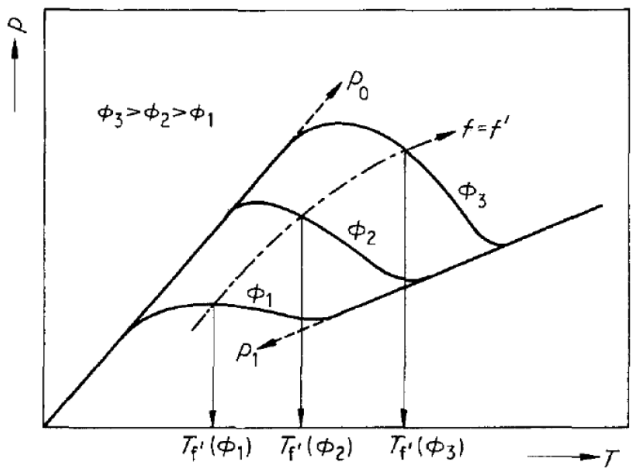

Figure 55. Schematic description of the graphical procedure for the calculation of the activation energy for the transformation applying an isothermal analysis (261). The temperature where a certain amount of transformation, f_1, is observed is a function of the temperature ramp. The temperature shift as a function of the ramping rate is determined by ΔE

Similar to isothermal analyses, the maximum transformation rate is a favorable choice for the calculation of ΔE since it occurs (in good approximation (261)) always for the same value of fraction transformed. *Isokinetic* reaction is generally assumed in case of isochronal investigations.

[40] This type of analysis is termed Kissinger-like after (264).

3.1.4. Applications of particular interest for this work

According to (261), the information that can be obtained from isothermal and isochronal analyses are equivalent, but the singular condition makes one or the other analysis preferable. The investigation of the different stages of tempering of ferrous martensites and the martensite transformation are the cases of interest for the present work.

In relation to tempering of ferrous martensite, which presents several overlapping processes, isochronal analyses are superior to isothermal analyses (261). The reason is that isochronal analysis allows the investigator to vary the heating rates in order to separate the different phenomena, while isothermal analysis does *not* provide this freedom for the investigator.

In relation to martensite formation, isothermal analysis is generally *not* adequate for determining ΔE. The reasons are twofold: (i) the transformation process possesses athermal components (see chapter 2), which may result in different initial conditions for different holding temperatures; (ii) the level of saturation for the transformation is defined by $\Delta G^*(T)$ determining different final conditions for different holding temperatures.[41]

3.2. The tempering of ferrous martensite

Among the purposes of the present work, there is the investigation of the effect of sub-zero Celsius treatment on the different stages of tempering. This paragraph describes in detail the different stages of tempering of ferrous martensites and the connected changes in physical properties. Thereafter, the sensitivity of different experimental techniques, which can be applied for the investigation of tempering, is addressed.

3.2.1. Description of the different stages

As anticipated in chapter 1, the tempering of ferrous martensite has been historically divided into four stages: (i) the precipitation of transition carbides; (ii) the decomposition of

[41] See paragraph 3.3.4.

retained austenite; (iii) the formation of cementite; (iv) the precipitation of alloy carbides. An additional (zero) stage could be the pre-precipitation stage that is usually referred to as aging of martensite (13) (14) (265) (266) (267).

The stages of tempering of ferrous martensites were generally investigated in iron-carbon and iron-nickel-carbon alloys / steels (13) (14) (16) (265) (266) (267) (268). It was demonstrated that the analysis is also valid for a Fe-1.5%Cr-1%C low alloyed bearing steel (15)(269)(270).

The pre-precipitation stage

During aging, carbon atoms in martensite diffuse to lattice defects and agglomerate into clusters (13) (265) (266) (267) (268). According to (265) (268) (after (271)), the chemical composition of the clusters is established in Fe_4C. The clustering (or segregation) of Carbon atoms at crystal defects such as dislocations can involve up to 0.2wt%C (< 0.1wt% according to (266)), which does not take part in the subsequent first stage of tempering.

Aging is accompanied with a (partial) relaxation of the tetragonal structure of martensite (266) and is rate controlled by carbon diffusion in martensite. This mechanism proceeds at temperatures as low as 228 K – 233 K (14) (265). Aging is an exothermic process (13) and results in a lower resistivity of the sample (265).

The first stage of tempering

The precipitation of transition carbides leads to the formation of hexagonal ε carbides, first reported in (272), and orthorhombic carbides, defined η carbides, and first reported in (273). According to (15), the orthorhombic structure of η carbides results from ordering of carbon atoms during growth of the ε carbides, which distorts the hexagonal lattice into orthorhombic. The hexagonal ε carbide structure is observable only for carbon contents $<$ 1wt% (15) in the steel (after (269)).

The formation of carbides is kinetically hindered at room temperature (12) and starts on heating above about 353 K – 373 K. The nucleation sites for the precipitates have not been clarified yet (15), but precipitation along twin boundaries is considered favorable (Figure 56).

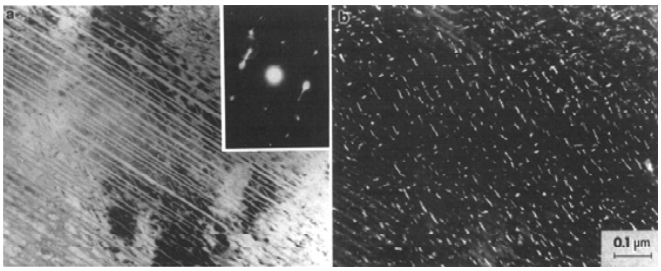

Figure 56. Transition carbide precipitation in the midrib of a plate of Fe-25Ni-0.4C martensite. TEM micrographs (a) bright-field/(b) dark-field pair obtained after tempering the material at 373 K for 1 hour (274).

In more macroscopic terms, the precipitation of transition carbides occurs uniformly throughout the martensite phase, is exothermic (13) (16) (269), results in a decreased resistivity of the sample (265) and in a significant volume contraction (16) (269). The precipitates are initially coherent with the matrix resulting in an increase in hardness, while a subsequent reduction in hardness results from loss of coherence with the matrix (13) (15).[42] Loss of coherence is associated with an almost complete relaxation of the tetragonal structure of martensite (13) (14).

The precipitation is rate controlled by pipe-diffusion of iron atoms in ferrite / martensite (13). The chemical composition of transition carbides is not clarified. According to (275), the chemical composition of the transition carbides is Fe_9C_4, which is in the range Fe_2C to $Fe_{2.4}C$ determined from prior studies (273) (276) (277) (278) (279). According to (15) the carbon concentration in the precipitate is reduced during their growth (i.e. describing the chemical composition as Fe_xC, X increases during growth).

The second stage of tempering

The decomposition of retained austenite into ferrite and *cementite* follows the first precipitation stage and starts at about 513 K – 523 K (13)(16). *Cementite* refers to the most stable form of Iron carbide, which possesses an orthorhombic crystal structure and a chemical composition Fe_3C (see for example (273)); cementite is indicated as θ (48).

[42] It is likely that the removal of carbon from solid solution in martensite also contribute to a reduction in hardness.

The decomposition of retained austenite is associated with an expansion of the sample (16) (269) and a noteworthy heat release (13) (16) (269). The reaction is rate controlled by the diffusion of carbon in austenite. In (13), it is suggested that the formation of cementite is kinetically hindered below about 498 K – 523 K; in this case, the decomposition is preceded by the transformation of a part of the austenite into ferrite, with simultaneous enrichment with carbon of the remaining austenite.

The third stage of tempering

The formation of cementite within the martensite phase represents the third stage of tempering. Cementite formation is rate controlled by volume diffusion of iron atoms in the ferrite phase and occurs within the same temperature range as the decomposition of austenite. According to (63) (after (18)), cementite grows at the expense of the fine ε/η transition carbides, which progressively disappear, leading to a considerable decrease in hardness. The formation of cementite is associated with a small enthalpy change and a noteworthy sample contraction (16) (269).

The fourth stage of tempering

The fourth stage of tempering depends on the presence of alloy elements. In presence of carbide formers stronger than iron, like molybdenum, chromium, vanadium, tungsten, niobium, tantalum, zirconium and aluminum (48) (17), cementite progressively disappears, while the precipitation of more stable forms of carbides takes place. This process generally leads to an hardness increase (4) (48).

The description of the stages of tempering indicates that, among other possibilities, the structural changes in the material can be followed recording the volumetric and enthalpy changes during the thermal cycle.

3.2.2. Evolution of specific volume and specific enthalpy

General description of the methods

The methods that are applied to record specific volume and specific enthalpy changes are d*ilatometry* and *Differential Scanning Calorimetry*, DSC, respectively.

In *DSC*, the energy necessary to equilibrate the temperature of the investigated sample and of an inert reference sample subjected to an identical thermal cycle is measured. The measure of the energy is associated with the enthalpy or the heat capacity changes in the sample.

In *dilatometry*, the dimensional changes of a sample, specifically its length changes, which is one third of the volume change assuming isotropic material, is recorded versus both temperature and time. Volume changes result from thermal expansion / contraction and from structural transitions.

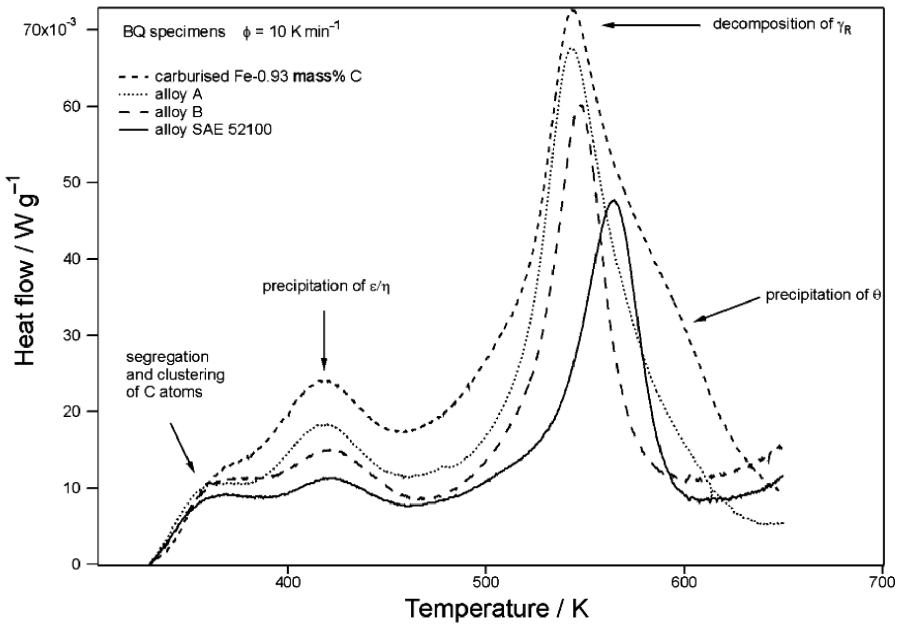

Figure 57. Example of DSC curves obtained during isochronal heating of different quenched steels. The different stages of tempering of ferrous martensites are visualized as a series of exothermic reactions (269). Alloy A, stands for Fe-1%C; alloy B for Fe-1.5%Cr-1%C; SAE 52100 is a commercial bearing steel containing 1.5%Cr and 1%C alloying elements.

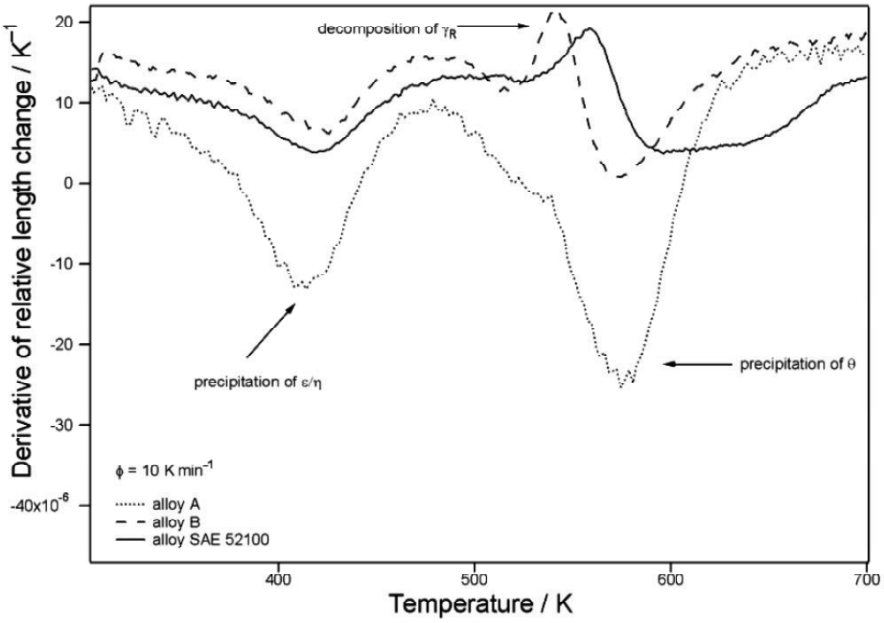

Figure 58. Example of dilatometry curve obtained during isochronal heating of different quenched steels. The precipitation stages are visualized as sample contractions, while the decomposition of retained austenite results in an expansion of the sample (269). Alloys are identical to those in Figure 57.

DSC and dilatometry, are both *indirect* methods because the structural changes can only be *inferred* from the changes in physical properties and the occurrence of concurrent overlapping phenomena cannot be excluded. The sensitivity of the two methods to the different stages of tempering was shown in (269), where the tempering of ferrous martensite was investigated isochronally in Fe-1%C and Fe-1.5%Cr-%C steels with DSC, (Figure 57) and dilatometry (Figure 58).

In (269), both the DSC and dilatometry investigations allowed to identify the different stages of tempering and to determine ΔE for the different stages. However, it is here noted that the different stages of tempering are identified more straightforwardly with the use of dilatometry than with DSC (compare Figure 57 and Figure 58), the reason being an opposite volumetric effect of stage 2 versus stage 1 and 3, while all process being exothermic.

The use of dilatometry for the investigation of the different stages of tempering is also reported in (280) for a low alloyed steels, in (281) for two Fe-Cr-N steels and in (282) for a

medium-carbon (C content 0.44wt%) steel. The physical principles for the investigation of the different stages of tempering by dilatometry is described in the following.

The first stage of tempering

The volumetric changes of a material during a solid state reaction can be evaluated from the estimation of the specific volume of the phases initially present in the sample as compared to the specific volume of the products of the reaction. For the first stage of tempering, the complete reaction is $\alpha' \rightarrow \frac{X \cdot C_C}{100 - C_C} \cdot \alpha + Fe_XC$, where C_C is the at.% concentration of carbon atoms dissolved in the martensite. This reaction is easily handled considering the specific volume of the Iron atoms in α', α and Fe_XC.

The volume of the unit cell of martensite, which contains two iron atoms, increases linearly with the carbon and nitrogen content (6). The $\alpha' \rightarrow \alpha$ is accompanied with a volume contraction of the unit cell of martensite and a reduction of the specific volume per iron atom, consequently leading to sample contraction, $\Delta V_{\alpha' \rightarrow \alpha} < 0$.[43] On the other hand, according to the data in (6) (after (276) (283) (284)), the specific volume per iron atom in the ε / η carbide phases is larger than the specific volume in both martensite and, accordingly, ferrite structures, resulting in a volume expansion, $\Delta V_{\alpha' \rightarrow Fe_XC} > 0$.

It follows that the volumetric changes in the sample are determined by the balance among the two reactions, which depend on the chemical composition of the carbide phase (i.e. of the X value) because of mass conservation in the sample. The volume change $\Delta V_{\alpha' \rightarrow \alpha + Fe_XC}$ can be calculated according to the following expression:

$$\Delta V_{\alpha' \rightarrow \alpha + Fe_XC} = \frac{X \cdot C_C}{2 \cdot (100 - C_C)} \cdot \Delta V_{\alpha' \rightarrow \alpha} + \Delta V_{\alpha' \rightarrow Fe_XC} \quad [4]$$

In (6) it is shown that, with the assumption $2 < X < 3$,[44] the volume contraction associated with the $\alpha' \rightarrow \alpha$ transition is only partially counterbalanced by the formation of

[43] Reference data on the lattice parameter of b.c.c. / b.c.t. Iron Carbon martensites are reported in (6) (7) (282) (285).

[44] Interval that includes both the composition of ε/η transition carbides ($2 < X < 2.4$) and the composition of θ cementite ($X = 3$).

Fe_XC carbides and the process results in sample contraction, $\Delta V_{\alpha' \rightarrow \alpha + Fe_XC} < 0$. Moreover, the larger X, i.e. the lower the carbon concentration in the carbide phase, the smaller the sample contraction.

Note that, since the analysis is performed isochronally, thermal expansion must be taken into account in the evaluation of the volume of the unit cells for the different phases.[45]

The second stage of tempering

The decomposition of retained austenite follows the precipitation of transition carbides. The complete reaction is $\gamma \rightarrow \alpha + \theta$, with $\theta = Fe_3C$. According to (6), the decomposition leads to a net expansion of the sample. This result is expected as the γ phase is closed packed, while α is *not* and the volume per iron atom of cementite is larger than for ferrite.[46]

The third stage of tempering

The precipitation of cementite within martensite follows either $\alpha' \rightarrow \alpha + Fe_XC \rightarrow \alpha + \theta$, as demonstrated in (15), in association with a further shrink of the sample as compared to the first formation of transition precipitates, or directly $\alpha' \rightarrow \alpha + \theta$, as assumed in (6), similarly associated with sample contraction.

Sample contraction for the $\alpha + \varepsilon/\eta \rightarrow \alpha + \theta$ reaction is determined by the more compact structure of orthorhombic θ as compared to ε/η (see data in (6)), which overcompensate the effect of a lower carbon concentration in θ as compared to ε/η, i.e. a larger value of X (see above).

The fourth stage of tempering

A general analysis is *not* possible for the precipitation of alloyed carbides, which present chemical composition and crystal structure depending of the individual system under investigation. In principle, the effect of the formation of each precipitate can be calculated *a*

[45] Reference data on thermal expansion of the different phases are listed in (6) (286).
[46] Reference data for γ are listed in (6)

priori providing that the crystal structures and the chemical composition of each phase are known.

3.3. The $\gamma \rightarrow \alpha$ transformations in steel

3.3.1. Description of transformation processes and products

Diffusive versus diffusionless $\gamma \rightarrow \alpha$ transformations in steel

The $\gamma \rightarrow \alpha$ transformation in steel can occur following different mechanisms (48) (144) (287). The transformation mechanism which applies to a certain case results in the formation of a specific transformation product.

In this paragraph, *massive transformations* and *bainitic transformations* are described according to (51) (288). Moreover, it is assumed that the carbon content in the material is negligible (i.e. the reaction $\gamma \rightarrow \alpha + Fe_XC$ is not considered), implying that the concepts described in paragraph 2.5.2 in relation to equilibrium temperature T_0 apply to all the transformation processes.

Massive transformations

According to (48) (288), in *massive transformations*, the product phase (i.e. α) forms by a *not* coordinated movement of atoms across the parent / product interface resembling a series of *in*dependent jumps. In massive transformations, growth of the product is rate-controlled by the thermally activated motion of the interface (i.e. the thermally activated occurrence of successful jumps) and results in irregular grains in the final product.

The products of the $\gamma \rightarrow \alpha$ massive transformations in low carbon-iron alloys are *equi-axed ferrite* and *massive ferrite*. *Equi-axed ferrite* nucleates at austenite grain corners (i.e. triple points) and is associated with a very small amount of strain energy. *Massive ferrite* nucleates at austenite grain boundaries and is associated with a relevant amount of strain energy.

In the $\gamma \rightarrow \alpha$ transitions which do not involve changes in the chemical composition of the phases, the amount of strain energy associated with the transformation defines the undercooling

below T_0 which is necessary for the transformation to start. Consequently, *equi-axed ferrite* start to form at higher temperatures as compared to *massive ferrite*.

Bainitic transformations

According to (288), in *bainitic transformations*, atoms move across the interface following a *coordinated* movement resembling a shear. This definition suggests that *bainitic transformations* are *diffusionless* and is in agreement with the observations of surface relief, habit plane and O.R. with austenite. On the other hand, there exists in the literature evidence, like for example recognizable differences between the carbide precipitates within the bainitic and the martensitic transformations products (see (62)), which indicate that the transformation is (partially) diffusive.

The nature of bainitic transformations, is still under debate (287). In the present work, bainitic transformations are defined as transformations which possess both diffusionless and diffusive character, being in between the massive and the martensitic cases.

The product of bainitic transformations is defined *bainite* in presence of carbon atoms and *bainitic ferrite* otherwise (288). In the present work, *Widmanstätten ferrite* is also classified as a product of bainitic transformations.[47] (144)

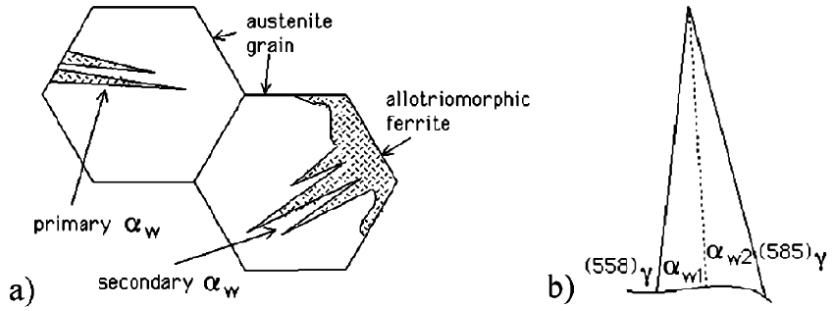

Figure 59. Schematic representation of Widmanstätten ferrite formation: a) nucleation processes; b) formation of coupled ferrite variants; the habit plane of the variants is also indicated (after (289)).

[47] According to (144), the difference between bainite and Widmästatten ferrite is in the mechanism controlling short-range diffusion of Carbon atoms during the transformation. To the author´s understanding, in absence of Carbon atoms the two transformation processes must be classified as identical.

According to (289), *ferrite* is defined primary when it nucleates on an austenite grain boundary, while it is defined secondary when it nucleates on a preexisting phase boundary between austenite and ferrite, so called allotriomorphic ferrite (Figure 59a). [48] *Widmanstätten ferrite* forms along $\{1\ 1\ 1\}\gamma$ by the simultaneous and cooperative growth of two adjacent coupled ferrite variants with $\{5\ 5\ 8\}\gamma$ habit plane, resulting in a tent like morphology (289) (Figure 59b). This formation mechanism is associated with a relatively small amount of strain energy (144). In relation to growth, in (290) (291), it was shown that thickening of each unit occurs by a ledge mechanism.

According to (144), *bainite / bainitic ferrite* shares the same nucleation sites of primary *ferrite*. Following (143) (292) (293), *bainite / bainitic ferrite* results from autocatalytic formation of small needle like ferrite units, defined laths and grouped into *sheafs* (Figure 60). Each *sheaf* possess plate like morphology and is oriented along $\{1\ 1\ 1\}\gamma$. In relation to growth, in (294), it was shown that thickening of each bainitic lath occurs by a ledge mechanism. The mechanism was previously suggested in (295) (296).

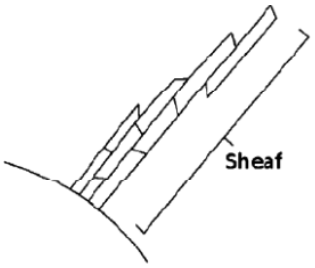

Figure 60.Schematic representation of sheaf composed by a series of bainitic laths (292)

The formation of a *sheaf* is associated with a noteworthy amount of strain energy. It follows that *bainite / bainitic ferrite* forms at lower temperature than *ferrite*. More generally, the formation of *bainite / bainitic ferrite* is associated with a larger amount of strain energy also as compared to massive transformation, while to the author´s knowledge no direct comparison between *ferrite* and *massive ferrite* is reported in the literature.

[48] Allotriomorphic ferrite is the product of a diffusive $\gamma \rightarrow \alpha$ transformation rate-controlled by long range diffusion (48).

Sheaf are comparable to *blocks* in lath martensite. For example, according to (142), parallel sheaves are grouped into packets and the simultaneous formation of differently oriented sheaves results in a decrease in strain energy, analogous to blocks in lath martensite.

A net criterion that allow to discriminate between martensite and *bainite / bainitic ferrite* has so far not been defined yet. This lack of a criterion makes it *im*possible to distinguish ex situ lath martensite and *bainitic ferrite*. [49] On the other hand, the strain energy term for bainitic transformations is lower than for martensitic transformations, (43), with the consequence that bainitic ferrite formation is observed at higher temperatures than martensite.

Finally, for both martensitic and bainitic transformations and contrary to massive transformations, the boundaries within the region presenting large misorientation (i.e corresponding to the block / Sheaf boundaries) in the final product are straight.

3.3.2. Measuring the changes in physical properties

Independently of the transformation product obtained during the $\gamma \rightarrow \alpha$ transition, the changes in physical properties, which can be monitored to follow the phase transition, are a shared characteristic between the different $\gamma \rightarrow \alpha$ transformations. The more relevant physical properties and the techniques which are applied for monitoring such properties are described in the following.

DSC

The $\gamma \rightarrow \alpha$ transformations in steel proceed by nucleation and growth. A transformation proceeding by nucleation and growth is defined a *first order transformation* (260). In a first order transformation heat is released /absorbed during the phase transition (297), i.e. there is an enthalpy change. Consequently, DSC is sensitive to the $\gamma \rightarrow \alpha$ transition.

From the quantitative point of view, the measured specific heat evolution (per mole/mass of material), $\Delta H(T)$, depends on the specific enthalpy of the transition, $\Delta H_{\alpha \rightarrow \gamma}(T)$. Following (298):

[49] For bainite the presence of carbon makes it possible to distinguish between bainite and martensites from the observation of the distribution of precipitates in the matrix (see (62)).

$$\Delta H_{\alpha\to\gamma}(T) = \Delta H_{\alpha\to\gamma}(T_s) + \int_{T_s}^{T} \left(C_{p_\alpha}(T) - C_{p_\gamma}(T) \right) dT \quad [5]$$

where T_s is the transformation start temperature, $\Delta H_{\alpha\to\gamma}(T_s)$ is the specific enthalpy change at the temperature and $C_{p_\alpha}(T)$ and $C_{p_\gamma}(T)$ are the specific heat capacities of α and γ, respectively and can be calculated theoretically (see for example (297) (298)). Assuming the heat released is an intrinsic property of the material, the fraction transformed versus time and temperature can be calculated according to the relationships:

$$f(t) = \int_0^t \frac{\Delta H(t)}{\Delta H_{\alpha\to\gamma}(T)} \cdot dt \quad [6]$$

$$f(T) = \int_{T_s}^{T} \frac{\Delta H(T)}{\Delta H_{\alpha\to\gamma}(T)} \cdot dT \quad [7]$$

referring to isothermal and isochronal analysis, respectively. Note that in the present description, the occurrence of concurrent overlapping processes, which also result in an enthalpy effect, is excluded. The presence of concurrent processes cannot be excluded *a priori* and the technique must be considered an *indirect* evidence of the γ → α transition.

The main limitations of the DSC technique as an indirect technique are twofold: it allows to follow the transformation in a few mg of material only ((63), after (299)); it is sensitive to the energy that is stored in the material in the form of crystal defects and retained strains (300), i.e. the heat release is not necessarily proportional to the amount of transformation.

Dilatometry

The γ → α transformations are associated with an increase in the specific volume of the material as a consequence of the transition from the close packed f.c.c. crystal structure to the less densely packed b.c.c. / b.c.t. crystal structures. Dilatometry is consequently sensitive to the γ → α transition.

From a quantitative point of view, the decrease in specific volume can be calculated from the specific volume per Iron atom in the two crystal lattices (see paragraph 3.2). In the case of martensite formation, the dilatation of the material can be expressed in the form of the dilatational component of the transformation strain (see paragraph 2.2.2), $\varepsilon_0(T)$, which is a

function of the chemical composition of the material and of temperature.[50] Following (76) (301) (302):

$$\varepsilon_0(T) = \frac{2 \cdot \left(a_\alpha(T_s) \cdot \left(1 + \int_{T_s}^{T} \lambda_\alpha(T)\, dT\right)\right)^3}{\left(a_\gamma(T_s) \cdot \left(1 + \int_{T_s}^{T} \lambda_\gamma(T)\, dT\right)\right)^3} \quad [8]$$

with $a_\alpha(T_s)$ and $a_\gamma(T_s)$ lattice parameters of α and γ, respectively, and $\lambda_\alpha(T)$ and $\lambda_\gamma(T)$ the linear expansion coefficients of α and γ, respectively. Assuming the specific volume as an intrinsic property of the phases and isotropic deformation, the measure of the sample elongation, $\frac{dl(t,T)}{l_0}$, gives the fraction transformed according to the relationships:

$$f(t) = \int_0^t \frac{dl(t)}{l_0} \cdot \frac{3}{\varepsilon_0(T)} \cdot dt \quad [9]$$

$$f(T) = \int_{T_s}^{T} \frac{dl(T)}{l} \cdot \frac{3}{\varepsilon_0(T)} \cdot dT \quad [10]$$

for isothermal and isochronal analysis, respectively and where $\frac{dl(T)}{l_0}$ is the measured expansion / contraction of the sample corrected for expected thermal expansion / contraction. Moreover, under the assumption of isotropic transformation:

$$\varepsilon_0(T) \cong \frac{2 \cdot \left(a_\alpha(T_s)^3 + 3 \cdot \int_{T_s}^{T} \lambda_\alpha(T)\, dT\right)}{a_\gamma(T_s)^3 + 3 \cdot \int_{T_s}^{T} \lambda_\gamma(T)\, dT} \quad [11]$$

Note that in the present description, the occurrence of concurrent overlapping processes which also result in dimensional changes is excluded (i.e. for example the formation of precipitates). The presence of concurrent processes cannot however be excluded *a priori* and the technique must be considered *indirect* evidence of the $\gamma \rightarrow \alpha$ transition.

The main limitation of dilatometry is its sensitivity to the buildup or relaxation of stresses / strains in the material, i.e. the specific volume of the phases is not necessarily proportional to the amount of transformation.

[50] The dilatation $\varepsilon_0(T)$ can be calculated from the Bain matrix (Figure 8) as the product of the values on its diagonal minus one (76).

Magnetometry

In magnetometry, the magnetization of the material, $\bar{M}$, is recorded versus temperature and time. The magnetization of a material is a function of the applied magnetic field, $\bar{H}$, and of the magnetic properties of the material according to the expression $\bar{M} = \chi(H) \cdot \bar{H}$, with $\chi(H)$ a material, temperature and geometry dependent dimensionless quantity defined *magnetic susceptibility*.

Under specific conditions, which corresponds to the application of a magnetic field sufficiently strong to bring $\bar{M}$ to so called *saturation*, $\bar{M}$ can be safely approximated to an intrinsic property of the material: $\bar{M} = \sum_j \bar{m}_j$, with $\bar{m}_j$ magnetic moments of the j atoms constituting the material. It follows for a multiphase material: $\bar{M} = \sum_i \bar{M}_i \cdot f_i$, (or similarly $\chi(H) = \sum_i \chi(H)_i \cdot f_i$) with i referring to the present phases and f_i to the molar fraction. For the $\gamma \rightarrow \alpha$ case:

$$\bar{M} = \bar{M}_\alpha \cdot f_\alpha + \bar{M}_\gamma \cdot f_\gamma = \left(\chi(H) \cdot f_\alpha + \chi(H) \cdot f_\gamma\right) \cdot \bar{H} \qquad [12]$$

The magnetic properties of a phase are determined by its crystal structure, defining the ability of the material to align the magnetic moments of the atoms constituting it, and the chemical composition, which defines $|m_j|$. In general terms, the γ and α phases possess different magnetic properties. Magnetometry is consequently sensitive to the $\gamma \rightarrow \alpha$ transition.

The values of $\chi(H)_i$ are a strong function of the form of magnetism possessed by the specific phase. Among the different forms, *paramagnetism*, *ferromagnetism* and *anti-ferromagnetism* are the one of interest for the present work.

A phase is *paramagnetic* when, in presence of a magnetic field, the magnetic moments of the atoms which constitute it (partially) align in the direction of the magnetic field, slightly enhancing its strength within the material; this form of magnetism is defined *paramagnetism*.[51] According to ((63) after (303)), the value for $\chi(H)$ for paramagnetic phases is in the order of $10^{-4} - 10^{-6}$.

[51] The strength of the field in the material is defined as magnetic flux, B, and follows the relationship $B = \mu \cdot (H + M)$with μ permeability of the material, which is a material dependent constant (18).

A phase is *ferromagnetic* when the magnetic moments in the atoms which constitute it align spontaneously in a specific direction. This alignment is a form of ordering and results in a spontaneous magnetization of the material also in absence of an applied field; in presence of an applied field, the strength of the field in the material increases noteworthy; this form of magnetism is defined *ferromagnetism*. According to ((63) after (303)), the value for $\chi(H)$ for ferromagnetic phases is in the order of 10^6. Ferromagnetic phases become paramagnetic above a certain critical temperature, the *Curie temperature* ((63) after (304)).[52]

In an *anti-ferromagnetic* phase, the magnetic moments of the atoms are also ordered, but ordering occurs coupling $\overline{m}_j$ in anti-parallel (i.e. opposite) directions so that the net macroscopic effect of the alignment is null. Anti-ferromagnetic phases becomes paramagnetic above a certain temperature defined Néel *temperature* ((63) after (304)). The value of $\chi(H)$ is continuous during the anti-ferromagnetic to paramagnetic transition and remains of the same order of magnitude $(10^{-4} - 10^{-6})$ (57) (305).

In conclusion, $\chi(H)$ for paramagnetic and anti-ferromagnetic phases is negligible as compared to $\chi(H)$ for ferromagnetic phases. Consequently, in a mixture of ferromagnetic and non ferromagnetic phases in a material, the magnetization will be determined by the molar fraction of the ferromagnetic phase only. In the following the magnetic properties of α and γ are considered.

The *Curie temperature* of α Iron is 1043 K and for low alloyed steel, is effectively independent of the alloying elements (Figure 1) (306). For the investigation of martensite formation, which always occurs well below 1073 K, the α phase can be safely assumed ferromagnetic.

For γ iron, both the *Curie temperature* and the *Néel temperature* have been reported. In the present discussion, only the *Curie temperature* is relevant. According to (307), the *Curie temperature* of γ iron is always in the order of a few Kelvin; for example, in (308), it is shown

[52] Specifically, the ferromagnetic to paramagnetic transition is an ordered to disordered transition promoted by the availability of thermal energy.

that γ in the iron-nitrogen system is paramagnetic down to 1.7 K. In conclusion, the γ phase can be safely assumed *not* ferromagnetic. It follows:

$$\bar{M} = \bar{M}_\alpha \cdot f_\alpha + \bar{M}_\gamma \cdot f_\gamma \cong \bar{M}_\alpha \cdot f_\alpha \qquad [13]$$

This relation implies that magnetometry is an extremely sensitive technique to follow the γ → α transition. Nevertheless, magnetometry remains an *indirect* technique since the occurrence of concurrent processes, like the formation of ferromagnetic phases other than martensite (i.e. for example ε, η and θ carbides, which possess a Curie temperatures of 520 K, 390 K and 440 K, respectively ((63) after (309)) cannot be excluded *a priori*.

Among other works, magnetometry was applied to investigate the kinetics of martensite formation, according to the principles presented above, in (60) (63) (183) (184) (310) (311) (312) (313). It is noted that several investigations (183) (184) (311) (312) (313) erroneously refer to f_α in terms of volume fraction of martensite instead of the molar fraction of martensite.

3.3.3. Rationalization of γ → α transformations

The γ → α transformation curves (determined by dilatometry, DSC, magnetometry, …), are used to construct transformation diagrams, where the formation of an α structure is reported versus parameters such as temperature, time, cooling rates and grain size of the original austenite.

In the present section, selected works are presented to convey the connections between the different γ → α transitions which emerge from the investigation of transformation diagrams. The description is according to the rationalization presented in (51).

In (51) internally slipped martensite is referred to as *lath martensite*, internally twinned martensite is referred to as *twinned martensite*. This corresponds to *Umklapp* and *Schiebung* martensite transformations in the present description.

Continuous cooling experiments

The kinetics of the γ → α transition during a continuous cooling experiments is reported in *Continuous-Cooling-Transformation*, CCT, diagrams (Figure 61). According to (51), during a continuous cooling experiment, the temperature where the product of a transformation is first observed is specific of the obtained transformation product, but providing that a specific

transformation product is considered, this temperature is *in*dependent of $\dot{T}$. In CCT diagrams, this concept corresponds to a series of horizontal lines.

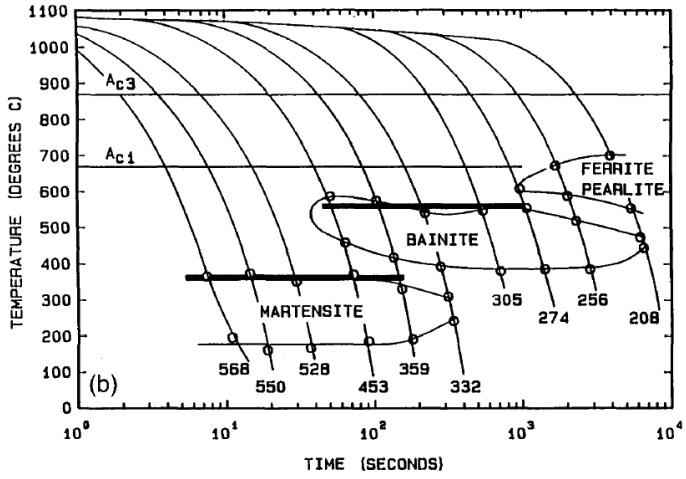

Figure 61. CCT diagram for a Fe-0.35%C-1.4%Mn-0.76%Si-0.%Cr-0.06%Ni-0.16%V ((51) modified after (314)).

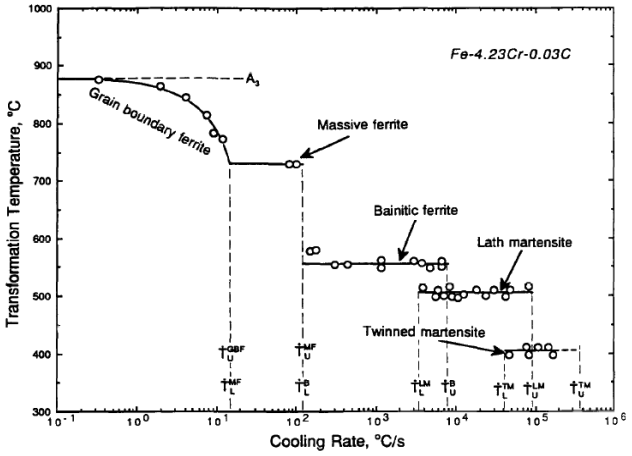

Figure 62. Schematic example of $T - \dot{T}$ diagram ((51) after (315)) based on experimental data from (151). Different cooling rates result in different transformation products. The lower and upper critical temperatures to obtain a specific product are named $\dot{T}_L$ and $\dot{T}_U$, respectively, while subscripts refer to the product of the transformation. Apart from grain boundary ferrite, the temperature where a specific product is first observed is independent of $\dot{T}$.

The independence of the transformation start temperature of $\dot{T}$, is conveyed more clearly in $T - \dot{T}$ diagrams (Figure 62). In $T - \dot{T}$ diagrams, the independence of the transformation start temperature of $\dot{T}$ appears as a series of plateau, where each plateau is associated with a specific transformation product.

Isothermal experiments

The kinetics of the γ → α transition during isothermal investigation is generally presented in *Time-Temperature-Transformation*, TTT diagrams (Figure 2, Figure 3).

In TTT diagrams, the plateaus typical of CCT diagrams are not observed, but the different transformations appear as *C-type* curves (Figure 63). According to (316), the plateau observed in CCT and $T - \dot{T}$ diagrams correspond, in good approximation, with the maximum transformation rate observed during isothermal experiments (Figure 63).

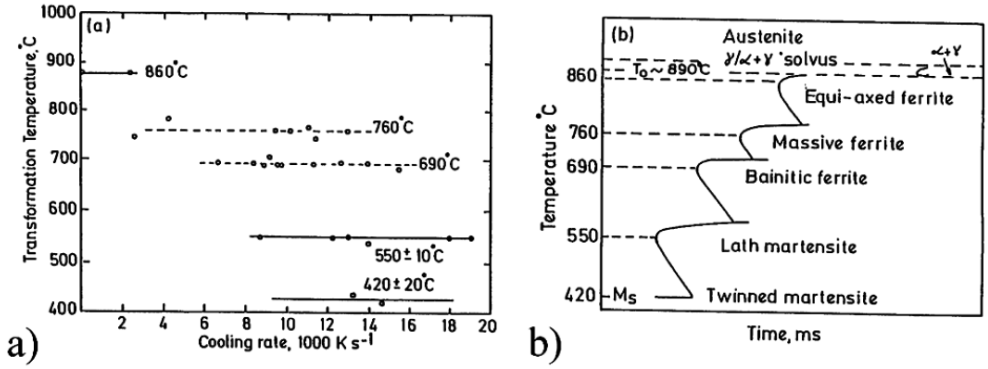

Figure 63. Correspondence between transformation plateau observed in $T - \dot{T}$ diagrams and transformation curves reported in TTT diagrams. The temperature of the plateau reported in $T - \dot{T}$ diagrams corresponds to the fastest isothermal kinetics for a specific transformation product, visible as a nose (or knee) of the C-type curves in TTT diagrams (316).

The observation of *C-type* curves in TTT diagrams is generally described in terms of a balance between the driving force for a transformation and the thermal energy (260). The driving force for the transformation increases with the undercooling (i.e. the lower the temperature) promoting the formation of a larger number of nuclei for the transformation process. The thermal energy sustains the occurrence of thermally activated mechanisms and decreases with falling temperature.

This interpretation appears *not* to apply for the transformation plateau observed in continuous cooling experiments. The presence of different plateaus indicates that there is a sort of athermal mechanism which is not recognized. Moreover, this mechanism can clearly be suppressed providing that sufficiently fast cooling is applied.

3.3.4. The temperature range for martensite formation and the stabilization of retained austenite

From CCT and TTT diagrams (Figure 2, Figure 61), it is observed that the $\gamma \rightarrow \alpha$ transition does *not* occur at a fixed temperature, but takes place in a certain temperature range. This concept applies also for martensite formation.

Martensite formation, irrespective of whether it is internally slipped or twinned, occurs in a temperature range between M_S and a temperature where the transformation is completed, defined as *martensite finish temperature*, M_f. The mechanisms which may lead to the occurrence of a temperature range $M_S \rightarrow M_f$ for the occurrence of the transformation are presented in this paragraph.

According to (115) (310) (317) (318), there is a direct relationship between the fraction of martensite that can form in the material, $f_{\alpha' max}$, and ΔG^*. Following (310) (318), $f_{\alpha' max} \propto \Delta G^* - \Delta G(M_S)$, where in (318) the expression is considered to apply in the interval $5\% < f_{\alpha'} < 55\%$. On the other hand, in (115) (317) the expression $f_{\alpha' max} = 1 - exp\big(-b \cdot (M_S - T)\big)$, originally presented in (49), is applied, with $b \propto \frac{d\Delta G^*}{dT}$.

It can be shown that the exponential expression actually originates from the linear relationship introducing a term $(1 - f_{\alpha'})$, which account for a progressive reduction of the content of retained austenite in the material during the transformation.[53] The two expression are consequently based on the same physical concept.

---

[53] It stands $\frac{df_{\alpha'}}{dT} = \rho \cdot \frac{d\Delta G}{dT} \cdot \big(1 - f_{\alpha'}\big)$ with ρ proportionality factor. Upon integration and the imposition of the boundary condition $f = 0$ for $T = M_S$, it follows: $f_{\alpha'} = 1 - \exp\Big(-\rho \cdot \frac{d(\Delta G)}{dT} \cdot (Ms - T)\Big)$.

However, on the basis of the description given so far, the existence of a temperature range $M_S \rightarrow M_f$ for the occurrence of the transformation is counterintuitive: provided that ΔG^* is sufficient for a spontaneous nucleus to trigger many autocatalytic nucleation events, each autocatalytically generated nucleus should equally be able to trigger new nuclei until the transformation goes to completion. Evidently, there exist one or more mechanisms which are responsible for a progressive stabilization of the austenite.

From (115) (310) (317) (318), it follows that the mechanism responsible for the existence of a temperature interval for the transformation, M_S to M_f, is a function of $f_{\alpha'}$ only, suggesting that the transformation process either progressively increases the energy (i.e. $-\Delta G_{\varepsilon_{rev}}$, $\Delta H_{\gamma \rightarrow \alpha'}$, $-\Delta G_{\varepsilon_{ir}}$) necessary for martensite formation, or decreases ΔG^*.

According to (5) (319), the mechanisms leading to the stabilization of the retained austenite can be of chemical origin, thermal origin or mechanical origin. The different mechanism are shortly discussed in the following.

The mechanisms which are of chemical and thermal origin are: changes in the chemical composition of the austenite (decrease of ΔG_{chem}, i.e. ΔG^* - chemical type); atomic ordering / formation of coherent precipitates, leading to hardening of the austenite phase (i.e. increase of ΔG_{ε} - chemical / thermal type); pinning of dislocation by interstitials, leading to hardening of the austenite phase and to loss of mobility of the austenite to martensite interface (increase of $\Delta H_{\gamma \rightarrow \alpha'}$ - thermal type).

The mechanisms which are of mechanical origin are: mechanical interaction among transformed / untransformed regions leading to a state of compression in austenite (decrease of ΔG^*); introduction of crystal defects during the transformation, leading to hardening of the austenite phase and to loss of mobility of the austenite to martensite interface.

Only the mechanisms of mechanical origin can be associated with the general existence of a temperature range M_S to M_f, because they depend on $f_{\alpha'}$. This is not the case for the chemical / thermal origin for stabilization. Unfortunately, no experimental evidence exist to corroborate the mechanical stabilization during spontaneous transformation, i.e. not assisted by external mechanical forces.

For example, the mechanical interaction between different phases during spontaneous transformation has been investigated only ex situ in a few works listed in (181), and in situ in (183); contradictory results were reported (see paragraph 2.5.3). The dependence of the yield strength of austenite on the fraction transformed has never been investigated, nor it can be investigated because its testing would assist / induce the transformation.

To summarize, there are indications that the fraction of martensite which can form in the material is controlled by the availability of the driving force for the transformation only and according to the expression $f_{\alpha'_{max}} = 1 - \exp\left(-\rho \cdot \frac{d(\Delta G)}{dT} \cdot (Ms - T)\right)$, with ρ material parameter. This expression is likely to be determined by the mechanical stabilization of retained austenite during the transformation, but so far remains *not* justified.

As a final remark, it is noted that in order to study the mechanical stabilization of austenite, it is necessary to exclude the occurrence of chemical and thermal stabilization mechanisms. In presence of carbon atoms in the material, this requires investigation temperatures below about 230 K (38) (39) (40).

3.4. Transformation curves and transformation mechanisms

Time dependent martensite formation was discussed in chapter 2 in terms of the characteristics of the transformation leading to time dependent spontaneous nucleation and / or time dependent growth of martensite.

However, when autocatalytic nucleation does *not* occur, or is poor, martensite formation remains confined to a few regions of material (Figure 64). Autocatalytic nucleation is a necessary condition for a relevant amount of transformation which can be followed in a kinetics analysis (see paragraph 2.7.3): time dependent transformation curves must be described in terms of time dependent autocatalytic nucleation of martensite.

The purpose of the present section is to analyze a series of transformation curves reported in the literature for different ferrous systems and to discuss time-dependence in terms of time dependent autocatalytic nucleation on the basis of time dependent mechanisms described in chapter 2.

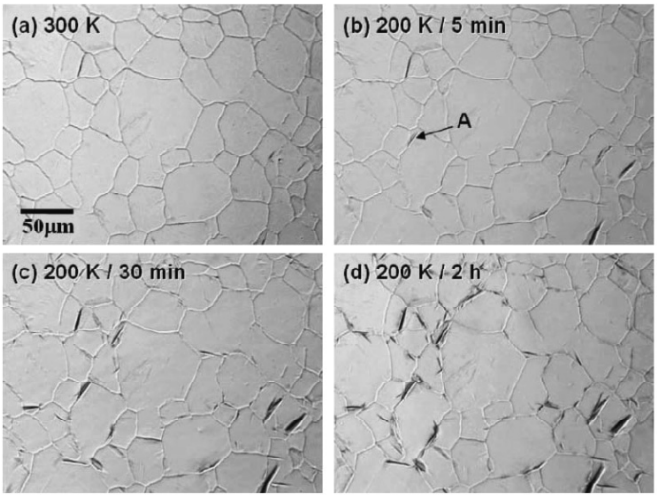

Figure 64. Optical micrographs showing in situ martensite formation during isothermal holding at 200 K in 18%Cr-8%Ni stainless steel: a) material prior to cooling to 200 K; b) nucleation of martensite has started after 5 minutes of isothermal holding and a few small nuclei are visible; c) after 30 minutes, more nuclei are visible and the initially small nuclei have grown further; d) both nucleation and growth have continued. Time dependent growth is emphasized for the martensite unit labeled A (56).

3.4.1. Discussion on the time dependent autocatalytic nucleation of martensite

Time dependent autocatalytic nucleation of martensite can result from: (i) spontaneous time dependent nucleation, which instantaneously triggers a large number of autocatalytic nucleation events (consider Figure 47); (ii) time dependent growth, which suddenly triggers autocatalytic nucleation events providing that a critical dimension to promote autocatalysis is reached (see Figure 44, Figure 45 and reconsider paragraph 2.7.3).

The first case represents a nucleation controlled description, with a transformation curve that results from the superposition of several bursts. These bursts can either spread over several austenite grains (Figure 47), appearing in the form of multiple *not* reproducible macroscopically observable transformation steps (see Figure 48, up to 30% transformation), or be confined to small portions of material, resulting in a continuous transformation rate (see Figure 48, for fraction transformed larger than 30%).

Localization of the burst to small portions of material is likely to result from the progressive partition of the material during martensite formation (Figure 65), and is favored the larger the fraction transformed. Under these conditions, the transformation is controlled by the

driving force for the transformation only, which triggers the transformation in new areas by spontaneous nucleation.

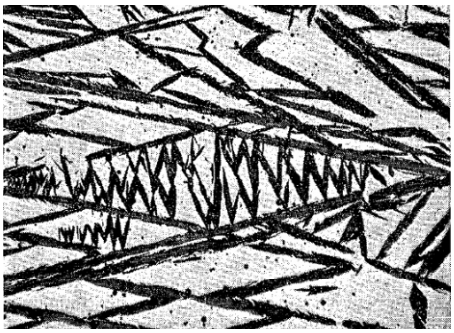

Figure 65. Optical micrograph showing progressive partitioning of the material in a Fe-24%Ni-0.5%C steel (247). Martensite appears black; austenite light grey. The micrograph refers to 33% fraction transformed.

The second case is representative of time dependent continuous propagation of transforming regions in the material. For this condition, the transformation is controlled by time dependent growth of martensite areas driven by the availability of driving force for the transformation, which determines the velocity of the martensite / austenite interface (see paragraph 2.8).

In the following, the reasoning is applied to interpret a series of transformation curves reported in the literature.

3.4.2. $\{2\ 5\ 9\}_\gamma$ *lenticular martensite*

In this paragraph, selected works (100) (247) (320) which reported time dependent formation of lenticular martensite are described. The works in (100) (247) (320) are chosen because of being the most systematic investigations of the kinetics of lenticular martensite formation available in the literature.

In (100), lenticular martensite was formed at sub-zero Celsius temperature in a series of iron-nickel-carbon alloys. The martensite formation was observed to start as a single burst, which transforms a large part of the material, followed by controlled transformation upon continuous cooling (Figure 66).

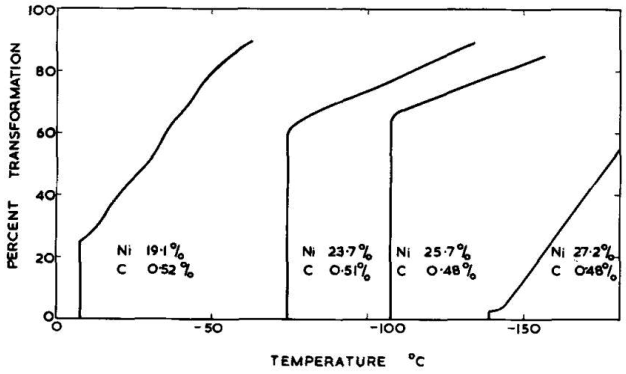

Figure 66. Martensite formation versus temperature reported for different Fe-Ni-C alloys. The transformation is observed to suddenly start at different temperatures with a burst, which transforms a large portion of the material into martensite. Continuous cooling after the burst results in progressive continuous increase of the fraction of martensite. For the Fe-19.1%Ni-0.52%C material, a series of accelerations and deceleration is observed (184).

According to (100), the martensite transformation after the initial burst was dependent of the cooling rate (i.e. was time dependent) and may show a behavior that is defined *irregular*, probably referring to the series of accelerations and decelerations in the transformation rate reported in Figure 66 for Fe-19.1%Ni-0.52%C steel. However, the dependence of the cooling rate was *not* shown in (100), while it is claimed to be well established after (248).

In (247), the martensite formation in a series of iron-nickel-carbon based alloys forming lenticular martensite was followed at sub-zero Celsius temperature during cooling and subsequent isothermal holding. It was reported that martensite formation during cooling occurred in terms of a series of bursts, which appears as multiple transformation steps (Figure 67). Bursts were claimed to be followed by time dependent transformation during continuous cooling, but time dependent martensite formation was *not* shown.

Moreover, according to (247), the multi-step transformation evolved into a continuous transformation (Figure 67) during the transformation (i.e. for larger fraction transformed). In this condition, bursts were smoothened into a series of *waves*. This behavior is referred to as *unusual*. Unusual behavior was particularly evident when the carbon content was reduced (Figure 68). The *waves* in (247) correspond to the *irregular* transformation according to (100).

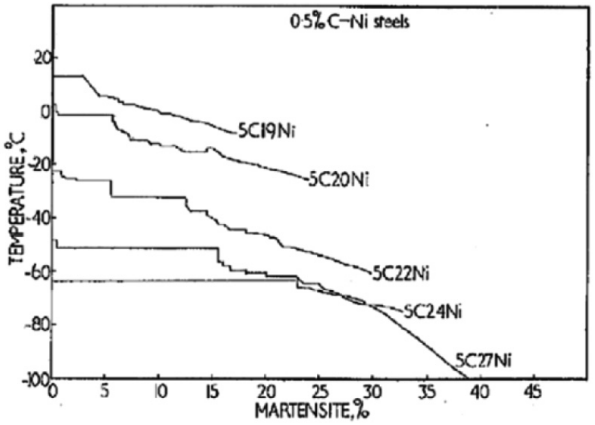

Figure 67. Martensite formation versus temperature reported for different Fe-Ni-C alloys. The transformation is observed to suddenly start at different temperatures with a burst, which transforms a large portion of the material into martensite. A series of bursts is reported at the beginning of the transformation. Thereafter, continuous cooling results in a progressive continuous increase in the martensite content. The numbers in the graph refer to the carbon content ($5 \times 0.1\% wt.$) and the Nickel content ($(X \times 1\% wt)$) (247).

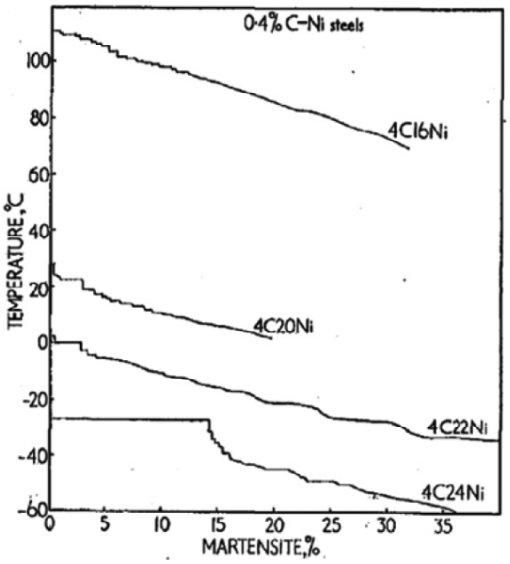

Figure 68. Martensite formation versus temperature reported for different Fe-Ni-C alloys. The transformation is observed to suddenly start at different temperatures with a burst, which transforms a large portion of the material into martensite. A series of smoothened bursts are reported during continuous cooling. The numbers in the graph refer to the carbon content ($5 \times 0.1\% wt.$) and the Nickel content ($(X \times 1\% wt)$) (247).

Time dependent martensite formation on cooling was shown in (320) (Figure 69). Initially, martensite formation was observed to start with a burst and to continue during cooling; the transformation showed a series of accelerations and decelerations and the transformation path was a function of the cooling rate. Time dependent martensite formation was observed also during isochronal heating and isothermal holding at different temperatures ranging from 5 to 117 K (Figure 70 and Figure 71). Clearly, the maximum transformation rate occurs at about 100 K for samples held below 100 K, irrespective of the holding temperature.

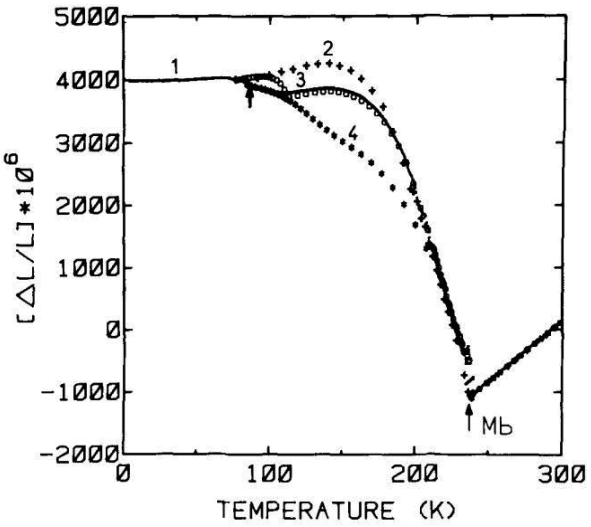

Figure 69. Sample elongation versus temperature during isochronal cooling. thermal holding at 77K. During cooling, martensite formation results in an expansion of the sample, which is counteract from thermal shrink. M_b indicates the temperature where martensite formation is first observed and takes place in a form of a burst (320).

In relation to martensite formation during isothermal holding, in (247), it was claimed that, when a cooling rate in the range of 100 K/min was applied, the transformation was observed to continue during isothermal holding after cooling. For a slower cooling, no isothermal transformation was observed. The isothermal transformation curves are named *isothermal tails* (see for example (232)).

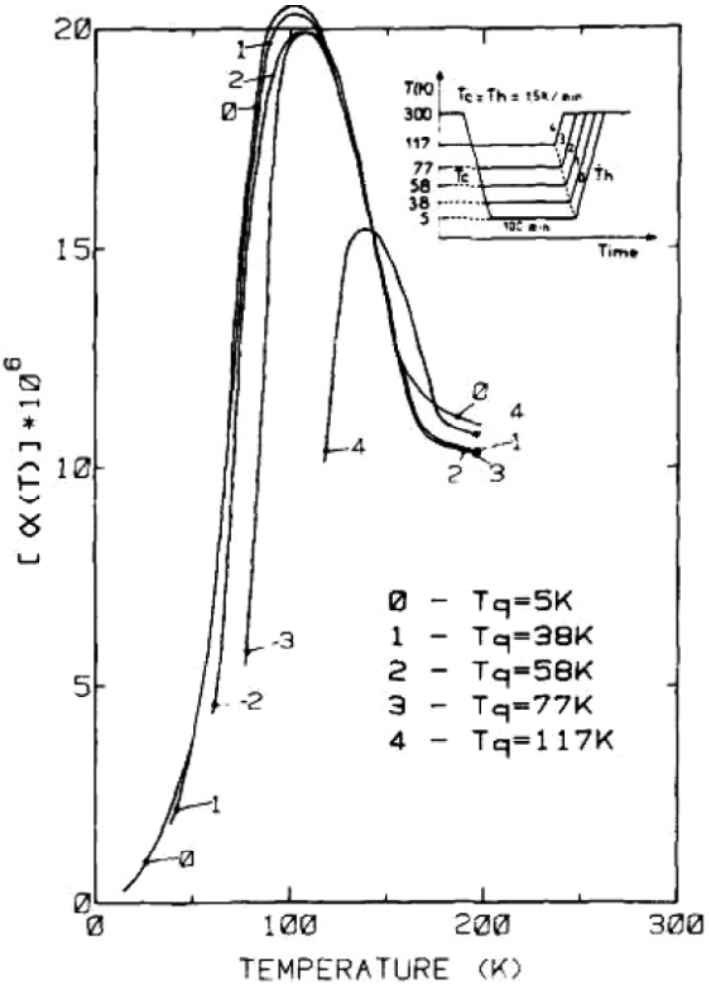

Figure 70. Sample elongation differentiated and plotted versus temperature during isochronal heating following controlled cooling at 1.5K/min to different temperatures. The peak is representative for the maximum transformation rate and occurs at about 100 K for the sample undercooled below 100 K. Martensite formation on reheating is a clear demonstration of thermal activation (320).

A dependence of the degree of transformation on the cooling rate, the observation of isothermal tails and martensite formation on reheating are clear experimental evidence of thermally activated, time dependent martensite formation of lenticular martensite in steel.

Isothermal tails have been extensively reported in the literature, for example in (60) (63) (232) (320). The mechanism responsible for the observation of isothermal tails remains *not*

clarified. In particular, the isothermal tails reported in (320) (Figure 71) are of significance. These isothermal tails were obtained during isothermal holding a Fe-19.1%Ni-0.51%C steel at 77 K, after isochronal cooling of the material at different rates (Figure 69). It was reported that the isothermal kinetics is function of the cooling rate.

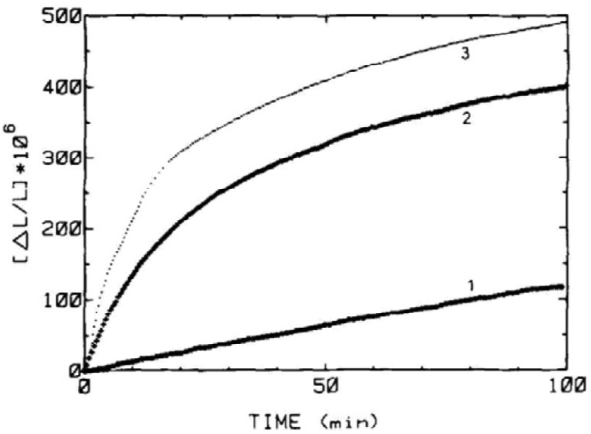

Figure 71. Sample elongation versus time during isothermal holding at 77K. Since the formation of the b.c.c. / b.c.t. crystal structure from f.c.c. iron is associated with an expansion of the material, the elongation of the sample is interpreted as an indication of martensite formation. The numbers in the graph refer to the cooling rate applied to reach the isothermal holding temperatures: 1, 0.15K/min; 2, 1.5K/min; 3, 33K/min (320). The isothermal part of the transformation is the larger the faster the cooling.

Following the currently accepted description that growth of lenticular martensite is *in*dependent of time (after (120)), i.e. nucleation controlled transformation, time dependent transformation curves in (100) (247) (320) can only be interpreted in terms of time dependent nucleation of martensite. In a nucleation controlled description, isothermal martensite formation results from time dependent spontaneous nucleation of martensite embryos possessing $\Delta G_{critical}$ larger than ΔG^* at the temperature of isothermal holding (i.e. 77 K). If a slow cooling rate is applied, a part of these embryos may be able to trigger martensite formation in new areas during cooling, hence increasing the fraction of martensite formed prior to the isothermal holding step, but at the same time reducing the intensity of the isothermal tail. However, this mechanism is inconsistent with the experimental data in (320). The dependence of the isothermal kinetics on the cooling rate shown in Figure 71 does not result from a partial suppression of the transformation on cooling (see arrow in Figure 69).

In the present text, consistent with the rationalization of the literature reported in paragraph 2.4.5, data in (100) (247) (320) is interpreted in terms of athermal formation of thin plate martensite that results in one / several bursts (Figure 66 and Figure 67, respectively), followed by (mainly) thermally activated, time dependent, growth into a lenticular shape, which results in a continuous transformation rate and in martensite formation during cooling, isothermal holding and reheating.[54]

This process is responsible for the initial observation of multi-step martensite formation which evolves into *waves* for larger fractions transformed. This evolution is a consequence of both a reduced effect of each instantaneous burst (i.e. because of progressive partition of the material) and a larger number of growing nuclei (i.e. which results in a stronger smoothening of the steps).

Finally, the work in (320) indicates that martensite formation is controlled by a balance between driving force for the transformation and thermal energy: the increase in driving force promotes martensite formation during cooling (Figure 66, Figure 67) and defines $f_{\alpha'_{max}}$ (Figure 69); the availability of thermal energy rate-control martensite formation at low temperature. The balance between driving force and thermal energy results in a maximum transformation rate during (re)heating (Figure 70), where martensite nucleated at temperatures too low to support their evolution into lenses are allowed to grow.

In conclusion, several works in the literature indicate that the formation of lenticular martensite is time dependent. Time dependent martensite formation in terms of time dependent nucleation of martensite appears inconsistent with a few observations in the literature. The rationalization reported in paragraph 2.4.5, leads to the conclusion that time dependent behavior results from time dependent evolution of thin plates into lenticular morphology.

In the following, a series of "wavy" transformation curves reported in the literature for different ferrous systems is presented. The transformations leading to reproducible smoothened multi-step transformation curves are hereby defined as *abnormal* after (298).

---

[54] Note that time dependent growth can yield a continuation of martensite nucleation in terms of autocatalytic nucleation assisted / induced by progressive thickening of lenticular martensite.

3.4.3. $\{2\ 2\ 5\}_\gamma$ *plate martensite*

In this paragraph, a transformation curve which was reported in (247) is presented. As far as the author´s is aware, the work in (247) is the only one in the literature where *abnormal* transformation behavior was reported for {2 2 5 } martensites.

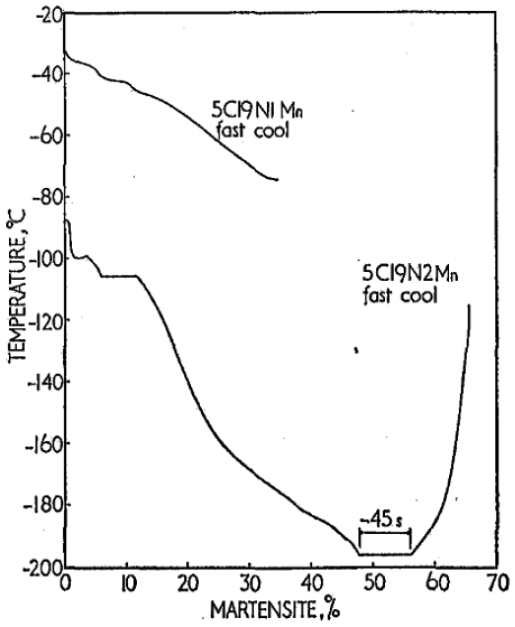

Figure 72. Martensite formation versus temperature reported for different Fe-Ni-C-Mn alloys. Martensite formation is reported on cooling, isothermal holding and reheating. A series of smoothened bursts are reported during continuous cooling. The numbers in the graph refer to the Carbon content ($5 \times 0.1\%wt.$) *and the Nickel and Manganese contents* ($X \times 1\%wt.$) *(247).*

As compared to iron-nickel-carbon systems, which generally develop $\{2\ 5\ 9\}_\gamma$ lenticular martensites and were extensively investigated in (247), in the present case, the nickel content was reduced and partially replaced by chromium and manganese, in order to generate {2 2 5 } martensite.[55] The product of the transformation was butterfly martensite (see paragraph 2.4.2).

[55] As discussed in paragraph 2.4.1, manganese and Chromium both promote a rotation of the habit plane towards $\{1\ 1\ 1\}_\gamma$.

According to (247), when chromium and manganese were added, the burst appeared smoothened and the time dependent part of the transformation was more evident. The transformation curves recorded during cooling, isothermal holing and reheating a Fe-0.5%C-19%Ni-1%Mn and Fe-0.5%C-19%Ni-2%Mn are reported in Figure 72. The transformation curves in Figure 72 can be interpreted consistently with the previous paragraph. The formation of twinned plates, which is *in*dependent of time, is responsible for the sharp near horizontal transformation steps; continuous growth of slipped martensite areas is responsible for thermally activated, time dependent martensite formation during cooling, isothermal holding and reheating and for smoothening of the transformation steps into *waves*.

Note that butterfly martensite does not partition the material during the transformation (compare Figure 73 with Figure 65). Consequently, the continuity of the transformation rate during the transformation cannot be interpreted in terms of reduced size of burst for larger fractions transformed.

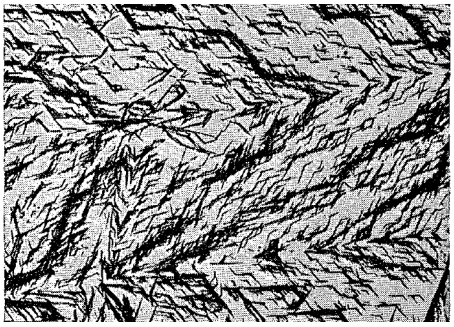

Figure 73. Optical micrograph showing butterfly martensite in Fe-0.5%C-19%Ni-1%Mn for 30% martensite transformation (247).

3.4.4. Lath martensite / bainitic ferrite

In this paragraph, a transformation curve which was reported in (321) is presented (Figure 74). The work in (321) is the only work in the literature where abnormal transformation was claimed for lath martensite.

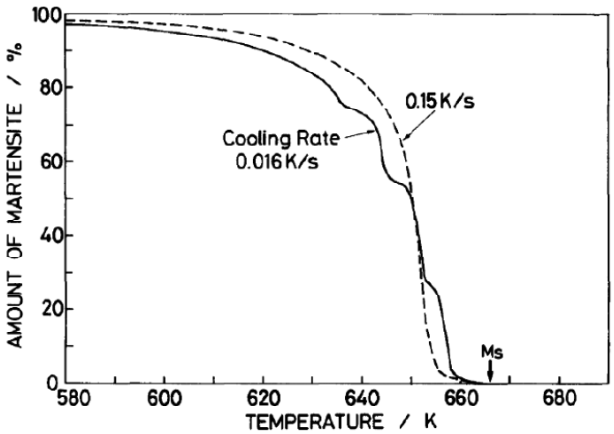

Figure 74. Martensite formation versus temperature reported for a Fe-15%Ni alloy cooled at different rates (321). Clearly, martensite / bainitic ferrite formation is time dependent. However, the fraction of the transformation is mainly determined by temperature, suggesting that the driving force controls the transformation.

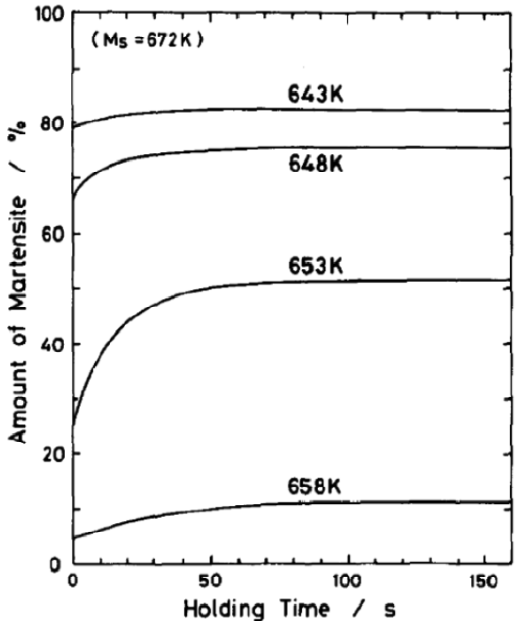

Figure 75. Isothermal tails recorded during isothermal holding of Fe-15%Ni alloy at different temperatures after isochronal cooling 0.2K/min (321). The transformation, reported versus time, was shown to start during cooling (i.e. the fraction transformed at $t = 0$ is not zero) and increases during isothermal holding.

However, later work in (322) (293) pointed out on the basis of the temperature interval where the transformation was observed, that the transformation discussed in (321) was most likely of bainitic type rather than martensitic. If this is indeed the case, abnormal martensite formation for lath martensite has never been reported.[56]

According to (321), the observation of abnormal transformation results from time dependent martensite formation. In (321), a series of isothermal tails is reported to corroborate the conclusion. Note that, as concluded in chapter 2, time dependent formation of lath martensite and bainitic ferrite is well-established.

Abnormal behavior for bainitic ferrite transformation has not been reported anywhere else.

3.4.5. Abnormal behavior in $\gamma \rightarrow \alpha$ massive ferrite formation

The most systematic investigation of multi-step controlled $\gamma \rightarrow \alpha$ transformations reported in literature refers to massive ferrite formation (298) (324) (325) (326) (327). The present paragraph describes the work in (298) (324) (325) (326), dealing with Fe-2.26at.%Mn, Fe-1.79at.%Co, 99.98wt% Iron and an Fe-0.005wt%N alloy.

In (298) (324) (325) (326), the $\gamma \rightarrow \alpha$ transformation was followed by dilatometry during isochronal cooling at different rates (Figure 76a). It was observed that ferrite formation suddenly starts at a certain temperature, which was the lower the faster the cooling. Moreover, the transformation rate showed a series of transformation maxima, which were larger and shifted to lower temperature the faster the cooling (Figure 76b). The maxima are all sharp maxima, but the last one (i.e. the second transformation peak in Figure 76b, the third in Figure 77).

In (298) (324) (325) (326), it was shown that the number of transformation rate maxima was independent of the cooling rate and similarly independent of the cooling rate was the

[56] Actually, new research (323) showing smoothened bursts (referred to as "unusual behavior") in lath martensite transformation was submitted for publication at the time the present text is written.

position of the sharp maxima versus fraction transformed (i.e. the sharp maxima always occurred at specific values of fraction transformed - Figure 77).[57]

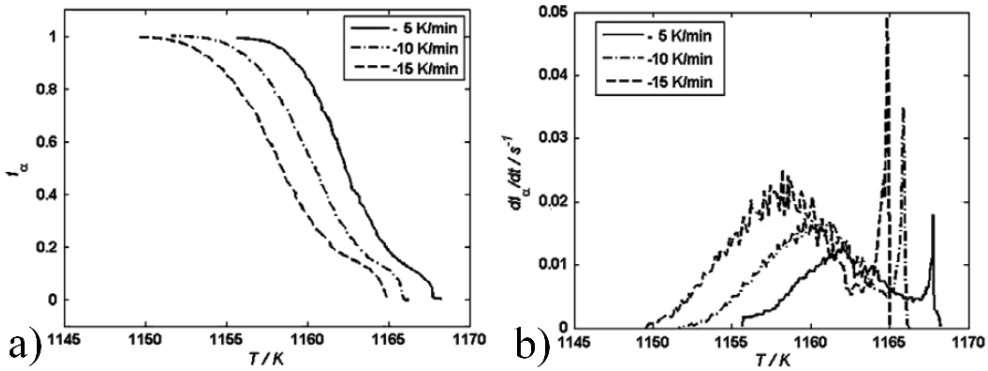

Figure 76. a) Massive ferrite formation during isochronal cooling. The transformation was shifted to lower temperatures the faster the cooling and showed abnormal behavior. b) The occurrence of a multi-peak transformation is readily visible from the transformation rate plotted versus temperature.

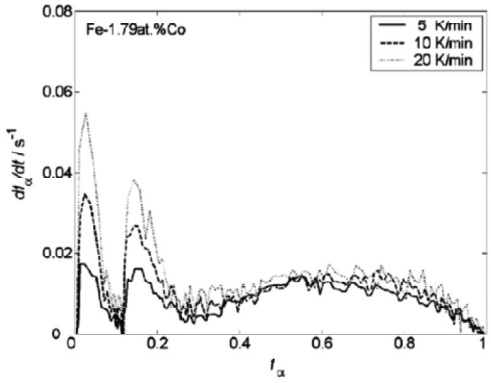

Figure 77. Example of multiple rate maxima reported for massive ferrite transformation in a Fe-1.79at.%Co alloy. The transformation shows three rate maxima positioned at specific values of the fraction transformed irrespective of the cooling rate.

[57] To emphasize that the independence of the rate maxima on the cooling rate was reported only for the investigation in (297) (323) (324) (325), where the γ → α transitions were recognized to be *interface-controlled*, and not in (326), where a *diffusion controlled* regime is included.

According to (170), the observation that the position of the sharp maxima versus fraction transformed is independent of the cooling rate and that the transformation rate increases with the cooling rate, both indicate athermal transformation. The last transformation peak results instead from thermal activation. According to (326), the transformation curves for massive ferrite formation can be described as follows.[58]

During initial cooling, the material is completely austenitic (Figure 78a). At the beginning of the transformation, ferrite nucleates at several locations and each nucleus starts to grow (Figure 78b). The strain energy which is introduced *locally* in the system, because of the volume misfit between ferrite and austenite, promotes autocatalytic nucleation of ferrite in front of the ferrite to austenite interface (Figure 78c). Autocatalytic nucleation results in a strong acceleration of the transformation and stops when the strain energy, introduced in the system, *averaged* over the whole sample, equals $\Delta G^* - \Delta G(F_S)$, with F_S ferrite start temperature. The interruption of nucleation results in a decrease of the transformation rate.

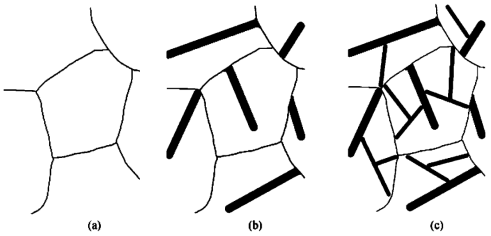

Figure 78. Schematic mechanism for abnormal austenite to massive ferrite formation according to (326): a) initial austenitic state; b) nucleation of ferrite in several places in the material; c) autocatalytic nucleation ahead of the moving austenite to ferrite interface (325).

Consistently with the observation of lower F_S temperatures for faster cooling, hence increasing $\Delta G^* - \Delta G(F_S)$, autocatalysis was the larger the faster the cooling. It follows that the observation of higher maxima (i.e. faster transformation rate) the faster the cooling was clarified.

The mechanism described for a single sharp peak, applies for multiple accelerations and decelerations, where each increase in the transformation rate results from autocatalytic nucleation of ferrite, promoted *locally* by the misfit energy, and each decrease of the

[58] The reader is referred to (170) (326) for a detailed description of the analysis.

transformation rate is a consequence of the misfit energy *averaged* over the whole sample reaching the value $\Delta G^* - \Delta G(F_S)$. Note that this mechanism is athermal in the sense that the *averaged* degree of transformation in the specimen is controlled by the availability of driving force only and *not* because of the transformation being *in*dependent of time. The transformation is indeed time dependent, as illustrated by the dependence of its transformation curve (and microstructure (170)) on the cooling rate.

The concept that the *average* degree of transformation in the sample is determined by $\Delta G^* - \Delta G(F_S)$ is equivalent to the presence of a temperature range $\mathrm{F_S} \rightarrow \mathrm{F_f}$ for the transformation (in absence of relaxation phenomena which promote the transformation reducing the strain energy in the system). Interestingly, the observation of none / one or more sharp maxima was observed to depend on the prior austenite grain size and on the ability of ferrite to growth to a relevant dimension prior to consuming the available energy for the transformation $\Delta G^* - \Delta G(F_S)$ (170).[59]

After one or multiple sharp peaks, a broad thermally activated peak was observed. This part of the transformation was claimed to be controlled by the mobility of the interface only, which is thermally activated. However, surpisingly, the interface moved in the material at a velocity which remained constant during the transformation process was estimated to be effectively *in*dependent of the cooling rate. This could be a direct consequence of progressive "consumption" of $\Delta G^* - \Delta G(F_S)$ by the transformation process, which maintains an about constant effective driving force, i.e. the difference between $\Delta G^* - \Delta G(F_S)$ and the misfit strain energy in the system constant. According to (324) (specifically table 2 in (324)), this value is of the order of $0.1\ J/mol$ independent of the analyzed system.[60]

Finally, the broad last maximum results because of progressive reduction of the fraction of austenite in the material while, according to (326), nucleation did *not* occur during this stage of the transformation.

---

[59] Note the similarities of the description introduced for the growth of massive ferrite with the description according to (142) presented for martensite blocks (and bainitic ferrite sheaf) discussed in paragraph 2.7.4.
[60] Data in (324) refers to for 50% fraction transformed.

3.5. Reconciliation of the mechanisms for the different γ → α transformations

In the last two sections, a series of connections between the different γ → α diffusionless and diffusive interface-controlled transformations were pointed out. The most relevant connections are summarized below.

Firstly, it has been shown that not only martensite, but also massive ferrite and bainite start to form at a temperature which is in good approximation independent on the cooling rate during a continuous cooling experiment (see paragraph 3.3.3).

Secondly, the transformation curves for the different γ → α transformations were reported to show comparable features, like smoothened transformation steps, which can be explained in terms of partially athermal, partially thermally activated transformation mechanisms (see section 3.4).

Thirdly, the γ → α transformations appear controlled by the misfit strain energy between γ and α phases. On the one side, the misfit strain energy *locally* promotes autocatalytic nucleation; on the other side it *macroscopically* determines the maximum fraction of α which can form in the sample.

These similarities suggest a rationalization of the γ → α transformations driving in particular to the understanding of two features: the observation of transformations plateaus in CCT and $T - \dot{T}$ diagrams; the existence of a temperature range for the occurrence of the transformation.

3.5.1. Observation of transformation plateaus in CCT and $T - \dot{T}$ diagrams

In a CCT diagram, the temperatures where the different products are first detected are plotted versus time for a series of cooling curves. These temperatures forms the series of plateau in $T - \dot{T}$ diagrams. Assuming autocatalysis as a necessary condition for the observation of γ → α transition, the plateaus in CCT and $T - \dot{T}$ diagrams represent the temperature where autocatalysis occurs first.

It appears that two conditions are necessary for autocatalysis to proceed: a sufficiently large driving force to compensate for the strain energy of a unit of α which is thick enough to assist the formation of a coupled variant (i.e. block, sheaf, or ferrite needle)[61]; a sufficient time for the α unit to reach such a critical dimension. When these two conditions are met, a transformation plateau is obtained. On the other hand, if the cooling rate is too fast to allow time dependent growth, the subsequent plateau is encountered at a lower temperature, where ΔG^* is sufficient to compensate for the higher value of strain energy associated with a different transformation mechanism, which however allows a higher mobility of the α to γ interface.

Under this interpretation, the plateaus cannot be horizontal lines in CCT and $T-\dot{T}$ diagrams because, as reported by (298) (324) (325) (326), the transformation is shifted to lower temperatures the faster the cooling. On the other hand, it is noted that the shift in temperature of a few degrees reported in (298) (324) (325) (326) applying high resolution dilatometry, is in the range of the uncertainties in the determination of the transformation temperatures, which was estimated in $\pm 12\ K$ for dilatometers (328) generally applied to determine the CCT and $T-\dot{T}$ diagrams available in the literature.

In conclusion, the transformation plateaus are the result of autocatalytic nucleation and characterizes all the γ → α transformations in steel which do *not* involve long range atomic diffusion.

Finally, the observation of the γ → α transformation at temperatures above the plateau in TTT diagrams is interpreted as a consequence of spontaneous nucleation of several variants, which results in the possibility for the transformation to take place at higher temperatures.

This process is expected to be more gradual as compared to forced nucleation of coupled variants during continuous cooling, hence not resulting in sudden transformation steps.

[61] When a coupled variant is obtained, martensite formation actually reduces the strain energy in the system, so that a relevant amount of transformation can occur.

3.5.2. Existence of the $M_S \rightarrow M_f$ temperature range

The existence of the $M_S \rightarrow M_f$ temperature range is equivalent to the existence of a $F_S \rightarrow F_f$ range described for massive ferrite. When martensite forms, it introduced a certain amount of strain energy in the system, which stabilizes austenite; a larger undercooling is necessary to increase $\Delta G^* - \Delta G(M_S)$ and to allow a continuation of the transformation.

So far, no direct experimental evidence of mechanical stabilization of the austenite due to the misfit strain energy term introduced during the transformation has been presented in the literature. Moreover, calculation of the misfit strain energy introduced in the system during martensite formation has *not* been reported.

A very rough estimation can be introduced on the basis of data calculated for massive ferrite in (324). It is noted that the calculated misfit strain energy introduced in the system is of about the same order of magnitude as the strain energy extrapolated at zero fraction transformed which, following paragraph 2.5.2, equals $\Delta G(M_S) - \Delta G(T_0)$. Provided that the analysis in (324) is correct and apply the reported observation to martensite transformation, it is roughly expected $M_S - M_f \sim T_0 - M_S$.

4. Materials and methods

4.1. Materials

4.1.1. Fe-12%Ni-0.6%C model alloy

The iron-nickel-carbon system was initially considered for the investigation of martensite formation at sub-zero Celsius temperature in high carbon steels.

The chemical composition of the material was tailored to obtain martensite with lenticular morphology and a M_S temperature in the range of 223 K to 373 K. A content of 0.8wt% carbon was selected on the bases of Figure 15. The influence of nickel and carbon on M_S was estimated from literature data (45). Three different nickel content, 11wt%, 14wt%, 17wt%, were selected in order to obtain different contents of retained austenite upon austenitization and quench heat treatment.

This temperature range for M_S was considered to investigate martensite formation at sub-zero Celsius after martempering in boiling water and quenching in water at 273 K. Martempering was applied to minimize the presence of thermal gradients in the sample and quench in water at 273 K was applied to obtain a stable microstructure at room temperature for the purpose of material storage.

The material was prepared by the Foundry Institute of Finland (329). The three casts were highly *in*homogeneous, presented high porosity and a carbon content of 0.6wt%, hence lower than expected.

The investigation of martensite formation in iron-nickel-carbon model alloys was soon abandoned because of poor reproducibility.

4.1.2. Fe-1.6%Cr-1%C commercial bearing steel

The investigation of martensite formation during sub-zero Celsius treatment in high carbon steels was continued with the use of commercial steel grade 100Cr6 (AISI 52100), which was chosen because of the high reproducibility and homogeneity generally required for bearing

steels and for the possibility to retain a large part of the austenite after austenitization and quench. The material used in the present work was a Ø 10 mm rod, supplied as extruded. The chemical composition is given in Table 2.

Table 2. Chemical composition of the steel 100Cr6 determined with Glow Discharge Optical Emission Spectroscopy (GDOES - Horiba Jobin Yvon GD2) given in wt%.

Fe	C	Cr	Ni	Si	Mn	Mo	Cu
Bal.	0.96	1.60	0.10	0.13	0.28	0.05	0.15

According to (63), industrial recommendations for heat treatment indicate austenitization at 1133 K for 1.8 ks, followed by oil quench at 393 K and tempering at 423 K for 7.2 ks. This heat treatment results in the retention of about 0.3wt%C in primary carbides and a certain amount of retained austenite.

In contrast with the recommended heat treatment, the material was austenitized at higher temperatures with the purpose to dissolve all carbides in austenite as to exclude their influence on martensite formation. Two austenitization processes were chosen: 1323 K for 0.9 ks, followed by martempering at 413 K for 0.18 ks and air quench (condition 1323-900); 1353 K for 60 s followed by martempering at 413 K for 20 s and air quench (condition 1353-60).

During high temperature heat treatment, oxidation was prevented by protecting the material with austenitic stainless steel grade X5 CrNiMo 17-12 (AISI 316). The samples were embedded in-between two 3 mm thick plates and 4 layers of 0.03 mm thick foils, for conditions 1323-900 and 1353-60, respectively.

4.1.3. Fe-17wt%Cr-7 wt%Ni-1wt%Al commercial Precipitation Hardenable, 17-7 PH, stainless steel

The investigation of martensite formation in 17-7 PH was performed with the purpose of investigating time dependent lath martensite formation at sub-zero Celsius temperatures. This steel grade is low Carbon and was selected to minimize thermal stabilization phenomena. The material used in the present work is a 17-7 PH, 0.15 mm thick foil, supplied by Goodfellow Cambridge Ltd (330), as rolled. The chemical composition of the material is reported in Table 3.

The chemical composition of 17-7 PH is adjusted to bring out a partially austenitic, partially martensitic, microstructure upon air quenching to room temperature after

austenitization. Accordingly, 17-7 PH is classified as semi-austenitic precipitation hardenable stainless steel.

Table 3. Chemical composition of the steel 17-7 PH (in wt%) determined with Energy Dispersive Spectroscopy, EDS. The Carbon content was measured with a LECO-CS230 Carbon analyzer. The chemical composition is according to standard specification (331).

Fe	C	Cr	Ni	Al	Mn	Si
Bal.	0.09	17.3	7.3	0.8	0.7	0.5

The standard heat treatments for 17-7 PH are described in (331): the material for fabrication is provided solution heat treated at 1339 ± 14 K or cold rolled at mill. Austenitization treatment of the fabricate is normally performed at 1228 ± 9 K for 0.6 ks, followed by air cooling. The full potential in terms of mechanical properties for the steel is obtained as a consequence of a fine precipitation of intermetallic compounds after complete transformation into martensite and martensite tempering, which is performed in the temperature interval 783-838 K, (332).

Complete martensite transformation into martensite in as-quenched 17-7 PH steel can be induced mechanically during metal forming, which is the as-receive state for the present work, or by increasing the driving force for martensite formation with further undercooling at sub-zero Celsius temperature (331) (332). According to standard heat treatment specifications, the latter is performed by cooling the material to 200 ± 9K, followed by isothermal holding at this temperature for 28.8 ks. This treatment is conveniently performed at the sublimation temperature of carbon dioxide (i.e. 194 K).

The occurrence of isothermal martensite formation in 17-7 PH was first suggested in (331) and can be inferred from (332) (specifically Fig. 32 in (332)), where ultimate tensile strength and 0.2% yield strength are reported as a function of time and temperature of sub-zero Celsius storage. However, a direct proof of the occurrence of isothermal martensite formation in 17-7 PH stainless steel grade has so far *not* been reported in the literature.

4.1.4. Fe-17%Cr-4%Ni commercial Precipitation Hardenable, 17-4 PH, stainless steel

The investigation in PH 17-4 was performed with the purpose to investigate time dependent lath martensite formation at temperatures above room temperature and compare the results with the sub-zero Celsius investigation, which was performed in 17-7 PH. The material

used in the present work was a Ø 20 mm rod, supplied as extruded. The chemical composition of the material is reported in Table 3.

Table 4. Chemical composition of the steel PH 17-4 (in wt%) determined with Energy Dispersive Spectroscopy, EDS. The Carbon content was measured with a LECO-CS230 Carbon analyzer. The chemical composition is according to standard specification (331).

Fe	C	Cr	Ni	Si	Mn	Nb	Cu
Bal.	0.06	15.9	4.6	0.5	0.6	0.2	3.2

The chemical composition of 17-4 PH is adjusted to bring about a fully martensitic structure after quenching to room temperature from the austenitizing temperature. Accordingly, PH 17-4 is classified as martensitic precipitation hardenable stainless steel.

The standard heat treatments for 17-4 PH are described in (331): according to specification, austenitization treatment is performed at 1339 ± 14 K for 1.8 ks, followed by air cooling (331). The temperature interval for martensite formation is indicated in 405 K to 305 K for M_S and M_f, respectively. The full potential in terms of mechanical properties for the steel is obtained after complete transformation into martensite and martensite tempering in the temperature interval 783-838 K, as a consequence of a fine precipitation of intermetallic compounds (332).

According to (331), when the transformation is not completed on cooling, it goes to completion during room temperature storage. However, a direct proof of isothermal martensite formation in 17-4 PH stainless steel grade has so far *not* been reported in the literature.

4.2. Vibrating Sample Magnetometry, VSM

4.2.1. Experimental details

Vibrating Sample Magnetometry was performed with a Lake Shore Cryotronics 7407 Vibrating Sample Magnetometer (VSM) equipped with a Janis SuperTran-VP continuous flow cryostat. The VSM equipment supplied by Lake Shore Cryotronics, Inc. is shown in Figure 79. The functioning principles of the equipment are described in the following (333) (334).

During the investigation, cylindrical samples of 3mm in diameter are mounted onto a fiber rod and placed in between two induction coils. Thereafter, an electric current is introduced

into the coils to generate an (ideally) uniform magnetic field in the region where samples are placed.

Figure 79. Photograph of the VSM equipment supplied by Lake Shore Cryonics, Inc. The sample is placed on the top of a non magnetic rod, in between of two induction coils. The motion of the sample generates an electrical signal which is collected and recorded (333).

Samples, magnetized by the application of a magnetic field, are subjected to controlled vertical vibration motion to induce an electric current in pick-up coils because of Faraday's law (63). The current generated in the pick-up coils is proportional to the sample magnetization, to the vibration amplitude and to the vibration frequency. The electric signal, which is modulated and amplified, represents the data collected by the instrument.

In order to establish the proportionality constant, collected data require a calibration. In the present work, calibration is performed with the use of a sample of known magnetization, according to the technical specification reported in (334).

Moreover, under practical conditions, the magnetic field is *not* uniform in the region where samples are placed determining a dependence of the induced current on temperature because of thermal expansion / shrink of the fiber rod, which results in a drift in the position of the sample. In the present work, the effect was corrected measuring a baseline, which was used to compensate for the temperature dependence of the signal.

The possibility for in situ investigation of martensite formation during thermal cycling is obtained with the use of a cryostat.

The sample is placed in the cryostat chamber, where the temperature is continuously monitored. Thermal cycles are performed setting the temperature in the cryostat chamber by a gas flow, which is heated up by means of a 50 Ω electrical resistor and a PID controller. The gas used in the present work is boiling nitrogen (i.e. at 77 K). The functioning of the cryostat supplied by Lake Shore Cryotronics, Inc. is presented in Figure 80.

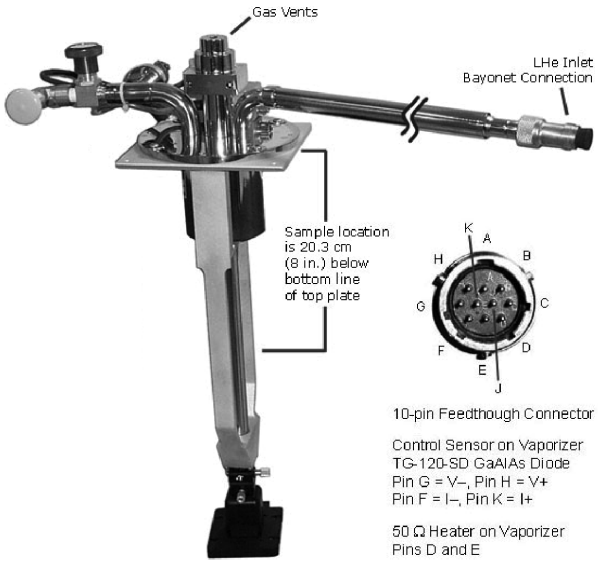

Figure 80. Photograph of the Janis SuperTran-VP continuous flow cryostat. A continuous gas flow is introduced in the chamber of the cryostat and heated by a resistor. The gas flow (at the correct temperature) reaches the sample, which is placed in the center of the chamber, from the bottom and leave the chamber from a gas vent placed on its top. (334)

As the temperature of the sample is not directly monitored, the thermal inertia of the system is of importance. *Thermal inertia* refers to the time delay between chamber cooling / heating and sample cooling / heating (i.e. the time elapsed between the moment when a defined temperature is recorded and the moment when the sample actually reaches that temperature).

The possibility for the sample to follow sudden temperature changes is determined by its thermal mass and by the gas flow, being the inertia the larger, the larger the thermal mass and the lower the gas flow.

The thermal mass is determined by the size of the sample, while the used experimental setup allows to set the gas flow in terms of gas pressure and aperture of an inlet valve. In the present work, the gas pressure is kept at about 5 bar, while the aperture is generally set to obtain 25-35% heating power for the 50 Ω resistor during the performed thermal cycles.

In these experimental conditions, the time delay was estimated from a comparison between a magnetic signal collected in a reference sample during opposite thermal cycling (i.e. signal during cooling versus signal during heating). The time delay was observed to be in the range 10-20 s for 0.2 mm thick samples and in the range 20-40 s for 2 mm thick samples.

For thermal cycles requiring a particularly short time delay, the flow was adjusted controlling the valve aperture manually, in order to minimize temperature overshoot and speed up temperature stabilization.

4.2.2. Quantitative evaluation of the fraction transformed

The VSM technique was applied to quantitatively follow the martensite formation at sub-zero Celsius temperatures. The method presented in the following was applied to the investigation in 100Cr6 and 17-7 PH commercial steels. Quantitative phase analysis is based on the following five assumptions:

1. no transformation takes place during baseline measurement, $M_b(T)$;
2. the temperature dependence of the saturation magnetization relative to the value at a reference temperature T_{ref} is given by $\frac{M_b(T)}{M_b(T_{ref})}$;
3. there is a reference condition where the amount of retained austenite is known and given by $f_{\gamma_{RS}}$;
4. the saturation magnetization M_{RS} of the reference sample at T_{ref} is known;
5. martensite is the only ferromagnetic phase in the sample.

With these assumption, the saturation magnetization of a fully transformed sample at temperature T can be calculated as:

$$M_{\alpha'}(T) = \frac{M_{RS}}{1 - f_{\gamma_{RS}}} \cdot \frac{M_b(T)}{M_b(T_{ref})} \quad [14]$$

where the first term equals the saturation magnetization of a fully transformed sample at T_{ref}, and the second term accounts for the temperature dependence of the magnetic moment at saturation.

Moreover, the fraction of martensite is given by:

$$f_{a'} = \frac{M(t,T)}{M_{\alpha'}(T)} = \frac{\left(1 - f_{\gamma_{RS}}\right) \cdot M(t,T)}{M_{RS}} \cdot \frac{M_b(T_{ref})}{M_b(T)} \quad [15]$$

where $M(t,T)$ represents the saturation magnetic moment measured during the thermal cycle, which is a function of temperature, T, and time, t. Assuming austenite as the only *not* ferromagnetic phase in the sample, the fraction of austenite is:

$$f_\gamma = 1 - f_{a'} = 1 - \frac{\left(1 - f_{\gamma_{RS}}\right) \cdot M(t,T)}{M_{RS}} \cdot \frac{M_b(T_{ref})}{M_b(T)} \quad [16]$$

The method requires to determine $f_{\gamma_{RS}}$ and M_{RS} of the sample at T_{ref}. The $f_{\gamma_{RS}}(T_{ref})$ data were obtained by transmission XRD quantitative phase analysis (see section 4.5). For the steel 100Cr6, the reference state was the content of retained austenite prior to sub-zero Celsius heat treatment, which was different for conditions 1332-900 and 1353-60. For 17-7 PH the as-rolled material was used as reference.

The M_{RS} was established upon measurement of the magnetic moment of the sample with known $f_{\gamma_{RS}}(T_{ref})$ and assuming linear proportionality.

The baseline was obtained fitting experimental data recorded during *ad-hoc* thermal cycles to a second order polynomial. For 100Cr6, the baseline was recorded after material stabilization, applying an additional thermal cycle at the end of the investigation. Baseline recording for 17-7 PH was performed on stable as-rolled material.

Note that, the reference state for 100Cr6 steel grade is internal, since each sample is used as self-reference for the investigation during sub-zero Celsius treatment. The investigation of 17-7 PH instead uses as reference state a sample which is *not* the object of the investigation.

In relation to the sensitivity of the measurement, with the experimental settings used in the present work, [62] a typical signal to noise ratio in the order of 10^5 was typically obtained. This set a resolution limit for the fraction transformed during a single run in the order of 0.01%.

On the other hand, in absolute terms, the uncertainty in quantitative phase analysis is much larger and is determined by a series of factors. The sources of experimental error for quantitative phase analysis differ for 100Cr6 and 17-7 PH as follows:

1. the error connected with the quantification of $f_{\gamma_{RS}}$, which results from limited statists in the XRD quantitative phase analysis, cannot be quantified and is particularly relevant for 100Cr6 material, where a relevant amount of retained austenite is present in the reference state;
2. the error connected with sample mounting / demounting, which is associated with charging of the fiber rod and sample misalignment and, according to (63), equals $\pm 0.7\%$ and does *not* depend of the material;[63]
3. the error associated with baseline recording, which is a function of the applied thermal cycle and instrument alignment and is in the order of $\pm 0.1\%$ per 100 K temperature shift and does *not* depend of the material;
4. The error associated with reproducibility of sample dimensions, which is relevant only in relation to the investigation of martensite formation in 17-7 PH, where the reference state is not the investigated sample itself, and is in the order of $\Delta f_{\alpha'}(t) = \pm 1\% \cdot f_{\alpha'}(t)$.

The sources of error for the temperature determination are mainly associated with thermal inertia of the sample, while the temperature control of the system is within ± 0.5 K.

[62] The reader is referred to (334) in relation to the optimization of the signal quality. The following settings where applied in the present work: time constant 0.1 s; continuous data acquisition; time per point depending on the investigation condition but in the range 0.33 s to 30 s; inlet valve aperture 180 to 230 degrees.

[63] Specifically the error is about $\pm 0.5\%$ of the detection limit of the instrument. Consequently it depends on the ratio between detection limit and actual signal. For a set of experiment performed with 17-7 PH steel, this error was estimated in $\pm 2.5\%$.

4.3. Dilatometry

4.3.1. Experimental details

Dilatometry was performed with a Bähr DIL 805 A/D quenching dilatometer at Rostock University, faculty of Mechanical Engineering and Marine Technology. The instrument settings were established by the colleagues in Rostock University and are not discussed in the present text. The functioning principles of the equipment are described in the following (335).

Samples are 10 ± 0.2 mm long (hollow / full) cylinders, 4 mm in external diameter, which are placed in between two silica pushing rods in the center of an induction coil inside the chamber of the dilatometer. The chamber is evacuated prior to thermal cycling to avoid oxidation. The chamber of the dilatometer supplied by Bähr is shown in Figure 81.

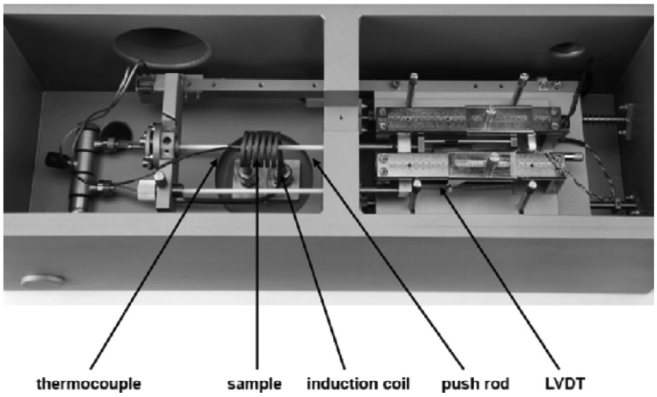

Figure 81. Photograph of the chamber of Bähr DIL 805 quenching dilatometer (336). The sample is placed in between two pushing rods. The position of the right pushing rod, which is determined by the sample length represents the collected and recorded data.

The elongation of samples during the investigation is monitored from the displacement of the pushing rod, which is measured by a Linear Variable Differential Transducer (LVDT) with a resolution of about 50 nm. The resolution of the LVDT sets the resolution of the dilatometer in the order of $5 \cdot 10^{-6}$ (i.e. $\frac{50 \cdot 10^{-9}\ m}{10 \cdot 10^{-3}\ m}$).

The temperature of investigated samples is monitored with a thermocouple, which is spot welded onto the sample surface prior to mounting. The temperature during thermal cycling is

adjusted by the counterbalancing effect of heating power supplied by the induction coil and a cooling power supplied by an inert gas flow. In the present gas helium was used as inert gas.

4.3.2. Quantitative evaluation of the fraction transformed

Dilatometry was applied to quantitatively follow the martensite formation in PH 17-4 commercial steels. The analysis is based on the assumption of isotropic phase transformation. Data were collected in a series of one thousand points per thermal step.

The atomic fraction of martensite was calculated following paragraph 3.3.2. Mathematically:

$$f_{\alpha'}(T,t) = \sum_i \left(\frac{3\cdot\left(\frac{l_i - l_{i-1}}{l_0} - f_{\alpha' i-1}\cdot\lambda_{\alpha'}(T)\cdot(T_i - T_{i-1}) - \left(1 - f_{\alpha' i-1}\right)\cdot\lambda_\gamma(T)\cdot(T_i - T_{i-1})\right)}{\varepsilon_0(T)_i} \right) \quad [17]$$

where $f_{\alpha'}(T,t)$ is the fraction transformed, $\frac{l_i - l_{i-1}}{l_0}$ is the measured length change per data point, $f_{\alpha' i-1}$ is the fraction transformed calculated for the data point $i-1$, $\lambda_{\alpha'}(T)$ the linear expansion coefficient of martensite, $\lambda_\gamma(T)$ the linear expansion coefficient of austenite, $(T_i - T_{i-1})$ the temperature change per data point and $\varepsilon_0(T)_i$ the transformation strain.

The linear expansion coefficient of austenite was extrapolated from experimental data obtained for pure austenite in the temperature interval 613 to 413 K and obeys:

$$\lambda_\gamma(T) = (15.2 + 0.0035 \cdot T\,[K]) \cdot 10^{-6}[K^{-1}]. \quad [18]$$

The linear expansion coefficient of martensite $\lambda_{\alpha'}(T)$ was assumed $11.8\cdot 10^{-6}[K^{-1}]$ (see APPENDIX C).

The value of $\varepsilon_0(T)_i$ was calculated according to paragraph 3.3.2 from experimental data of austenite and martensite lattice parameters at room temperature. Measurements were performed by transmission XRD (see section 4.5) using a 17-7 PH with a $f_{a'} \approx 0.08$.

The value of the lattice parameter were:

$$a_{\alpha'}(T = 300\ K) = 2.868\ \mathring{A} \quad [19]$$

$$a_{\alpha'}(T = 300\ K) = 3.596\ \mathring{A} \quad [20]$$

For PH 17-4 steel grade measurement was not possible, because of complete transformation into martensite after austenitization and storage at room temperature. It was obtained:

$$\varepsilon_0(T) = 1.51\% - (10.2 + 0.01 \cdot T\ [K]) \cdot 10^{-6} \cdot (T[K] - 300) \quad [21]$$

In relation to the sensitivity of the measurement, the resolution of the equipment and the value of the transformation strain set the sensitivity in the order of 0.1% (i.e. $\frac{3\cdot(5\cdot10^{-6})}{2.3\cdot10^{-2}} \sim 10^{-3}$).

4.4. Electron backscatter Diffraction, EBSD

4.4.1. Introduction to diffraction and EBSD

In a diffraction experiment, coherent radiation (i.e. a beam of particles / an electromagnetic wave with a defined direction, energy and phase) is directed towards a crystalline material. The radiation interacts with the periodic arrangement of atoms in the crystal and is scattered elastically or inelastically (i.e. the radiation conserves its energy or loses a part of its energy).

As a consequence of interference of radiation elastically scattered by atoms at different positions in the crystal structure, specifically by atoms in a set of parallel crystal planes, intensity maxima (constructive interference) and intensity minima (destructive interference) occur. The pattern of intensity maxima is the diffraction pattern, which yield information on the crystal structure. On the other hand, inelastic scattering results in a part of the energy which is transferred to the sample and a part of the radiation which is absorbed during its interaction with the material.

The intensity of a radiation is attenuated when it traverses a distance in a substance according to $I = I_0 \cdot exp(-\mu(E) \cdot z)$, with I_0 intensity of the incident radiation, z traversed distance, $\mu(E)$ energy dependent absorption coefficient. The absorption of the radiation determines the information depth of the diffraction technique which is defined as the distance yielding $\frac{I}{I_0} = 1 - 1/e$, with e Euler's number.

Constructive interference of elastically scattered radiation occurs only at specific scattering angles, 2θ, from the incident beam, which are defined by the energy of radiation and the interplanar distance according to:

$$sin(\theta) = \frac{hc}{E} \cdot \frac{1}{2 \cdot d(hkl)} \qquad [22]$$

where h is Planck's constant, c is the speed of light, E is energy of the radiation and d is the interplanar distance (337). [64]

Diffraction techniques allow to investigate the crystalline structure of a material recording its diffraction patterns. Among diffraction techniques are: neutron diffraction; X-ray diffraction and electron diffraction. In the following, EBSD is described according to (84) (339) (340) (341).

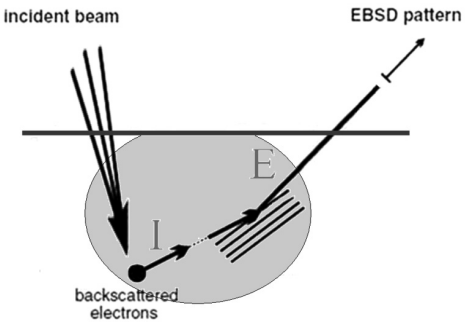

Figure 82.Schematic representation of the principles for EBSD. The incident electron beam interacts with the atoms in the crystalline sample. A part of the radiation, I, is inelastically back-scattered by the atoms towards the sample surface. The part of inelastically back-scattered electrons that are subsequently subjected to elastic scattering by a set of parallel crystal planes, E, generate the Kikuchi pattern (after (341)). The interaction volume is schematically represented with a grey area.

EBSD makes use of an electron backscatter diffraction pattern, the Kikuchi pattern, which is generated by the part of the incident radiation escaping from the sample surface after being subjected to an inelastic (back-) scattering event followed by an elastic scattering event (Figure 82).

[64] The energy of a particles and of an electromagnetic wave is $E = \frac{hc}{\lambda} = mv^2$, with λ wavelength of the electromagnetic waves, m mass of the particles and v velocity of the particles (338).

A Kikuchi pattern is shown in Figure 83 and appears as a series of bands with characteristic wideness and reciprocal orientation, which depend on crystal planes, angles between crystal planes (i.e. the crystal structure) and interplanar distances. The position of the lines in diffraction pattern depends on the crystal orientation. Consequently, a Kikuchi pattern for a given crystal is determined by the crystal structure as well as by the orientation of the crystal with respect to the measurement geometry.

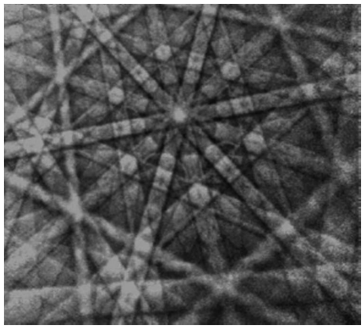

Figure 83 Example of a backscatter Kikuchi pattern (341). In a Kikuchi pattern, the information about the crystal structure is contained in the band width and pattern geometries / symmetries; the position of the angular diffracted pattern indicates the orientation of the crystal.

The region of the sample where the signal is collected from is the *interaction volume* of the radiation, which defines the resolution limit and the information depth of the technique. The resolution limit and the information depth decrease the smaller the angle between sample surface and electron beam. The relative orientation between the sample surface and the incident beam also determines the yield of radiation which escape from the sample surface. The yield increases the smaller the angle between sample surface and incident beam.

In EBSD, the best compromise between electrons yield and resolution / penetration depth, which results in the best quality for the electron diffraction pattern, is obtained tilting the samples 70° about the direction of the beam (i.e. for setting an angle of 20° between sample surface and incoming beam).

At 70° tilting, the penetration depth of electrons for the energies generally applied in EBSD (i.e. about 15 KeV to 18 KeV) is in the order 20-30 nm for iron based materials; consequently, EBSD is a surface sensitive technique.

The resolution limit for the technique is also in the range of a few tens of nm. Due to the 70° tilting the resolution is asymmetric and in iron based materials is about 30 nm in the direction parallel to the tilt axis and 90 nm perpendicular to the tilt-axis.

To summarize, EBSD is an electron diffraction technique which allows to assess the crystal structure and the crystal orientation of the sample in the close surface region with a depth resolution and a lateral resolution in the order of a few tens of nm.

4.4.2. Experimental details

The EBSD system is composed by an hardware to acquire the data and software to analyze the data. The EBSD technique is performed in a Scanning Electron Microscope, SEM. A general description of an EBSD system is reported in Figure 84.

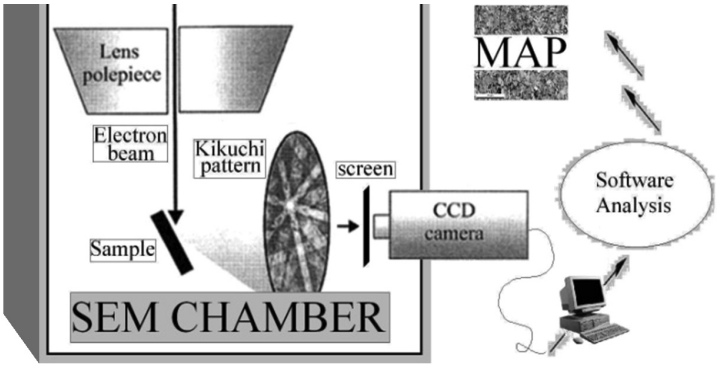

Figure 84. Schematic representation of the EBSD system. The diffraction pattern is detected on a transmission phosphor screen and recorded with a sensitive CCD camera. After background subtraction, the patterns are analyzed with the use of software (according to (341)).

EBSD measurements were carried out at the Technical University of Denmark, the Center of Electron Nanoscopy, DTU-CEN. The investigation was performed in a dual beam FEG-SEM FEI Helios Nanolab 600 SEM equipped with an EBSD system from EDAX-TSL and a Hikari camera. Calibration of the EBSD camera was performed by the colleagues at DTU-CEN and is not discussed in the present text. The OIM TSL 6.1 software was used to analyze the EBSD results.

All measurements were performed with an electron probe current of 11 nA at an acceleration voltage of 18 kV; samples were tilted 70° about the direction of the beam. The scan areas and the step size were chosen on the basis of the dimension of the microstructural features under investigation.[65]

In the present work, EBSD was applied to investigate ex situ martensite formation in 17-7 PH and 17-4 PH stainless steel. Investigation of 17-7 PH material was performed setting the scan areas to 80 µm × 80 µm and the step size to 80 nm. Investigation of 17-4 PH material, was performed setting the scan areas to 150 µm × 150 µm and the step size to 150 nm. In both cases the step size was larger than the physical resolution of the technique, hence determining the actual resolution.

4.5. X-Ray Diffraction, XRD

4.5.1. Principles of XRD

In XRD, X-Ray radiation is used to investigate crystalline materials. XRD is performed either using conventional X-Ray tubes, where X-Rays are produced from bombardment of a metal anode by electrons, or at synchrotron facilities, where high-intense X-Rays are obtained by high-energy electrons accelerated in a storage ring. In the following, XRD is described according to (342) (343). The description refers to polycrystalline materials.

In XRD, the diffraction pattern is generated by the part of the incident radiation which escaped from the sample surface after being subjected to an elastic scattering event. In an elastic scattering event, the radiation is "reflected" by (the atoms arranged in) a set of parallel crystal planes with the scattering angle, 2θ. The normal to the scattering planes is defined scattering vector, s_V.

In the generally applied geometry, the incident beam reaches the surface of the material under investigation under the angle θ and is diffracted under the same angle, implying that s_V is

[65] The parameters for software analysis are not discussed in the present work. It is mentioned that the parameters were set to maximize indexing of the crystal structure (i.e. give a solution with confidence index > 0.1 in the largest number of acquisition points).

parallel to the surface normal. In this set-up, only lattice plane parallel to the surface contribute to diffraction (Figure 85).

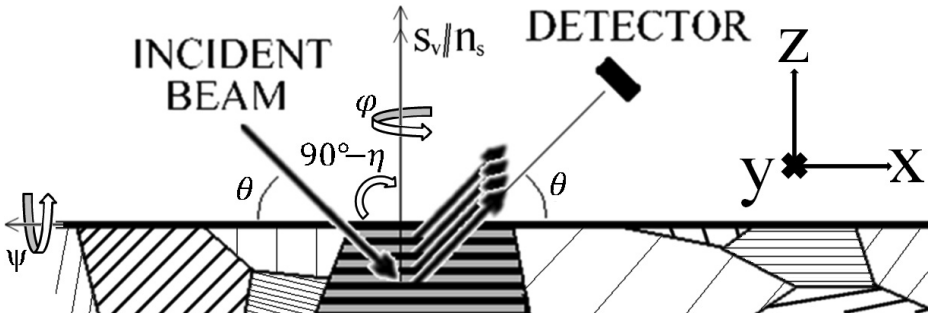

Figure 85.Schematic representation of the principles for XRD. Incoming radiation is diffracted by a set of parallel atomic planes. The scattered radiation forms a diffraction pattern which is collected by a detector. The description refers to symmetric XRD in absence of tilt along the axis, where the scattering vector, s_V, is parallel to the sample normal, n_S. Only crystallographic planes parallel to the surface contribute to diffraction. Differently oriented planes can be brought into a diffraction condition by a change of the measurement geometry.

The distribution of intensity maxima in the diffraction pattern gives indication on the crystal structure of the material. The scattering angle, 2θ, or the energy value, E, yielding intensity maxima in the diffraction pattern gives information on the interplanar distance (see Eq. 22).

In angular dispersive XRD, an (ideally) monochromatic (i.e. with a defined energy) radiation is used, and the diffraction pattern is recorded versus scattering angle 2θ (see Eq. 22) by moving the scattering arrangement during the recording of the pattern. For a fixed radiation, different sets of parallel crystal planes, (hkl), with different interplanar distances, $d(hkl)$, yield intensity maxima in a diffraction pattern at different scattering angle, θ. Tthe energy of the applied radiation determines their absolute position on the angular scale.

In energy dispersive XRD, white radiation (i.e. distributed in energy) is used and the scattering arrangement is kept constant (i.e. the detector, the sample and the beam are all fixed) and determines the position of the reflections in the energy scale. In energy dispersive XRD, the position of the reflections in the energy scale are a function of the scattering angle 2θ, which is kept constant during the experiment.

For both techniques, different sets of crystal planes yield diffraction maxima with different intensity, $I(hkl)$. The intensity of the diffraction maxima is proportional to the number of atoms which contribute to the diffraction signal (i.e. the number of atoms which compose a crystalline phase multiplied the number of equivalent sets of crystal planes) and is a function of the type of atoms responsible for scattering (i.e. the chemical composition of the phase), the scattering angle and the investigation temperature.

The number of equivalent sets of crystal planes leading to diffraction is referred to as multiplicity factor, $m(hkl)$. The effect of chemical composition, scattering angle and temperature can be predicted according to three factor named *atomic scattering factor,* $f_0\left(X_{Fe,Ni,C,Cr,\dots}, \theta\right)$*, Lorentz polarization factor,* $LP(\theta)$, and *Debye-Waller factor,* $DW(\theta, T)$, which are calculated theoretically.

XRD is a direct technique sensitive to phase transformations involving a modification of the crystal structure. Moreover, phase transformation can be followed from the quantitative point of view by recording various diffraction peaks for the constituting phases and comparing the experimentally measured intensities to those predicted for an ideal polycrystalline sample (i.e. a powder (344)).

However, for a specific measurement geometry, only a few crystallites meet the conditions for diffraction (consider Figure 85). Consequently, a large number of grains ($>10^4$) must be irradiated in order for the diffracted intensity to be statistically reliable for quantitative phase analysis.

Furthermore, the material can present a preferential orientation of the crystallite (i.e. texture), which result in not correct estimation of the phases fraction when only a single scattering arrangement or few crystal reflections are recorded.

In an additional application, XRD is used to analyze the presence of residual stresses in the sample (see paragraph 4.5.4). In the evaluation of residual stresses ψ-geometry is generally applied.

In ψ-geometry, an angle Ψ is obtained between the scattering vector and the normal to the sample surface by tilting the sample, either along the plane defined by the incident and diffracted

beams,(tilt defined by an angle $90° - \eta$), or along the plane perpendicular to the plane where the beam lies perpendicular to the sample surface, (tilt defined by an angle ψ).

It is noted that, on the other hand, the rotation of the sample around the normal to its surface (defined by an angle φ) does *not* affect the measurement geometry (Figure 85).

4.5.2. Experimental details

In the present work, all XRD experiments were performed at the synchrotron facility HZB-BESSY II at the experimental stations MagS (345) and EDDI (346). The radiation at MagS and EDDI is delivered by a superconductive 7 Tesla multipole wiggler in form of a energy spectrum (i.e. X-Ray show an energy distribution) given in (347).

At the experimental stations MagS and EDDI, different experimental setups are applied: at EDDI, energy dispersive XRD is used; at MagS, XRD is angular dispersive.[66]

At Mags, a monochromatic beam of 12.4 KeV is obtained with the use of a monochromator and Bragg-Brentano geometry (symmetric and with $\Psi = 0$) is applied. Consequently, the movements of the sample and the detector during the acquisition of the diffraction pattern correspond to θ and 2θ, respectively. The applied radiation correspond to an information depth of 11μm (absorption data from (349)).

At EDDI a scattering angle $2\theta = 8°$ was initially applied. Thereafter, $2\theta = 20°$ was considered to obtain information from more crystal reflections, loosing however in resolution. To reduce sample heating because of the energy transferred by the beam, a low energy X-Ray stopper of several mm graphite was inserted in the primary beam. It is emphasize that the energy range yielding good diffraction patterns at EDDI is 15 KeV to 65 KeV corresponding to an information depth of a few tens up to several hundreds μm.

Note that, in energy dispersive XRD, the intensity maxima associated with the different sets of crystallographic planes, are recorded simultaneously during the investigation; this is *not* the case for angular dispersive XRD during θscans. Unfortunately, a cryostat for in situ

[66] For further experimental details on the XRD at the synchrotron facility HZB-BESSY II at the experimental stations MagS and EDDI, the reader is referred to (347) (348).

investigation was available only at MagS station at the time this work is performed. This aspect suggested the minimum acquisition time per diffractogram as top priority during settings of the acquisition parameters.

The cryostat applied at MagS was a Beryllium dome, which was evacuated during the experiments. The temperature is recorded by a thermocouple placed in thermal contact with the copper holder where the sample is placed. The temperature is controlled by the opposite effect of the compressor and of an electrical resistor.

All instrumental calibrations were performed by the colleagues at the synchrotron facility and are not discussed in the present work.

4.5.3. Quantitative evaluation of the fraction transformed

Synchrotron XRD was applied to quantify the atomic fraction of martensite and retained austenite in the sample. The analysis was performed for Fe-12%Ni-0.6%C model alloy and 100Cr6 commercial steel.

Quantitative phase analysis is based on the following assumptions: (i) martensite and austenite are the only phases present; (ii) the austenite and martensite grains are randomly oriented; (iii) the number of grains which contribute to the diffracted intensity is statistically reliable. The following relationships apply:

$$R = m(hkl) \cdot |F_0(f_0, hkl)|^2 \cdot n^{-2} \cdot DW(\theta, T) \cdot LP(\theta) \cdot \mu(E)^{-1} \cdot (E)^{-3} \quad [23]$$

$$f_\gamma = \frac{1}{1 + \frac{R_\gamma}{R_{\alpha'}} \cdot \frac{I_{\alpha'}}{I_\gamma}} \quad [24]$$

$$f_\gamma = 1 - f_{\alpha'} \quad [25]$$

where R (i.e. $R_{\alpha'}$ and R_γ) is theoretical integrated intensity (calculated for a powder sample), $|F_0(f_0, hkl)|^2$ is the structure factor, n is the number of atoms per unit cell, $I_{\alpha'}$ and I_γ are the measured integrated intensity of the diffraction peaks fitted to Lorentian / Gaussian / pseudo-Voigt functions. In particular:

- the doublets of b.c.t. martensite, which is fit as two separate peaks, was assigned to a single position on the angular scale corresponding to its centroid;
- $m(hkl)$ for f.c.c. and b.c.c. crystals are tabulated in (344); for b.c.t. was calculated summing up the multiplicity factors of the doublet of martensite;
- For f.c.c. crystals $|F_0(f_0, hkl)|^2 = 0$ when h, k, l are all odd or even; $|F_0(f_0, hkl)|^2 = (n \cdot f_0)^2$ otherwise;
- For b.c.c. crystals $|F_0(f_0, hkl)|^2 = 0$ when $h + k + l$ is even; $|F_0(f_0, hkl)|^2 = (n \cdot f_0)^2$ otherwise; martensite was approximated by b.c.c. in the calculation of $|F_0(f_0, hkl)|^2$;
- f_0 was calculated by linear interpolation among the tabulated $\frac{sin(\theta)}{hc} \cdot E$ in (350);
- $LP(\theta)$ is reported in (342) (344);
- the temperature factor contained in $DW(\theta, T)$ was assumed to be linearly dependent on temperature and equal to 0.71 at 296K (344);
- $\mu(E)^{-1}$ was given by the colleagues at EDDI experimental station and is also tabulated in (350).

4.5.4. Evaluation of residual stresses

Residual stresses indicate the stresses which are present in a sample in absence of applied mechanical forces. Consequently, equilibrium of forces imposes that residual stresses balance over the sample thickness (i.e. there is a balance between stresses at different position and concentrated in different phases). In the following, residual stresses evaluation is described according to (351) (352). However, a different notation is introduced to comply with the description given in the present text.

The determination of residual stresses with XRD relies of the determination of lattice strains, $\varepsilon_{\varphi\psi}$, which are obtained from the lattice spacing $d_{\varphi,\psi}(hkl)$ measured at sample tilting angles φ, ψ in comparison with a strain-free lattice parameter $d_0(hkl)$.

Residual stresses are distinguished in micro-stresses, which vary over sub-grain distances, and macro-stress, which vary continuously along different grains. Micro-stresses result in both broadening and shifting of the diffraction peak in the diffraction pattern while macro-stresses result in peak shift only. In the following, the discussion is limited to peak shift, which was

considered in the present work to determine the macro state of stress in the austenite. Residual strains which result in peak shifting are obtained as:

$$\varepsilon_{\varphi,\psi} = \frac{d_{\varphi,\psi}(hkl) - d_0(hkl)}{d_0(hkl)} \quad [26]$$

with $d_0(hkl)$ strain free lattice interplanar spacing, which is defined by chemical composition and crystal structure of the phase in unconstrained conditions. Defining a sample coordinate system, (x, y, z), like shown in (Figure 85), and $\psi = \Psi$, it holds:

$$\begin{aligned}\varepsilon_{\varphi,\psi} = {}& ½S_2{}^{(hkl)} \cdot sin^2(\psi) \cdot \left(\sigma_{xx} \cdot cos^2(\varphi) + \sigma_{xy} \cdot sin(2\varphi) + \sigma_{yy} \cdot sin^2(\varphi) - \sigma_{zz}\right) \\ & + ½S_2{}^{(hkl)} \cdot cos^2(\psi) \cdot \sigma_{zz} + S_1{}^{(hkl)} \cdot \left(\sigma_{xx} + \sigma_{yy} + \sigma_{zz}\right) + ½S_2{}^{(hkl)} \\ & \cdot \left(\sigma_{xz} \cdot cos(\varphi) + \sigma_{yz} \cdot sin(\varphi)\right) \cdot sin(2\psi)\end{aligned} \quad [27]$$

where $½S_2{}^{(hkl)}$ and $S_1{}^{(hkl)}$ are crystallographic planes dependent on X-Ray Elastic Constant, XEC. The XEC applied in the present work were given by the colleagues at EDDI experimental station and are not discussed in the present text. The diffraction elastic constants were taken from the single crystal constants for ferrite (353) and austenite (354) applying the Eshelby/Kröner model (355) (356) for elastic grain interaction. Eq. 27 requires several measurements at different sample orientations in order to determine the whole stress tensor, σ_{ij}.

The problem is generally simplified introducing the following assumptions: (i) biaxial state of stress, which always applies at the sample surface, where stresses along z are easily relaxed, $\sigma_{zz} = 0$, $\sigma_{xz} = 0$, $\sigma_{yz} = 0$; (ii) rotational symmetric state of stress along the sample surface, which applies in absence of a preferential orientation for the stress components, $\sigma_{xx} = \sigma_{yy}$ and $\sigma_{xy} = 0$. Hence, Eq. 27 simplifies to:

$$\varepsilon_{\varphi,\psi} = ½S_2{}^{(hkl)} \cdot \sigma_{//} \cdot sin^2(\psi) + 2 \cdot S_1{}^{(hkl)} \cdot \sigma_{//} \quad [28]$$

where $\sigma_{//} = \sigma_{xx} = \sigma_{yy}$ is the stress along the sample surface. Under these assumptions, $\sigma_{//}$ is the only unknown component of σ_{ij} and can be evaluated from the slope of $d_{\varphi,\psi}(hkl)$ plotted versus $sin^2(\psi)$, provided that $S_1{}^{(hkl)}$ is known.

Clearly, the simplified analysis does *not* apply when a triaxial state of stress exists. For example, an hydrostatic state of stress would lead to $d_{\varphi,\psi}(hkl) \neq d_0(hkl)$ together with the observation of no slope in the $d_{\varphi,\psi}(hkl)$ versus $sin^2(\psi)$ plot.

5. Results

5.1. The martensitic transformation and its effect on the stress state in austenite

5.1.1. Investigation of Fe-12wt%Ni-0.6wt%C model alloy

The reader is referred to the manuscripts included as APPENDIX A and APPENDIX B at this point of the text.

The investigation performed with Fe-12wt%Ni-0.6wt%C model alloy indicates that synchrotron XRD at BESSY II at the MagS experimental station can be applied to detect in situ martensite formation with a sensitivity close to 0.1% fraction transformed with time sampling of a few minutes. Also, results show that quantitative phase analysis with VSM requires a calibration method (see paragraph 4.2.2).

In regard to the martensitic transformation, in spite of the presence of large compositional *in*homogeneities in the material, which do *not* allow definitive conclusions on the transformation process, the following indications were put forward: (i) the transformation requires a certain undercooling with respect to quenching / storage temperature to (re)start; (ii) the transformation is (partially) thermally activated; (iii) a state of compression builds up in austenite during the transformation.

These indications are further investigated applying XRD and VSM techniques to martensite formation at sub-zero Celsius temperature in a 100Cr6 commercial steel.

5.1.2. Investigation of as quenched 100Cr6 commercial steel: condition 1323-900

Austenitization at 1323 K for 900 s of 100Cr6 steel fully dissolves carbon in the austenite. The microstructure is dual phase containing martensite and retained austenite; no carbides were present in the microstructure. Martensite has lenticular morphology and partitions the austenite grains (Figure 86).

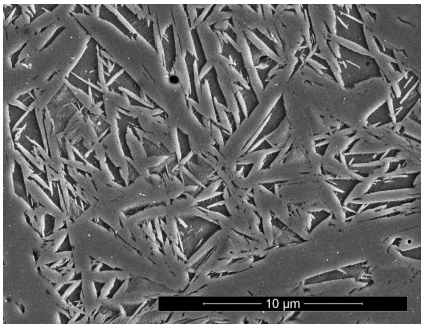

Figure 86. Micrograph showing the microstructure of the material in condition 1323-900; SEM, secondary electron image, electro-etching with A2 Struers electrolyte, applying a potential of 30V for 40 s: small regions of retained austenite are embedded in between the lenses of martensite.

It is emphasize that the XRD investigation on material in condition 1323-900 suffered from poor grain statistics, because the intensity of the austenite reflections varied about 10% for different sample positions. The grain size of the prior austenite grains was in the order of a few tens of micrometers (Figure 87). This limitation was overcome averaging the results obtained at different sample locations.

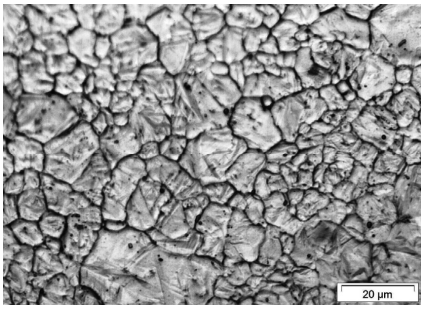

Figure 87. Micrographs showing the appearance of the material in condition 1323-900 at the surface: prior austenite grain boundaries and surface relieves generated by surface martensite are visible. Light Optical Microscopy.

5.1.3. The state of stress in retained austenite during sub-zero Celsius martensite formation

The investigation of Fe-12wt%Ni-0.6wt%C model alloy (APPENDIX A, APPENDIX B) suggests that the formation of martensite at sub-zero Celsius temperature builds up a state of compression in the retained austenite.

The work in APPENDIX D, which refers to 100Cr6 material in condition 1323-900, shows a series of experiments that were conducted to assess if sub-zero Celsius martensite formation builds up a state of compressive stress in austenite and if this state of stress is (mainly) hydrostatic or presents relevant deviatoric components.

In particular, the measurement of the strain-free lattice parameter of austenite and the proof of build-up of (mainly) hydrostatic compressive state of stress was obtained with a *sample slicing* method that has *not* been reported in the literature yet.

The reader is referred to the manuscript reported as APPENDIX D at this point of the text.

As follows from (176) (177), the result in APPENDIX D is relevant for the thermodynamics of the transformation, since hydrostatic pressure stabilizes austenite against martensite formation. The thermodynamic effect of the state of compression introduced in austenite by the martensitic transformation is taken into account in the description of the kinetics of martensite formation in APPENDIX E.

5.1.4. The effect of the state of stress on the kinetics of martensite formation at sub-zero Celsius temperature

The main propose of the activity described in APPENDIX E was to investigate the kinetics of the martensite formation and to deepen the understanding of the relationship between XRD results and magnetometry measurements.

APPENDIX E reports abnormal kinetics of martensite formation on isochronal cooling; also it shows that the martensite formation rate is continuous upon interruption of the cooling step and continuation of the transformation on isothermal holding.

The experimental data in APPENDIX E is interpreted by describing the kinetics of the transformation in terms of a-thermal spontaneous nucleation and thermally activated growth, which induces / assists autocatalytic nucleation.

The thermodynamic effect of the state of compression in austenite during martensite formation is introduced in the analysis and yields a consistent explanation for the observation of abnormal transformation of austenite into lenticular martensite.

The reader is referred to the manuscripts reported as APPENDIX E at this point of the text.

5.1.5. Additional experimental data

Magnetometry – Sub-zero Celsius investigation

In the following, additional experimental data for the material austenitized at 1323 K for 900 s are reported. For these additional experiments, the storage time at room temperature was about 2 Ms (3 weeks) versus 4 Ms (6-7 weeks) storage time at room temperature which was applied to the material prior to the sub-zero Celsius investigations presented in APPENDIX D and APPENDIX E.

After storage at room temperature, all samples were subjected to isochronal cooling at a rate of 0.5 K/min to a predefined temperature and thereafter held for 7 h at this temperature. After isothermal holding, each sample was isochronally (re)heated at 1.5 K/min. All samples are named after the temperature (in K) of isothermal holding.

The evolution of martensite formation in the samples was followed in situ by magnetometry. Quantitative phase analysis was performed as described in APPENDIX E and taking as initial content of martensite a value of $f_{\alpha'} = 0.633$. Figure 88 report the results of quantitative phase analysis and is intended for a direct comparison with Figs. 2 and 3 in APPENDIX E.

Figure 88 shows that austenite is initially stable on cooling. After a certain degree of undercooling, the transformation restarts at a temperature, $M_{(re)s} = 245$ K (Figure 88a). Thereafter, martensite formation continues during isochronal cooling and occurs in association with a multi-step mechanism, defined abnormal (APPENDIX E).

The temperature where the transformation first restart (i.e. $M_{(re)s} = 245$ K) is higher than $M_{(re)s} = 240$ K reported in APPENDIX E. Evidently, the shorter storage time applied in the present investigation (i.e. 2 Ms) as compared to the storage time applied in APPENDIX E (i.e. 4 Ms) resulted in a 5 K lower undercooling for martensite formation. Moreover, it is observed that the overall transformation of austenite into martensite is enhanced in the present

case. These two observations are interpreted in terms of thermal stabilization of retained austenite during room temperature storage (319), which is larger for samples stored 4 Ms.

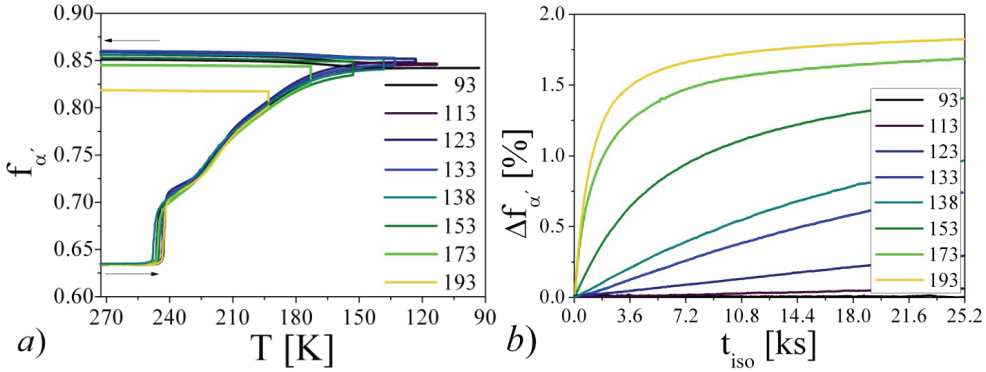

Figure 88. Magnetometry investigation: a) Molar fraction of martensite $f_{\alpha'}$ plotted versus temperature T. b) Isothermal martensite formation platted versus time of isothermal holding t_{iso}. Samples are named after the temperature of isothermal holding (in K).

In Figure 88b, isothermal martensite formation is reported. All investigated isothermal holding temperatures are lower than the temperature region where abnormal behavior is observed on isochronal cooling. Consequently, no anomalies like the one reported in APPENDIX E for sample 223 and 233 are expected. Consistently, isothermal martensite formation is the larger and the faster, the higher the temperature of isothermal holding.

Martensite formation is observed also during (re)heating the samples isothermally held at temperatures below 173 K (Figure 88b). The maximum transformation rate during reheating is in the temperature interval 160–170 K, in agreement with the data reported in APPENDIX E.

Figure 89 shows the transformation rate versus time and is intended for a direct comparison with Fig. 6 in APPENDIX E. From Figure 89, abnormal martensite formation is clearly observed. The transformation rate is reported to be continuous upon interruption of the isochronal cooling step, while its derivative versus time is *not* continuous. The transformation suddenly decelerates faster when the cooling step is interrupted at $T > 173\,K$, while the transformation is favored by the interruption of the cooling step for $T < 173\,K$. These results are consistent with those included in APPENDIX E.

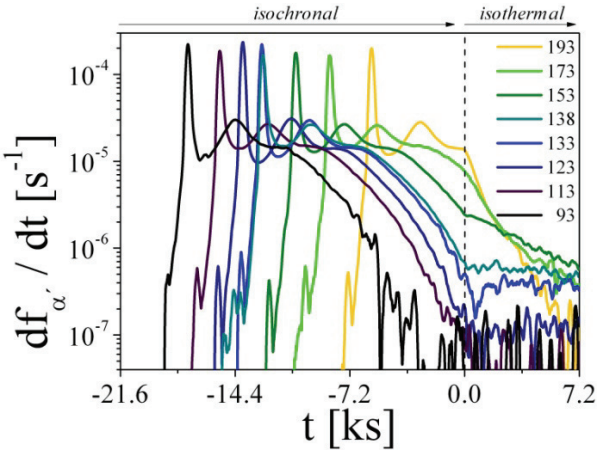

Figure 89. Transformation rate df_{γ}/dt (calculated within 480 s time intervals) plotted versus time t. Data is presented relative to the beginning of the isothermal step (defining $t = 0$), consequently negative time values apply in the isochronal cooling step.

XRD – in situ investigation of the different stages of tempering

APPENDIX E shows in situ martensite formation at sub-zero Celsius temperature during cooling, isothermal holding and (re)heating.

The sub-zero Celsius thermal cycle was reported in APPENDIX E: after cooling at 0.5K/min to different temperatures, cooling was interrupted and the samples were isothermally held for 7 h at different temperatures. After isothermal holding, samples were reheated at 1.5K/min. For the purpose of the discussion in APPENDIX E, only the sub-zero Celsius investigation is mentioned.

In reality, samples were continuously heated 1.5K/min to 650 K to investigate the tempering response of the material. The thermal cycle down to 93 K was performed twice and interrupted at 300 K during the second tests, in order to have a reference sample for the ex situ investigation (please consider APPENDIX D and Fig. 1b in APPENDIX E).

All collected data are presented in the following. The obtained information should be considered as preliminary results and were confirmed during a more extensive investigation of the tempering stages performed taking condition 1353-60. In particular, data are hereby only shortly described, while the reader is referred to section 5.2 for interpretation and discussion of the results.

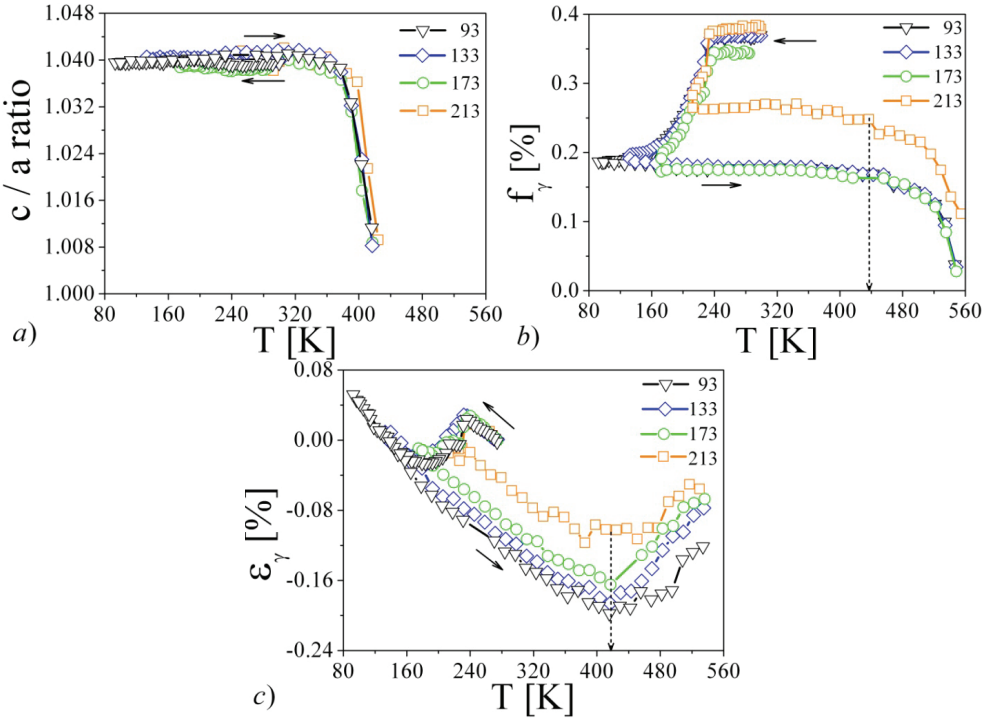

Figure 90. In situ XRD, sample 93, 133, 173 and 213 according to APPENDIX E. a) Tetragonality of martensite (i.e. c/a ratio) versus temperature T. (b) Fraction of retained austenite f_γ normalized to the initial content $f_{\gamma i}$ versus temperature T. (c) Lattice strain ε_γ for austenite versus temperature T corrected for expected thermal expansion / contraction as reported in APPENDIX E.

Figure 90a shows the tetragonality of the b.c.t. unit cell of martensite as measured by XRD. Results were averaged over the 200/002 and the 211/112 reflections. Figure 90a shows that the tetragonality of martensite increases during sub-zero Celsius treatment (compared the value at 273 K). Also, it is observed that the tetragonality is constant during isothermal holding at sub-zero Celsius temperatures. During heating to the tempering region, martensite loses is tetragonality in the temperature interval 350 K to 420 K, irrespective on the applied thermal cycle.

Figure 90b shows sub-zero Celsius martensite formation during cooling, isothermal holding and, for samples 93 and 133, (re)heating. The sub-zero Celsius martensite formation is described and discussed in APPENDIX E. During heating to the tempering region, the

reflections of austenite start to disappear at about 450 K. Austenite is no longer present in the material after heating above 560 K.

Figure 90c shows the lattice strain of austenite corrected for expected unconstrained compression / expansion. The build-up of compressive strain during sub-zero Celsius martensite formation is described in APPENDIX E. During heating to the tempering region, austenite experiences progressive contraction up to about 420 K; where after, a discontinuity is observed at 420 K and a trend toward expansion of the lattice of austenite appears at higher temperature.

Results in Figure 90 are particularly interesting from the technological point of view, because it is indicated that the compressive state of stress which builds up in austenite during the sub-zero Celsius treatment is retained after tempering at relatively low temperature.

5.2. Martensite formation during sub-zero Celsius treatment of 100Cr6 and its effects on tempering

5.2.1. Investigation of as quench 100Cr6 commercial steel: condition 1353-60

Austenitization at 1353 K for 60 s and quenching resulted in a (mainly) dual phase material containing martensite and retained austenite. The presence of primary carbides (Figure 91) was revealed by electron microscopy investigation after tempering and deep Nital etching of the material. Martensite presented lenticular morphology.

It is explicitly mentioned that the austenitization procedure 1353-60 granted excellent grain statistics for the XRD investigation at the synchrotron facility. Consequently, the difficulties which where faced during in situ investigation of the material in condition 1323-900 were overcome applying a different austenitization procedure, i.e. higher temperature and shorter time.

In relation to chemical homogeneity, regions of material enriched in chromium were pointed out by deep Nital etching and appear as lighter macro-areas. Investigation with EDS chemical analysis indicated that the chromium content in this regions is lower than 3wt%

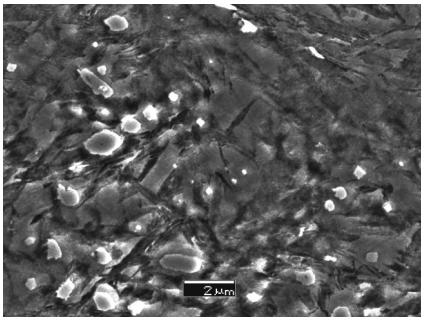

Figure 91. Micrograph showing carbides visualized after deep Nital etching of the material tempered at 463 K for 1h: carbides stand out of the surface and appear lighter than the matrix. The carbides are placed in the regions of retained austenite (relieved regions) being consequently primary.

5.2.2. The evolution of lattice strain in austenite during sub-zero Celsius heat treatment and tempering.

In paragraph 5.1.5, the evolution of lattice strain in austenite during tempering is presented and it is mentioned that the state of compression introduced in austenite during martensite formation is retained after tempering. This point is discussed in APPENDIX G.

The reader is referred to the manuscript reported as APPENDIX G at this point of the text.

5.2.3. The effect ***of martensite formation at cryogenic temperatures and the first stage of tempering.***

APPENDIX G suggests that the formation of martensite at temperatures below say, 140 K, may lead to a modification of the first stage of tempering, yielding an increased and more uniform precipitation of transition carbides. This concept is further investigated in APPENDIX C, APPENDIX F and an additional manuscript entitled "*The effects of cryogenic treatment on the first stage of tempering – The role of the thermal path*", which is in preparation.

The reader is referred to the manuscripts reported as APPENDIX C, APPENDIX F and at this point of the text.

In APPENDIX C it is shown that the first stage of tempering is more pronounced when the material is subjected to a long isothermal holding at cryogenic temperature. The study excludes that this effect results from a modification in the tetragonality of martensite during the

sub-zero Celsius treatment, whereas it indicated that isothermal martensite formation is likely to be the metallurgical process responsible for the modification of the tempering reaction.

The study in APPENDIX F presented the effect of different parameters, like storage time at room temperature, time of isothermal holding at cryogenic temperature, cooling and heating rates applied, on the formation of martensite during sub-zero Celsius treatments. The purpose of APPENDIX F is to establish the experimental condition to prove that martensite formation at cryogenic temperature is the phenomenon responsible for the modification of the tempering reaction.

The manuscript entitled "*The effects of cryogenic treatment on the first stage of tempering – The role of the thermal path",* has the purpose to apply the knowledge acquired from APPENDIX F and is targeted for technical journals. The manuscript will contain a suggestion for consistent classification of sub-zero Celsius treatment as follows:

- For the highest temperature pre-treatment, __/__ as indication of time in h / temperature in K;
- SZ", to indicate that the material was sub-zero Celsius treated;
- "-" used as a separator for different thermal steps;
- "q" for quenching or "c__" followed by the (average) cooling rate in K/h for controlled cooling;
- "/__" followed by the temperature reached during the thermal step;
- "i__" followed by the time in h for isothermal holding;
- "h__" followed by the (average) heating rate in K/h for controlled heating.

As a matter of fact, the lack of a classification drove to often unspecified treatment conditions in several technical articles, which determines the impossibility for a reader to establish the effectiveness of the applied treatments.

All related experimental data which pertain to "*The effects of cryogenic treatment on the first stage of tempering – The role of the thermal path"* are presented in the following. The experimental method is also described.

Five 10 mm high hollow cylinders with outer and inner diameter of Ø 4.0 and Ø 3.6, respectively, were prepared for dilatometry investigation. After preparation, samples were austenitized and stored at room temperature for 2 Ms (condition 1353-60).

Dilatometry was performed during isochronal heating at 1.5 K/min from room temperature to 1173 K. The thermal cycle of interest for the present discussion is up to 650 K, but additional data were collected to check the possibility for future investigations.

Prior to dilatometry investigation, the five cylinders were sub-zero Celsius treated in the VSM cryostat and thereafter additionally stored at room temperature for 2 Ms (consequently, the overall storage time at room temperature was 4Ms for all samples). Sub-zero Celsius heat treatments were as follows:

1. No treatment [AsT];
2. Direct air (nitrogen atmosphere) quench to 123 K, 1 minute holding for temperature homogenization, direct air heating to RT [1000/300-SZ-q/123];
3. Direct air (nitrogen atmosphere) quench to 123 K, isothermal holding 16h, direct air heating to RT [1000/300-SZ-q/123-i16];
4. Controlled cooling 0.15K/min to 123 K (nitrogen atmosphere), isothermal holding 16h, direct air heating to RT [1000/300-SZ-c9/123-i16];
5. Direct air (nitrogen atmosphere) quench to 123 K, (re-heating) 0.15K/min [1000/300-SZ-q/123-h9].

The transformation path followed by the material during these thermal cycles is established in APPENDIX F. Figure 92 selectively presents the result of interest for the present discussion.

Figure 92 shows that all sub-zero Celsius treatments lead to the reduction of the content of retained austenite in the material. However, a relevant amount of martensite formation at temperatures below 140 K is obtained only for sample SZ-q/123-i16 (Fig. Figure 92c).

Evidently, for the mechanism presented in APPENDIX G to be acceptable, the observation of a more pronounced contraction peak during dilatometry investigation as reported in APPENDIX C for the sample soaked long time at 123 K, should be observed only for the sample 1000/300-SZ-q/123-i16.

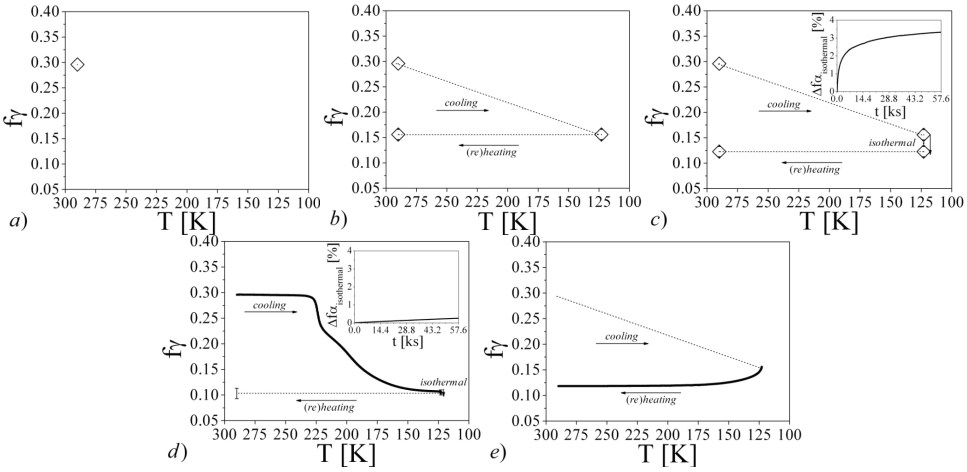

Figure 92. Fraction of retained austenite f_γ plotted versus temperature T for different thermal paths: a) AsT; b) 1000/300-SZ-q/123; c) 1000/300-SZ-q/123-i16; d) 1000/300-SZ-c9/123-i16; e) 1000/300-SZ-q/123-r9. The insets in c) and d) report the isothermal part of the transformation at 123 K.

The dilatometry results during tempering are reported in Figure 93. The temperature region of interest for the present discussion is reported in the inset in Figure 93.

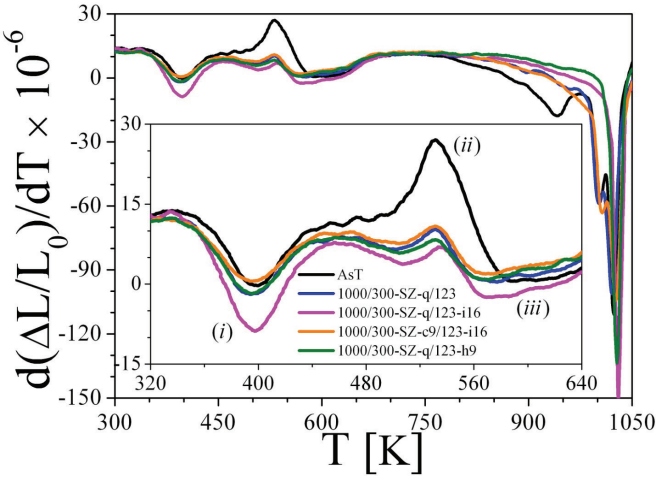

Figure 93. Dilatometry. Relative sample elongation during isochronal heating differentiated with respect to temperature $d(\Delta L/L_0)/dT$ versus temperature T. Precipitation of secondary carbides and formation of cementite are associated with volume reductions, indicated as (i) and (iii), respectively, decomposition of retained austenite induces volume expansion (ii)

Figure 93 appears consistent with the interpretation given in APPENDIX G, APPENDIX C and APPENDIX F and indicates that the isothermal formation of martensite is indeed responsible for a modification of the tempering reaction in high Carbon steels.

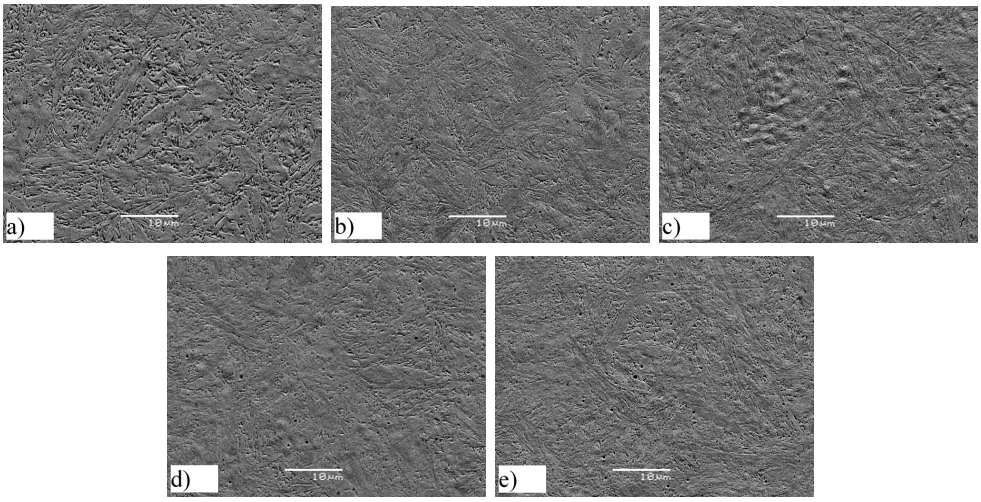

Figure 94. Micrographs showing the microstructure of the material prior to tempering. Secondary Electron Image. Electrolytic etching in Struers A-2 solvent at 30V for 40s: a) AsT; b) 1000/300-SZ-q/123; c) 1000/300-SZ-q/123-i16; d) 1000/300-SZ-c9/123-i16; e) 1000/300-SZ-q/123-r9.

The following additional observations require further experimental investigation and validation to be of scientific interest:

- after tempering 1h in the temperature interval 353 K to 573 K no differences in micro-hardness (Vickers, 500g) are observed between samples 1000/300-SZ-q/123-i16 and 1000/300-SZ-q/123;
- the surface appearance (i.e. color) for samples 1000/300-SZ-q/123-i16 differs after tempering *in air* as compared to all other conditions, where it is invariant of the applied sub-zero Celsius treatment; this observation applies to 1h tempering in the temperature interval 473 K to 523 K;
- a general tendency to lose the primary carbides during polishing and Nital etching is observed for samples 1000/300-SZ-q/123-i16 as compared to all other conditions;
- after electro-polishing, the presence of primary carbides in the material is evident for samples 1000/300-SZ-q/123-i16 only (Figure 94);

- the thermal path followed during sub-zero Celsius treatment has a relevant effect also during heating in the temperature interval 750 K to 1050 K (Figure 93).

5.2.1. Additional experimental data

Investigation of martensite formation with sub-zero Celsius dilatometry

Sub-zero Celsius dilatometry was applied to validate the VSM investigation and to investigate stress relaxation in the material. Unfortunately the investigations failed because of insufficient stability of the equipment.[67]

Samples were hollow cylinders, 10mm long, 4mm in diameter, 0.2mm thick. The wall thickness was chosen to match the thickness of the samples investigated with VSM and XRD in APPENDIX F and APPENDIX G.

After 3.6 Ms (i.e. 1000 h) storage at room temperature, the cylinders were subjected to sub-zero dilatometry. Figure 95 reports martensite formation during isochronal cooling at 15 K/min for three different samples named, A, B and C and is considered for a direct comparison with Fig. 2 in APPENDIX F.

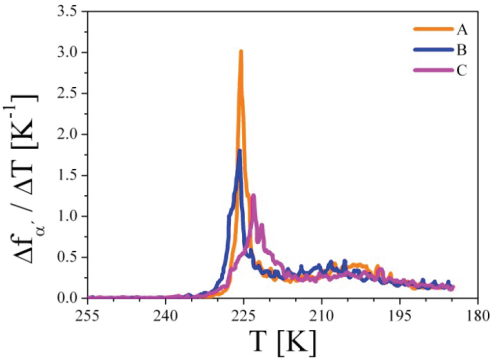

Figure 95. Dilatometry investigation with a Bähr 805 A/D quenching dilatometer equipped for sub-zero Celsius cooling. Martensite formation in three different samples A,B,C is plotted as transformation rate $\frac{\Delta f_{\alpha'}}{\Delta T}$ versus temperature T.

[67] It is meaningful to mention that relaxation was observed at temperatures as low as 180 K. Relaxation resulted in an initial decrease of sample dimensions upon interruption of the cooling step.

Misalignment of the instrument was observed during the sub-zero Celsius investigation making the analysis meaningless from the quantitative point of view. From the *qualitative* point of view, two transformation peaks are observed: a first transformation peak at about $225 \pm 2\ K$; a second transformation peak at lower temperatures.

From a comparison between Figure 95 and Fig. 2 in APPENDIX F, it is visible that the temperature for the first transformation peak is consistent for dilatometry and VSM investigations. In conclusion, dilatometry *qualitatively* validates the observation of martensite formation by VSM.

Cooling curves for the material sub-zero Celsius quenched in the cryostat chamber

APPENDIX F reports 2 sets of experimental data which were obtained upon quenching the material into the cryostat chamber pre-cooled to 93 K and 123 K, respectively. This method does *not* allow to follow martensite formation on cooling, because the actual temperature of the sample is unknown (see paragraph 4.2.1).

To follow martensite formation on (re)heating, the material must have experienced thermal stabilization prior to the (re)heating step. The time necessary for thermal stabilization of the sample during a quenching experiment was estimated from temperature measurements with a thermocouple, which was placed on the top of the fiber rod, where samples are generally mounted, and fixed with Kapton tape prior to the insertion of the fiber rod in the cryostat.[68]. Data were collected using an APPA-55II digital thermometer. The recorded cooling curves are shown in Figure 96.

Figure 96 shows that thermal stabilization of the thermocouple required 20 s to 40 s depending on the quenching temperature. Since the time to start data acquisition after sample mounting is about 60 s, it can safely be assumed that thermal stabilization is reached prior to reheating.

[68] Consequently, it is assumed that the thermal inertia of the sample / thermocouple is negligible as compared to the thermal inertia of the fiber rod.

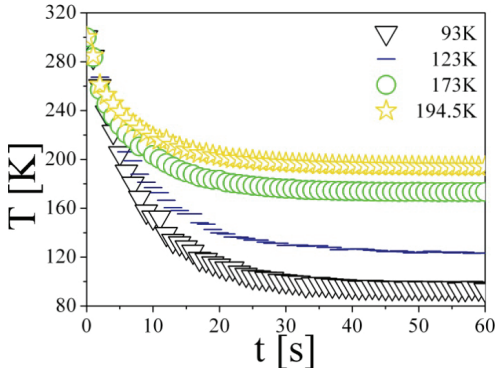

Figure 96. Cooling curves for the material quenched in the cryostat chamber pre-cooled to different temperatures.

Additional investigation of martensite formation during reheating

Martensite formation during isochronal reheating was followed after quenching the material in the cryostat chamber pre-cooled to the quenching temperature. Two sets of data are reported in APPENDIX F. In the following, data obtained with two additional sets of samples are reported. Several other spare data are omitted.

The samples were isochronally heated at 1.5 K/min and 15 K/min, respectively. The applied thermal cycles are illustrated in Figure 97a and Figure 97b, respectively. Experimental data are reported in Figure 98.

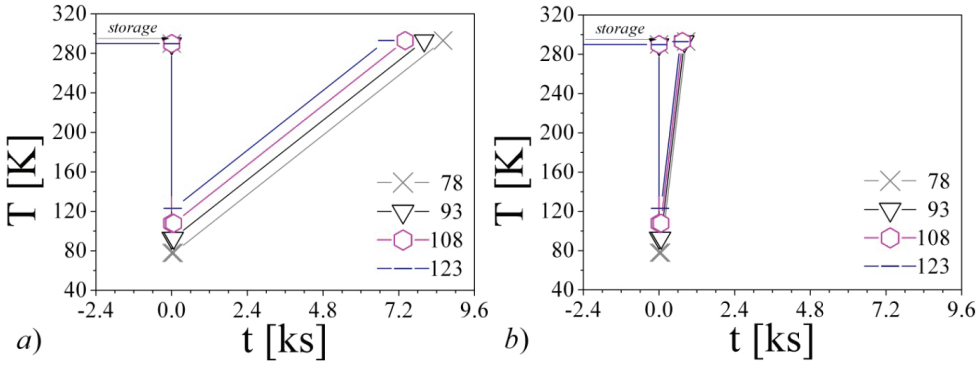

Figure 97. Sub-zero Celsius treatment of the sample quenched and reheated: the quenching step is assumed infinitively rapid; after 60s isothermal holding, samples were reheated at a) 15 K/min and b) 1.5 K/min.

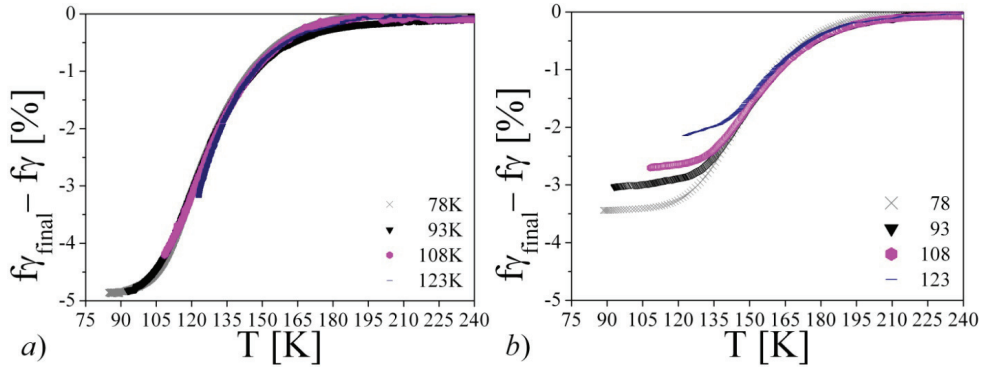

Figure 98. Magnetometry investigation. Reduction in the content of retained austenite (i.e. martensite formation) during reheating of samples quenched in the cryostat chamber pre-cooled to different temperatures: a) heating rate of 1.5 K/min; b) heating rate of 15 K/min.

Figure 98 shows martensite formation during reheating and is complementary to Figs. 3 and 4 in APPENDIX F. Direct comparison of Figure 98a and Figure 98b shows that martensite formation is partially suppressed during fast reheating.

Moreover, Figure 98a shows that the lower the quenching temperature, the larger the fraction of martensite forming on reheating. This observation suggests that a-thermal nucleation of martensite on cooling is promoted by an increase in the driving force for the transformation, i.e. a larger undercooling.

Figure 98a reveals a saturation level in the transformation for quenching temperatures $T_q \leq 93\ K$ (Figure 98a bottom left). In the frame of a-thermal nucleation, this observation suggests leveling out of the driving force at $T < 93\ K$ as indeed is generally the case (see APPENDIX E).

5.3. A-thermal versus thermally activated nucleation and growth of lenticular martensite

5.3.1. Description of the transformation kinetics

In APPENDIX E, APPENDIX F and APPENDIX G it is claimed that the kinetics of lenticular martensite formation can be described in terms of a-thermal nucleation of thin plate

martensite (i.e. the midrib) followed by thermally activated, time dependent growth into lenticular morphology. Time dependent spontaneous nucleation is neglected.

This description, which is only (partially) consistent with the literature of martensite presented in chapter 2 (i.e. spontaneous nucleation is time dependent – see section 2.7.2), was based on extensive experimental activity performed by VSM using 100Cr6 material in 1353-60 condition. The present section presents the part of experimental data which leads to the proposed description of the transformation kinetics.

If not differently specified, samples are intended as stored at room temperature for 2 Ms to 4 Ms prior to the sub-zero Celsius investigation. Thereafter, different sets of samples were subjected to different types of sub-zero Celsius treatment, which is described in detail at the beginning of each sub-paragraph. The baseline was measured on a stabilized sample[69] and data were fitted with a second order polynomial.

5.3.2. The existence of master curves for isothermal martensite formation and their significance for the transformation kinetics

In this paragraph, experimental data obtained on two different sets of samples are reported.

A first set of samples was isochronally cooled to 183 K applying different rates. Thereafter, samples were isothermally held 16 h at 183 K. The thermal cycles are illustrated in Figure 99. Figure 100a reports martensite formation during isochronal cooling plotted versus undercooling below the martensite (re)start temperature, $M_{(re)s}$. Figure 100b shows martensite formation during isothermal holding.

As expected, martensite forms on cooling (Figure 100a) and isothermal holding (Figure 100b). Martensite formation on cooling is particularly pronounced at about 20 K undercooling below $M_{(re)s}$ and is time dependent. At 183 K, the fraction transformed during the isochronal

[69] A sample in which no more martensite forms upon cooling to the lower temperature of investigation and reheating. This condition is reached upon double cooling to boiling nitrogen temperature.

cooling step is about equal for the different samples, in spite of a different transformation path followed on cooling.

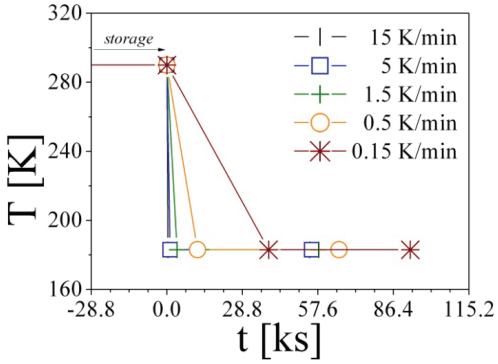

Figure 99. Sub-zero Celsius thermal cycles for the samples isochronally cooled at different rates to 183 K and thereafter isothermally held 16 h at 183 K.

Figure 100b shows that martensite formation on isothermal holding at 183 K depends on the applied cooling rate to reach this temperature. Specifically, isothermal martensite formation is the more pronounced the faster the cooling. Interestingly, this dependence is observed in spite of equal initial contents of martensite in the samples.

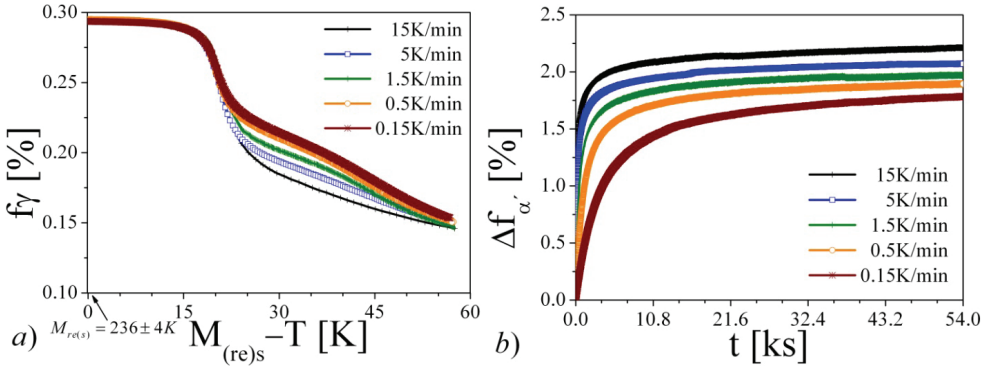

Figure 100. Martensite formation during sub-zero Celsius treatment. a) Fraction of retained austenite f_γ as a function of cooling rate plotted versus undercooling below the martensite (re)start temperature $M_S - T$. Thin lines represent the transformation rate in arbitrary units. b) Isothermal martensite formation $\Delta f_{\alpha'}$ at 183 K plotted versus time t after isochronal cooling at the indicated rates.

The observation that the fraction of martensite at the beginning of the isothermal holding is about equal for all samples, while the isothermal kinetics is not, indicates that isothermal

martensite formation does not arise from a (partial) suppression of the martensite formation on cooling, but has different origin.

It is explicitly mentioned that this observation invalidates nucleation-controlled explanations (see paragraph 3.4.2). To deepen the understanding of the isothermal process, in the following an alternative presentation of the data is introduced.

As reported in APPENDIX E and APPENDIX F, the transformation rate is continuous upon interruption of isochronal cooling (see also paragraph 5.1.5). This observation, which is confirmed in the present case (not shown), suggests to plot isothermal data differently than in Figure 100. In Figure 101a, the fraction isothermally transformed is plotted against the product of holding time and applied cooling rate.

Apparently (Figure 101a), when the fraction transformed isothermally is plotted against the product of holding time and applied cooling rate, isothermal martensite formation is presented by a master curve. Hence, not only the transformation rate during isochronal cooling is about proportional to the cooling rate, but also is the degree of transformation on isothermal holding.

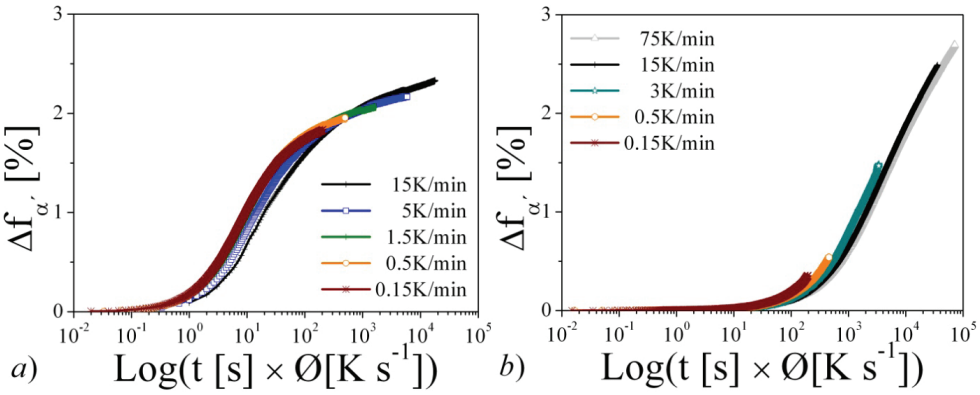

Figure 101. Isothermal martensite formation $\Delta f_{\alpha'}$ plotted versus the product between holding time t and applied cooling rate Ø: a) at 183 K; b) at 123 K. The isothermal transformation follows a master curve in a n approximate way; the master curve is a function of the holding temperature.

The observation of a master curve reported in Figure 101a has not been noticed before and is confirmed for the series of samples cooled to 123 K (Figure 101b). Note that the observation of master curves changes the description of the isothermal kinetics. Isothermal

martensite formation is not larger the faster the cooling, it is simply the faster the faster the cooling. In the following, the significance of the observation of master curves is further discussed.

As previously mentioned, a nucleation controlled description is incompatible with the present data. Consequently, an attempt is made to describe isothermal martensite formation as determined by continuous growth of a-thermally formed nuclei on cooling.

In absence of isothermal nucleation (and relaxation phenomena), the maximum fraction of martensite which can form in the material, and consequently on isothermal holding, is defined by complete growth of the martensite units, as determined by thermodynamics (paragraph 2.8.1).

Assuming growth as a single activated process and controlled by the movement of the martensite-austenite interface, the isothermal transformation rate can be described as:

$$\dot{f} = v_i \cdot (f_{max} - f) \qquad [29]$$

where f is the fraction transformed isothermally, f_{max} is the fraction corresponding to saturation of the transformation (i.e. complete growth) and v_i is the transformation rate at the beginning of isothermal holding. This expression can be integrated analytically to give $\ln\left(\frac{f}{f_{max}-f}\right) = v_i \cdot t$, with t time. The first order dependence on t agrees with the description in (357).

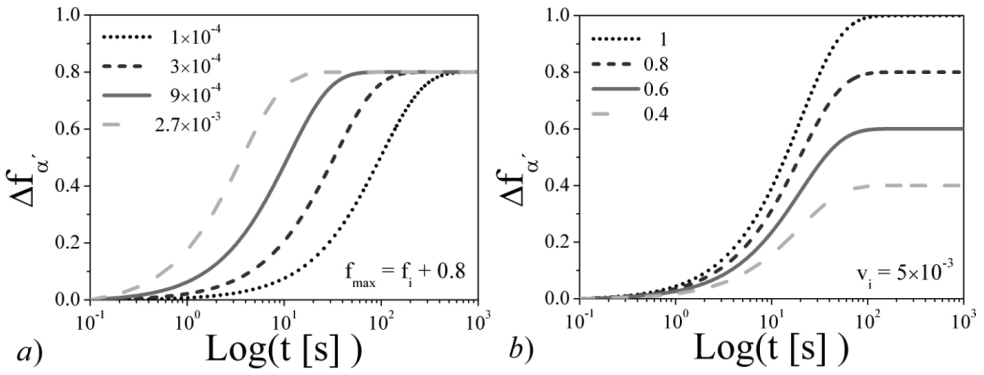

Figure 102 Isothermal transformation curve for continuous growth of preexisting nucleation sites: a) as a function of the initial transformation rate v_i taking $f_{max} = f_i + 0.8$, with f_i starting fraction; b) as a function of the fraction of martensite at saturation f_{max} , taking $v_i = 5 \cdot 10^{-4}$.

In the present analysis, the fraction transformed isothermally $f_J = \sum_{j=1}^{J} \Delta f_j$ was calculated numerically for a series of time step j, with $j = 1,2,3$ ..., where the fraction transformed per time steps, Δt, is $\Delta f_j = v_i \cdot \left(f_{max} - f_{j-1}\right) \cdot \Delta t$. Figure 102 reports graphically the transformation curves that result from numerical integration versus v_i (Figure 102a) and f_{max} (Figure 102b).

Evidently, if nucleation does *not* take place on isothermal holding, the master curve plot should yield a sigmoid shape, which is clearly *not* the case for the data in Figure 101. Moreover, Figure 101 shows that the shape of the master curve is a function of temperature, which is not compatible with a unique process occurring on isothermal holding. Consequently, isothermal martensite formation cannot be interpreted as growth of pre-existing nuclei only. Time dependent isothermal nucleation of martensite is invoked to explain the experimental results.

Time dependent nucleation of martensite during isothermal holding can occurs for the following reasons: (i) thermally activated, time dependent nucleation of martensite embryos which would require a lower temperature for a-thermal nucleation; (ii) time dependent nucleation induced / assisted by the continuous growth of the martensite units. The existence of master curves undoubtedly indicates that time dependent nucleation is a function of the fraction transformed only and it is indeed induced / assisted by growth of pre-existing nuclei.

In conclusion, time dependent, thermally activated nucleation of martensite can be neglected in the description of the kinetics of isochronal martensite formation, while it is *not* possible to describe isothermal martensite as growth of pre-existing nuclei only. Time dependent autocatalytic nucleation of martensite as promoted by thermally activated growth gives a finite contribution to the isothermal kinetics.

5.3.3. Isothermal transformation as a function of holding temperature and cooling rate

In this paragraph, additional experimental activity which contributes to the understanding the isothermal kinetics of lenticular martensite formation is presented.

Two sets of samples, sI and sII, were isochronally cooled at 15K/min and 1.5 K/min, respectively. Isochronal cooling was interrupted and followed by isothermal holding at different temperatures for 1h and 16 h. The applied thermal cycles are illustrated in Figure 103.

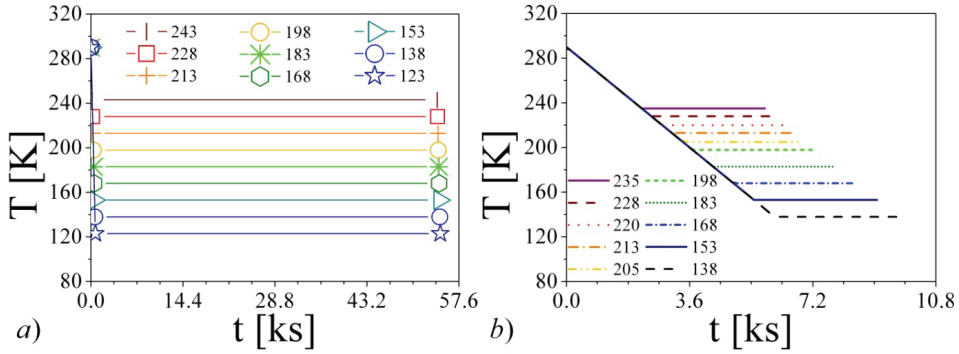

Figure 103. Sub-zero Celsius treatment of samples a) cooled 15 K/min to different temperatures and held 16 h isothermally (set sI); b) 1.5 K/min to different temperatures and held 1 h isothermally. Samples are named after the temperature of isothermal holding (set sII).

The fraction of retained austenite versus undercooling below $M_{(re)s}$ is plotted in Figure 104 for all the samples cooled 15K/min. Figure 105 shows the isothermal part of the transformation.

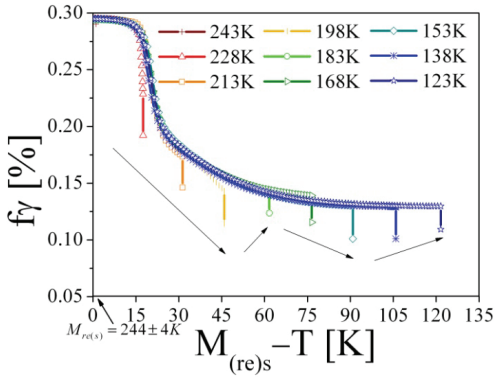

Figure 104. Set sI. Fraction of retained austenite f_γ plotted versus undercooling below the martensite (re)start temperature $M_S - T$ for the sample isochronally cooled 15 K/min and thereafter isothermally held 16 h.

Consistently with the data presented so far, martensite starts to form after a certain degree of undercooling with respect to the storage (room) temperature, at a temperature $M_{(re)s}$. Thereafter, a sudden acceleration of the transformation is observed upon continuous cooling, which results in a first maximum in the transformation rate at about 20 K undercooling below

$M_{(re)S}$. A second maximum is not observed for the samples cooled at 15 K/min (see APPENDIX F).

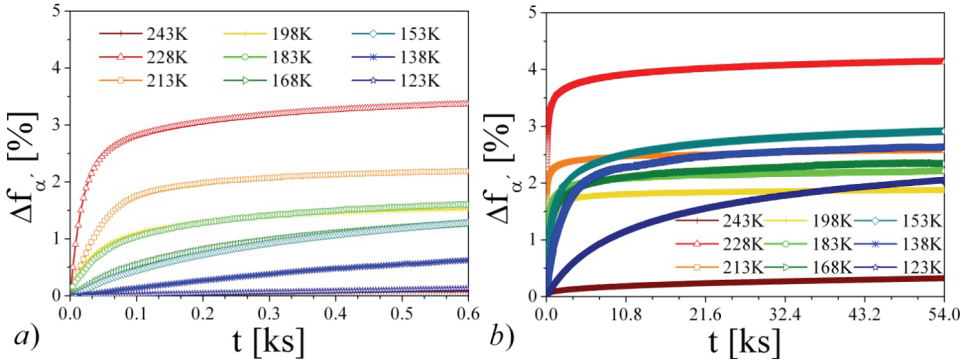

Figure 105. Set sI. Isothermal martensite formation $\Delta f_{\alpha'}$ after isochronal cooling 15K/min to the indicated temperatures plotted versus time t: a) during the first 10 minutes of isothermal holding; b) during the all recorded isothermal step of 16 h.

From Figure 104, it is observed that the total fraction of martensite that forms on cooling and isothermal holding strongly depends on temperature and does *not* immediately show a rational pattern. The largest degree of transformation is obtained upon isochronal cooling to 153 K followed by isothermal holding.

A (partially) rational pattern is observed for the isothermal transformation (Figure 105) where, at the beginning of the isothermal holding, the degree of transformation is the larger the faster the transformation on continuous cooling.

The isothermal transformation depends on temperature and reaches a saturation level. The level of saturation for the transformation appears strongly dependent on temperature and is particularly low for isothermal holding at 198 K. A rational pattern for the continuous evolution of the isothermal transformation is *not* recognized. Most isothermal transformation is reched at 228 K, in correspondence with a sudden acceleration of the transformation on isochronal cooling (Figure 104), while it is minimal at 243 K, in proximity of $M_{(re)S}$.

In Figure 106, the isothermal transformation after isochronal cooling 15 K/min is plotted as a function of $log(t) \times \emptyset$. Figure 106 helps to visualize the differences in the isothermal kinetics of the transformation at different temperatures. Following the description in paragraph

5.3.2, these differences are explained from different nucleation rates during the isothermal holding. In particular, the steeper the isothermal curve at long holding time, the larger the nucleation rate is expected to be.

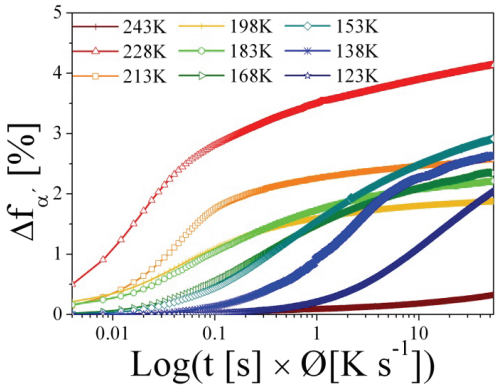

Figure 106. Set sI. Isothermal martensite formation $\Delta f_{\alpha'}$ plotted versus the product between holding time t and applied cooling rate Ø.

Martensite formation for the next set of samples, sII is presented in the following. The isochronal part of the transformation is shown in Figure 107a, while the isothermal part is shown in Figure 107b.

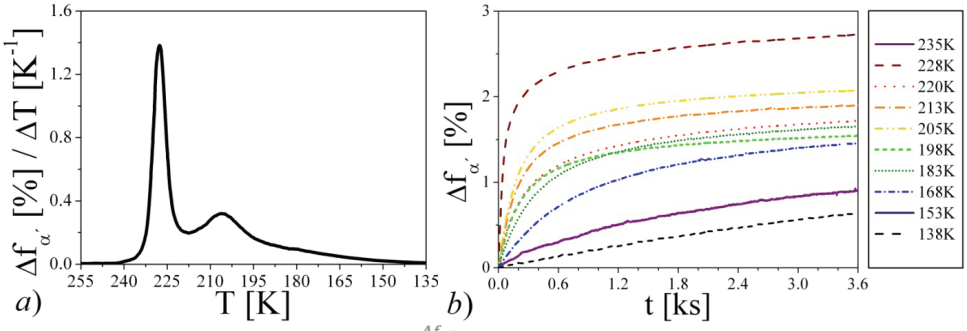

Figure 107. Set sII. a) Transformation rate $\frac{\Delta f_{\alpha'}}{\Delta T}$ plotted versus temperature for a sample isochronally cooled 1.5K/mi to 123 K; differentiation was done on 4K temperature interval. b) Isothermal martensite formation $\Delta f_{\alpha'}$ after isochronal cooling 1.5K/min to the indicated temperatures plotted versus time t.

Figure 107a shows that martensite starts to form at about 240 K. The transformation rate suddenly increase up to a maximum at about 220 K. A second transformation peak occurs at

lower temperatures. Following APPENDIX E, Figure 107a shows abnormal martensite formation.

Figure 107b shows isothermal martensite formation upon interruption of the cooling step. The observation that isothermal martensite formation is strongly dependent on temperature is confirmed in Figure 105. Figure 105 also confirmed that the isothermal transformation is largest at 228 K, in correspondence with the transformation peak in Figure 107a.

Similarly to all previously reported observations, at the beginning of isothermal holding, the transformation is the more pronounced the faster it is on cooling. A rational pattern is not recognized for the saturation level for isothermal transformation, which appears minimal at 198 K, consistent with data reported for set sI.

At this point it is again remarked that the steeper the isothermal curve at long isothermal holding time, the larger the nucleation rate during isothermal holding is expected to be. This concept is investigated further in the next section.

5.3.4. The nucleation rate experiment

This paragraph presents a method to qualitatively estimate the rate of isothermal nucleation. The method is purely empirical.

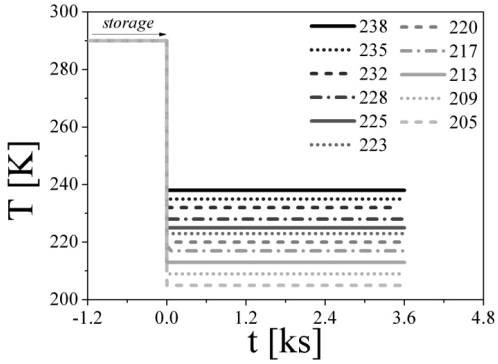

Figure 108. Sub-zero Celsius treatment of the sample quenched and isothermally stored at different temperatures.

A series of samples was stored at room temperature for 4 Ms prior to sub-zero Celsius investigation. The whole sub-zero investigation reported in this section was performed in a single

day. A sample, R, was cooled at 1.5 K/min to 123 K and used as a reference for the formation of martensite during isochronal cooling. All the other samples were quenched in the cryostat chamber pre-cooled to different temperatures, meanwhile martensite formation was followed during 1 h of isothermal holding.

The applied thermal cycles are reported in Figure 108. The results of the investigation are shown in Figure 109 and Figure 110.[70]

Specifically, Figure 109 shows martensite formation during the isothermal step. Figure 110 reports a comparison between the transformation rate obtained on isochronally cooling sample R and a qualitative estimation of the nucleation rate on isothermal holding, which was obtained as described in the following.

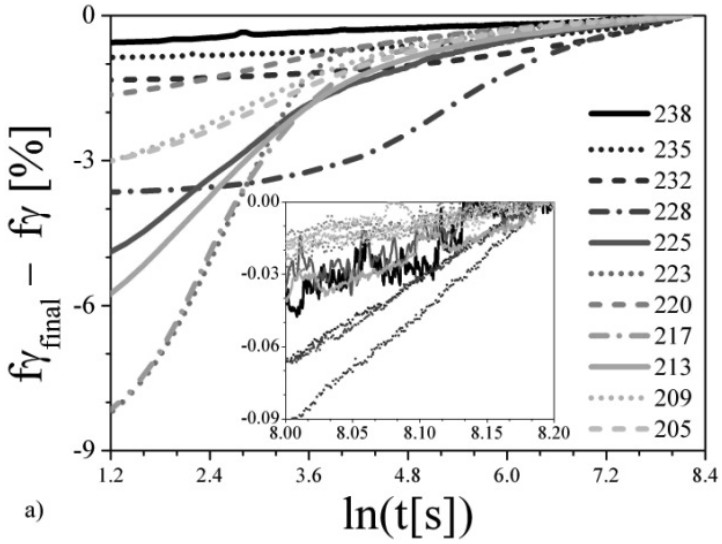

Figure 109. Magnetometry investigation. Reduction of the content of retained austenite (i.e. martensite formation) during isothermal holding of the sample. Inset: last 600s of isothermal holding. The final content of retained austenite is taken as reference point; good linearity of the data justifies the fit to a straight line.

[70] Please note that the experimental setup allow to start the measurement about 60s after inserting the sample in the pre-cooled chamber, hindering the visualization of a large part of transformation.

A qualitative estimation of the nucleation rate of martensite versus temperature is obtained in two steps. Firstly, the formation of martensite is plotted versus the logarithm of time in Figure 109; secondly, the slope of the plot in the time interval $3000 < t < 3600\ s$ (inset in Figure 109) is estimated by linear fitting of the data. As mentioned in paragraph 5.3.3, the slope of the plot of isothermal martensite formation versus the logarithm of time is indicative of the nucleation rate in the material.

The slope of the data is shown in Figure 110. Figure 110 shows that data obtained from Figure 109 reproduces the multistep pattern measured in sample R albeit shifted to higher temperature by about 9 K. The analysis leads to the conclusion that the nucleation rate is highest at temperatures just above the transformation peaks, while it is inhibited by the occurrence of a transformation peak on cooling.

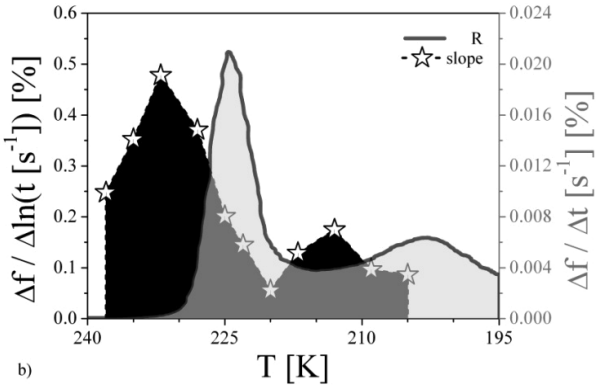

Figure 110. Magnetometry investigation. Comparison between the slope obtained by fitting to a straight line the data in the inset in Figure 109 and of the transformation rate plotted versus temperature for sample R.

5.3.5. Demonstration of (partially) a-thermal growth of lenticular martensite

In this paragraph, the consistence of the so far presented description is considered. The analysis starts from evaluating five different scenarios, where nucleation and growth of martensite are assumed time dependent and / or time independent. Also, it is assumed that martensite formation is observed on continuous cooling.

In a first scenario, both nucleation and growth are purely a-thermal. No martensite forms isothermally. This is not the present case.

In a second scenario, both nucleation and growth are purely thermally activated. Isothermal transformation results from the combination of isothermal nucleation and growth and the transformation rate is continuous upon interruption of the cooling step. However, fast cooling would completely suppress martensite formation, which does *not* apply for the present case. [71]

In a third scenario, martensite nucleation is partially, or fully, a-thermal and growth is purely thermally activated. Isothermal transformation results from the combination of isothermal nucleation and growth and the transformation rate is continuous upon interruption of the cooling step, while the nucleation rate is not, resulting in a discontinuity in the acceleration/deceleration rate. This may be the present case.

In a fourth scenario, nucleation is purely thermally activated and growth is partially, or fully, a-thermal. Isothermal transformation results from the combination of isothermal nucleation and growth and the transformation rate is similarly continuous upon interruption of the cooling step, while the nucleation rate is not,[72] resulting in a discontinuity in the acceleration/deceleration rate. This may also apply for the present case.

In a fifth scenario, the nucleation of martensite is partially, or fully, a-thermal and growth is also partially, or fully, a-thermal. Isothermal transformation results from the combination of isothermal nucleation and growth and the transformation rate is *not* continuous upon interruption of the cooling step. In the results presented above, this discontinuity was never observed.

However, instantaneous formation of the midrib in lenticular martensite is established (chapter 2), invalidating the third scenario. Consequently, either nucleation is *not* at all a-thermal, implying that the analysis so far developed is completely wrong, or conditions must exist where a discontinuity in the transformation rate is observed. The visualization of the discontinuity was obtained as follows.

---

[71] This statement was validated by directly quenching the material into liquid nitrogen. This process results in a degree of transformation which is comparable with a the one obtained with a fast cooling in the pre-cooled chamber (see APPENDIX F).

[72] Because of a different rate of autocatalytic nucleation as promoted by a-thermal growth which is lost on interrupting the cooling step.

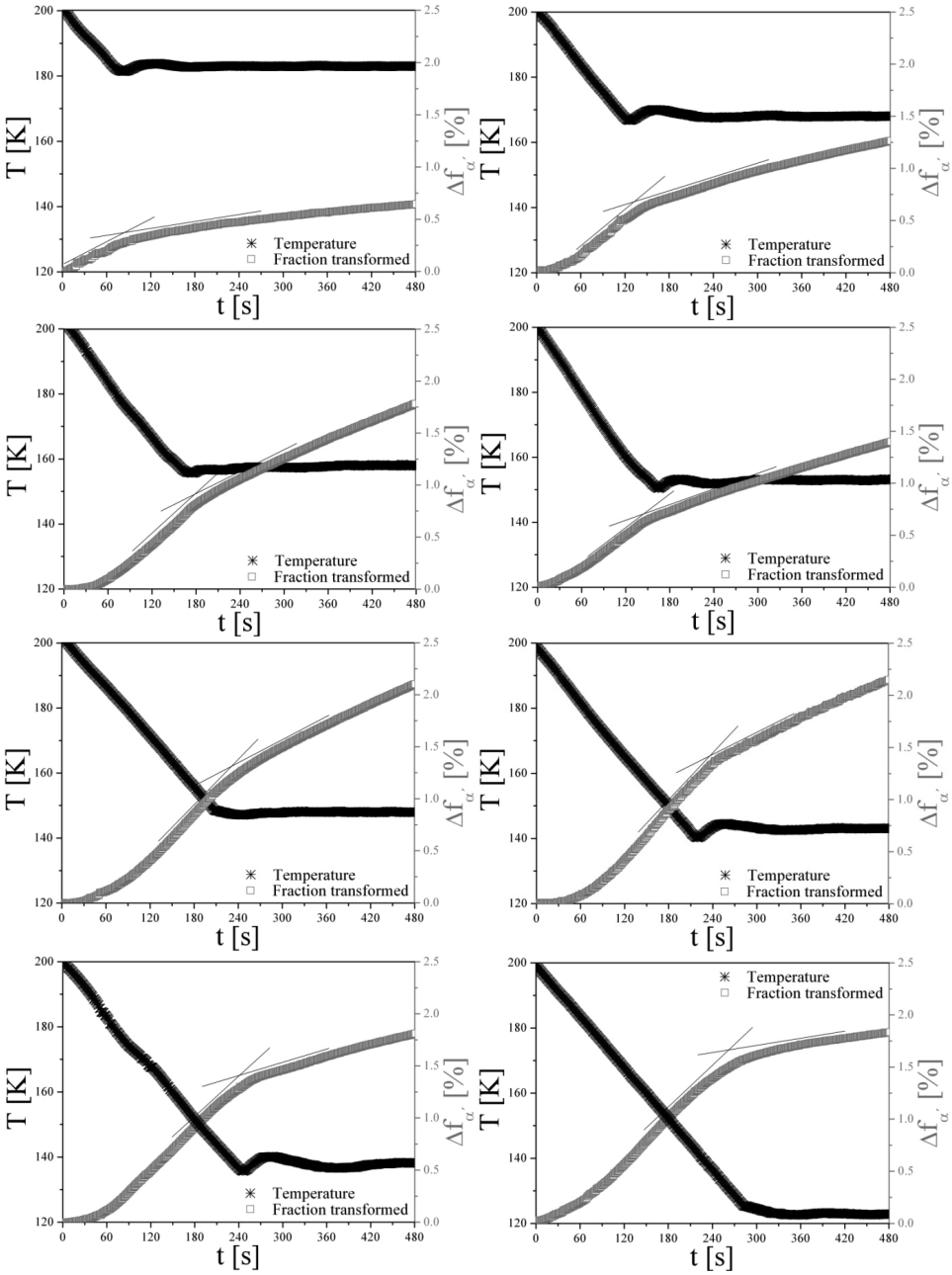

Figure 111. Magnetometry investigation. Martensite formation $\Delta f_{\alpha'}$ during continuous cooling from 205 K at 15K/min plotted versus time. Recorded temperature data is also shown versus time.

A set of samples was sub-zero Celsius treated after 4 Ms storage at room temperature. Initially, samples were quenched in the cryostat chamber pre-cooled to 205 K, which is just on the right side of the second transformation peak in Figure 110, and held 1h at 205.[73] A second stage of martensite formation was promoted by continuous cooling at 15 K/min from starting from 205 K. Thereafter, continuous cooling was interrupted at different temperatures T in the interval $123 < T < 183\ K$ and isothermal martensite formation is recorded.

Figure 111 shows martensite formation versus time for the different samples and is representative of both the isothermal and isochronal step. The distinction between isothermal and isochronal is left to the reader on the bases of the cooling curves, which are also reported.

Evidently, a discontinuity in the transformation rate upon interruption of the isochronal cooling followed by isothermal holding is observed in all investigated samples, as a confirmation of a (partially) a-thermal character of both nucleation and growth of lenticular martensite.

It is concluded that the a-thermal component for growth can generally be neglected for the present system, as validate from the generally observed continuity of the transformation rate, but is existing, as proved in the present paragraph.

5.4. Time dependent growth of lath martensite in 17-7 PH stainless steel

5.4.1. In situ observation of martensite formation at sub-zero Celsius treatment

As mentioned in paragraph 4.1.3 experimental evidence of isothermal martensite formation in 17-7 PH commercial stainless steel grade has not been reported yet. Isothermal martensite formation is demonstrated in APPENDIX H.

The reader is referred to the manuscripts reported as APPENDIX H at this point of the text.

[73] Indeed, to visualize the theorized (partially) a-thermal behavior, it is necessary to minimized the continuous growth of pre-existing nuclei. This is the purpose of quench to 205 K followed by isothermal holding.

5.4.2. Investigation of the mechanism for isothermal martensite formation

The mechanism for isothermal martensite formation is investigated in APPENDIX I. In APPENDIX I it is shown that isothermal martensite formation arises as a consequence of purely thermally activated, time dependent growth of lath martensite. It is emphasized that this description is consistent with the description in chapter 2.

The reader is referred to the manuscripts reported as APPENDIX I at this point of the text.

5.4.3. Additional experimental data

The manuscript in APPENDIX I referred to the present text for the validation of the following experimental data: lattice parameter of austenite and martensite; negligible amount of retained austenite in the as rolled material.

The Energy Dispersive X-Ray spectrum collected in transmission for the as-rolled material is reported in Figure 112. A scattering angle 2θ=20° was applied during data acquisition. Acquisition time was 900 seconds.

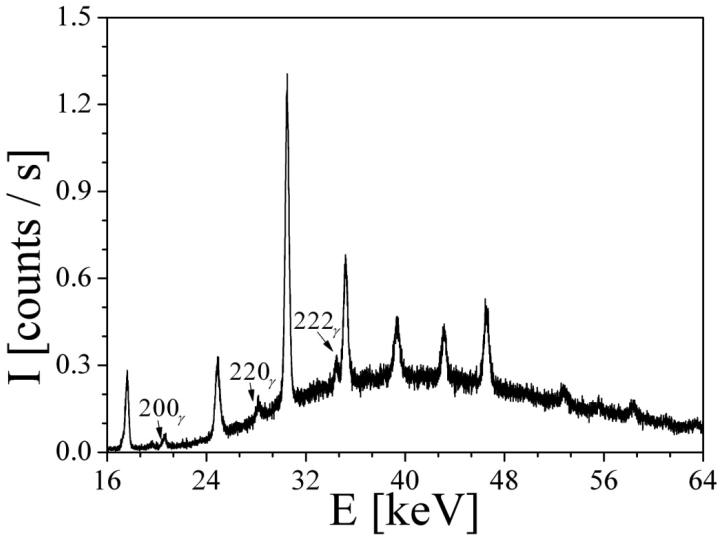

Figure 112. Energy Dispersive X-Ray spectrum collected in transmission for the as-rolled material. The sharper peaks refer to $110_{\alpha'}$, $200_{\alpha'}$, $211_{\alpha'}$, $220_{\alpha'}$, $310_{\alpha'}$, $222_{\alpha'}$ and $321_{\alpha'}$. The following reflections of austenite are not observed in the same energy range: 311_{γ}, 420_{γ}, 422_{γ}. The reflections 111_{γ}, 400_{γ}, 311_{γ}, are overlapping with the reflections of martensite and no conclusions are allowed.

Figure 112 reports the presence of all reflection of martensite expected for the energy interval under investigation, whereas only few reflections of austenite are observed. The observation of few austenite reflections only was expected because of rolling operation, which is likely to yield a strong preferential orientation of the austenite grains in specific directions (texture).

Consequently, quantitative phase analysis performed taking into account all reflections of martensite and the 200_{γ}, the 220_{γ} and 311_{γ} reflection of austenite would result in a overestimation of the phase fraction of austenite. The fraction of austenite calculated according to paragraph 4.5.3 gave a content of retained austenite of 2.7%.

The lattice parameter of austenite and martensite at room temperature, which was applied in APPENDIX I, was measured on as quenched material austenitized as presented in APPENDIX H. The following lattice parameters were obtained: $a_{\alpha'} = 2.868\ \AA$; $a_{\gamma'} = 3.595\ \AA$

5.5. Observation of abnormal lath martensite formation in 17-4 PH stainless steel

Abnormal lath martensite formation was observed also for 17-4 PH stainless steel. Data are reported in a manuscript form.

The reader is referred to the manuscripts reported as APPENDIX J at this point of the text.

6. Summary

The performed work started from the investigation of the metallurgical reasons leading to improved performance of high carbon steel parts subjected to sub-zero Celsius treatment. A literature survey suggested that isothermal martensite formation at cryogenic temperature leading to an enhanced and more uniform precipitation of carbides during tempering is the most likely mechanism for improved performance of sub-zero Celsius treated steel parts.

Isothermal martensite formation can result either from time dependent growth of martensite, or from time dependent nucleation. The investigation of isothermal martensite formation at sub-zero Celsius temperature on 100Cr6 steel grade lead to the conclusion that time dependent growth of lenticular martensite is occurring in the system, while time dependent nucleation can be neglected for engineering purposes.

This conclusion is *not* aligned with the general belief that the formation of lenticular martensite occurs instantaneously. From the analysis of the literature on martensite formation, the conclusions obtained from the work on 100Cr6 steel grade appear to be consistent with previous observations, while instantaneous growth of martensite appears *in*consistent.

The investigation of the kinetics of martensite formation gave the possibility to test whether isothermal martensite formation at cryogenic temperatures can be appointed as the process responsible for enhanced performances of high carbon steel products. Experimental evidence of a more abundant precipitation of carbides during tempering was reported. A thorough investigation of the precipitation products by high resolution microscopy and mechanical testing is necessary for stronger claims on the effect of the precipitates on the performance of high carbon steel parts under service conditions.

In relation to the theory of martensite formation, the investigation of 100Cr6 steel grade material indicated that martensite formation builds up a compressive state of stress in the remaining austenite. This process is likey to be a general characteristic of the martensitic transformations in steels and results from the mechanical interaction between austenite and martensite phases.

This aspect of the martensitic transformations was shown to be fundamental for the investigation of the transformation kinetics and leads to a progressive stabilization of the remaining austenite. Abnormal transformations, which are characterized by a series of reproducible accelerations and decelerations of the transformation during cooling, were systematically observed in the present work.

The observation of abnormal transformations was reported several times in the literature for various transformations of f.c.c. austenite into b.c.c. products. In the present work it was demonstrated that the reason for abnormal transformations is the interplay between driving force and self induced strain energy, which on one side promote autocatalytic nucleation of the b.c.c. products, on the other mechanically stabilizes austenite against its trasnfomration into b.c.c..

Specifically, how the abnormal trasnformation is manifested depends on whether the b.c.c. product is already present at the most nucleation sites. For virginal austenite, nucleation starts at the most potent nucleation sites, while the shear strain introduced by the transformation promotes autocatalityc nucleation of new variants of b.c.c. product. For a sample where austenite is encapsulated as a minority phase by the b.c.c. product, this leads to hydrostatic compressive stress and a deceleration of the transformation.

Exploitation of insights may lead to optimized heat treatment of martensitic steel products.

7. References

(1) **Nicodemi, W.** *Introduzione agli acciai inossidabili.* Paderno Dugnano, MI, Italy : Associazione Italiana di Metallurgia, 2008.

(2) **ASM Handbook.** *Carbon and Alloy Steels.* (OH) : ASM International, 1996.

(3) **Davis, J.R.** *Tool Materials.* (OH) : ASM International, 1995.

(4) **ASM Handbook.** *Volume 4 - Heat Treating.* (OH) : ASM International, 1991.

(5) **Nishiyama, Z.** *Martensitic Transformation.* New York : Academic Press., 1978.

(6) **Cheng, L.; Böttger, A.; De Keijser, Th.H; Mittemeijer, E.J.** Lattice parameters of Iron-Carbon and Iron-Nitrogen martensites and austenites. *Scripta Mater.* 1990, Vols. 24, pp. 509-514.

(7) **Roberts, C.S.** *Transaction AIME.* 1951, Vols. 191, pp. 203.

(8) **Speich, G.R.** *Metall. Trans.* 1972, Vols. 3, pp. 1045.

(9) **Honeycombe, R.W.K.** *Steels Microstructure and Properties.* London : Edward Arlond, Ltd., 1981.

(10) **Massalski, T.B.; Murray, J.L.; Bennett, L.H.; Baker, H.** *Binary Alloy Phase Diagrams - Vol 1.* s.l. : American Society of Metals, 1986.

(11) **Speich, G.R.; Taylor, K.A.** Tempering of Ferrous Martensites. [book auth.] G.B. Olson and W.S. Owen. *Martensite.* (OH) : ASM International, 1992.

(12) **Van Gendered, M.J.; Böttger, A.; Cernik, R.J.; Mittemeijer, E.J.** Early stages of decomposition in iron-carbon and iron-nitrogen martensites: Diffraction analysis using synchrotron radiation. *Metall. Trans. A.* 1993, Vols. 24, pp. 1965-1973, 9.

(13) **Van Genderen, M.J.; Isac, M.; Böttger, A.; Mittemeijer, E.J.** Aging and tempering behavior of Iron-Nickel-Carbon and Iron-Carbon martensite. *Metall. and Mater. Trans. A.* 1997, Vols. 28, pp. 545-561, 3.

(14) **Chen, P.C.; Winchell, P.G.** Martensite lattice changes during tempering. *Metall. Trans. A.* 1980, Vols. 11, pp. 1333-1339, 8.

(15) **Barrow, A.T., Kang, J-H and Rivera-Diaz-del-Castillo, P.E.J.** *Acta Mater.* 2012, Vols. 60, pp. 2805-2815.

(16) **Cheng, L.; Brakman, C.M.; Korevaar, B.M.; Mittemeijer, E.J.** Tempering of Iron-Carbon Martensite; Dilatometric and Calorimetric Analysis. *Metall. Trans. A.* 1988, Vols. 19, pp. 2415-2426.

(17) **Briggs, J.Z.; Parker, T.D.** *The super 12% Cr steels.* New York : Climax Molybdenum company, 1977.

(18) **Callister Jr., W.D.** *Materials science and engineering - An introduction.* s.l. : John Wiley & Sons, Inc., 2007.

(19) **Jaswin, M.A., Shankar, G.S.; Mohan Lal, D.** *Int. J. Precision Eng. and Manuf.* 2010, Vols. 11-1, pp. 97-105.

(20) **Mohal Lal, D., Renganarayanan, S.; Kalanidhi, A.** *Cryogenics.* 2001, Vols. 41, pp.149-155.

(21) **Amini, K., Nategh, S. and Shafyei, A.** *Mater. And Design.* 2012, Vols. 31, pp. 4666-4675.

(22) **Barron, R.F.** *Cryogenics.* 1982, Vols. 22, pp. 409-413.

(23) **Das, D., Dutta, A.K., Ray, K.K.** *Mat. Sci. Eng. A.* 2010, Vols. 527, pp. 2182-2193.

(24) **Meng, F., Tagashira, K.; Sohma, H.** Wear Resistance and Microstructure of Cryogenic Treated Fe-1.4%Cr-1%C steel. *Scripta Mater.* 1994, Vols. 31:7, pp. 865-868.

(25) **Harish, A.; Bensely, A.; Mohan Lal, D.; Rajadurai, A.; Lenkey, G.B.** Microstructural study of cryogenically treated EN 31 bearing steel. *J. of Mater. Sci. Processing Technology.* 2009, Vols. 209, pp. 3351-3357.

(26) **Gill, S.S.; Singh, H.; Singh, R.; Singh, J.** *Int. J. Adv. Manuf. Technol.* 2010, Vols. 48, pp. 175-192.

(27) **Gill, S.S.; Singh, J.; Singh, R.; Singh, H.** *Int. J. Adv. Manuf. Technol.* 2011, Vols. 54, pp. 59-82.

(28) **Reitz, W. and Pendray, J.** *Mater. Manuf. Processes.* 2001, Vols. 16:6, pp. 829-840.

(29) **Collins, D.N.** *Heat treatment of Metals.* 1997, Vols. 3, pp. 71 .

(30) **Meng, F., et al.** Role of Eta-carbide Precipitations in wear resistance Improvements of Fe-12Cr-Mo-V-1.4C Tool Steel by Cryogenic Treatment. *ISIJ Int.* 1994, Vols. 34, pp. 205-210.

(31) **Stratton, P.F.** *Mat. Sci. Eng., A.* 2007, Vols. 449-451, pp. 809-812.

(32) **Huang, J.Y., et al.** *Mat. Sci. Eng., A.* 2003, Vols. 339, pp. 241-244.

(33) **Mohal Lal, D.; Renganarayanan, S.; Kalanidhi, A.** *Cryogenics.* 2001, Vols. 41, pp. 149-155.

(34) **Das, D., Dutta, A.K.; Ray, K.K.** *Wear.* 2009, Vols. 266, pp. 297-309.

(35) **Das, D., Dutta, A.K.; Ray, K.K.** *Phil. Mag.* 2009, Vols. 89, pp. 55-76, 1.

(36) **Collins, D.N.; Dormer, J.** *Heat Treat. Metals.* 1997, Vols. 3, pp. 71.

(37) **Meng, F.; Tagashira, K.; Azuma, R.; Sohma, H.,** ISIJ Int. 1994, 34, pp. 205-210

(38) **Tyshchenko, A.I.; Theisen, W.; Oppenkowski, A.; Siebert, S.; Razumov, O.N.; Skoblik, A.P.; Sirosh, V.A.; Yu.; Petrov, N.; Gavriljuk, V.G.** *Mat. Sci. Eng., A.* 2010, Vols. 527, pp. 7027-7039.'

(39) **Kaputkin, D.E.** *Mat. Sci. Eng., A.* 2006, Vols. 438-440, pp. 207-211.

(40) **P.C. Chen, B.O. Hall, P.G. Winchell.** *Metall. Trans., A.* 1980, Vols. 11, pp. 1323-1331.

(41) **Bensely, A.; Venkatesh, S.; Mohan Lal, D., Nagarajan, G.; Rajadurai, A.; Junik, K.** *Mat. Sci. Eng. A.* 2008, Vols. 479, pp. 229-235.

(42) **Wierszylloski, I.; Samolczyk, J.; Wieczorek, S.; Andrzejewska, E.; Marcinkowska, A.** *Def. Diff. Forum.* 2008, Vols. 273-276, pp. 731-739.

(43) **Bhadeshia, H.K.D.H.** Developments in martensitic and bainitic steels: the role of shape strain. *Mat. Sci. Eng. A.* 2004, Vols. 378, pp. 34-39.

(44) **Gavriulik, V.G.; Theisesn, W.; Siroshm, V.V.; Polshin, E.V.; Kortmann, A.; Mogilny, G.S.; Petrov, Yu.N.; Tarusin, Ye.V.** Low-temperature martensitic trasnformation in tool steels in relation to their deep cryogenic treatment. *Acta Mater.* 2013, Vols. 61, pp. 1705-1715.

(45) **Voort, G.F.V.** *Atlas of Time-Temperature Diagrams for Irons and Steels.* s.l. : ASM International, 1991.

(46) **Mittemeijer, E.J.** *Fundamentals of Materials Science.* s.l. : Springer, 2011.

(47) **Ashby, M., Shercliff, H.; Cebon, D.** *Materials – engineering, science, processing and design.* s.l. : Elsevier Ltd., 2007.

(48) **Porter, D.A., Easterling, K.E.; Sherif, M.Y.** *Phase Transformations in Metals and Alloys.* s.l. : CRC Press, 2008.

(49) **Koistinen, D.P.; Marburger, R.E.** A general equation prescribing the extent of the austenite-martensite transformation in pure iron-carbon alloys and plain carbon steels. *Acta Metallurgica.* 1959, Vols. 7, pp. 59-60, 1.

(50) **Zhang, Z.; Farrar, R.A.** *An atlas of continuous cooling transformation (CCT) diagrams applicable to low carbon low alloy weld metals.* s.l. : Maney Publishing for IOM3, the Institute of Materials, Minerals and Mining, 1995.

(51) **Zhao, J.-C.; Notis, M.R.** Continuous cooling transformation kinetics versus isothermal transformation kinetics of steels: a phenomenological rationalization of experimental observations. *Materials Science & Engineering R: Reports.* 1995, Vols. R15, pp. 135-207, 4-5.

(52) **Kurdjumov, G.V.; Maksimova, O.P.** *Dokl. Akad, Nauk SSSR.* 1948, Vol. 61, 83

(53) **Thadhani, N.N.; Meyers, M.A.** Kinetics of isothermal martensitic transformation. *Progress in Materials Science.* 1986, Vols. 30, pp. 1-37, 1.

(54) **Shih, C. H.** Some characteristics of isothermal martensitic transformation. *Journal of metals.* 1955, Vols. 7, pp. 183-187, 1.

(55) **Reed, R.P.** The Spontaneous Martensitic Transformation in 18% Cr, 8% Ni Steels. *Acta Metall.* 1962, Vols. 10, pp. 865-877.

(56) **Post, J.** *On the constitutive behaviour of Sandvik Nanoflex.* PhD Thesis; Opende, The Netherlands : Ponsen & Looijen, 2004.

(57) **Lee, J.H., Fukuda, T.; Kakeshita, T.** Isothermal Martensitic Transformation in Sensitized SUS304 Austenitic Stainless Steel at Cryogenic Temperature. *Mater. Trans.* 3, 2009, Vols. 50, pp. 473 to 478.

(58) **Kakeshita, T; Sato, Y.; Saburi, T.; Shimizu, K.; Matsuoka, Y.; Kindo, K.** Effects of magnetic field on athermal and isothermal martensitic transformations in Fe-Ni-Cr alloys. *Materials transactions, JIM.* 1999, Vols. 40, pp. 100-106, 2.

(59) **Liu, Y. Zhang, L., Sommer, F. and Mittemeijer, E.J.** Kinetics of Martensite formation in Substitutional Fe-Al Alloys: Dilatometric Analysis. *Metall. snd Mater. Trans. A.* 2012, Vols. DOI: 10.1007/S11661-012-1497-6.

(60) **Stojko, A.; Hansen, M.; Slycke, J.; Somers, M.A.J.** Isothermal martensite formation at sub-zero Celsius Temperatures. *ASTM Special Technical Publication.* 2012, Vols. 1532, pp. 44-56.

(61) **Kim, D., Speer, J.G.; De Cooman, B.C.** Isothermal transformation of a CMnSi Steel Below the Ms Temperature. *Metall. and Mater. Trans. A.* 2011, Vols. 42, pp. 1575-1585.

(62) **Kim, D., Lee, S-J; De Cooman, B.C.** Microstructure of Low C Steel Isothermally transformaed in the Ms to Mf Temperature Range. *Metall. and Mater. Trans. A.* 2012, Vols. 43, pp. 4967-4983.

(63) **Stojko, A.** *The effect of cryogenic treatment on structural and phase transformations in iron-carbon martensite.* PhD Thesis; Lyngby, Denmark : The Technical University of Denmark, 2006.

(64) **Floreen, S.** The physical metallurgy of maraging steels. *Metall. Reviews.* 1968, Vols. 13, pp. 115-128.

(65) **Ludwigson, D.C.; Hall, A.M.** *The physical metallurgy of precipitation-hardenable stainless steels.* Columbus, Ohio, United States : Battelle Memorial Inst. Defense Metals Information Center, 1959.

(66) **Korotushenko, G.V.; Grigorkin, V.I.** Mechanical Properties of Nickel Steels with Isothermal and Athermal Martensite. *Metallovedenie i Termicheskaya Obrabotka Metallov.* 1974, Vols. 1, pp. 41-46.

(67) **Venables, J. A.** The martensite transformation in stainless steel. *Philosophical Mag.* 1962, Vols. 7, pp. 35-44, 73.

(68) **McDougall, P.G. and Wayman, C.M.** Crystallography and Morphology of Ferrous Martensite. [book auth.] G.B. Olson and W.S. Owen. *Martensite.* (OH) : ASM International, 1992.

(69) **Olson, G.B;Owen, W.S.** *Martensite.* (OH) : ASM International, 1992.

(70) **Olson, G.B.** Introduction: Martensite in perspective. [book auth.] G.B. Olson and Owen S.W. *Martensite.* (OH) : ASM International, 1992.

(71) **Christian, J.W.** Interfacial Structure. [book auth.] G.B. Olson and Owen W.S. *Martensite.* (OH) : ASM International, 1992.

(72) **Kaufman, L.; Hillert, M.** Thermodynamics of Martensitic Transformations. [book auth.] G.B. Olson and W.S. Owen. *Martensite.* (OH) : ASM International, 1992.

(73) **Olson, G.B.; Roitburd, A.L.** Martensitic Nucleation. [book auth.] G.B. Olson and W.S. Owen. *Martensite.* (OH) : ASM International, 1992.

(74) **Sinha, A.K.** Martensite. *Physical Metallurgy Handbook.* New York : McGraw-Hill, 2003.

(75) **Cohen, M., Olson, G.B.; Clapp, P.C.** Cambridge, Massachussetts USA : International conference on the martensitic transformation - ICOMAT, 1979. p. 1.

(76) **Bhadeshia, H.K.D.H.** *Worked examples in the Geometry of Crystals.* Second. London : Institute of Materials, 2001. ISBN 0-904357-94-5.

(77) **Kulin, A.S. and Cohen, M.** On martensitic transformation at temperatures approaching absolute zero. *American Institute of Mining and Metallurgical Engineers -- Journal of Metals.* 1950, Vols. 188, pp 1139-1143, 9.

(78) **Bunshah, R. F. and Mehl, R. F.** Rate of propagation of martensite. *Journal of metals.* 1954, Vols. 6, pp.681-682, 5.

(79) **Ghosh, G.; Olson, G.B.** Kinetics of f.c.c. --> b.c.c. heterogeneous martensitic nucleation - II. Thermal activation. *Acta Mater.* 1994, Vols. 42, pp. 3371-3379, 10.

(80) **Krauss, G.; Marder, A. R.** The morphology of martensite in iron alloys. *Metallurgical Transactions.* 1971, Vols. 2, pp. 2343-2357, 9.

(81) **Klostermann, J.A.** The concept of the habit plane and the phenomenological theories of the martensite transformation. *Journal of The Less-Common Metals* . 1972, Vols. 28, pp. 75-94, 1.

(82) **The Iron and Steel Institute.** *Physical properties of martensite and bainite.* London, UK : Humpries & Co Ltd., 1965.

(83) **Brooks, J.W., Loretto, M.H.; Smallman, R.E.** Direct observations of martensite nuclei in stainless steel. *Acta Metallurgica.* 1979, Vols. 27, pp. 1839-1847, 12.

(84) **Hammond, C.** *The Basics of Crystallography and Diffraction.* 3rd. Oxford : Oxford Press, 2009.

(85) **Miller, W.H.** *Treatise on Crystallography.* s.l. : J. & J. J. Deighton, 1839.

(86) **Kurdjumov, G.; Sachs, G.** *Z. Phys.* 1930, Vol. 64, 325.

(87) **Nishiyama, Z.** *Sci. Rep. Res. Insts Tôhoku Univ.* 1934, Vol. 23, 639.

(88) **Wassermann, G.** *Arch. Eisenhütt Wes.* 1933, Vol. 16, 647.

(89) **Greninger, A.B.; Troiano, A.R.** *Trans. Metall. Soc. A.I.M.E.* 1949, Vol. 185, 590.

(90) **Barcelo, F., Bechade, J.L.; Fournier, B.** Orientation relationship in various 9%Cr ferritic/martensitec steels - EBSD comparison between N-W, K-S and G-T. *Phase transitions.* 2010, Vols. 83, pp. 601-614, 8.

(91) **Cayron, C., Barcelo, F; De Carlan, Y.** The mechanisms of the fcc–bcc martensitic transformation revealed by pole figures. *Acta Mater.* 2010, Vols. 58, pp. 1395–1402.

(92) **Bowles, J.S.; Mackenzie, J.K.** Crystallography of martensite transformations . *Acta Metallurgica* . 1954, Vol. 2, 1.

(93) **Wechsler, M.S., Lieberman, D.S.; Read, T.A.** On theory of formation of martensite. *Journal of Metals.* 1953, Vols. 5, pp. 1503-1515, 11.

(94) **Bullough, R; Bilby, B A.** Continuous Distributions of Dislocations: Surface Dislocations and the Crystallography of Martensitic Transformations. *Proceedings of the Physical Society. Section B* . 1956, Vols. 69, pp. 1276-1286, 12.

(95) **Bhadeshia, H.K.D.H., Kundu, S.; Abreu, H.** Mathematics of Crystallographic Texture in Martensitic and Related Transformations. [book auth.] A. Haldar, S. Suwas and D. Bhattacharjee. *Microstructure and Texture in Steels.* s.l. : Springer, 2009.

(96) **Kostorz, G.** *Phase Transformations in Materials.* s.l. : VCH, 2001. ISBN 3527302565.

(97) **Bain, E.C.** The nature of martensite. *American Institute of Mining and Metallurgical Engineers -- Transactions* . 1924, 1299.

(98) **Frank, F.C.** Martensite. *Acta Metallurgica.* 1953, Vols. 1, pp. 15-21, 1.

(99) **Dunne, D.P.; Wayman, C.M.** The crystallography of ferrous martensites. *Metallurgical Transactions.* 1971, Vols. 2, pp. 2327-2341, 9.

(100) **Entwisle, A. R.** The kinetics of martensite formation in steel . *Metallurgical Transactions.* 1971, Vols. 2, pp. 2395-2407, 9.

(101) **Watanabe, M.; Wayman, C.M.** The morphology and substructure of highly tetragonal martensites in Fe-7 ptc Al−C steels. *Metal. Trans. B.* 1971, Vols. 2, pp. 2221-2227, 8.

(102) **Wakasa, K.; Wayman, C.M.** The Morphology and Crystallography of Ferrous Lath Martensite Studies of Fe-20%Ni-5%Mn—I. Optical microscopy. *Acta Metall.* 1981 , Vols. 29, pp. 973–990, 6.

(103) **Shibata, A.; Morito, S.; Furuhara, T.; Maki, T.**Substructure of lenticular martensites with different martensite start tempeatures in ferrous alloys. *Acta Materialia.* 2009, Vol. 57, 483-492.

(104) **Davies, R.G.; Magee, C.L.** Influence of Austenite and martensite strenght on Martensite Morphology. *Metall. Trans.* 1971, Vols. 2, pp. 1939-1947.

(105) **Maki, T.; Shimooka, S.; Fujiwara, S.; Tamura, I.** Formation Temperature and Growth Behavior of Thin Plate Martensite in Fe-Ni-C Alloys. *Trans. JIM.* 1975, Vol. 16, 35-41.

(106) **Magee, C.L.; Davies, R.G.** The structure, deformation and strength of ferrous martensites. *Acta Metall.* 1971, Vols. 19, pp. 345–354, 4.

(107) **Lo, K.H., Shek, C.H.; Lai, J.K.L.** Recent developments in stainless steels. *Mat. Sci. Eng. R.* 2009, Vols. 65, pp. 39–104.

(108) **Zhao, J.** Continuous cooling transformations in steels. *Mater. Sci. and Tech.* 1992, Vols. 8, pp. 997-1003, 11.

(109) **Davies, R. G.; Magee, C. L.** Influence of austenite and martensite strength on martensite morphology. *Metallurgical Transactions.* 1971, Vols. 2, pp. 1939-1947, 7.

(110) **Maki, T.; Wayman, C. M.** Substructure of ausformed martensite in Fe-Ni and Fe-Ni-C alloys. *Metallurgical Transactions A.* 1976, Vols. 7,pp. 1511-1518, 9.

(111) **Shibata, A.; Murakami, T.; Morito, S.; Furuhara, T.; Maki, T.** The origin of Midrib in Lenticular Martensite. *Materials Transactions.* Vol. 49:6, 1242-1248.

(112) **Lee, H.Y.; Yen, H.W.; Chang, H.T; Yang, J.R.** Substructures of martensite in Fe-1C-17Cr stainless steel. *Scripta Materialia.* 2010, Vol. 62, 670-673.

(113) **Shibata, A.; Morito, S.; Furuhara, T.; Maki, T.***Morphology and Crystallography of Martensite in Ferrous Alloys.* s.l. : Kyoto University. http://www.msm.cam.ac.uk/phase-trans/2002/martensite.html.

(114) **Shibata, A.; Morito, S.; Furuhara, T.; Maki, T.** Local orientation change inside lenticular martensite plate in Fe-33Ni alloy. *Scripta Materialia.* 2005, Vol. 53, 597-602.

(115) **Bhadeshia, H.K.D.H.** An aspect of the nucleation of burst martensite. *Journal of Materials Science.* 1982, Vols. 17, pp. 383-386, 2.

(116) **Sarma, D. S., Whiteman, J. A.; Keown, S. R.** The structure of burst and isothermal martensites in an Fe-24 wt% Ni-0.5 wt%C alloy. *Journal of Materials Science.* 1979, Vols. 14, pp. 693-698, 3.

(117) **Umemoto, M., Minoda, K.; Tamura, I.** Some characteristics of the substructure of Lenticular Martensite in Fe-Ni-C Alloys. *Metallography.* 1982, Vol. 15, 177-191.

(118) **Shibata, A., Furuhara, T.; Maki, T.** Interphase boundary structure and accommodation mechanism of lenticular martensite in Fe–Ni alloys. *Acta Materialia.* 2010, Vols. 58, pp. 3477-3492, 9.

(119) **Miyamoto, G.; Shibata, A.; Maki, T.; Furuhara, T.** Precise measurement of strain accommodation in austenite matrix surrounding martensite in ferrous alloys by electron backscatter diffraction analysis. *Acta Materialia.* 2009, Vols. 57, pp. 1120-1131, 4.

(120) **Patterson, R.L.; Wayman, G.M.** The crystallography and growth of partially-twinned martensite plates in Fe-Ni alloys. *Acta Metallurgica.* 1966, Vols. 14, pp. 347-369, 3.

(121) **Yeo, R.B.G.** Growth of Martensite in an Iron - 28.8% Nickel Alloy. *Transactions of the ASM.* 1964, Vols. 57, pp.48-59.

(122) **Raghavan, V.; Cohen, M.** Measurement and interpretation of isothermal martensitic kinetics. *Metallurgical Transactions.* 1971, Vols. 2, pp. 2409-2418, 9.

(123) **Okada, M.; Arada, Y.** *Tech. Rep. Osaka. Univ.* 5, 1955, Vol. 169.

(124) **Shimizu, K., Oka, M. and Wayman, C.M.** The association of martensite platelets with austenite stacking faults in an Fe-8Cr-1C alloy . *Acta Metallurgica.* 1970, Vols. 18, pp. 1005-1011, 9.

(125) **Yang, D-Z, Sandvik, B.P.J.; Wayman, C.M.** On the Substructure of Athermal ans Isothermal Martensites Formed in an Fe-21Ni-4Mn Alloy. *Metall. Trans. A.* 1984, Vols. 15, pp. 1555-1562.

(126) **Thomas, G.** Electron Microscopy Investigations of Ferrous Martensite. *Metall. Trans. A.* 1971, Vols. 2, pp. 2373-2385.

(127) **Yang, D.; Zhu, M.** Growth of isothermal martensite. *Acta Metall.* 1989, Vols. 2, pp. 16-21, 1.

(128) **Kajiwara, S.** Morphology and Crystallography of the isothermal martensite transformation in Fe-Ni-Mn alloys. *Philosophical Magazine A.* 1981, Vols. 43, pp. 1483-1503, 6.

(129) **Roitburd, A.L.; Kurdjumov, G.V.** The nature of martensitic transformations. *Materials Science and Engineering.* 1979, Vols. 39, pp. 141-167, 2.

(130) **Christian, J.W.** Accommodation strains in martensite formation, and the use of a dilatation parameter . *Acta Metallurgica.* 1958, Vols. 6, pp. 377-379, 5.

(131) **Kelly, P.M.** Martensite crystallography—The role of the shape strain. *Materials Science and Engineering A.* 2006, Vols. 438-440, pp. 43-47.

(132) **Bowles, J.S.;Dunne, D.P.** Role of lastic accommodation in (225) Martensite Transformation. *Acta Metallurgica.* 1969, Vols. 17, pp. 677-685, 5.

(133) **Kelly, P.M.** Crystallography of martensite transformations in steels. [book auth.] E. Perelova and D.V. Edmonds. *Phase transformations in steels: Diffusionless transforamtions, high strenght steels, modelling and advanced analytic techniques (Volume 2).* s.l. : Woodhead Publishing Ltd., 2012.

(134) **Shidao, W.; Zukun, H.** Substructures of the (252) ferrous martensite and their crystallographic significance. *Scripta Materialia* . 1999, Vols. 40, pp. 1157-1164, 10.

(135) **Schoen, F.J.; Owen, W.S.** On the multiple shear theories of martensite crystallography. *Scripta Mater.* 1971, Vols. 5, pp. 315-318.

(136) **Sandvik, B. P. J.; Wayman, C. M.** Characteristics of lath martensite. *Metallurgical Transactions A.* 1983, Vols. 14, pp. 809-822, 4.

(137) **Sandvik, B. P. J.; Wayman, C. M.** Characteristics of lath martensite: Part I. Chystallography and substructural Features. *Metallurgical Transactions A.* 1983, Vols. 14, pp. 809-822, 4.

(138) **Morito, S.; Huang, X.; Furuhara, T.; Maki, T.; Hansen, N.** The morphology and crystallography of lath martensite in alloy steels. *Acta mater.* 2006, Vols. 54, pp. 5323-5331.

(139) **Morito, S.; Igarashi, R.; Kamiya, K.; Ohba, T.; Maki, T.** Effect of cooling rate on the morphology and Crystallography of Lath Martensite in Fe-Ni Alloys. *Mater. Sci. Forum.* 2010, Vols. 638-642, pp. 1459-1463.

(140) **Marder, J.M.; Marder, A.R.** Morphology of iron-nickel massive martensite. *ASM Transaction.* 1969, Vols. 62, pp. 1-10, 1.

(141) **Kitahara, H.; Ueji, R.; Tsuji, N.; Minamino, Y.** Crystallographic features of lath martensite in low-carbon steel. *Acta Mater.* 2006, Vols. 54, pp. 1279–1288.

(142) **Furuhara, T., Takayama, N., Miyamoto, G.** Key Factors in Grain Refinement of Martensite and Bainite. *Materials Science Forum.* 2010, Vols. 638-642, pp. 3044-3049.

(143) **Gourgues, A. F., Flower, H. M.; Lindley, T. C.** Electron backscattering diffraction study of acicular ferrite, bainite, and martensite steel microstructures. *Mater. Sci. Technol.* . 2000, Vols. 16, pp. p. 26.

(144) **Bhadeshia, H.K.D.H.** A rationalization of shear transformations in steels. *Acta Metall.* 1981, Vols. 29, pp. 1117-1130, 6.

(145) **Morito, S.; Tanaka, H.; Konishi, R.; Furuhara, T.; Maki, T.** The morphology and crystallography of lath martensite in Fe-C alloys. *Acta Mater.* 2003, Vols. 51, pp. 1789–1799.

(146) **Tamura, I., Tsuzaki, K.; Maki, T.** Morphology of lath martensite formed from deformed austenite in 18%Ni maraging steel. *J. de Physique.* 12, 1982, Vols. 43, 551-556, Colloque C4.

(147) **Tsuzaki, T.; Maki, T.** The effect of Cooling Rate on the Morphology of lath Martensite in Fe-Ni Alloys. *J. Japan Inst. Metals.* 1981, Vols. 45, p. 126-134, 2.

(148) **Shteynberg, M.M., Mirzayev, D.A.;Ponomareva, T.N.** Gamma -> Alfa Transformation of Iron-Manganese Alloys during Cooling. *Fiz. Metal. Metalloved.* 1977, Vols. 43, pp. 166-172, 1.

(149) **Ansell, G.S., Donachie, S.J.; Messler, R.W.** The effect of quench rate on the martensitic transformation in Fe−C alloys. *Metallurgical Transactions.* 1971, Vols. 2, pp. 2443-2449, 9.

(150) **Yang, D-Z.; Wayman, C.M.** Athermal Martensitic Transformation with an isothermal Component in an Fe-21Ni-4Mn Alloy. *Metallography.* 1984, Vols. 17, pp. 131-137.

(151) **Mirzayev, D.A.; Karzunov, S.Ye.; Schastlivtsev, V.M.; Yakovleva, I.L.** *Phys. Met. Metall.* 1986, Vols. 61, pp. 114.

(152) **Stheynberg, M.M., Mirzayev, D.A.; Ponomavera, T.N.** *Phys. Met. Metall.* 1977, Vols. 43, pp. 143.

(153) **Mirzayev, D.A., Morozov, O.P.; Shteynberg, M.M.** *Phys. Met. Metall.* 1973, Vols. 36, pp. 99.

(154) **Yang, D-Z; Wayman, C.M.** Slow Growth of isothermal lath martensite in an Fe-21Ni-4Mn alloy. *Acta Metall.* 1984, Vols. 32, pp. 949-954, 6.

(155) **Kelly, P.M., Jostsons, A.; Blake, R.G.** The orientation relationship between lath martensite anf austenite in low carbon, low alloy steels. *Acta Metall. Mater.* 1990, Vols. 38, pp. 1075-1081, 6.

(156) **Miyamoto, G., Takayama, N.; Furuhara, T.** Accurate measurement of the orientation relationship of lath martensite and bainite by electron backscatter diffraction analysis. *Scripta Mater.* 2009, Vols. 60, pp. 1113-1116.

(157) **Narashima Rao, B.V.** On the orientation Relationship between Retained Austenite and Lath martensite. *Metall. Trans. A.* 1979, Vols. 10, pp. 645-648.

(158) **Takeuchi, S., Suzuki, H.; Honma, T.** *Jpn. Inst. Metals.* 1950, Vols. 65, pp. 21.

(159) **Easterling, K.E.; Tholen, A.R.** On the growth of martensite in steel. *Acta Metall.* 1980, Vols. 28, pp. 1229-1234.

(160) **Wu, J., Howe, J.M.; Zhang, W.-Z.** An in situ transmission electron microscopy study of interface growth during martensitic transformation. *Acta Mater.* 2011, Vols. 59, pp. 3297-3303.

(161) **Edmondson, B.; Ko, T.** Spontaneous Deformation of Austenite during Martensitic Transformations. *Acta Metall.* 1954, Vols. 2, pp. 235-241.

(162) **Liu, D.Z., Bergeon, N.; Kikuchi, T.; Kajiwara, S.; Shinya, N.** Observation of Plastic Accommodation of Shape Strain in Martensitic Transformation in Fe-Ni-C Shape Memory Alloys. *Mater. Sci. Forum.* 2000, Vols. 327-328, pp. 405-408.

(163) **Lysac, L.I., Artemyak, S.A.; Rybakova, E.A.** *Ordena Lenina Akademiya Nauk USSR, Inst. Metallofiziki.* 1970, Vol. 70, 3.

(164) **Yershov, V.M.; Oslon, N.L.** *Fiz. Met. Metalloved.* 1972, Vols. 33:1, pp. 215-217.

(165) **Araki, T.; Shibata, K.; Asakura, K.; Wada, H.** Direct Observation of the gamma yields alpha prime isohtermal Martensitic Transformation of iron alloys in electron microscope. *ISIJ.* 1975, Vols. 15, pp. 175-184, 4.

(166) **Suzuki, H.** *Sci. Rep. Tohoku Univ.* 1954, Vols. A6, pp. 30.

(167) **Dash, S.; Brown, N.** Nucleation and Groth of Martensite in Fe-32.2%Ni Alloy. *Acta Metall.* 1966, Vols. 14, pp. 595-603.

(168) **Shimizu, K., Oka, M.; Wayman, C.M.** *Modern Diffraction and Imaging Techniques in Material Science.* s.l. : North Holland Publishing Comp., 1970.

(169) **DeHoff, R.T.** *Thermodynamics In Materials Science.* New York : McGraw-Hill, 1993.

(170) **Liu, Y.C., Sommer, F.; Mittemeijer, E.J.** Nature and kinetics of the massive austenite-ferrite phase transformations in steels. [book auth.] E. Pereloma and D.V. Edmonds. *Phase transformations in steels: Fundamentals and diffusion-controlled transformations (Volume 1).* s.l. : Woodhead Publishing Ltd., 2012.

(171) **Christian, J.W.** *Thermodynamics and Kinetics of Martensite.* Cambridge, Massachussetts USA : International conference on the martensitic transformation - ICOMAT, 1979.

(172) **Bhadeshia, H. K. D. H.** Martensite in Steels. [Online] [Cited: May 22, 2013.] http://www.msm.cam.ac.uk/phase-trans/2000/C9/lectures45.pdf.

(173) **Eshelby, J.D.** *The Determination of the Elastic Field of an Ellipsoidal Inclusion, and RelatedProblems.* s.l. : Proceedings of the Royal Society of London. Series A, Mathematical and Physical Sciences, 1957. 241:1226, pp. 376-396.

(174) **Olson, G.B.; Cohen, M.** Thermoelastic behavior in martensitic transformations. *Scripta Metall.* 1975, Vols. 9, pp. 1247-1254.

(175) **Lee; B.; Millman, S.; MacDougall, I.L.** Entalpy of the Martensitic Trasnformation in Steels Containing Nickel and Chromium. *Metal Science.* 1977, Vols. 7, pp.261-271.

(176) **Patel, J.R.;Cohen, M.** Criterion for the action of applied stress in the martensitic transformation. *Acta Metallurgica.* 1953, Vols. 1, pp. 531-538, 5.

(177) **Kakeshita, T., Saburi, T.; Shimizu, K.** Effects of hydrostatic pressure and magnetic field on martensitic transformations. *Materials Science and Engineering A* . 1999, Vols. 273, pp. 21-39.

(178) **Xie, Z.L.; Sundqvist, B.; Hänninen, H.; Pietikäinen, J.** Isothermal martensitic transformation under hydrostatic pressure in an Fe-Ni-C alloy at low temperatures. *Acta Metall. Mater.* 1993, Vols. 41, pp. 2283–2290, 8.

(179) **Kundu, S.; Bhadeshia, H.K.D.H.** Crystallographic texture and intervening transformations. *Scripta Materialia.* 2007, Vols. 57, pp. 869-872, 9.

(180) **Meng, Q.P., Rong, Y.H.; Hsu, T.Y.** Effect of internal Stress on Autochatalytic Nucleation of Martensitic Transformation. *Metall. Mater. Trans. A.* 2006, Vols. 37, pp. 1405-1411.

(181) **Golovchiner, K. Ya.** Changes in the austenite lattice parameter during the martensitic transforamtion in steel. *Fiz. Meta.. Metalloved.* 1974, Vols. 37, No 363-368, pp. 126-130, 2.

(182) **San Martin, D.; Jimenez-melero, E.; Duffy, J.A.; Honkimaki, V.; Van der Zwaag, S.; van Dijk, N.H.** Real time synchrotron X-Ray diffraction study on the isothermal martensite transforamtion of maraging steel in high magnetic fields. *J. Appl. Cryst.* 2012, Vols. 45, pp. 718-757.

(183) **San Martin, D.; van Dijk, N.H.; Jimenez-Melero, E.; Kampert, E.; Zeitler, U.; Van der Zwaag, S.** Real-time martensitic transformation kinetics in maraging steel under high magnetic fields. *Mat. Sci. Eng. A.* 2010, Vols. 527, pp. 5241-5245.

(184) **San Martin, D.; Aarts, K.W.P.; Rivera-Diaz-del-Castillo, P.E.J., van Dijk, N.H.; Bruck, E.; van der Zwaag, S.**Isothermal martensitic transformation in a 12Cr-9Ni-4Mo-2Cu stainless steel in applied magnetic fields. *J. Magnetism and Magn. Mater.* 2008, Vols. 320, pp. 1720-1728.

(185) **Satyanarayan, K.R., Eliasz, W.; Miodownik, A.P.** *Acta Metall.* 1966, Vols. 16, pp. 877.

(186) **Pati, S.R., Cohen, M.** Kinetics of isothermal martensitic transforamtions in an Iron-Nichel-Manganese alloy. *Acta Metall.* 1971, Vols. 19, pp. 1327-1332.

(187) **Guimaraes, J.R.C.** Athermal martensite: Genesis of microstructure and transformation curves. *Mat. Sci. Eng. A.* 2008, Vols. 476, pp. 106-111.

(188) **Guimaraes, J.R.C.; Rios, P.R.** Initial nucleation kinetics of martensite transformation. *J. Mater. Sci.* 2008, Vols. 43, pp. 5206-5210.

(189) **Guimaraes, J.R.C.; Rios, P.R.** Unified Model for Plate and Lath Martensite with Athermal Kinetics. *Metall. and Mater. Trans. A.* 2010, Vols. 41, pp.1928-1935.

(190) **Foster, F.; Scheil, E.** *Ztsch. Metallkunde.* 1936, Vols. 28, pp. 295.

(191) **Yu, Z.Z.; Clapp, P.C.** Growth Dynamics Study of the Martensitic Transformation in Fe-30%Ni Alloys: Part I. Quantitative measurements of Growth Velocity. *Metall. Trans. A.* 1989, Vols. 20, pp. 1601-1615.

(192) **Takashima, K., Higoa, Y.; Nunomura, S.** *Philosophical Mag. A.* 1984, Vols. 49:2, pp. 231-241.

(193) **Bunshah, R.; Mehl, R.F.** *Trans. AIME.* 1953, Vols. 197, pp. 1251-1258.

(194) **Olson, G.B.; Cohen, M.** A general mechanism of martensitic nucleation. *Metallurgical Transactions A (Physical Metallurgy and Materials Science).* 1976, Vols. 7A pp. 1905-1914, 12.

(195) **Kajiwara, S.** Mechanism of isothermal martensitic transformation. *Materials transactions, JIM.* 1992, Vols. 33, pp. 1027-1034, 11.

(196) **Fisher, J.C., Hollomon, J.H.; Turnbull, D.** *J. Applied Physics.* 1948, Vols. 19, pp. 775.

(197) **Kakeshita, T.; Kuroiwa, K.; Shimizu, K.; Ikeda, T.; Yamagishi, A.; Date, M.** A New Model Explainable for Both the Athermal and Isothermal Natures of martensitic Transformation in Fe-Ni-Mn Alloys. *Mat. Trans. JIM.* 1993, Vols. 34, pp. 423-428, 5.

(198) **Kakeshita, T. and Saburi, T.** Kinetics of martensitic transformation in some ferrous and non-ferrous alloys. *Philosophical Magazine.* 2000, Vols. 80, pp.171-181, 2.

(199) **Forster, F • Scheil, E.** Measurement of the formation of martensite needles. *Naturwissenschaften.* 1937, Vols. 25, pp. 439-440.

(200) **Beisswenger, H.; Scheil, E.** *Arch. Eisenhuttenwes.* 1956, Vols. 27, pp. 413.

(201) **Kimmich, H. and wachtel, E.** *Arch. Eisenhuttenwes.* 1964, Vols. 35, pp. 1193.

(202) **Kajiwara, S. and Kikuchi, T.** On the abnormally large tetragonality of martensite in Fe-Ni-C alloys. *Acta Metall. Mater.* 1991, Vols. 39, pp. 1123-1131, 6.

(203) **Ullakko, K. and Gavriljuk, G.V.** Effects of coherent interfaces in the freshly formed Iron-Nickel-Carbon martensites. *Acta Metall. Mater.* 1992, Vols. 40, pp. 2471-2482, 10.

(204) **Ulakko, K. and Gavriljuk, V.G.** Origin of an Internal Friction peak at 145 K in Fe-Ni and Fe-Ni-C Martensites. *Scripta Metall.* 1993, Vols. 28, pp. 593-598.

(205) **Prokoshin, S.D., Kaputkina, L.M.; Bernshtein, M.L.** The Mechanism of Low-Temperature Lattice Changes of Martensite with Abnomal Tetragonality. Part I. Abnormally low Tetragonality. *Scripta Metall.* 1986, Vols. 20, pp. 293-298.

(206) **Prokoshkin, S.D., Kaputkina, L.M..; Bernshtein, M.L.** The Mechanisms of Low-Temperatures Lattice Change of Martensite with Abnormal Tetragonality. Part 2 Martenisites with Abnormally High Tetragonality. *Scripta mater.* 1986, Vols. 20, pp. 299-304.

(207) **Lysak, L.I., Kondratiev, C.P.; Polishchuk, Yu.M.** Dependence of the crystal structures of κ'- and α-martensites on carbon concentration. *Met. Metalloved.* 1973, Vols. 36, pp. 546-550, 3.

(208) **Kurdjumov, G.V.** Martensite with Abnormal Crystal Lattice. *Journal of the Less-Common Metals* . 1972, Vols. 28, pp. 153-155.

(209) **Kurdjumov, G. V.; Khachaturyan, A.** Nature of the Axial Ratio Anomalies of the Martensite Lattice and Mechanism of Diffusionless g->a Trasnformation. *Acta Metall.* 1975, Vols. 23, pp. 1077-1088.

(210) **Kurdjumov, G. V.** Behaviour of Carbon in Quenched Steels. *Mem. Sci. Rev. Met.* 1970, Vols. 67, pp. 755, 12.

(211) **Magee, C.L.** The kinetics of martensite formation in small particles. *Metallurgical Transactions.* 1971, Vols. 2, pp. 2419-2430, 9.

(212) **Cech, R.E.; Turnbull, D.** Heterogeneous nucleation of martensite transformation. *Journal of Metals.* 1956, Vols. 8, pp. 124-132, 2.

(213) **Saburi, I.; Nenno, H.** Stress-induced martensitic transformations in Cu-Zn-Al and Cu-Zn-Ga alloys. *J. de physique colloque.* 1982, Vols. 43, pp. 633-638, C-4.

(214) **Cao, W., Krumhansl, A.; Gooding, R.J.** Defect-induced heterogeneous transformations and thermal growth in athermal martensite. *Physical Review B.* 1990, Vols. 41,319-325, 16.

(215) **Hull, D.; Bacon, D.J.** *Introduction to dislocations.* Oxford, MA, U.S. : Butterworth-Heinemann, 1965.

(216) **Olson, G.B.** Advances in theory: Martensite by design. *Materials Science & Engineering A.* 2006, Vols. 438-440, pp. 48-54.

(217) **Kajiwara, S.** Roles of Dislocations and Grain Boundaries in Martensite Nucleation. *Metall. Trans. A.* 1986, Vols. 17, 1693-1702.

(218) **Jiewu, Z., Yan, X.; Liu, Yongning.** Lath martensite in 1.4%C ultra-high carbon steel and its grain size effect. *Mat. Sci. and Eng. A.* 2004, Vols. 385, pp. 440-444.

(219) **Warlimont, H..** *Trans. AIME.* 1962, Vols. 224, pp. 495.

(220) **Honma, T.** *Bull. Jpn. Inst. Met.* 1957, Vols. 21, pp. 122.

(221) **Pak, J., Suh, D.W.; Bhadeshia, H.K.D.H.** Displacive Phase Transformation and Surface Effects Associated with Confocal Laser Scanning Microscopy. *Metall. And Mater. Trans. A.* 2012, Vols. 43, pp.4520-4524.

(222) **Olson, G. B.; Cohen, M.** Dislocation theory of martensitic transformations. [book auth.] F.R.N. Nabarro. *Dislocations in Solids - Vol 7.* Amsterdam, The Netherlands : North Hollande Physics Pubblishing, 1986.

(223) **Ghosh, G.; Raghavan, V.** The Kinetics of Isothermal Martensitic Transformation in an Fe-23.2wt%Ni-2.8wt. %Mn Alloy. *Mat. Sci. Eng.* 1986, Vols. 80, pp. 65-74.

(224) **S.R Pati, S.R.; Cohen, M.** Nucleation of the isothermal martensitic transformation. *Acta Metall.* 1969, Vols. 17, pp. 189–199, 3.

(225) **Chang, S.N.; Meyers, M.A.** Martensitic Transformation Induced by a Tensile Stress Pulse in Fe-22.5 wt% Ni-4 wt% Mn Alloy. *Acta Metall.* 1988, Vols. 36, pp. 1085-1098, 4.

(226) **Entwisle, A.R.** unpublished work carried out in the Department of Metallurgy, M.I.T. 1963.

(227) **Kakeshita, T., Fukuda, T.; Saburi, T.** Time dependent Nature of the Athermal Martensitic Transformation in Fe-Ni Alloy. *Scripta Mater.* 1995, Vols. 34, pp. 147-150, 1.

(228) **Kakeshita, T.; Kuroiwa, K.; Shimizu, K.; Ikeda, T.; Yamagishi, A.; Date, M.** Effect of Magnetic Fields on Athermal and Isothermal Martensitic Transformations in Fe-Ni-Mn Alloys. *Mater. Trans. JIM.* 1993, Vols. 34, pp. 415-422, 5.

(229) **Kajiwara, S.** Continuous observation of Martensite Formation in Fe-Ni-Mn alloys. *Acta Metall.* 1984, Vols. 3, pp. 404-413.

(230) **Datta, R., Ghosh, G.; Raghavan, V.** Plastic accomodation during growth of the martensic plates in Fe-Ni alloys. *Scripta Mater.* 1986, Vols. 20, pp. 559-563, 4.

(231) **Li, D. F.; Zhang, X. M.; Gautier, E.; Zhang, J. S.** Morphology transitions of deformation-induced thin-plate martensite in Fe–Ni–C alloys. *Acta Mater.* 1998, Vols. 46, pp. 4827-4834, 13.

(232) **Lin, M., Olson, G.B.; Cohen, M.** Distributed-activation kinetics of heterogeneous martensitic nucleation. *Metall. Trans. A.* 1992, Vols. 23, pp. 2987-2998, 11.

(233) **Shih, C.G., Averbach, B.L.; Cohen, M.** *Trans. AIME.* 1955, Vols. 203, pp. 183.

(234) **Rios, P.R.; Costa Guimarães, J.R.** Formal analysis of isothermal martensite spread . *Materials Research.* 2008, Vols. 11, pp. 103-108, 1.

(235) **Ghosh, G.; Raghavan, V.** Autocatalysis and the extent of plate association in isothermally formed martensite in an Fe-Ni-Mn alloy. *Scripta Mater.* 1986, Vols. 79, pp. 223-231, 2.

(236) **Raghavan, V.; Entwisle, A.R.** Isothermal martensite kinetics in iron alloys. *Iron and Steel Institute.* 1965, Vols. Special Report, pp. 30-37.

(237) **Diani, J. M.; Parks, D. M.** Effects of strain state on the kinetics of strain-induced martensite in steels. *Journal of the Mechanics and Physics of Solids.* 1998, Vols. 46, pp. 1613-1635, 9.

(238) **Liu, C; Yao, Ke-Fu; Liu, Z.; Gao, G.** Study of the effects of stress and strain on martensite. *Journal of Computer-Aided Materials Design.* 2000, Vols. 7, pp. 63–69.

(239) **Breinan, E.M.; Ansell, G.S.** The influence of austenite strength upon the austenite-martensite transformation in alloy steels. *Metall. Trans.* 1970, Vols. 1, pp. 1513-1520, 6.

(240) **Kundu, A.; Chakraborti, P.C.** Effect of strain rate on quasistatic tensile flow behaviour of solution annealed 304 austenitic stainless steel at room temperature. 2010, Vols. 45, pp. 5482-5489, 20.

(241) **Chen, A. Y.; Ruan, H. H.; Wang, J.; Chan, H. L.; Wang, Q.; Li, Q.; Lu, J.** The influence of strain rate on the microstructure transition of 304 stainless steel. *Acta Mater.* 2011, Vols. 59, pp. 3697-3709, 9.

(242) **Maxwell, P. C., Goldberg, A.; Shyne, J. C.** Stress-Assisted and strain-induced martensites in Fe-Ni-C alloys. *Metall. Trans.* 1974, Vols. 5, pp. 1305-1318, 6.

(243) **Pradhan, R.; Ansell, G. S.** Kinetics of the martensite transformation in athermal Fe-C-Ni-Cr alloys. *Metall. Trans. A.* 1978, Vols. 9, pp. 793-801, 6.

(244) **Meng, Q.P., Rong, Y.H.; Hsu, T.Y.** Effect of internal stress on autocatalytic nucleation of martensitic transformation. *Metal. and Mater. Trans. A.* 2006, Vols. 37, pp. 1405-1411, 5.

(245) **Olson, G.B.; Cohen, M.** Kinetics of strain-induced martensitic nucleation. *Metallurgical Transactions A (Physical Metallurgy and Materials Science).* 1975, Vols. 6, pp. 791-795, 4.

(246) **Bokros, J.C.; Parker, E.R.** Mechanism of martensite burst transformation in Fe-Ni single crystals. *Acta Metall.* 1963, Vols. 11, pp. 1291-1301, 12.

(247) **Brook, R.; A. Entwisle, A.** Kinetics of burst transformation to martensite. *Journal of the Iron and Steel Institute.* 1965, Vols. 203, pp. 905.

(248) **Machlin, E. S.; Cohen, M.** Burst phenomenon in martensitic transformation. *Trans AIME.* 1951, Vols. 191, pp. 746.

(249) **Durlu, T.N.; Christian, J.W.** Effect of prior deformation on the martensite burst transformation in single crystals of an Fe-Ni-C alloy. *Acta Metall.* 1979, Vols. 27, pp. 663-666, 4.

(250) **Samuels, L.E.** *Optical microscopy of carbon steels.* Metals Park, Ohio : American society for metals, 1980. ISBN 0-87170-082-4 .

(251) **Marder, A.R.; Krauss, G.** Formation of low Carbon martensite in Fe-C- alloys. *ASM Trans. Quart.* 1969, Vols. 62, pp. 957-64, 4.

(252) **Wasaka, K.; Wayman, C.M.** The morphology abn cristallography of ferrous lath martensite. Studeis of Fe-20%Ni.5%Mn - II. Transmission Electron Microscopy. *Acta Metallurgica.* 1981, Vols. 29, pp. 991-1001.

(253) **Ling, H.C.; Owen, W.S.** *Acta. Metall.* 1981, Vols. 29, pp. 1721.

(254) **Wakasa, K.; Wayman, M.** Isothermal Martensite Formation in a Fe-20Ni%-5%Mn Alloy. *Metallography.* 1981, Vols. 14, pp. 37-48, 37.

(255) **Araki, T., Shibata, K.; Wada, H.** Kinetic Study of the Interaction among Three Types of γ◊α´ Martensite Transforation in iron Alooys. *ISIJ.* 1974, Vols. 60, pp.258-268, 2.

(256) **Grujicic, M., Olson, G.B.; Owen, W.S.** Mobility of Martensitic Interfaces. *Metall. Trans. A.* 1985, Vols. 16, pp. 1713-1722.

(257) **Ogawa, K.; Kajiwara, S.** High-resolution electron microscopy study of ledge structures and transition lattices at the austenite-martensite interface in Fe-based alloys. *Philosophical Mag.* 2004, Vols. 21, pp. 2919-2947.

(258) **Schoen, F. J.; Owen, W. S.** Interfacial drag and the growth of martensite. *Metallurgical Transactions.* 1971, Vols. 2, pp. 2431-2442, 9.

(259) **Christian, J.W.** *The Theory of Transformations in Metals and Alloys.* Oxford : Pergamon Press, 1975, 2nd edition.

(260) **Ragone, D.V.** *Thermodynamics of Materials - Volume II (Mit Series in Materials Science and Engineering).* s.l. : John Wiley & Sons Ltd., 1995.

(261) **Mittemeijer, E.J.** Review Analysis of the kinetics of phase transformation. *Journal of material science.* n° 27 1992, pp. 3977-3987.

(262) **Henderson, D.W.** Thermal analysis of non-isothermal crystallization kinetics in glass forming liquids. *J. Non-Cryst. Solids.* 1979, Vols. 30, pp. 301-315.

(263) **Meisel, L.V. and Cote, P.J.** *Acta Metall.* 1983, Vols. 31, pp. 1053.

(264) **Kissinger, H.E.** Reaction Kinetics in Differential Thermal Analysis. *Anal. Chem.* 1957, Vols. 29, pp. 1702–1706, 11.

(265) **Sherman, A.M., Eldis, G.T. and Cohen, M.** The aging and tempering of Iron-Nickel-Carbon martensites. *Metal. Trans. A.* 1983, Vols. 14, pp. 995-1005, 6.

(266) **Cheng, L.; Van der Pers, N.M.; Böttger, A.; de Kejser, Th. H.; Mittemeijer, E.J.** Lattice changes of iron-carbon martensite on aging at room temperature. *Metall. Trans. A.* 1991, Vols. 22, pp. 1957-1967, 9.

(267) **Chen, P.C., Hall, B.O.; Winchell, P.G.** Atomic displacements due to C in Fe Ni C martensite. *Metall. Trans. A.* 1980, Vols. 11, pp. 1323-1331.

(268) **Miller, M.K., Beaven, P.A. and Smith, G.D.** A study of the early stages of tempering of iron-carbon martensites by atom probe field ion microscopy. *Metall. Trans. A.* 1981, Vols. 12, pp. 1197-1204, 7.

(269) **Morra, P.V., Bottger, A.J. and Mittemeijer, E.J.** Decomposition of Iron-based Martensite. A kinetic analysis by means of differential scanning calorimetry and dilatometry. *J. of Thermal Analysis and Calorimetry.* 2001, Vols. 64, pp. 905-914.

(270) **Perez, M., Sidoroff, C. and Vincent, A., Esnouf, C.** Microstructural evolution of martensitic 100Cr6 bearing steel during tempering: From thermoelectric power measurements to the prediction of dimensional changes. *Acta Mater.* 2009, Vols. 57, pp. 3170-3181.

(271) **Izotov, V.I. and Utevskiy, L.M.** Structure of martensite crystals of high-Carbon steel. *Phys. Met. Metallog.* 1, 1968, Vols. 25, pp. 86-96.

(272) **Jack, K.H.** Binary and Ternary Interstitial Alloys III. The Iron-Carbon System: The Characterization of a New Iron Carbide. *Proceedings of the royal society of London, A.* 1948, Vols. 195, pp. 56-61, 1040.

(273) **Nagakura, S., et al.** Crystallographic study of the tempering of martensitic carbon steel by electron microscopy and diffraction. *Metall. Trans. A.* 1983, Vols. 14, pp. 1025-1031, 6.

(274) **Taylor, K.A., et al.** Carbide precipitation during stage I Tempering of Fe-Ni-C Martensites. *Mater. Trans. A.* 1989, Vols. 20, pp. 2749-2765.

(275) **Genin, J-M. R.** On the morphology of the modulated precipitation of extended multiplets and Fe9C4 epsilon or eta carbide obtained by aging and tempering in Fe-C martensite. *Metal. Trans. A.* 1988, Vols. 19, pp. 2901-2909, 12.

(276) **Jack, K.H.** *J.I.S.I.* 1951, Vols. 169, pp. 26-36.

(277) **Lement, B.S.** *Trans. ASM.* 1953, Vols. 45, pp. 597-598.

(278) **Arbuzov, M.P.; Khayenko, B.V.** *Fiz. Metal. Metalloved.* 1962, Vols. 13, pp. 686-692.

(279) **Ruhl, R., Cohen, M.** *Trans. TMS-AIME.* 1969, Vols. 245, pp. 241-251.

(280) **Servant, C. and Cizeron, G.** Investigation into the structural evolutions of a low alloy steel during tempering. *Mater. Sci. Eng. A.* 1989, Vols. 117, pp. 175–189.

(281) **Wiedermann, J., Zalecki, W. and Malec, M.** The influence of nitrogen on the structure and properties of Fe–10Cr–N and Fe–10Cr–1Mo–N steels after tempering in the

temperature range of 650–750 8C. *J. of Mater. Process and Technology.* 2003, Vols. 133, pp. 225–229.

(282) **Jung, M., Lee, S.J. and Lee, J.K.** Microstructural and Dilatational Changes during Tempering and Tempering Kinetics in Martensitic Medium-Carbon Steel. *Metall. and Mater. Trans. A.* 2009, Vols. 40, pp. 551-559.

(283) **Hirotsu, Y. and Nagakura, S.** *Acta Metall.* 1972, Vols. 20, pp. 645-655.

(284) **Nagakura, S.** *J. Phys. Soc. Japan.* 1959, Vols. 14, pp. 186-95.

(285) **Winchell, P.G., Cohen, M.** Strength of martensite. *ASM - Transaction.* 1962, Vols. 55, pp. 347-361, 2.

(286) **Lifshitz, B.G.** *Physical Properties of Metals and Alloys.* Moscow : Mashgiz, 1965.

(287) **Fielding, L.C.D.** The Bainite Controversy. *Mat. Sci. Technology.* 2013, Vols. 29, pp. 383-399, 4.

(288) **Wilson, E.A.** The g->a Transformation in Low Carbon Irons. *ISIJ International.* 1994, Vols. 34, pp. 615-630, 8.

(289) **Bhadeshia, H. K. D. H.** Widmanstatten Ferrite. [Online] [Cited: 07 29, 2013.] http://www.msm.cam.ac.uk/phase-trans/2000/C9/lecture7.pdf.

(290) **Yang, Z-G, et al.** Ledges in Widmanstatten ferrite observed by scanning tunnelling microscopy. *J. Mater. Sci. letters.* 1998, Vols. 17, pp. 331-333.

(291) **Bo, X-Z; Fang, H-S.** Surface relief effects associated with the formation of grain boundary allotriomorph in an Fe-C alloy. *Acta Mater.* 1998, Vols. 46, pp. 2929-2936, 8.

(292) **Oblak, J.M.; Hehemann, R.F.** Structure and growth of widmanstatten ferrite and bainite. [book auth.] Climax Molybdenum. *Transformations and hardenability in steels.* Ann Arbor, MI : s.n., 1967.

(293) **Wilson, E.A., Shtanky, D.V.; Ohmori, Y.** A kinetics and Electronmicroscopic Study of Transformations in Continuously Cooled Fe-15%Ni Alloys. *ISIJ International.* 2001, Vols. 41, pp. 866-875, 8.

(294) **Liu, Y.; Degui, Z.; Jun, Z.; Jian, C.** In situ observation of growth of bainite in Fe-Ni alloy. *Acta Metall. Sinica.* 1994, Vol. 30, 8.

(295) **Aaronson, H.I., Laird, C.; Kinsman, K.R.** *Phase Transformations.* OH : ASM Metal Park, 1970.

(296) **Aaronson, H.I.** *Metall. Trans. A.* 1993, Vols. 24, pp. 24.

(297) **Ragone, D.V.** *Thermodynamics of Materials - Volume I (Mit Series in Materials Science and Engineering).* s.l. : John Wiley & Sons Ltd., 1995.

(298) **Liu, Y.C., Sommer, F.; Mittemeijer, E.J.** Abnormal austenite-ferrite transformation behaviour in substitutional Fe-based alloys. *Acta Mater.* 2003, Vols. 51, pp. 507-519.

(299) **Blazek, A.** *Thermal Analysis.* London : Van Nostrand Reinhold, 1973.

(300) **Bhadeshia, H. K. D. H.** Differential Scanning Calorimetry. [Online] [Cited: 7 25, 2013.] http://www.uzaktanegitimplatformu.com/UEP/uep_ylisans/ey2/ey2_download/DSC%20Thermal2.pdf.

(301) **Zhao, J.Z., Mesplont, C.; De Cooman, B.C.** Kinetics of Phase Transformations in steels: A new Method for Analysing Dilatometric Results. *ISIJ International.* 5, 2001, Vols. 41, pp. 492-497.

(302) **Takahashi, M., Bhadeshia, H.K.D.H.** The interpretation of dilatometric data for trasnformations in steels. *J. of Mater. Sci. Letters.* 1989, Vols. 8, pp. 477-478.

(303) **O´Handley, R.C.** *Modern Magnetic Materials - Principles and Applications.* s.l. : John Wiley & Sons Inc., 2000.

(304) **Cahn, R.W., Haasen, P.; Luborwshy, F.E.** *Physical metallurgy.* s.l. : North Holland Publishing, 1983.

(305) **Zhang, S.Y.; Lu, X.; Tian, X; Qin, Z.** Compositional dependence of the Néel transition, structural stability, magnetic properties and electrical resistivity in Fe–Mn–Al–Cr–Si alloys. *Mat. Sci. Eng. A.* 2002, Vols. 334, pp. 19–27.

(306) **McGraw-Hill Encyclopedia of Science & Technology.** *Vol 20 - "Curie Temperature".* s.l. : McGraw-Hill, 1997.

(307) **Koyano, T.** Isothermal Martensitic trasnformation of g-FeN in a magnetic Field. *Mater. Trans.* 12, 2003, Vols. 44, pp. 2541-2544.

(308) **Yamaoka, T.; Mekata; M.; Takaki, H.** *J. Phys. Soc. Jpn.* 1973, Vols. 35, pp. 63-67.

(309) **Mathalone, Z.; Ron, M.; Pipman, J.; Niedzwiedz, S.** *Journal of Applied Physics.* 1971, Vols. 42, pp. 687-695, 2.

(310) **Koyano, T.** Isothermal martensitic trasnoformation of g-FeN in a Magnetic Field. *Mater. Trans. A.* 12, 2003, Vols. 44, pp. 2541-2544.

(311) **Zhao, L., et al.** Magnetic and X-Ray Diffraction Measurements for the Determination of Retained Austenite in TRIP Steels. *Mater. Sci. Eng. A.* 2001, Vols. 313, pp. 145-152.

(312) **Radu, M.; Valy, J.; Gourgues, A.F.; Le Strat, F.; Pineau, A.** Continuous Magnetic Method for Quantitative Monitoring of Martensitic Transformation in Steels Containing Metastable Austenite. *Scripta Mater.* 2005, Vols. 52, pp. 525-530.

(313) **Xie, Z.L., Liu, Y.; Hanninen, H.** Stabilization of Retained Austenite due to Partial Martensitic Transformation. *Acta Metall.* 1994, Vols. 42, pp. 4117-4133, 12.

(314) **Thompson, S.W.; Krauss, G.** *31st Mechanical Working and Steel Processing Proceedings.* Warrendale, PA : The Iron Steel Society of AIME, 1990.

(315) **Zhao, J.-C., Notis, M.R.** *J. Phase equilibria.* 1993, Vols. 303, pp. 14.

(316) **Wilson, E.A.** *PhD Thesis.* Liverpool, UK : University of Liverpool, 1965.

(317) **Van Bohemen, S.M.C.; Sietsma, J.** Martensite Formation in Partially and Fully Austenitic Plain Carbon Steels. *Metal. and Mater. Trans. A.* 2009, Vols. 40, pp. 1059-1068.

(318) **Brook, R., Entwisle, A.R.; Ibrahim, E.F.** The effect of chemical composition on the shape of martensite trasnformation curves. *Journal of the Iron and Steel Institute.* 1960, Vols. 195, pp. 292-298.

(319) **Mohanty, O.N.** On the stabilization of retained austenite: mechanism and kinetics. *Materials science & engineering. B, Solid-state materials for advanced technology.* 1995, Vols. B32, pp. 267-278, 3.

(320) **Rodrigues, C.A.V., Prioul, C.; Hyspecka, L.** Isothermal martensitic Transformation in Fe-Ni and Fe-Ni-C Alloys at Subzero Temperatures. *Metall. Trans. A.* 1984, Vols. 15, pp.2193-2203.

(321) **Tsuzaki, K., Maki, T.; Tamura, I.** Isothermal Character and Cooling Rate Dependence of Lath Martensitic Transformation in Fe-15%Ni Alloy. *Scripta Mater.* 1987, Vols. 21, pp. 1693-1698.

(322) **Wilson, E.A., Allen, S.P.; Butler, J.** *Met. Sci.* 1982, Vols. 16, pp. 539, 11.

(323) **Löwy, S., et al.** Unusual Martensitic Formation Kinetics in Steels:Observation of Discontinuous Transformation Rates. *submitted for pubblication.*

(324) **Liu, Y.C., Sommer, F.; Mittemeijer, E.J.** Kinetics of the abnormal austenite-ferrite trasnformation behaviour in substitutional Fe-based alloys. *Acta Mater.* 2004, Vols. 52, pp. 2549-2560.

(325) **Liu, Y.C., Sommer, F.; Mittemeijer, E.J.** Abnormal Austenite-Ferrite Trasnformation Behaviour in Pure Iron. *Chinese Sci. Bullettin.* 2004, Vols. 49, pp. 972-975.

(326) **Liu, Y.C., Sommer, F.; Mittemeijer, E.J.** Abnormal Austenite-Ferrite Transformation Kinetics of Ultra-Low-Nitrogen Fe-N alloy. *Metall. and Mater. Trans. A* . 2008, Vols. 39, pp. 2306-2318.

(327) **Liu, Y.C., Sommer, F.; Mittemeijer, E.J.** The austenite–ferrite transformation of ultralow-carbon Fe–C alloy; transition from diffusion- to interface-controlled growth. *Acta Mater.* 2006, Vols. 54, pp. 3383-3393, 12.

(328) **Yang, H.-S. and Bhadeshia, H. K. D. H.** Uncertainties in Dilatometric Determination of Martensite Start Temperature. 2007, Vols. 23, pp. 556-560, 5.

(329) [Online] [Cited: 08 08, 2013.] http://www.valimoinstituutti.fi/en/home.php.

(330) **Goodfellow Cambridge Ltd.** [Online] [Cited: 08 12, 2013.] http://www.goodfellow.com/.

(331) **Ludwigson, D.C. and Hall, A.M.** *The Physical Metallurgy of Precipitation-Hardenable Stainless Stee - Report III.* s.l. : Defence Metals information center, 1959.

(332) **Slunder, C.J., Hoenie, A.F. and Hall, A.M.** *Thermal and Mechanical Treatment for Precipitation-Hardening Stainless Steel.* Washington, D.C. : NASA, 1967.

(333) **Lake Shore Cryonics, Inc.** [Online] [Cited: 08 12, 2013.] http://www.lakeshore.com/products/Vibrating-Sample-Magnetometer/Pages/Model-Landing.aspx.

(334) **Lake Shore Cryotronics, Inc.** Help file - 7400 Series - VSM System software. *Version 1.5.* s.l. : Lake Shore Cryotronics, Inc., 2005.

(335) **TA Instruments.** [Online] [Cited: 08 13, 2013.] http://thermophysical.tainstruments.com/instruments/dilatometers/dil-805ad-quenching-and-deformation-dilatometer/.

(336) **TA Instrument – Bähr Thermoanalyse.** *Quenching Dilatometers Model DIL805.* Hüllhorst / Germany : TA Instrument, 2013.

(337) **Giessen, C.B.; Gordon, G.E.** *Science.* 1968, Vols. 159, pp. 973 – 975.

(338) **Griffiths, D. J.** *Introduction to Quantum Mechanics.* New Jersey : Prentice Hall., 2004.

(339) **Randle, V. and Engler, O.** *Introduction to texture analysis. macrotexture, Microtexture & Orientation Mapping.* s.l. : CRC Press, 2000.

(340) **Goodhew, P.J., Humphreys, J. and Beanland, R.** *Electron Microscopy and Analysis.* s.l. : Taylor & Francis, 2001.

(341) **Schwartz, A. J., et al.** *Electron Backscatter Diffraction in Material science.* s.l. : Springer Science, 2009.

(342) **Jenkins, R. and Snyder, R.** *Introduction to X-Ray Powder Diffractometry.* New York : John Wiley & Sons, Inc., 1996.

(343) **Grunibetiere, R.** *X-Ray Diffraction by Polycystalline Materials.* London : ISTE, Ltd., 2007.

(344) **ASTM.** *ASTM International Standard designation E 975-03, Standard Practice for X-ray Determination of Retained Austenite in Steel with near Random Crystallographic Orientation.*

(345) **Feyerherm, R. and Dudzik, E.** [Online] [Cited: 08 23, 2013.] http://www.helmholtz-berlin.de/forschung/magma/magnetismus/instrumentierung/synchrotron/mags/mags-experiment_en.html.

(346) **Klaus, M.** [Online] [Cited: 08 23, 2013.] https://www.helmholtz-berlin.de/pubbin/igama_output?modus=einzel&sprache=en&gid=1630&typoid=35423.

(347) **Genzel, Ch., Denks, I.A. and Klaus, M.** The materials science Beamline EDDI for Energy-Dispersive Analysis of subsurface Residual Stress Gradients. *Mater. Sci. Forum.* 2006, Vols. 524-525, pp. 193-198.

(348) **Dudzik, E; Feyerherm, R.; Diete, W.; R., Signorato; Zilkens, C.** The new HMI beamline MAGS: an instrument for hard X-ray diffraction at BESSY. *J. of synchotron radiation.* 2006, Vols. 13, pp. 421-425, 6.

(349) **NIST.** [Online] [Cited: 09 15, 2013.] http://physics.nist.gov/PhysRefData/XrayMassCoef/ElemTab/z26.html.

(350) **MacGillavry, C.H. and Rieck, G.D.** *International Tables for X-Ray Crystallography - Vol. III physical and chemical tables.* s.l. : Kynoch Press, 1963.

(351) **Hauk, V.** *Structural and Residual Stress Analysis by Non-Destructive Methods: Evaluation – Application –Assessment.* s.l. : Elsevier Science, 1997.

(352) **Welzel, U., et al.** Stress analysis of polycrystalline thin films and surface regions by X-Ray Diffraction. *J. Appl. Cryst.* 2005, Vols. 38, pp. 1-29.

(353) **Landoldt-Börnstein.** *New Series, Group III Vol. 11.* Berlin : Springer, 1979.

(354) **Behnken, H.** *"Berechnung und Ermittlung der röntgenographischen Elastizitätskonstanten sowie der Mikro- und Makro-Spannungen heterogener und texturierter Werkstoffe", PhD thesis.* Aachen : s.n., 1992.

(355) **Kröner, E.** *Z. Physik.* 1958, Vols. 151, pp. 504 – 518.

(356) **Eshelby, J.D.** The Determination of the Elastic Field of an Ellipsoidal Inclusion, and Related Problems. *Proc. Roy. Soc. (London) A.* 1957, Vols. 241, pp. 376 – 396.

(357) **Christian, J.W.** *The Theory of Transformations in Metals and Alloys.* s.l. : Pergamon Press, 1965.

8. Appendixes

APPENDIX A

In situ investigation of the martensitic transformation in Fe–12wt%Ni–0.6wt%C steel at subzero temperatures

PUBLISHED

M. Villa, K. Pantleon, M. A.J. Somers, J. Alloy Compd., (2012) in press

DOI: 10.1016/j.jallcom.2011.12.162

Work was planned and the results were interpreted by all co-authors. First author performed the majority of the experimental activity and wrote the first draft of the manuscript. K. Pantleon supported the activity at the synchrotron facility. Comments and suggestions from K. Pantleon and Marcel A.J. Somers were incorporated iteratively in the subsequent versions of the manuscript.

Errata Corrige:

XRD quantitative phase analysis was affected by computational errors. The correct quantification can be obtained from the reported data according to the expression:

$$f_\gamma = \frac{4 \cdot f_{RA}}{(1 - f_{RA}) + 4 \cdot f_{RA}}$$

with f_γ actual content of retained austenite calculated according to the method reported in the manuscript and f_{RA} content of retained austenite indicated in the manuscript itself.

Journal of Alloys and Compounds 577S (2013) S543–S548

Contents lists available at ScienceDirect

Journal of Alloys and Compounds

journal homepage: www.elsevier.com/locate/jallcom

In situ investigation of the martensitic transformation in Fe–12 wt.%Ni–0.6 wt.%C steel at subzero temperatures

Matteo Villa*, Karen Pantleon, Marcel A.J. Somers

Technical University of Denmark, Department of Mechanical Engineering, Produktionstorvet, Building 425, 2800 Kgs. Lyngby, Denmark

ARTICLE INFO

Article history:
Received 15 September 2011
Accepted 29 December 2011
Available online 11 January 2012

Keywords:
Phase transformation
Magnetometry
X-ray diffraction
Martensite
Retained austenite

ABSTRACT

Martensitic transformation in a Fe–12 wt.%Ni–0.6 wt.%C alloy was investigated with magnetometry and in situ (synchrotron) X-ray diffraction at sub-zero Celsius temperature. In situ X-ray diffraction at the HZB-BESSY II synchrotron facility was applied to quantitatively determine the fractions of retained austenite and martensite formed during: (i) isochronal transformation, while cooling at a rate of 3 K/min from room temperature to 138 K, and (ii) isothermal transformation, while holding at 138 K. X-ray diffraction analysis was also used for a qualitative evaluation of the stress evolution in austenite during the transformation. Magnetometry was applied to monitor the overall kinetics for the same isochronal and isothermal transformations. The results are discussed in the light of the current theories on martensitic transformations.

1. Introduction

Martensitic transformations in steel are usually considered to be athermal, i.e. the transformation is instantaneous and the degree of transformation depends only on the lowest temperature reached, not on time. In contrast with this athermal behavior, for Fe–Ni–C alloys forming martensite at sub-zero Celsius temperature, the austenite-to-martensite transformation was observed to show a time dependent behavior during isothermal holding at a temperature below the martensite start temperature, M_S [1,2]. Such isothermal behavior was observed to occur above M_S as well [3] and was firstly revealed by Kurdyumov and Maksimova [4] on Fe–1.6%C and Fe–Ni–Mn alloys forming martensite during isothermal holding at sub-zero temperature.

As rationalized by Zhao and Notis [5] the time dependent behavior could be an intrinsic characteristic of the martensitic transformation and, thus, shared by all steels. The notion of an athermal process should then be ascribed to the very fast progression of the austenite to martensite transformation and the inability of existing experimental techniques to monitor this. This rationalization appears consistent with the results reviewed by Thandhani and Meyers [6], the ones analyzed by Borgenstam and Hillert [7] as well as the experimental observations reported by Stojko et al. [8] and Kim et al. [9], where the thermally activated formation of martensite in different steels and at different temperatures was described and discussed.

On the other hand, the reason for a time dependence (hence, for thermal activation) of the martensitic transformation, is unclear. Various explanations have been put forward [10,11], but no actual experimental evidence for a confirmation or rejection of these hypotheses has been presented.

In this study, the martensitic transformation was investigated with a combination of magnetometry and in situ synchrotron X-ray diffraction under both isochronal and isothermal transformation conditions.

2. Experimental

2.1. Material and heat treatments

The model alloy used in the present work is an iron alloy containing 12 wt.% Ni and 0.6 wt.% C. The material was prepared by vacuum induction melting as a 20 kg cast (permanent mold) from electrolytic iron, electrolytic nickel and graphite.

The as-cast material was tempered for 10 h at 723 K to improve machinability and formability. Thereafter, the material was deformed by forging to $\varepsilon = -0.44$ and subsequently tempered for 4 h at 723 K to obtain a homogeneous microstructure. The characteristic transformation temperatures of the material in this initial state were determined by dilatometry (DIL 805A/D) on cylindrical samples with a diameter of 4 mm and 10 mm height. The obtained temperatures are $A_1 = 878$ K, $A_3 = 919$ K, $M_s = 379$ K. Dilatometry was also used to determine the linear expansion coefficient of homogeneous austenite in the temperature range 573–423 K during cooling.

For investigating the martensitic transformation, the samples were austenitized at 1173 K for 30 min, quenched in boiling water, quenched in an ice-bath, and maintained at 273 K for 10 min. After austenitization, the samples were stored at room temperature for 4–6 days. The microstructure of this as-prepared state is shown in Fig. 1a.

For sub-zero treatment the samples were isochronously cooled at a rate of 3 K/min from room temperature to 138 K and isothermally kept at 138 K for 6 h. Two samples, referred to as sample 1 and sample 2, were subjected to synchrotron X-ray investigation during sub-zero treatment. After isothermal holding at 138 K,

* Corresponding author. Tel.: +45 4525 2215; fax: +45 4593 6213.
E-mail address: matv@mek.dtu.dk (M. Villa).

0925-8388/$ – see front matter © 2012 Elsevier B.V. All rights reserved.
doi:10.1016/j.jallcom.2011.12.162

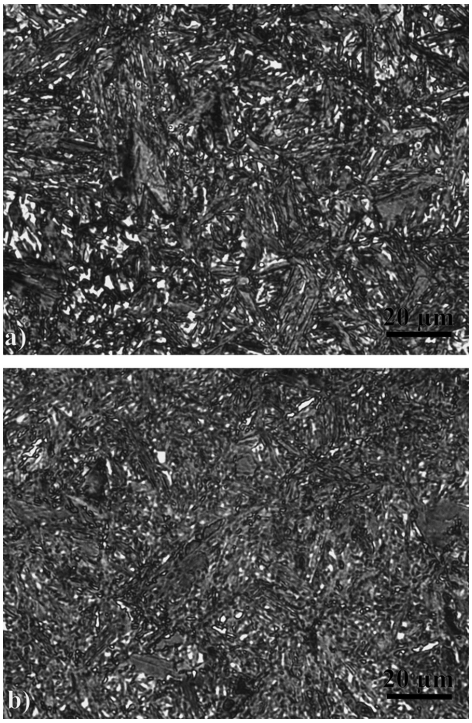

Fig. 1. Reflected light microscopy of: (a) the microstructure of the material in the as-prepared state and (b) the microstructure of the material after the sub-zero treatment. The material was tempered at 423 K for 1 h before surface preparation in order to increase the contrast by partial tempering of martensite. Etching: 2% Nital etching 20 s at 298 K; illumination: monochromatic green light. Retained austenite appears as tiny light areas; martensite appears dark.

sample 1 was reheated at 3 K/min to room temperature. The final microstructure of this sample is shown in Fig. 1b. For the purpose of baseline correction, sample 2 and the magnetometry sample were subjected to further cooling to 108 K, reheated to 198 K, cooled again to 108 K and reheated to room temperature. For all thermal cycles a heating or cooling rate of 3 K/min was applied.

2.2. Magnetometry

Vibrating sample magnetometry was performed with a Lake Shore 7400 Cryotronics VSM equipped with a cryostat on cylindrical samples (⌀3 mm, 4 mm height), which were mounted onto rigid fiber pole using non-magnetic Kapton tape. A magnetic field of 1.5 T was used to bring the sample at saturation. Recording was performed every 0.5 K during the isochronal cooling and every 30 s during the isothermal treatment. The degree of transformation can be followed recording the magnetic moment of the sample at saturation. The extremely high signal to noise ratio, better than 10^4, of this technique makes it the proper choice to describe the kinetics of the transformation. As the magnetic moment is temperature dependent, the signal has to be baseline corrected for the isochronal measurements. The baseline was recorded in the reference state (see Section 2.1).

Magnetometry should be considered an indirect method, as the technique itself cannot prove the formation of martensite, because different phenomena influencing the magnetic signal cannot be excluded a priori. Moreover, it does not allow a direct transformation of the signal in terms of the fraction transformed without the assumption of at least one condition where the phase content is known. In the quantitative analyses of the fraction transformed a linear relationship between magnetic moment at saturation and fraction of martensite was assumed.

2.3. X-ray diffractometry

In situ synchrotron X-ray diffraction was performed at MagS station (HZB-BESSY II) [12] with a radiation with wavelength λ = 0.1 nm focused on a 1 mm spot, applying Bragg–Brentano geometry. Samples 1 and 2 are 0.8 mm-thick disks with a diameter of 15 mm. Investigation was performed in the center on the surface of sample 2,

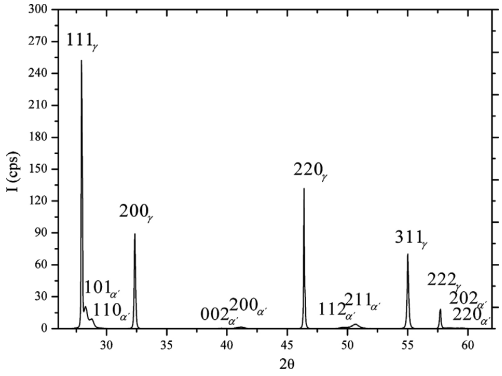

Fig. 2. Diffractogram for sample 1 showing the intensity "*I*" versus scattering angle "2θ" of the material in the as-prepared condition.

where the material was homogeneous in microstructure. For sample 1, the diffracted intensities indicated an inhomogeneous microstructure across the surface and, thus, the recording position on sample 1 was chosen at the location where highest intensity was measured for the austenite peaks. Hence, data from samples 1 and 2 are not comparable in absolute sense and sample 1 is not quantitatively representative.

The applied measurement conditions are collected in Table 1.

For sample 1, the 1 1 1, 2 0 0, 2 2 0, 3 1 1 and 2 2 2 reflections of the f.c.c. austenite and the 1 1 0/1 0 1, 2 0 0/0 0 2, 2 1 1/1 1 2 and 2 2 0/2 0 2 doublets of the b.c.t. martensite were recorded, while for sample 2 only the 1 1 1, 2 0 0, 3 1 1 and 2 2 2 reflections of austenite and the 1 1 0/1 0 1 and 2 2 0/2 0 2 doublet reflections of martensite were measured in the isochronal stage. By means of example, the diffractogram for sample 1 is given in Fig. 2. Diffractograms were recorded every 7 K for sample 1 and every 9 K for sample 2 in the isochronal stage and every 16 min in the isothermal stage.

X-ray diffraction analysis allows a direct observation and quantification of the f.c.c. to b.c.t. transformation by recording various Bragg peaks for the two constituting phases and comparing the experimentally measured intensities to those predicted for a powder sample [13]. The quantification of the fraction transformed during cooling was performed by fitting Lorentzian functions to the recorded line profiles and considering the integrated intensity of the 2 0 0, 2 2 0 and 3 1 1 peaks of austenite and of the 2 0 0/0 0 2 and 2 1 1/1 1 2 peaks of martensite. All reflections were included in the quantification, as to minimize the effect of crystallographic texture on the calculated fraction. The 1 1 1 reflection of austenite and the 1 1 0/1 0 1 reflections of martensite were not considered, because of their strong overlap and corresponding uncertainties in peak profile fitting. The austenite peaks recorded during isothermal holding at 138 K allowed fitting of pseudo-Voigt functions, because of their higher quality as compared to the isochronal stage, consistent with the smaller step size and longer counting time (Table 1).

On fitting, special care was taken to avoid artifacts that can result from a slight overlap of 2 0 0 and 2 2 0 austenite peaks with the tails of 1 0 1 and 1 1 2 martensite reflections. For the reflections of martensite (2 0 0/0 0 2 and 2 1 1/1 1 2) the intensity factor was calculated assuming the angular position of the doublets in their centroid position and summing up their multiplicity factors (cf. [13]). In the quantification procedure the atomic scattering factor was calculated from the value reported in [14] by linear interpolation among the tabulated $\sin\theta/\lambda$ values. The temperature factor was assumed to be linearly dependent on temperature and equal to 0.71 at 296 K [13].

Lattice (macro-)strains generated during the thermal cycle can be evaluated in the direction parallel to the diffraction vector, comparing the change of the lattice parameter of the material with that expected due to unconstrained thermal contraction. This investigation was performed in situ by measuring the average distance between the atomic planes parallel to the sample surface and was used to estimate the stress accumulating in austenite during transformation. The linear expansion coefficient of austenite at the temperature of investigation was obtained by linear extrapolation of dilatometry results.

3. Results and discussion

3.1. Isochronal transformation

The magnetization relative to the baseline recorded in the isochronal and isothermal stage is shown in Fig. 3. Clearly, the magnetization increases for temperatures below 230 K and continues in

Table 1
Measurement conditions for in situ synchrotron X-ray diffraction investigations at $\lambda = 0.1$ nm.

	Isochronal			Isothermal		
	2θ range	Step size	Time per step [s]	2θ range	Step size	Time per step [s]
Sample 1	26–62°	0.015°	0.05	26–62°	0.015°	0.5
Sample 2	25–34° 53–62°	0.005°	0.1	25–62°	0.015°	0.5

the isothermal stage, consistent with results presented earlier for AISI 52100 and 1070 steels in [8]. The magnetization corresponds to an, as yet, unknown fraction of transformed austenite. X-ray diffractograms for sample 2 recorded in the isochronal stage are collected in Fig. 4a. As anticipated the intensities of austenite and martensite peaks decrease and increase, respectively. Comparison of the diffractograms for sample 2 in Fig. 4a and that for the initial state on sample 1 in Fig. 2 show convincingly that different amounts of retained austenite are present in these samples, and that the highest amount is present in sample 1. A comparison of the fraction of transformed austenite, calculated from a quantification of the diffracted intensities of austenite and martensite, and the evolution of the magnetization is provided in Fig. 4b for sample 1. No accurate quantification of the austenite fraction in sample 2 was possible, due to a limited number of available peaks (see Fig. 4a) as a consequence of the chosen 2θ range (Table 1).

Both diffractometry and magnetometry show consistently that thermal stabilization of austenite occurs down to the temperature range 250–230 K, where martensite formation commences. Thermal stabilization of austenite occurs whenever the transformation is interrupted below the M_s temperature [15] and is more pronounced for lower initial contents of retained austenite [16]. Seemingly, the martensitic transformation starts at a higher temperature in the diffraction analysis of sample 1 (at 250 K) than in the magnetometry analysis (230 K). This discrepancy is consistent with the initially larger content of retained austenite present in sample 1, where a location on the sample surface with a higher austenite content was selected deliberately. Consequently, austenite is stabilized to lower temperatures in sample 2 than in sample 1. Also, temperatures indicating stabilization from magnetometry results are lower than the ones from XRD. In this respect it should be realized that magnetometry averages over the entire sample, while diffractometry refers to a local region on the sample, which, as mentioned above, was not representative for the whole sample 1. Consequently data in Fig. 4a cannot be used for a calibration of the magnetic moment against the fraction of austenite.

The evolution of the (macro-) lattice strain derived from the relative peak shift of various reflections corresponding to different $h\,k\,l$ is given in Fig. 5 for both sample 1 (2 0 0, 2 2 0 and 3 1 1 reflections) and sample 2 (2 0 0 and 3 1 1 reflections). The strains are corrected for unconstrained contraction as calculated from a linear expansion coefficient of $23.2 \times 10^{-6}\,K^{-1}$ at 290 K decreasing linearly to $22.6 \times 10^{-6}\,K^{-1}$ at 138 K, which was derived from linear extrapolation of the dilatometry measurements. The evolution of the lattice strain is qualitatively consistent for the investigated Bragg reflections; all data indicate that compressive lattice strain builds up in austenite upon martensitic transformation.

It was anticipated that after the correction for unconstrained thermal contraction, tension would be observed to build up in the stage of thermal stabilization, because application of the unconstrained linear expansion coefficient of austenite leads to an overestimation of thermal shrink, which is counteracted by the smaller contraction of the martensite. The scatter in the data does not allow a conclusion as to whether this trend actually occurs. Qualitatively, the development of compressive stress in austenite at temperatures below 240 K is consistent with the volume expansion associated with the f.c.c. to b.c.t. transformation. Realizing that the austenite is present as isolated crystals embedded in a martensite matrix (see Fig. 1), a hydrostatic triaxial state of stress is assumed to exist in austenite. This leads to the conclusion that it would not be possible for the transformation to go to completion, because an increase of hydrostatic pressure in the remaining austenite will stabilize it against transformation [17].

Adopting a state of hydrostatic stress in austenite, the (macroscopic) hydrostatic stress, σ_h, related to the measured lattice strain, ε_{33}, obeys:

$$\varepsilon_{33} = \left(3S_1^{h\,k\,l} + \tfrac{1}{2}S_2^{h\,k\,l}\right)\sigma_d \tag{1}$$

where $S_1^{h\,k\,l}$ and $(1/2)S_2^{h\,k\,l}$ are the X-ray elastic constants, which depend on the $h\,k\,l$ under investigation and the assumed elastic interaction model between the crystallites. No data is available for the elastic interaction between martensite and austenite grains. It is therefore assumed that the elastic constants for monophase polycrystalline austenite prevail (this could imply a severe simplification), i.e. [18,19]: $S_1^{h\,k\,l} = (-2.35 + 3.73\Gamma) \times 10^{-6}\,MPa^{-1}$ and

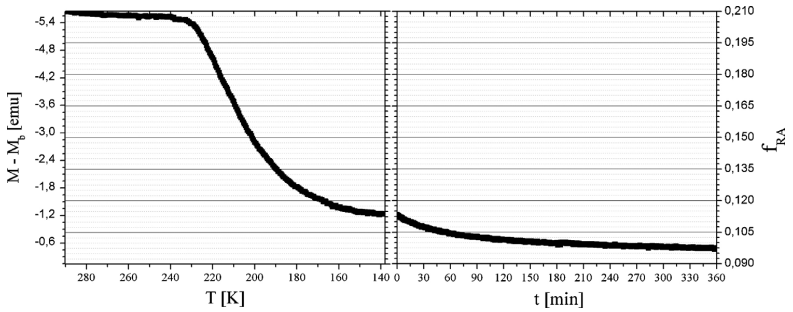

Fig. 3. Fraction of retained austenite "f_{RA}" versus temperature "T" and time "t" as determined from the magnetometry data assuming a final fraction of retained austenite during baseline recording of 8.74% (see text in Section 3.2).

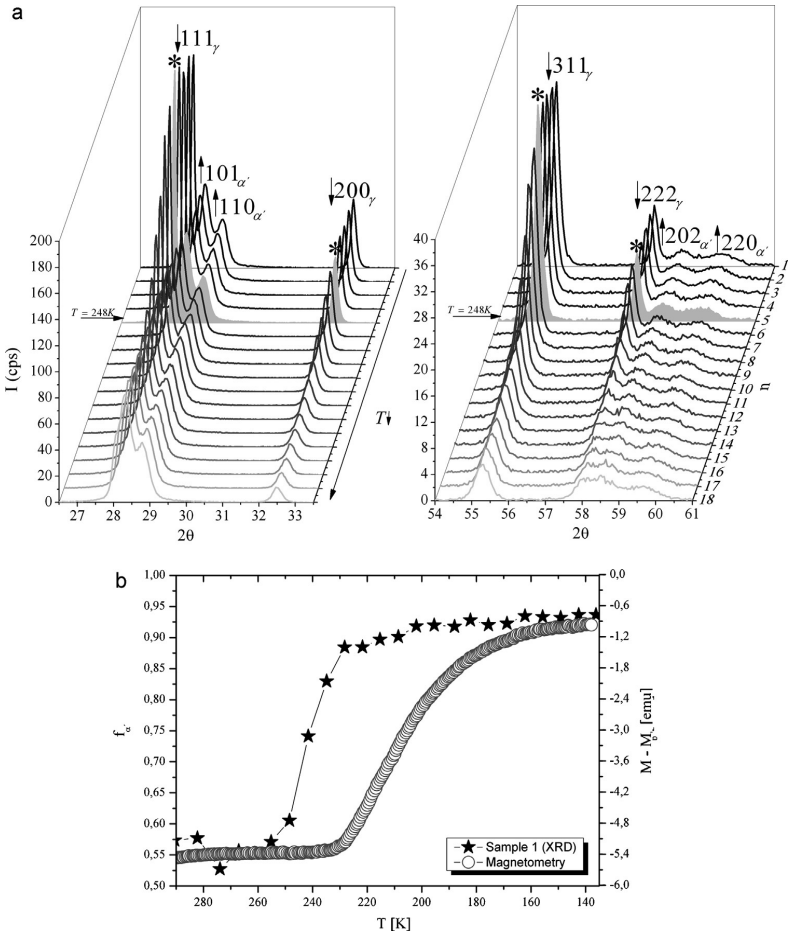

Fig. 4. (a) Diffractograms, intensity "*I*" versus scattering angle "2*θ*", at 9 K intervals recorded during isochronal cooling of sample. The diffractogram indicated with an asterisk (number 5) was recorded at 248 K and is the last diffractogram where no indication of new martensitic transformation is observed. (b) Fraction of martensite "f_α" versus temperature "*T*" as measured with in situ X-ray diffraction, and evolution of the magnetic moment at saturation relative to the background "$M_s - M_b$" as measured with magnetometry.

$(1/2)S_2^{hkl} = (8.32 - 11.2\Gamma) \times 10^{-6}\,\mathrm{MPa}^{-1}$ with $\Gamma = (h^2k^2 + k^2l^2 + l^2h^2)/(h^2 + k^2 + l^2)^2$. The values of the X-ray elastic constants for the various *h k l* investigated are given in Table 2, together with the stress values calculated from the average levels attained for ε_{33} in Fig. 5.

Quantitatively, the residual stresses in austenite vary for the different *h k l* investigated in accordance with the scatter among the lattice strains (for all *h k l* the effective elastic constant between hydrostatic strain and stress equals $1.33 \times 10^{-6}\,\mathrm{MPa}^{-6}$). On the basis of the present results it is not possible to conclude whether the variation in (lattice) strain/stress is an actual difference among the different orientations of austenite or an artifact of the evaluation procedure, i.e. presuming a state of hydrostatic stress and elastic grain interaction as for austenite.

An attempt was made to determine the lattice strain in martensite from shifts of the 2 0 0/0 0 2 and 2 1 1/1 1 2 reflections. As the quality of the data obtained is a compromise between accuracy and measurement time, the quantification of overlapping peaks is ambiguous and the stress effects in martensite are relatively small (as compared to austenite) the data did not allow a thorough

Table 2
X-ray elastic constants of austenite (presuming elastic grain interaction among austenite grains), and the hydrostatic stress σ_h, calculated from the average strain levels ε_{33}.

h k l	S_1^{hkl} [10^{-6} MPa^{-1}]	$(1/2)S_2^{hkl}$ [10^{-6} MPa^{-1}]	ε_{33}	σ_h [MPa]
200	−2.35	8.38	−0.00104	−781
220	−1.42	5.58	−0.00153	−1153
311	−1.76	6.62	−0.00109	−820

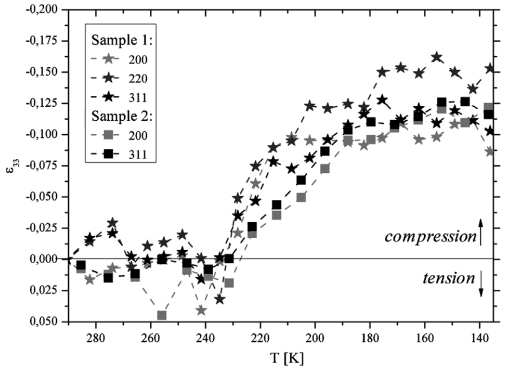

Fig. 5. Percentage lattice strain "ε_{33}" versus temperature "T" corrected for the expected thermal contraction.

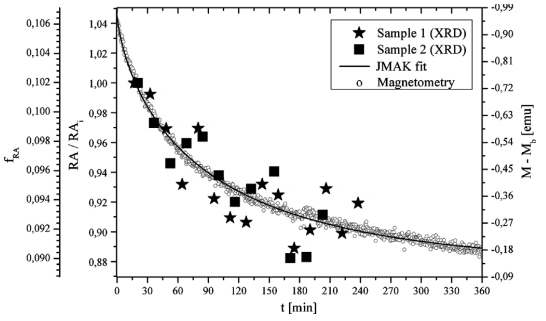

Fig. 6. Evolution of the isothermal martensitic transformation versus time "t" during holding at 138 K. The normalized results from XRD and magnetometry are compared in terms of content of retained austenite. The magnetic moment at saturation relative to the base line "$M_s - M_b$" versus time is reported scaled on the right side of the graph. The drawn line is the JMAK fitting result: $n = 0.75$, $k = 0.011\ \text{min}^{-1}$, $a_n = 1.04$ and $b_n = -0.16$.

quantification. Qualitatively, a weak trend showing the development of a state of tensile stress was observed on increasing the martensite content.

3.2. Isothermal transformation

After isochronal cooling to 138 K, a temperature overshoot of 6 K was recorded and the time for thermal stabilization of the sample holder before the isothermal step started was 8 and 10 min for sample 1 and sample 2, respectively. During this time interval, three diffractograms were recorded maintaining the instrumental set up used during isochronal cooling. These diffractograms are not included in the above reported analysis of the isochronal stage. Instead, the period of time necessary to achieve thermal stabilization of the system is considered to be part of the isothermal stage. During this short time the amount of retained austenite in sample 1 decreased from 6.3% to 5.3%.

The content of retained austenite calculated from the first diffractogram in the isothermal stage is 4.1% and 1.5% for sample 1 and sample 2, respectively. The different contents of austenite between the two samples originate from the initially higher amount of retained austenite in the recording position for sample 1. The discrepancy between the content of retained austenite at the end of the isochronal stage and at the beginning of the isothermal holding in sample 1 is attributed to the net result of the fast transformation in the first part of the isothermal stage (thermal stabilization) and the different fitting procedures applied for the austenite peaks in isochronal and isothermal stages (see Table 1).

The evolution of the austenite content obtained from X-ray diffraction on isothermal holding is shown by the data points in Fig. 6 for both samples 1 and 2. In order to compare the obtained results for different initial contents of retained austenite, the fraction of retained austenite was normalized to the content of austenite calculated for the first diffractogram ($(RA)_{1st}/RA_i) = 1$). In an attempt to calibrate the isothermal magnetometry results against the isothermal XRD results, identical kinetics, i.e. "n" and "k" values of a JMAK type fitting equation $f(t) = a_n + b_n \times (1 - \exp(-(k \times t)^n))$, of the transformation on the isothermal stage is assumed. The value of the content of retained austenite during baseline recording (reference state) was iteratively varied to match the JMAK curve obtained for the normalized XRD results with the experimental data from magnetometry. When a reference state is assumed, a correspondence between magnetic moment at saturation and fraction of martensite in the sample is established, and this correspondence can be used to calculate the reference state that provides a best match of the results. In order to compare the fraction transformed calculated from magnetometry for different reference states and the XRD results, the fraction of austenite calculated was normalized to the content of austenite calculated for an isothermal holding of 18 min ($((RA)_{18'}/RA_i) = 1$).

The reference state, i.e. the content of retained austenite during baseline recording, that provides the best match of the results is 9.3%. This provides the outer scale on the left hand side of the graph in Fig. 6 and the right hand scale of the graph in Fig. 3. An excellent correspondence between normalized experimental data obtained from magnetometry after the establishment of the reference state and the JMAK curve obtained from the XRD data is obtained (Fig. 6).

The obtained value for the final content of retained austenite (9.3%) is higher than the retained austenite content at the beginning of isothermal holding of sample 1 and sample 2 (4.1% and 1.5%, respectively). This discrepancy can most likely be attributed to the sensitivity of the measurement techniques (i.e. temperature induced instabilities of the optics and, hence, movement of the X-ray focus on the sample) as well as the part of the (slightly inhomogeneous) sample that contributes to the recorded signal in the applied technique. Magnetometry has a high signal to noise ratio and the recorded response is an average over the entire sample. These conditions imply that the technique provides an excellent statistical average. This makes magnetometry the optimal choice for a detailed study of the kinetics. On the other hand, XRD has a detection limit of approximately 2–3% retained austenite [13]. Furthermore, the technique investigates only a part of the sample and averages over a relatively shallow depth range. In this respect it is not surprising that the absolute values for the fraction of retained austenite obtained with magnetometry and XRD show a systematic difference. In regions close to the surface the stress state will generally deviate from hydrostatic, as stresses in the direction perpendicular to the plane of the sample surface can relax (partly). Consequently, shear stresses σ_{i3} are invoked leading to continued transformation of austenite into martensite. As a consequence, a measurement technique that does not include the bulk of the sample will show a lower content of retained austenite than techniques that average over the entire sample, as observed for the present investigations.

4. Conclusions

The transformation of austenite into martensite was followed by in situ synchrotron X-ray diffraction in a model alloy Fe–12 wt.%Ni–0.6 wt.%C under isochronal and isothermal conditions. The data confirm the possibility of thermally activated

martensitic transformation as suggested by magnetometry. During the transformation large (hydrostatic) compressive stress develop in the remaining austenite, which contribute to a stabilization of austenite against prolonged transformation.

Magnetometry is a sensitive technique for monitoring the kinetics of the martensitic transformation in both isochronal and isothermal stages and allows a quantitative description according to the Johnson–Mehl–Avrami–Kolmogorov transformation kinetics.

Coupling the information obtained from in situ synchrotron XRD investigation and magnetometry, the intrinsic limitations of both techniques are overcome: insufficient statistics and impossibility to study the average properties of the bulk connected with an X-ray investigation are supplemented by excellent statistics and sample-averaged information from magnetometry. On the other hand, indirect information and the impossibility to obtain quantitative data on the austenite fraction by magnetometry is supplemented by direct X-ray diffraction identification of austenite and martensite (and other phases if present) and quantitative determination of the fractions of these phases in the analyzed volume.

Acknowledgments

The “Foundry Institute of Finland” is acknowledged for supplying the material.

M.F. Hansen, Technical University of Denmark, is gratefully acknowledged for constant support with the magnetometry measurements and precious suggestions for the optimization of the experimental conditions.

O. Kessler and M. Reich, University of Rostock, are gratefully acknowledged for dilatometry investigations.

R. Feyerherm, E. Dudzik, C. Genzel and M. Klaus are acknowledged for their support during in situ experiments at the Berlin synchrotron facility HZB-BESSY II.

References

[1] C.A.V. de Rodrigues, C. Prioul, L. Hyspecka, Metall. Mater. Trans. A 15 (1984) 2193–2203.
[2] D.S. Sarma, J. Mater. Sci. 14 (1979) 693–698.
[3] V. Raghavan, M. Cohen, Met. Trans. 2 (1971) 2409–2418.
[4] G.V. Kurdyumov, O.P. Maksimova, Dokl. Akad. Nauk SSSR 61 (1948) 83–86.
[5] J.-C. Zhao, M.R. Notis, Mater. Sci. Eng. Rep. 15 (1995) 135–207.
[6] Naresh N. Thandhani, Marc A. Meyers, Prog. Mater. Sci. 30 (1986) 1–37.
[7] A. Borgenstam, M. Hillert, Acta Mater. 45 (2) (1997) 651–662.
[8] A. Stojko, M.F. Hansen, J. Slycke, M.A.J. Somers, J. ASTM Int. 8 (4) (2011) 1–9.
[9] D. Kim, J.G. Speer, B.C. de Cooman, Metall. Mater. Trans. A 42 (2011) 1575–1585.
[10] G.B Olson, W.S. Owen, Martensite, ASM International, 1992.
[11] S. Kajiwara, Mater. Trans. 33 (11) (1992) 1027–1034.
[12] E. Dudzik, R. Feyerherm, W. Diete, R. Signorato, C. Zilkens, J. Synchrotron Radiat. 13 (2006) 421–425.
[13] ASTM International Standard designation E 975-03, Standard Practice for X-ray Determination of Retained Austenite in Steel with near Random Crystallographic Orientation.
[14] C.H. MacGillavry, G.D. Rieck, International Tables for X-Ray Crystallography, vol. III, Physical and Chemical Tables, Kynoch Press, 1963.
[15] O.N. Mohanty, Mater. Sci. Eng. B32 (1995) 267–278.
[16] K.R. Kinsman, J.C. Shyne, Acta Metall. 15 (1967) 1527–1543.
[17] J.R. Patel, M. Cohen, Acta Metall. 1 (5) (1953) 531–538.
[18] K. Salmutter, F. Stangler, Z. Metallkd. 51 (1960) 544–548.
[19] V. Hauk, H. Kockelmann, Arch. Eisenhüttenwes. 50 (1979) 347–350.

APPENDIX B

Sub-zero Austenite to Martensite Transformation in a Fe-Ni-0.6wt% C alloy

PUBLISHED

M. Villa, K. Pantleon, Marcel A.J. Somers, Proceedings of the 19th IFHTSE Congress, 2011

Work was planned and the results were interpreted by all co-authors. First author performed the majority of the experimental activity and wrote the first draft of the manuscript. K. Pantleon supported the activity at the synchrotron facility. Comments and suggestions from K. Pantleon and Marcel A.J. Somers were incorporated iteratively in the subsequent versions of the manuscript.

Errata corrige:

XRD quantitative phase analysis was affected by computational errors. The correct quantification follow can be obtained from the reported data according to the expression:

$$f_\gamma = \frac{4 \cdot f_{RA}}{(1 - f_{RA}) + 4 \cdot f_{RA}}$$

with f_γ actual content of retained austenite calculated according to the method reported in the manuscript and f_{RA} content of retained austenite indicated in the manuscript itself.

Sub-zero Austenite to Martensite Transformation in a Fe-Ni-0.6wt%C alloy

Matteo Villa, Karen Pantleon, Marcel A.J. Somers

Technical University of Denmark, Department of Mechanical Engineering

DK 2800 Kongens Lyngby, Denmark

matv@mek.dtu.dk, kapa@mek.dtu.dk, somers@mek.dtu.dk

Abstract

Martensitic transformation in a model Fe-Ni-0.6wt%C alloy was investigated at sub-zero Celsius temperature. The influence of the thermal path in determining the conditions leading to the formation of martensite was studied. In the investigation, samples were austenitized and quenched, whereafter isochronal (constant cooling rate) and isothermal sub-zero Celsius treatments were applied. Magnetometry was used for describing the overall kinetics of the transformation in terms of the Johnson-Mehl-Avrami-Kolmogorov kinetics. The evolution of the transformation was also investigated with in situ synchrotron X-ray diffraction by evaluating austenite and martensite Bragg reflections. Also, the state of internal strain in austenite was determined.

Introduction

Martensitic transformations in steel are usually considered athermal, i.e. the transformation is instantaneous and the degree of transformation depends only on the lowest temperature reached, not on time. This approach resulted in the Koistinen-Marburger equation [1], where the transformation is modeled as a function of temperature only, and in the erroneous practice of drawing horizontal lines for the martensite formation in TTT diagrams pointed out by Zhao and Notis [2].

Similarly, when martensite is the only product of the transformation, the morphology of martensite is usually considered to be determined by the chemical composition of the steel and the austenitization process (time, temperature and imposed plastic deformation [3,4] only, and not on the thermal path followed during the quenching process in the M_s-M_f region.

Ansell et al. [5] were the first showing this concept to be only approximate, reporting the possibility for high cooling rates to suppress the formation of lath martensite in favor of a plate like morphology in a Fe-Ni-C alloy. The recent work of Sato et al. [6] for a Fe-Ni system confirmed that different morphologies (lath, butterfly and lenticular) can form as a function of cooling rate and the final quenching temperature. They showed that a larger fraction of austenite can be retained in the portion of material that is cooled faster and to a lower final quenching temperature due to the suppression of those emerging morphologies requiring a large plastic accommodation through the movement of dislocations.

These effects are appointed to the thermally activated nature of the martensitic transformation, first revealed by Kurdyumov and Maksimova [7], and recently demonstrated by the present authors during direct in situ observation at sub-zero temperature [8], and could get a relevant technological importance to design new advanced steels with improved characteristics. Nowadays, after the observation of the isothermal formation of martensite at high temperature in low carbon steel by Kim et al. [9], enforcing the rationalization by Zhao and Notis regarding the possibility for time dependency to be an intrinsic characteristic of the martensitic transformation in steel, and the exploitation of the isothermal formation

of martensite in commercial alloys [10], the thermally activated nature of the martensitic transformation needs to be considered for optimization of heat treatments for steel.

In this paper the influence of the thermal cycle at sub-zero temperature on the transformation path in a Fe-Ni-C model alloy, and on the consequent buildup of stresses in the material due to transformation shape strain and interaction between martensite and retained austenite during the thermal cycle is reported and analyzed.

Experimental

Material and heat treatments

The model alloy used in the present work is an iron alloy containing 12wt% Ni and 0.6wt% C. The material was prepared by Vacuum Induction Melting as a 20 kg cast (permanent mold) from electrolytic iron, electrolytic nickel and graphite.

The as-cast material was tempered for 10h at 723K, deformed by forging to ε=-0.44 and subsequently tempered for 4h at 723K. The characteristic transformation temperatures of the material in this initial state were determined by dilatometry (DIL 805A/D) and amount to: A_1=878 K, A_3=919 K, M_s=379 K. Dilatometry was also used to determine the linear expansion coefficient of homogeneous austenite in the temperature range 573-423 K: a value of $(22.05 + 0.004 \cdot T) \cdot 10^{-6} K^{-1}$ was obtained. For investigating the martensitic transformation, the samples were austenitized at 1173 K for 30min, quenched in boiling water, quenched in ice water, and maintained at 273 K for 10 minutes. After austenitization, the samples were stored at room temperature for 1-7 days before further analysis. Thereafter the samples were subjected to different subzero treatments. The treatment conditions are reported in Table 1.

Table 1: Thermal cycle for the sub-zero treatments. Final reheating for the sample subjected to magnetometry investigation (Vibrating Sample Magneotemtry – VSM) was performed for the purpose of baseline correction and represents the reference state for the magnetometry investigation.

Sample VSM	Cooling 3K/min to:	Isothermal holding:	Further cooling 3K/min to:	Reheating 3K/min to:	Second cooling 3K/min to:	Final reheating 3K/min
143	143K	3h, 143K	103K	203K	103K	290K
163	163K	3h, 163K	103K	203K	103K	290K
203	203K	3h, 203K	103K	203K	103K	290K
Sample XRD	Cooling 3K/min to:		Isothermal holding:	Further cooling 3K/min to:		Reheating 3K/min
1	143K		6h, 143K	103K		290K
2	88K		4h, 88K	23K		290K

Magnetometry

Vibrating Sample Magnetometry was performed with a Lake Shore 7400 Cryotronics VSM equipped with a cryostat on cylindrical samples (Ø 3mm, 4mm height), which were mounted onto a rigid fiber pole using non-magnetic Kapton tape. A magnetic field of 1.5 T was used to bring the samples at saturation. Recording was performed every 0.5 K during the isochronal cycles and every 30 seconds during the isothermal treatment. The transformation can be followed recording the magnetic moment of the sample at saturation "M". The signal to noise ratio of this technique is better than 10^4, and makes it the proper choice to describe the kinetics of the transformation. As the magnetic moment is temperature dependent,

the signal has to be baseline corrected for the isochronal measurements. The baseline was recorded in the reference state (see 2.1).

Magnetometry is an indirect method, as the technique itself cannot prove the formation of martensite. However, a comparative analysis of the fraction transformed between different samples can be performed assuming equivalent sample dimensions and mounting conditions in the VSM equipment (standard deviation in measured magnetization ±0.7% [11]).

X-Ray Diffraction

In situ synchrotron X-ray diffraction, XRD, was performed at MagS station (HZB-BESSY II) [12] with a radiation of wavelength λ=0.1nm focused onto a 1mm spot, applying Bragg-Brentano geometry. Samples are 0.8 mm-thick disks with a diameter of 15 mm. The measurement conditions for f.c.c. (austenite)and b.c.t. (martensite) are collected in Table 2. Diffractograms were recorded every 16 minutes in the isothermal stage and every 9 K during isochronal treatments.

The quantification of the fraction transformed during isochronal cycles was performed considering the 200_{γ} and 311_{γ} reflections of austenite and the $110/101_{\alpha'}$, $220/202_{\alpha'}$ reflections of martensite, and fitting the recorded line profiles with Lorentzian functions. The 111_{γ} and the 222_{γ} reflection of austenite where not considered due to large overlap with the more intense martensite peaks. The quantification during isothermal holding was done considering all reflections to reach best statistics and weighting only 50% of the 111_{γ}-$110/101_{\alpha'}$ triplet and its second order as to avoid double counting of equally oriented grains. For the reflections of martensite the intensity factor was calculated assuming the angular position of the doublets in their centroid position and summing up their multiplicity factors (cf. [13]). In the quantification procedure the atomic scattering factor was calculated from the value reported in literature [14] by linear interpolation among the tabulated sinθ/λ values. The temperature factor was assumed to be linearly dependent on temperature and equal to 0.71 at 296 K [13].

Table 2: Measurement conditions for in situ synchrotron X-ray diffraction investigations at λ=0.1 nm.

	2θ range	Step size 2θ	time per step [s]	hkl (f.c.c.): γ	hkl (b.c.t.): α′
Isochronal	25°-34° 53°-62°	0.03°	0.1	111, 200, 311, 222	110/101, 220/202
Isothermal	25°-34° 38°-62°	0.02°	0.5	111, 200, 220, 311, 222	110/101, 200/002, 211/112, 220/202

Lattice (macro-)strains in austenite generated during the cooling and reheating cycle were evaluated in the direction parallel to the diffraction vector, comparing the change of the lattice parameter of the material with that expected due to unconstrained thermal contraction. This investigation was performed in situ on austenite by measuring the distance between the atomic planes parallel to the sample surface averaged for the 200 and 311 reflections.

Results and discussion

Isochronal treatments

It is observed from Fig. 1 that different thermal cycles affect the transformation path. In the samples, the final amounts of retained austenite “RA” (see caption Fig. 1) are comparable, but the transformation paths followed differ.

Assuming that the final content of RA is similar for the samples 143, 163 and 203, the results indicate different contents of RA at the beginning of the sub-zero treatment ($RA_{203}<RA_{143}<RA_{163}$); probably due to differences in the thermal path followed during quenching. Fig. 1 shows that after storage at room temperature, austenite is stabilized, because a restart of the transformation can only proceed upon further cooling [15]. Under the reported assumption, the temperature where martensite restarts to form is the lower the higher the initial fraction of martensite is, in agreement with previous studies [16].

At the beginning of the restart, martensite forms very slowly and the process accelerates during further cooling. This indicates that the transformation involves the development of new martensite nuclei. After isothermal holding in the sub-zero Celsius range, the same stabilization effect is observed for sample 203, where the isochronal transformation was interrupted at a transformed fraction before the bending point in the S-shaped curve (Fig.1). Clearly, a continuation of the transformation after isothermal holding at 203 K proceeds through a stage of nucleation. Similar effects, albeit to a much lesser extent, are observed for samples 163 and 143. Evidently, nucleation of martensite does occur during cooling in the entire temperature range investigated. On reheating only samples 143 and 203 show a continuation of the transformation to martensite, sample 163 has reached completion of the transformation on reaching 103 K.

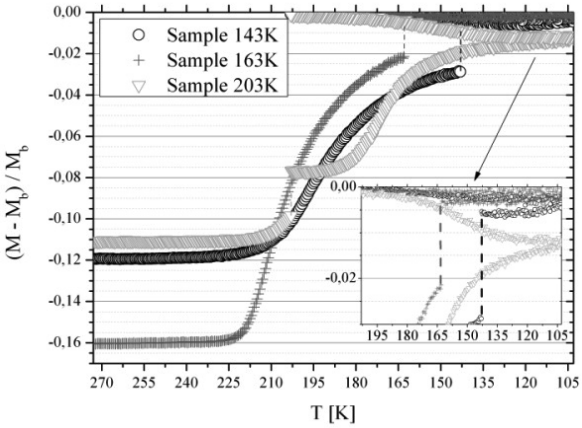

Figure 1. Baseline corrected magnetic moment at saturation, normalized to the baseline, "$(M - M_b)/M_b$" versus temperature "T" during cooling and first reheating to 203K. The discontinuities at 203K, 163K and 143K represent the isothermal part of the transformation. The magnetization at 203K during baseline recording Mb in the 2 samples was 41.43±0.02emu, indicating that comparable contents of retained austenite were obtained after the sub-zero treatment.

The effect of the thermal path on the lattice strains in austenite was investigated with XRD. Elastic straining of austenite was investigated for the thermal cycle of sample 143, albeit for an extended isothermal holding time of 6 h (SAMPLE 2). For comparison, a sample was isochronally cooled to 88 K, maintained at 88 K for 4h, further cooled to 23 K and thereafter reheated to room temperature (SAMPLE 1). The data are shown in Fig.2a, which reports the elastic strains in austenite for the two samples corrected for the thermal expansion in unconstrained conditions (taking the lattice parameter at room temperature as a reference), and in Figure 2b, which shows the fraction of retained austenite in the samples during the thermal cycle.

From Fig. 2 it is observed that the lattice strain is influenced by both transformation strain and interaction between phases. Since the austenite regions are very small, a state of hydrostatic strain is assumed in the following discussion of the results. During initial cooling from room temperature of the stabilized austenite, the coherency between austenite and martensite promotes a state of tension in austenite as a consequence of a larger unconstrained thermal shrink of austenite as compared to martensite, which is the majority phase in the sample.

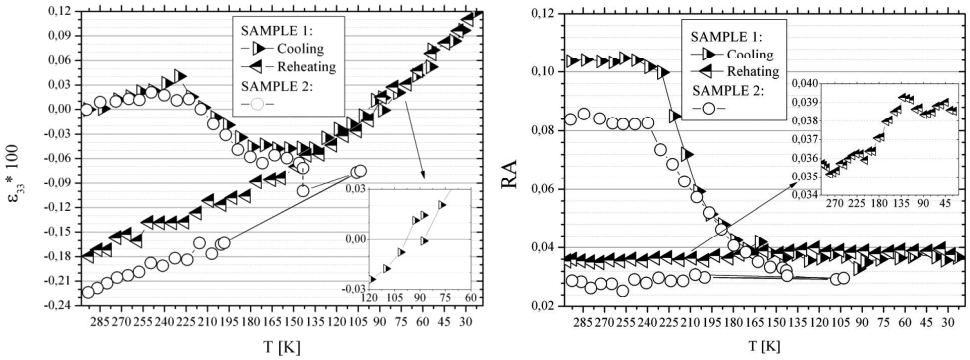

Figure 2. a) Evolution of lattice strain in austenite in the direction perpendicular to the sample surface "ε33" versus temperature "T"; b) Fraction of retained austenite "RA" as a function of temperature "T". The enlarged area shows the evolution of the transformation during reheating; the data have been smoothed considering 3 points per time. For SAMPLE 2 the data in the interval region 203-103K after isothermal holding are reported only for: end of the isothermal step, first cooling to 103K, first reheating to 203K, second cooling to 103K, final reheating at 203K.

The tension generated in austenite by constrained thermal shrink, is overcompensated by the transformation strain, because the formation of martensite in iron alloys occurs in association with a volume expansion. Consequently, when the transformation (re)starts at about 225 K (Fig. 2b), the f.c.c. lattice becomes compressed by the transformation strain, and compression increases until a temperature where the transformation rate is high enough to overcompensate the tension resulting from thermal shrink: this condition is reached at about 160 K. On continued cooling the transformation strain is visible until about 140 K, while during further cooling to 23 K only reversible elastic strain builds up (Fig.2a). This implies that only the difference in thermal shrink between austenite and martensite contributes to this strain and no irreversible volume changes associated with continued transformation or plastic deformation occur. It is noted that, since the martensite content has increased during the transformation, the strain is accommodated almost exclusively by austenite.

A very small change in compressive strain during the 4h isothermal holding at 88 K indicates that only a small amount of isothermal transformation occurs at this temperature. On reheating, the transformation restarts at about 135 K, while austenite experiences a compressive strain (Fig. 2). This temperature compares favorably with the temperature where the transformation ceased during cooling. Considering the role of straining of austenite it can be expected that compressive stress in austenite reduces the driving force for the transformation to martensite and that tension promotes this transformation. The onset of the transformation and its ceasing during cooling is consistent with this interpretation. However, the restarting of the transformation during heating, while compressive strain has built up and is further increased by continued transformation, contradicts this. Hence, the state of stress in austenite is not the

only parameter determining its transformation. Most likely also a (thermally activated) mechanism is required for the transformation to be able to proceed.

Regarding the overall effect of the sub-zero treatment from the technological point of view, it is important to underline that a large compressive strain in austenite at the end of the thermal cycle is observed in SAMPLE 1. Since compression stabilizes austenite [17], austenite is not only reduced, but is stabilized by the applied sub-zero treatment and reheating to room temperature.

Finally, comparing both applied thermal cycles, it is visible that isothermal holding at 143 K, allows the continuation of the transformation and a further stabilization of austenite.

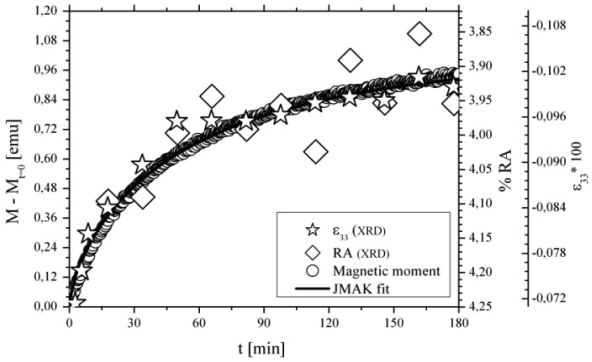

Figure 3. Evolution of the fraction of retained austenite "RA" and of the transformation strain calculated for the 200 and 311 reflections in the direction perpendicular to the surface "ε33" versus time "t" during isothermal holding. Data are compared with the increment of magnetic moment at saturation and the JMAK fit of the magnetometry results.

Isothermal holding at 143K

The evolution of the austenite-to-martensite transformation at143 K is reported in Fig.3. This graph compares the evolution of the magnetic moment at saturation with the fraction of retained austenite and the elastic strain in austenite. The axes for austenite fraction and strain were scaled to obtain overlap with the time evolution of the magnetic moment (cf. Ref. 8). Evidently, all data recorded during the isothermal stage show similar time dependence. Qualitatively, a continuous decrease of the rate of the transformation with time implies that no nucleation of new martensite occurs in the isothermal stage, only growth of nuclei developed in the isochronal stage of the transformation. For a quantitative description of the kinetics the magnetic moment appears most appropriate, since it gives a statistical average over the entire sample, while XRD based data only apply for the information depth close to the surface of the sample.

Kinetics analysis

Kinetic analysis of the magnetometry data in the isothermal stage was performed in terms of the JMAK equation (cf. Refs. 8 and 21 for the fitting procedure). The kinetics parameter resulting from the JMAK fit, i.e. the transformation rate *k* and the exponent *n* are collected in Table 3 for the present samples as well as for data at 138 K [18]. As an example, the fit for the isothermal stage of sample143 is given in Fig.3.

Table 3: Kinetic parameters for isothermal transformation at temperature T, resulting from JMAK fit of the isothermal holding. The rate of the transformation is related to the "k" parameter, the "n" exponent is connected with the mechanism of phase transformation.

T [K]	k $[min]^{-1}$	n
203	0.096	0.43
163	0.043	0.59
143	0.018	0.71
138	0.011	0.74

Table 3 shows that the isothermal formation of martensite evolves faster at higher temperature. Moreover, the "n" exponent is the higher the lower the transformation temperature is, indicating that the transformation mechanism depends on the transformation temperature. This is consistent with previous findings and has been suggested to be related to a change of the morphology of the developing martensite[18].

In an attempt to obtain further information on the phenomenon controlling the isothermal formation of martensite, an Arrhenius dependence for "k", i.e. $k = k_0 \cdot exp\left(-\frac{E}{RT}\right)$ was assumed [19], where k_0 is a pre-exponential factor and E is the activation energy. It is noted that since the exponent n of the transformation changes with transformation temperature, strictly speaking an Arrhenius relation for k cannot be expected. Indeed, the obtained activation energy appears to increase from 7 to 17 kJ/mol with decreasing transformation temperature. The order of magnitude of the activation energy is incompatible with solid state diffusion (apart from H diffusion) of the alloying elements, which would be consistent with the characteristics of a diffusionless transformation.

Conclusions

Martensite formation at sub-zero temperature in a model Fe-Ni-C alloy was investigated by in situ synchrotron XRD and magnetometry. In the isochronal stage of the transformation both nucleation and growth of martensite occurred, while only growth of pre-existing nuclei occured in the isothermal stage. After the isothermal transformation retained austenite was stabilized, implying that a restart of the transformation to martensite on continued isochronal cooling required an additional undercooling, which is consistent with the development of new martensite nuclei.

The interaction between martensite and austenite during the thermal cycle, together with the transformation strain, is important for the final stress state in the material. The difference in thermal shrink between martensite and austenite induces a tensile strain in austenite during cooling, while the transformation to martensite imposes a compressive strain onto austenite. The combination of thermal and transformation strains leads to a compressive strain in austenite after reheating to room temperature, which contributes to the stability of retained austenite.

A kinetic analysis of the austenite-to-martensite transformation in the isothermal stage indicates that the transformation mechanism depends on the sub-zero Celsius temperature and that the thermal activation involves a (diffusionless) low activation energy mechanism.

Acknowledgements

The "Foundry Institute of Finland" is acknowledged for supplying the Fe-Ni-C alloy. M.F. Hansen, Technical University of Denmark, is gratefully acknowledged for constant support with the

magnetometry measurements and precious suggestions for the optimization of the experimental conditions. O. Kessler and M. Reich, University of Rostock, are gratefully acknowledged for dilatometry investigations. R. Feyerherm, E. Dudzik, C. Genzel and M. Klaus, Helmholtz Zentrum für Materialien und Energy (HZME), are acknowledged for their support during in situ experiments at the Berlin synchrotron facility HZB-BESSY II. Financial support for the synchrotron measurements by the EU – Transnational Access Program is gratefully acknowledged.

References

[1] D.P. Koistinen and R.E. Marburger , Acta Metall., 7 (1959) 59
[2] Ji-Cheng Zhao, Michael R. Notis, Mater. Sci. Eng., R 15 (1995) 135-207
[3] M. Umemoto and W.S. Owen, Metall. Trans., 5 (1974) 2041-2045
[4] T.N. Durlu, J. Mater. Sci., 36 (2001) 5665-5671
[5] G.S. Ansell, S.J. Donachie and R.W. Messler, JR, Metall. Trans., 2 (1971) 2443-2449
[6] H. Sato, A. Nakashima, T. Tanaka, E.M. Fujiwara, Y. Watanabe, Presented at Int. Conf. on Martensitic Transformations, Osaka, Japan, September 2011.
[7] G.V. Kurdyumov, O.P. Maksimova, Dokl Akad. Nauk SSSR 61 (1948) 83-86
[8] M. Villa, K. Pantleon, Marcel A.J. Somers, Submitted for Proc. Int. Conf. on Martensitic Transformations, Osaka, Japan, September 2011.
[9] Donghwi Kim, John G. Speer, B.C. de Cooman, Metall. Mater. Trans. A 42 (2011) 1575-1585
[10] M. Holmquist, J.O. Nilsson, A. Hultin Stigenberg, Scripta Metall. Mater., 33 (1995) 1367
[11] A. Stojko, PhD Thesis, Technical university of Denmark, Lyngby, DK, 2005
[12] E. Dudzik, R. Feyerherm, W. Diete, R. Signorato, C. Zilkens, J. Synchr. Rad. 13 (2006) 421-425
[13] ASTM International Standard designation E 975-03
[14] C.H. MacGillavry, G.D. Rieck: International Tables for X-Ray Crystallography-Vol. III physical and chemical tables, Kynoch Press
[15] O.N. Mohanty, Mater. Sci. Eng., B32 (1995) 267-278
[16] K.R. Kinsman, J.C. Shyne, Acta Metall. 15 (1967) 1527-1543
[17] J. R. Patel, M. Cohen, Acta Metall. 1:5 (1953) 531-538
[18] A. Stojko, M. F. Hansen, J. Slycke, M.A.J. Somers, J. ASTM Int. 8(4) (2011) 1-9
[19] E.J. Mittemeijer: J. Mater. Sci. Vol. 27, 1992, pp. 3977-3987

APPENDIX C

Enhanced carbide precipitation during tempering of sub-zero Celsius treated AISI 52100 bearing steel

PUBLISHED

M. Villa, K. Pantleon, Marcel A.J. Somers, Proceeding of the Heat Treat and Surface Engineering Conference and Expo 2013, 2013, Chennai, India

Work was planned and the results were interpreted by all co-authors. First author performed the majority of the experimental activity and wrote the first draft of the manuscript. Comments and suggestions from K. Pantleon and Marcel A.J. Somers were incorporated iteratively in the subsequent versions of the manuscript.

Enhanced carbide precipitation during tempering of sub-zero Celsius treated AISI 52100 bearing steel

Matteo Villa, Karen Pantleon, Marcel A.J. Somers

Technical University of Denmark, Department of Mechanical Engineering
DK 2800 Kongens Lyngby, Denmark

matv@mek.dtu.dk, kapa@mek.dtu.dk, somers@mek.dtu.dk

Keywords: martensite, tempering, sub-zero Celsius treatment, (synchrotron) XRD, dilatometry

Abstract

A 1.5%Cr, 1%C bearing steel was sub-zero Celsius treated after quenching. Transmission and reflection (synchrotron) X-Ray Diffraction were applied ex situ at the HZB-BESSY II synchrotron facility to quantify the phase fractions of martensite and austenite and determine the stress state in austenite.
The tempering response of the sub-zero treated material was studied with high resolution dilatometry and compared with the behavior of a reference as-quenched sample.
X-Ray Diffraction indicates that sub-zero Celsius treating reduces the content of retained austenite in the material and introduces a state of compression in austenite. Dilatometry indicates that a long isothermal holding at cryogenic temperatures enhanced the precipitation of transition carbides during tempering.

Introduction

High carbon steels are used for bearings, cutting tools, dies and more generally applications that require mechanical stability, high hardness and wear resistance.

As an additional step in quenching and tempering heat treatment, sub-zero Celsius treating may improve the performance of high carbon steels, particularly with regard to wear resistance [1−6]. This improvement is of particular technological interest, since it drives to noteworthy economical savings enhancing life service of steel products.

The metallurgical mechanisms that cause enhanced wear resistance are not fully understood yet. Reviews on the topic [7−11] put forward the following interpretations: (i) a reduction of the content of retained austenite; (ii) an enhanced and more uniform precipitation of transition carbides; (iii) a modification of the sub-structure of martensite; (iv) a more favorable macro-stress state.

Among these possibilities, observations in [6,11−14] support enhanced and more uniform precipitation as the key point. However, the mechanism responsible for the modification of the precipitation process is not clarified.

It is documented that, both wear resistance and precipitation of carbides are promoted by an isothermal, i.e. thermally activated, process occurring at cryogenic temperatures (lower than −80°C) [3,15−18].

The following interpretations for the thermally activated process have been put forward [7−11]: (i) diffusion of carbon atoms to nearby lattice defects, resulting in the formation of carbon clusters that may act as nucleation sites for the precipitation of carbides, is an interpretation that appears inconsistent with the availability of thermal energy for the diffusion of carbon atoms in iron, insufficient at temperatures below −50°C [19−21]; (ii) modification of the martensite sub-structure and stress state (martensite

conditioning) during isothermal holding at cryogenic temperatures, is an interpretation that remains phenomenological; (iii) modified tetragonality of martensite upon sub-zero Celsius treating [22−24] is a phenomenon that does not require isothermal holding, hence it is an interpretation that does not appear consistent; (iv) thermally activated martensite formation.

Martensite formation occurs in connection with a noteworthy transformation strain and may introduce lattice defects and a new state of stress in the material [24,25]. Also it can assist the formation of carbon clusters [19].

Thermally activated martensite formation was first reported in [26] and is reviewed in [27]. In 1%C, 1.5%Cr bearing steels, thermally activated martensite formation was reported in [24,28−29], and is a particularly relevant phenomenon at cryogenic temperatures.

In [24], it was suggested that below a critical temperature (about −140°C), the transformation strain associated with martensite formation is accommodated in the existing martensite and generates nucleation sites for the precipitation of transition carbides during tempering.

This paper seeks to investigate the effect of a long isothermal holding at cryogenic temperature on the precipitation of transition carbides during tempering and aims to contribute to the understanding of the thermally activated process responsible for enhanced and more uniform precipitation.

Experimental

Material and sample geometries

The alloy investigated is a commercial AISI 52100 steel with the composition given in Table 1 and extruded to a 10mm rod. For dilatometry 10 mm high hollow cylinders were prepared with outer and inner diameter of Ø 4.0 and Ø 3.6, respectively; for (synchrotron) X-Ray Diffraction (XRD) Ø3mm, 0.2mm thick disks were prepared.

Table 1: Chemical composition (in wt-%) of AISI 52100 as determined by Glow Discharge Optical Emission Spectrometry (GDOES)

Fe	C	Cr	Ni	Mn	Si	Mo	Cu
Bal.	0.96 ±0.02	1.60 ±0.05	0.10 ±0.01	0.28 ±0.04	0.13 ±0.04	0.05 ±0.01	0.15 ±0.01

Heat treatments

The applied heat treatments are schematically reported in Fig. 1. Austenitization (Fig. 1a) was performed at 1080 °C for 60s, followed by a quench in oil at 140 °C; the material was kept in the oil bath for 20 s and air cooled before storage at room temperature for about 2 Ms (3-4 weeks). Protection from oxidation during austenitization was ensured through embedding the samples in 4 layers of 30 µm thick foils of stainless steel AISI 316.

Three different thermal cycles were performed after austenitization and 2 Ms storage (Fig. 1b): “AsQ” refers to samples not subjected to any sub-zero Celsius treatment, but stored further 2 Ms at room temperature; “C” refers to samples cooled at 15 K/min to −150°C and thereafter (re)heated at 15K/min to room temperature before a second storage period of 2 Ms at room temperature; “C+H” refers to samples that were cooled at 15K/min to −150°C, held 72h at −150°C, (re)heated at 15 K/min to −110°C, held 24h at −110°C and finally (re)heated at 15K/min to room temperature before a second storage period of 2 Ms at room temperature. In the sequel samples are referred to as “starting” condition AsQ, C and C+H,

depending on the performed thermal cycle. For the samples in the starting conditions, the total storage time at room temperature after initial quenching is about 4 Ms.

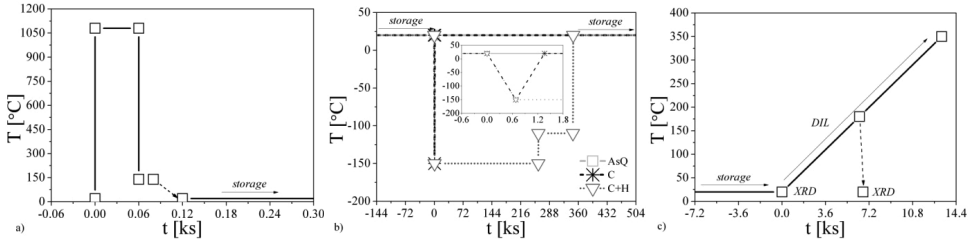

Figure 1. Heat treatments: a) austenitization; b) sub-zero Celsius treatments; c) tempering.

The material in the three different starting conditions was thereafter subjected to tempering. The tempering (Fig. 1c) of martensite was followed with dilatometry during isochronal heating of the material at 1.5K/min up to 350°C. XRD was applied at room temperature on samples heated at 1.5K/min to 180°C only and air cooled.

Methods

XRD was performed at the synchrotron facility HZB-BESSY II at the experimental station EDDI [30]. XRD investigation was performed prior to tempering and after heating at 1.5K/min to 180°C (Fig. 1c). These measurements were performed at room temperature in transmission geometry and averaged over the whole samples thickness. Details on the measurement conditions, the quantitative phase analysis and the determination of the lattice parameter of austenite are reported in [24]. The stress state in austenite was evaluated in reflection geometry applying the $\sin^2\psi$ method [31]; experimental details were reported in [25].

Dilatometry was performed in a Bähr DIL 805A/D dilatometer. The length change of the samples was measured during isochronal heating at 1.5K/min up to 350°C (Fig.1c).

Results

X-Ray Diffraction, XRD

The results of the (synchrotron) XRD investigations prior to the tempering step and after isochronal heating at 1.5K/min to 180°C are reported in Table 2.

The XRD investigations show that both the applied sub-zero Celsius treatments reduce the content of retained austenite in the material. As follows from the last column in Table 2, the difference in in-plane and normal macro-stress components in austenite is nil within experimental accuracy. Comparing the lattice parameters determined for the various *hkl* of austenite in the three samples prior to tempering shows clearly that austenite is in a compressed state of stress after sub-zero Celsius treatment. Hence, with $\sigma_{\parallel} - \sigma_{\perp} \approx 0$ austenite experiences a state of hydrostatic compression, most specifically for C+H. Locally, strains appear concentrated along specific crystallographic directions (the measured lattice parameter of austenite depends on the probed reflection). The tetragonality of martensite does not depend on the starting condition.

During heating to 180°C, martensite loses its tetragonality. The stress state in austenite is (mainly) hydrostatic, albeit with a slight net compression in the plane of the sample disc. Evidently, the local strain direction is observed to change during heating and to depend on the starting condition.

Table 2: Results of the XRD investigations: content of retained austenite, fγ; lattice parameter of austenite, aγ, probed for the (h k l) 200, 220, 311 and 420 reflections; tetragonality of martensite expressed as the ratio between the crystallographic axes c and a, c/a ratio; macro-stresses in austenite reported in terms of $\sigma_{\parallel} - \sigma_{\perp}$ (average and standard deviation for probed 200, 220, 311 and 420 reflections), where ∥ is a general direction parallel to the sample surface and ⊥ is the surface normal.

Starting condition	f_γ [%]	Treatment	c/a ratio	a_γ [Å]				$\sigma_{\parallel} - \sigma_{\perp}$ [MPa]
				2 0 0	2 2 0	3 1 1	4 2 0	
AsQ	29.2	Prior tempering	1.036	3.606	3.602	3.604	3.605	5±24
		After heating	*≈1*	*3.607*	*3.598*	*3.599*	*3.599*	*-23±9*
C	11.9	Prior tempering	1.037	3.604	3.597	3.599	3.601	23±29
		After heating	*≈1*	*3.608*	*3.598*	*3.598*	*3.599*	*-48±29*
C+H	7.7	Prior tempering	1.036	3.600	3.595	3.598	3.600	3±9
		After heating	*≈1*	*3.608*	*3.594*	*3.597*	*3.594*	*-71±23*

Dilatometry (DIL)

The results of dilatometry investigations are reported in Fig. 2: the linear thermal expansion coefficient at the beginning of the tempering step is given in Fig. 2a, while Fig. 2b shows the contraction/expansion of the samples during solid state transformation.

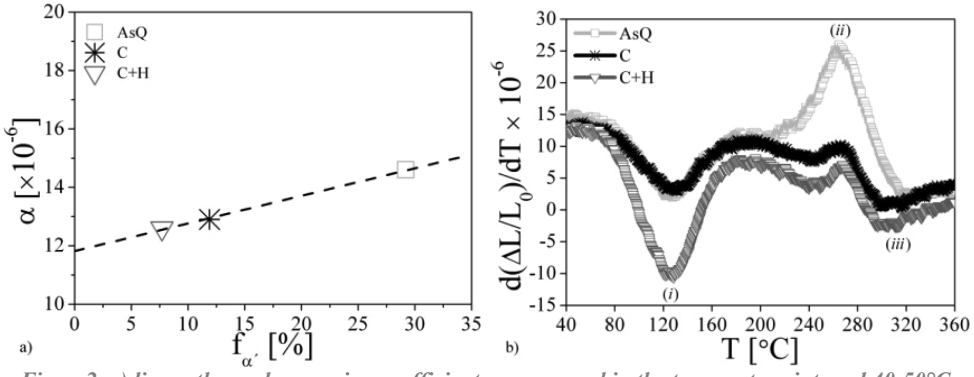

Figure2. a) linear thermal expansion coefficients α measured in the temperature interval 40-50°C during isochronal heating at 1.5K/min. b) differentiated relative sample elongation, d(ΔL/L0)/dT, vs. temperature, T, during isochronal heating.

Fig. 2a shows that the linear thermal expansion coefficient scales with the variation in austenite fraction. In Fig. 2b three phase transitions are discerned, indicated by (i), (ii) ad (iii). Transition (i) is most pronounced for the sample subjected to C+H treatment, while peak (ii) is largest for sample AsQ. No clear differences can be observed for peak (iii).

Interpretation

X-Ray Diffraction

As expected sub-zero Celsius treatment reduces the amount of retained austenite in AISI 52100. The observation of a lower content of retained austenite for condition C+H as compared to condition C indicates that isothermal treatment is an important step in the treatment. During the long isothermal cryogenic treatment thermally activated martensite formation occurs. In situ observation and investigation of thermally activated martensite formation for the present AISI 52100 is reported elsewhere and shows that mainly thermally activated growth of martensite nuclei, developed during cooling, into lenticular martensite occurs [24,32].

Martensite formation introduces a (macroscopically hydrostatic) state of compression in austenite that depends locally (microscopically) on the probed crystallographic direction [25]. It has been suggested that the compression is concentrated along the shape strain direction [25] and results from a partial elastic accommodation of the transformation strain in austenite. The compression is the larger, the more martensite forms [29]. In the present study, the introduction of (additional) compressive stress in austenite as observed between the starting condition AsQ and the condition C and C+H is directly ascribed to martensite formation. Also, the observation of a larger compression for the starting condition C+H as compared to the starting condition C is ascribed to the larger amount of transformation occurring in C+H.

Concerning martensite tetragonality, at temperatures above about −40°C, the availability of thermal energy is sufficient for the movement of carbon atoms of short distances [19−21] in iron and the tetragonal cell of martensite can relax [33−36]. At room temperature, relaxation is close to saturation after about 0.2 Ms [36]. The apparent insensitivity of martensite tetragonality on the starting condition as observed in the present study is ascribed to saturation of the relaxation phenomena during long time storage at room temperature (> 2 Ms).

For 1.5K/min heating rates, the crystal lattice of martensite becomes cubic in the temperature interval 90−140°C, as a consequence of the precipitation of transition carbides [24,37,38]. Data in the present study shows that the unit cell of martensite does not show any tetragonality upon heating to 180°C where precipitation of transition carbides is finished (cf. peak (i) in Fig. 2b).

The present investigation does not allow definitive conclusions on the stress state of the material after heating to 180°C due to the fact that carbon atoms may have diffused enriching or depleting the different phases (modifying their lattice parameters). Moreover, carbon redistribution is known to be influenced by sub-zero treating for the present system [24]. On the other hand, the strain (re)distribution between different probed crystallographic directions cannot be appointed to carbon redistribution between phases.

Transition carbides precipitate in association with a volumetric contraction of the material and a defined orientation relationship with the parent martensite phase [39−41]; also, it was suggested that a modification in the martensite sub-structure may alter the orientation relationship [42]. Data in the present study suggests that the precipitation of transition carbides has altered the local stress state in the material in a systematic way. The macroscopic state of stress in austenite, $\sigma_{\parallel} - \sigma_{\perp}$, has changed to a net compressive stress within the plane of the sample. Further, additional elastic strains are introduced along specific crystallographic directions of austenite (that is related to martensite with an orientation relationship). The observation of a quantitative difference between starting conditions C and C+H for the 220 and 420 probed reflections may indicate either a difference in the amount of precipitation, a different precipitation mechanism, or a combination of both.

Dilatometry

As a consequence of the closer packing of the f.c.c. lattice than the b.c.t. lattice, the linear thermal expansion of austenite is larger than the linear thermal expansion of martensite. The linear proportionality

of the linear expansion coefficient with the austenite content in Fig. 2b is consistent with this expectation. Extrapolation to pure martensite and pure austenite gives 11.9 10^{-6} K^{-1} and 21.3 10^{-6} K^{-1}, respectively. These values are in reasonable agreement with literature values of 10.9 10^{-6} K^{-1} and 23.4 10^{-6} K^{-1} [29], respectively.

The transformation peaks in Fig. 2b are interpreted on the basis of the analysis in [35,43]. According to [35,43], precipitation of secondary transition carbides (peak (i)) and formation of cementite (peak (iii)) are associated with volume reductions, while decomposition of retained austenite (peak (ii)) induces a volume expansion. From Fig. 2b, a significant reduction of the retained austenite content in cryogenic treated samples is demonstrated: peak (ii) is largely reduced for sample C and C+H as compared to sample AsQ.

Interestingly, peak (i) is equivalent for starting conditions C and AsQ, but differs spectacularly for sample C+H. Dilatometry results show that enhanced precipitation of transition carbides (peak (i)) is promoted only by long isothermal holding at cryogenic temperatures, while no effects are reported for (controlled) sub-zero Celsius cooling to the same cryogenic temperature.

Discussion

The present study strongly supports the notion that enhanced precipitation of transition carbides during tempering can be ascribed to a thermally activated process in the isothermal stage during sub-zero Celsius treatment.

Among the interpretations listed in the introduction section, the present experimental data exclude the tetragonality of martensite as a key parameter in governing enhanced precipitation during tempering.

Further investigation, including in situ investigation and direct observation of the precipitation products is necessary to definitively establish the nature of the thermally activated process.

On the basis of previous experimental activity by the present authors [24], enhanced precipitation is hereby interpreted as a consequence of thermally activated martensite formation at cryogenic temperatures that conditions existing martensite and generates new nucleation sites for the carbides precipitates during tempering.

This interpretation suggests that the investigation of the effects of sub-zero Celsius treatments should be driven towards the theory of the martensitic transformation in steel.

Conclusions

Sub-zero Celsius treatments are effective in reducing the content of retained austenite in high carbon steels.

The main microstructural difference between a simple sub-zero Celsius cooling and a sub-zero Celsius cooling followed by a long isothermal holding at cryogenic temperature, analyzed before tempering, is a further reduction of the amount of retained austenite. No effect of cryogenic treatment is observed on the tetragonality of martensite.

Sub-zero Celsius cooling alone is not effective in promoting enhanced precipitation of transition carbides. The present work demonstrates that enhanced precipitation can be obtained during tempering after a long isothermal holding at cryogenic temperatures. In the isothermal stage thermally activated martensite develops.

Acknowledgements

The authors are indebted Mikkel F. Hansen from the Technical University of Denmark for the controlled sub-zero Celsius treatments. M. Reich, University of Rostock, is gratefully acknowledged for performing the dilatometry experiments. The authors acknowledge the Danish Natural Science Research Council for financial support of the work at the Berlin synchrotron facility HZB-BESSY II via Danscatt.

References

[1] M.A. Jaswin, G. S. Shankar, D. Mohan Lal, Int. J. Precision Eng. and Manuf., 11-1 (2010) 97-105
[2] D. Mohal Lal, S. Renganarayanan, A. Kalanidhi, Cryogenics, 41 (2001) 149-155
[3] K. Amini, S. Nategh, A. Shafyei, Mater. And Design, 31 (2012) 4666-4675
[4] R.F. Barron, Cryogenics, 22 (1982) 409-413
[5] D. Das, A. K. Dutta, K.K. Ray, Mat. Sci. Eng. A, 527 (2010) 2182-2193
[6] F. Meng, K. Tagashira, H. Sohma, Scripta Mater, 31:7 (1994) 865-868
[7] S.S. Gill, H. Singh, R. Singh, J. Singh, Int. J. Adv. Manuf. Technol., 48 (2010) 175-192
[8] S.S. Gill, J. Singh, R. Singh, H. Singh, Int. J. Adv. Manuf. Technol., 54 (2011) 59-82
[9] W. Reitz, J. Pendray, Mater. Manuf. Processes, 16:6 (2001) 829-840
[10] D. N. Collins, Heat treatment of Metals, 3 (1997) 71
[11] D. Das, A.K. Dutta, K.K. Ray, Mat. Sci. Eng., A 527 (2010) 2182-2193
[12] F. Meng, K. Tagashira, R. Azuma, H. Sohma, ISIJ Int., 34 (1994) 205-210
[13] P.F. Stratton, Mat. Sci. Eng., A 449-451 (2007) 809-812
[14] J.Y. Huang, Y.T. Zhu, X.Z. Liao, I.J. Beyerlein, M.A. Bourke, T.E. Mitchell, Mat. Sci. Eng. A, 339 (2003) 241-244
[15] D. Mohal Lal, S. Renganarayanan, A. Kalanidhi, Cryogenics, 41 (2001) 149-155
[16] D. Das, A.K. Dutta, K.K. Ray, Wear 266 (2009) 297-309
[17] D. Das, A.K. Dutta, K.K. Ray, Phil. Mag., 89 1 (2009) 55-76
[18] D.N. Collins, J. Dormer, Heat Treat. Metals, 3 (1997) 71
[19] A.I. Tyshchenko, W. Theisen, A. Oppenkowski, S. Siebert, O.N. Razumov, A.P. Skoblik, V.A. Sirosh, Yu.N. Petrov, V.G. Gavriljuk, Mat. Sci. Eng. A, 527 (2010) 7027-7039
[20] D.E Kaputkin, Mat. Sci. Eng., A 438-440 (2006) 207-211
[21] P.C. Chen, B.O. Hall, P.G. Winchell, Metall. Trans., A 11 (1980) 1323-1331
[22] A. Bensely, S. Venkatesh, D. Mohan Lal, G. Nagarajan, A. Rajadurai, K. Junik, Mat. Sci. Eng. A, 479 (2008) 229-235
[23] I. Wierszylloski, J. Samolczyk, S. Wieczorek, E. Andrzejewska, A. Marcinkowska, Def. Diff. Forum, 273-276 (2008) 731-739
[24] M. Villa, K. Pantleon, M.A.J. Somers, "*Evolution of compressive strains in retained austenite during sub-zero martensite formation and tempering*", submitted
[25] M. Villa, K. Pantleon and Marcel A.J. Somers, Scripta Mater. 67 (2012) 621-624
[26] G.V. Kurdjumov, O.P. Maksimove, Dokl. Akad, Nauk SSSR, 61 (1948) 83
[27] N.N. Thadhani, M.A. Meyers, Progress in Mater. Sci., 30 (1986) 1-37
[28] A. Stojko, M.F. Hansen, J. Slycke, M.A.J. Somers, J. of ASTM Int., 8:4 (2011)
[29] M. Villa, K. Pantleon, M.A.J. Somers, "*Abnormal martensite formation during sub-zero treatment of ball bearing steel*", submitted
[30] Ch. Genzel, I.A. Denks, J. Gibmeier, M. Klaus, G. Wagener. Nuclear Instruments and Methods in Physics Research A, 578 (2007) 23–33
[31] V. Hauk, Structural and Residual Stress Analysis by Non-Destructive Methods: Evaluation – Application – Assessment, Elsevier Science, Amsterdam, 1997
[32] M. Villa, PhD thesis, in preparation
[33] P.C. Chen, P.G. Wichell, Metall Trans., A 11 (1980) 1333-1339
[34] A. M. Sherman, G.T. Eldis, M. Cohen, Metall. Trans., A 14 (1983) 995-1005
[35] L. Cheng, C.M. Brakman, B.M. Korevaar, E.J. Mittemeijer, Metall. Trans., A 19 (1988) 2415-2426

[36] L. Cheng, N.M. van der Pers, A. Bottger, Th.H. de Keijser, E.J. Mittemeijer, Metall. Trans. A 22A (1991) 1957–1967
[37] M.J. van Genderen, M. Isac, A. Bottger, E.J. Mittemeijer, Metall. Trans., A 28 (1997) 545-561
[38] A.T.W. Barrow, J-H. Kang, P.E.J. Rivera-Diaz-del-Castillo, Acta mater., 60 (2012) 2805-2815
[39] M.G.H. Wells, Acta Mater, 12 (1964) 389-399
[40] S. Nagakura, Y. Hirotsu, M. Kusunoki, T. Suzuki, Y. Nakamura, Metall. Trans., A 14 (1983) 1025-1031
[41] H.K.D.H. Bhadeshia, Worked Examples in the Geometry of Crystals, The Institute of Metals, London, 1987
[42] K.A. Taylor, G.B: Olson, M. Cohen, J.B. Vander Sande, Metall. Trans., A 20 (1989) 2749-2765
[43] P.V. Morra, A.J. Böttger, E.J. Mittemeijer, J. Thermal Analysis and Calorimetry, 64 (2001) 905-914

APPENDIX D

Martensitic transformation and stress partitioning in a high-carbon steel

PUBLISHED

M. Villa, F. B. Grumsen, K. Pantleon, Marcel A.J. Somers, Scripta Mater. 67, (2012) 621-624

Work was planned and the results were interpreted by all co-authors. First author performed the majority of the experimental activity and wrote the first draft of the manuscript. F. B. Grumsen supported the activity at the synchrotron facility. Comments and suggestions from K. Pantleon and Marcel A.J. Somers were incorporated iteratively in the subsequent versions of the manuscript.

Errata corrige:

In situ XRD quantitative phase analysis was affected by computational errors. The correct quantification follow can be obtained from the reported data according to the expression:

$$f_\gamma = \frac{4 \cdot f_{RA}}{(1 - f_{RA}) + 4 \cdot f_{RA}}$$

with f_γ actual content of retained austenite calculated according to the method reported in the manuscript and f_{RA} content of retained austenite indicated in the manuscript itself.

Available online at www.sciencedirect.com

SciVerse ScienceDirect

Scripta Materialia 67 (2012) 621–624

Scripta MATERIALIA

www.elsevier.com/locate/scriptamat

Martensitic transformation and stress partitioning in a high-carbon steel

Matteo Villa,* Flemming B. Grumsen, Karen Pantleon and Marcel A.J. Somers

Technical University of Denmark, Department of Mechanical Engineering, DK 2800 Kgs. Lyngby, Denmark

Received 18 May 2012; revised 18 June 2012; accepted 19 June 2012
Available online 1 July 2012

Martensitic transformation in a high-carbon steel was investigated with (synchrotron) X-ray diffraction at sub-zero Celsius temperature. In situ angular X-ray diffraction was applied to: (i) quantitatively determine the fractions of retained austenite and martensite; and (ii) measure the evolution of the lattice strain in retained austenite. Ex situ (synchrotron) energy-dispersive X-ray diffraction was performed to assess the effects of the martensitic transformation on the development of stresses in austenite.

Keywords: Martensitic phase transformation; X-ray diffraction (XRD); Martensite; Retained austenite; Residual stresses

Martensitic transformation followed by appropriate tempering is the most effective mechanism to obtain steel products with high strength. Also, in modern multiphase steels, like advanced high-strength steels, it plays a decisive role in maximizing the mechanical characteristics of a steel product.

The mechanical behavior of a multiphase material is determined not only by the properties of the phases considered individually, but (mainly) by the mechanical interaction between the phases [1,2]. In recent years, the distribution of stresses, and consequently strains, in a multiphase steel during applied deformation has been widely studied [3,4]. In contrast, almost no work has been devoted to the natural effect of the self-standing transformation promoted during cooling, for example in the sub-zero Celsius range, despite the fact that cryogenic treatment to improve steel performance has gained popularity in heat treatment practice.

The purpose of the present work is to investigate the stress state that is evoked in austenite by the martensitic transformation during a controlled sub-zero Celsius treatment of a partially transformed steel, containing austenite and martensite, after quenching to room temperature.

To the authors' knowledge, only a few contradictory experimental studies regarding the effect of martensite formation on the stress state of austenite have been published: compression of retained austenite due to martensitic transformation in steel is reported from in situ synchrotron X-ray diffraction (XRD) experiments [5,6], while the build-up of hydrostatic compression was suggested on the basis of conventional laboratory XRD experiments [7–9]. In contradiction, neutron diffraction experiments have indicated that martensite formation has no influence on the stress state in austenite [10].

The alloy used in the present work is a commercial AISI 52100 steel that was extruded to a Ø 10 mm rod. The chemical composition of the material as determined with glow discharge optical emission spectroscopy (GDOES; Horiba Jobin Yvon GD2) is reported in Table 1.

Disks of thickness 0.33 mm and diameter 10 mm were austenitized at 1323 K for 15 min, to dissolve all carbides. After austenitization, samples were quenched in oil and kept for 3 min at an austempering temperature of 413 K to promote temperature homogenization. Thereafter, the samples were air cooled to room temperature. The initial microstructure thus obtained is shown in Figure 1a and compared with a sample that was additionally cooled at 0.5 K min^{-1} to 93 K, held 7 h at 93 K and then reheated to room temperature at 1.5 K min^{-1}.

In situ (synchrotron) angular XRD was performed at MagS station (HZB-BESSY II) [11] with a radiation of wavelength $\lambda = 0.1$ nm focused onto a 1 mm spot, applying Bragg–Brentano geometry. A quantification of the volume fraction of retained austenite was obtained by considering the 200_γ, 220_γ and 311_γ Bragg peaks of austenite, and the $200/002_{\alpha'}$ and $211/112_{\alpha'}$ doublet peaks of martensite (see Ref. [5] for more details). Lattice (macro-) strains in austenite in the direction

* Corresponding author. E-mail: matv@mek.dtu.dk

1359-6462/$ - see front matter © 2012 Acta Materialia Inc. Published by Elsevier Ltd. All rights reserved.
http://dx.doi.org/10.1016/j.scriptamat.2012.06.027

Table 1. Chemical composition (in wt.%) of the material used in the present work as determined by GDOES.

Fe	C	Cr	Ni	Mn	Si	Mo	Cu
Bal.	0.96 ± 0.02	1.60 ± 0.05	0.10 ± 0.01	0.28 ± 0.04	0.13 ± 0.04	0.05 ± 0.01	0.15 ± 0.01

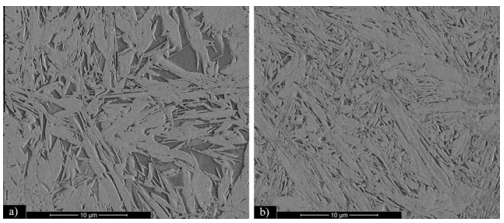

Figure 1. Back-scatter electron micrographs of AISI 52100: (a) austempered and cooled to room temperature; and (b) after additional sub-zero treatment.

perpendicular to the sample surface were evaluated from shifts of the above-mentioned austenite Bragg peaks. Figure 2 presents both the austenite phase fraction and the lattice strains, ε_{33}, in austenite for the different reflections.

No transformation occurred during the first 60 K of cooling, due to thermal stabilization of the austenite upon storage at room temperature [12]. At an undercooling of about 60 K with respect to room temperature, the martensitic transformation (re)started suddenly and continued until a temperature of about 140 K was reached. No transformation was observed during isothermal holding at 93 K. On reheating the transformation restarted at about 140 K, i.e. the same temperature at which it had stopped on cooling, and proceeded until 200 K. The occurrence of martensitic transformation on heating indicates the (partly) thermally activated nature of the transformation.

On cooling, thermal and transformation lattice strains, relative to the condition at room temperature, are expected to build up in austenite. In the first 60 K, at which no transformation occurred, compressive strain (relative to the initial condition) is experienced in austenite as a consequence of thermal shrink. It is noted that the thermal shrink of austenite is constrained by the smaller thermal shrink of the surrounding martensite. The martensitic transformation commencing at 60 K undercooling leads to an additional compressive strain in austenite. Below 140 K the elastic strain introduced on continued cooling is fully recovered on heating, which is consistent with no transformation in this temperature regime. After reheating to room temperature, a state of compression remains in the austenite; this is transformation strain. The magnitude of the remaining compression in the austenite appears to depend on the crystallographic direction probed, and is appreciably smaller for the 200 than for the 220 and 311 reflections. At this stage, it is not possible to conclude whether the stress state causing the observed strain is tri- or biaxial, or whether its *hkl* dependency is determined by the presence of macrostresses in the sample or if it arises from anisotropy of the transformation strain.

Ex situ synchrotron energy-dispersive X-ray diffraction was performed at the EDDI station (HZB-BESSY II) [13]. Reflection geometry was applied for stress analysis in a θ–2θ configuration; the scattering angle was kept fixed at $2\theta = 8°$. The aperture of the beam slit was 0.5 mm × 0.5 mm; the vertical aperture of the detector slit was 0.03 mm.

The stresses in austenite were evaluated applying the $Sin^2\psi$ method [14], where ψ is the angle formed between the scattering vector and the normal to the sample surface. The stresses within the plane of the sample are presumed rotationally symmetric; hence the stress values determined are $\sigma_{//} - \sigma_{33}$ in the sample reference system. The ψ angle was varied from 0 to 72° in steps of 4°; an additional measurement was performed at $\psi = 74°$. The diffraction elastic constants (DEC) were taken from the single crystal constants for ferrite [15] and austenite [16] applying the Eshelby/Kröner model [17,18] for elastic grain interaction.[1] By choosing different diffraction lines, *hkl* (i.e. corresponding to different energies E^{hkl}), an average over different depth ranges is obtained for the different *hkl*s. Further details of the $sin^2\psi$ method, and of the stress vs. information depth can be found elsewhere [13,14]. Figure 3 reports the results of the $sin^2\psi$ investigation. The values obtained for $\sigma_{//} - \sigma_{33}$ are close to zero, indicating that σ_{33} is of about the same magnitude as $\sigma_{//}$, while the build-up of *hkl*-dependent compressive strain is further observed.

In order to evaluate the strains/stresses averaged over the sample thickness, ex situ synchrotron energy-dispersive X-ray diffraction was performed in transmission geometry by aligning the scattering angle parallel to the "in plane" direction of the sample. Again, the 200_γ, 220_γ and 311_γ Bragg peaks of austenite and the $200/002_{\alpha'}$ and $211/112_{\alpha'}$ Bragg doublets of martensite were investigated. The austenite data are included in Figure 3 for $sin^2\psi = 1$, and are consistent with the $sin^2\psi$ and the angular dispersive investigations. For $sin^2\psi = 1$, compressive strain increments of 0.16%, 0.23% and 0.21% relative to the initial condition were measured for the 200_γ, 220_γ and 311_γ reflections, respectively. These values are systematically higher than those determined for ε_{33} in Figure 2, which is explained by the larger sample depth probed for $\varepsilon_{//}$ and the occurrence of a depth gradient (cf. Fig. 4).

Recognizing the very low stress values $\sigma_{//} - \sigma_{33}$ in Figure 3 and the additional compression upon martensitic transformation, a state of hydrostatic stress is assumed in austenite for convenience. Then, for the DEC reported in Refs. [15,16], the (macroscopic) hydrostatic stress for the measured strains $\epsilon_{//}$ amount to −880, −1270 and −1170 MPa for the 200_γ, 220_γ and 311_γ reflections, respectively. These values are indeed very different

[1] It should be noted that the Eshelby/Kröner model for the present case is an approximation, as it assumes elastic interaction of grains with identical single crystal elastic constants (SCECs), while the present two-phase material is composed of crystals with different SCECs.

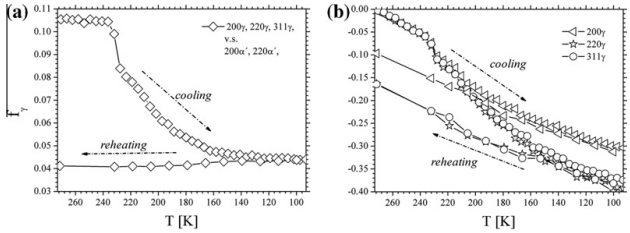

Figure 2. Temperature dependence of a) austenite phase fraction "f_γ" and b) austenite lattice strain in the direction perpendicular to the sample surface "ε_{33}", taking the initial condition at 273 K as a reference. (Measurement step size 0.04° 2θ in the 2θ range 25°–34°, 0.1° 2θ in the 2θ range 34°–62°).

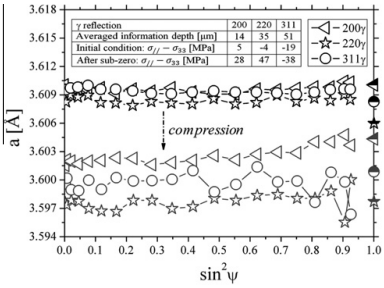

Figure 3. Lattice parameter "a" for different austenite reflections: black initial condition; grey after sub-zero treatment. In the table: stress evaluated from the slope of the interplanar distance vs. relation. Half filled symbols indicate the measurements performed in transmission geometry.

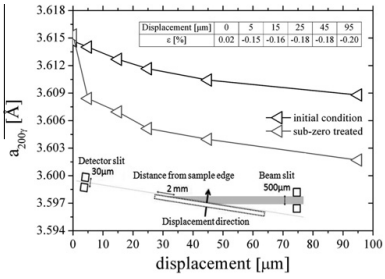

Figure 4. Lattice parameter $a_{200\gamma}$ vs. sample displacement along the surface normal, as measured with energy-dispersive diffraction. The reference for sample displacement is a location as close as possible to the sample surface that still gives a reasonable peak intensity for the most intense austenite reflection. Note that the abscissa does not contain direct information on the actual depth range probed. Surface roughness, imperfect sample planarity and local quench distortions all play a major role in the first points of analysis. In the table the additional strain introduced by the sub-zero treatment is reported.

from the values for $\sigma_{//}-\sigma_{33}$, thereby justifying the assumption of hydrostatic stress.

The lattice parameters of martensite measured in transmission were $a = 2.861$ Å, $c = 2.960$ Å in the initial condition and $a = 2.859$ Å, $c = 2.967$ Å after the sub-zero treatment, corresponding to a change of the sample's averaged c/a ratio (i.e. tetragonality) from 1.035 to 1.038. This apparent sample-averaged increase in tetragonality is explained by the occurrence of carbon segregation at lattice defects and carbon clustering during long-term room-temperature storage for the initial condition, together with an associated reduction in the tetragonality of martensite [19]. The additional martensite formed at sub-zero Celsius temperature has not experienced a similar relaxation and therefore has a higher tetragonality and higher carbon content in solid solution in martensite. The expansion of the volume unit cell of martensite measured from the above reported data is 0.136%. No conclusion concerning the state of stress in martensite can be drawn, because the observed "volume expansion" could be a consequence of the above-mentioned effect of relaxation during long-term storage at room temperature.

A series of experiments was additionally performed with the experimental set-up shown in Figure 4. The diffracted intensity was measured in a 30 μm slit on the side of the sample. In this experimental set-up, the diffracted radiation travels through 2 mm steel before reaching the detector. The gauge volume measures $0.5 \times 3.6 \times 0.03$ (mm^3) and averages over a depth range of 30 μm. Averages at different depths were investigated by displacing the sample along the direction normal to the surface, causing the gauge volume to shift deeper into the sample. The $(200)_\gamma$ lattice spacing was investigated for both as-quenched and sub-zero Celsius treated samples for various displacements (Fig. 4).

The results are interpreted as follows. Identical lattice spacings for zero displacement are explained from surface roughness and accordingly measurement in strain-free austenite. With increasing sample displacement, the lattice parameter for both the as-quenched and sub-zero treated samples decreases as compared to the strain-free condition at the surface, indicating that the deeper the austenite grains are located in the sample the more compression they experience as compared to a (rotationally symmetric) biaxially strain-free state. The systematic difference between the as-quenched and sub-zero treated samples proves that an additional compression is introduced by the martensitic transformation.

The systematic differences in lattice strains obtained for the different *hkl* (cf. Fig. 3) need an explanation. Such differences cannot be ascribed to DEC of the selected reflections, because (i) the stress state is (close to) hydrostatic and thus the same elastic constants apply for all *hkl* and (ii) in the case where the stress state is

biaxial, in terms of elasticity, $[1\,0\,0]_\gamma$ is the softest direction and would therefore be expected to experience the largest strain, in contrast to the observations.

It is known that the most significant aspect of martensitic transformation is its shape strain, which occurs along a specific crystallographic direction in the parent phase [20,21]. The importance of the shape strain direction in the accommodation of the transformation strain in the parent phase is shown in Ref. [22].

The Phenomenological Theory of Martensite Crystallography [23] was applied to predict the shape strain direction for the reported value for the lattice parameters. The lattice invariant shear $(1\,0\,1)[\bar{1}\,0\,1]_\gamma = (1\,1\,2)[\bar{1}\,\bar{1}\,1]_{\alpha'}$ was assumed (see Ref. [24] for more details), giving the habit plane $(0.262\ 0.831\ 0.491)_\gamma$ and the shape strain direction $[-0.303\ 0.764\ -0.569]_\gamma$. The obtained theoretical habit plane lies in-between $(2\,9\,5)_\gamma$ and $(2\,5\,2)_\gamma$, as expected for martensite with a lenticular morphology [25]. The smallest angle between the $\langle 2\,0\,0\rangle_\gamma$ direction and the calculated shape strain direction is 40.2°, while for the $\langle 3\,1\,1\rangle_\gamma$ and $\langle 2\,2\,0\rangle_\gamma$ directions the smallest angles are 19.5 and 17.4°, respectively. Then, assuming that the transformation strain in austenite is concentrated along the shape strain direction, the resolved stress on the different crystallographic planes of austenite would qualitatively correspond to approximately equally high stress values on the $\{3\,1\,1\}_\gamma$ or $\{2\,2\,0\}_\gamma$ planes, while the resolved stress on $\{2\,0\,0\}_\gamma$ is smaller; this is in qualitative agreement with the experimental data.

It is noted that the measured strains are elastic strains, while plastic accommodation of the transformation strain in austenite is relevant for lenticular martensite [22]. Hence, the above-reported theory should be considered as only a qualitative explanation of the observed reflection dependency for the transformation strain.

In conclusion, the build-up of compressive stress in austenite invoked by martensitic transformation during sub-zero Celsius cooling was proved. Ex situ XRD stress analysis revealed that stresses are macroscopically hydrostatic and their magnitude depends on the crystallographic plane. This dependency is suggested to originate from the specific orientation of the shape strain direction.

Ralf Feyerherm, Esther Dudzik, Christoph Genzel and Manuela Klaus, from Helmholtz Zentrum für Materialien und Energy (HZME), are acknowledged for their enthusiastic support during the in situ experiments at the Berlin synchrotron facility HZB-BESSY II. Financial support for the synchrotron measurements by the EU – Transnational Access Program is gratefully acknowledged.

[1] A.J. DeArdo, ISIJ International 35 (1995) 946–954.
[2] J. Bouquerel, K. Verbeken, B.C. De Cooman, Acta Mater. 54 (2006) 1443–1456.
[3] S. Harjo, Y. Tomota, P. Lukas, D. Neov, M. Vrana, P. Mikula, M. Ono, Acta Mater. 49 (2001) 2471–2479.
[4] J.H. Ryu, D.I. Kim, H.S. Kim, H.K.D.H. Bhadeshia, D.W. Suh, Scripta Mater. 63 (2010) 297–299.
[5] M. Villa, K. Pantleon, Marcel A.J. Somers, J. Alloys Compd, (2012). <http://dx.doi.org/10.1016/j.jalcom.2011.12.162>, in press.
[6] M. Villa, K. Pantleon, Marcel A.J. Somers, Sub-zero Austenite to Martensite Transformation in a Fe-Ni-0.6 wt.% C alloy, Proceedings of the 19th IFHTSE Congress, 2011. Available from: <http://orbit.dtu.dk/fedora/objects/orbit:72635/datastreams/file_6371300/content> [17th July 2012].
[7] K.Ja. Golovchiner, Phys. Metals Metallogr. 37 (1974) 126.
[8] V.M. Jershov, N.L. Oslon, Fix. Metal. 25 (1968) 874.
[9] V.N. Grindev, V.I. Trephilov, Dokl. Akad. Nauk SSSR 116 (1957) 60.
[10] K. Ulakko, V.G. Gavriljuk, Acta Metal. Mater. 40 (1992) 2471–2482.
[11] E. Dudzik, R. Feyerherm, W. Diete, R. Signorato, C. Zilkens, J. Synchr. Rad. 13 (2006) 421–425.
[12] O.N. Mohanty, Mater. Sci. Eng. B32 (1995) 267–278.
[13] Ch. Genzel, I.A. Denks, J. Gibmeier, M. Klaus, G. Wagener, Nucl. Instrum. Methods Phys. Res. A 578 (2007) 23–33.
[14] V. Hauk, Structural and Residual Stress Analysis by Non-Destructive Methods: Evaluation – Application – Assessment, Elsevier Science, Amsterdam, 1997.
[15] Landoldt-Börnstein, New Series, Group III, vol. 11. Springer, Berlin, 1979.
[16] H. Behnken, Ph.D. thesis, RWTH Aachen, 1992.
[17] E. Kröner, Z. Physik 151 (1958) 504–518.
[18] J.D. Eshelby, Proc. Roy. Soc. (London) A 241 (1957) 376–396.
[19] L. Cheng, N.M. van der Pers, A. Böttger, Th.H. de Keijser, E.J. Mittemeijer, Metall. Trans. A 22A (1991) 1957–1967.
[20] P.M. Kelly, Mater. Sci. Eng. A 438–440 (2006) 43–47.
[21] G.B. Olson, W.S. Owen, Martensite, ASM, International, 1992.
[22] G. Miyamoto, A. Shibata, T. Maki, T. Furuhara, Acta Mater. 57 (2009) 1120–1131.
[23] J.S. Bowles, J.K. Mackenzie, Acta Metall. 2 (1954) 129–137.
[24] H.K.D.H. Bhadeshia, Worked Examples in the Geometry of Crystals, The Institute of Metals, London, 1987.
[25] A. Shibata, T. Furuhara, T. Maki, Acta Mater. 58 (2010) 3477–3492.

APPENDIX E

In situ investigation of abnormal formation of lenticular martensite during sub-zero Celsius treatment

DRAFT

M. Villa, M.F. Hansen, K. Pantleon, Marcel A.J. Somers

Work was planned and the results were interpreted by all co-authors. First author performed the experimental activity and wrote the first draft of the manuscript. Comments and suggestions from M. F. Hansen, K. Pantleon and Marcel A.J. Somers were incorporated iteratively in the subsequent versions of the manuscript.

In situ investigation of abnormal formation of lenticular martensite at sub-zero Celsius temperature

Matteo Villa[1], Mikkel F. Hansen[2], Karen Pantleon[1], Marcel A.J. Somers[1]

1. Technical University of Denmark, Department of Mechanical Engineering, DK 2800 Kongens Lyngby, Denmark
2. Technical University of Denmark, Department of Micro and Nanotechnology, DTU Nanotech, DK 2800 Kongens Lyngby, Denmark

matv@mek.dtu.dk, mikkel.hansen@nanotech.dtu.dk; kapa@mek.dtu.dk, somers@mek.dtu.dk,

Keywords: isothermal martensite; steels; (synchrotron) X-Ray diffraction, magnetometry

Abstract

The formation of lenticular martensite in a high Carbon steel was investigated in situ at sub-zero Celsius temperature with vibrating sample magnetometry and (synchrotron) X-Ray diffraction. In situ magnetometry was applied to monitor and quantify the transformation from austenite to martensite during isochronal cooling, isothermal holding and isochronal (re)heating. In situ (synchrotron) X-Ray diffraction was applied to validate the magnetometry investigation and to assess the evolution of the lattice strain in austenite. X-Ray diffraction and magnetometry indicated that the formation of lenticular martensite is associated with multiple retardations and accelerations during isochronal cooling. Such abnormal transformation is interpreted in terms of the combined effect of autocatalytic nucleation of lenticular martensite and self-induced mechanical stabilization of the austenite.

Introduction

Martensite formation in iron-based alloys can proceed athermally, i.e. *in*dependent of time, or isothermally, i.e. dependent of time. The distinction between "*athermal*" and "*isothermal*" kinetics during martensite formation was first introduced [1] after the observation of time dependent martensite formation at sub-zero Celsius temperature [2], which did not fit into the general understanding of the transformation as strictly athermal at the time. The occurrence of time dependent martensite formation is well documented, and reviewed in Ref. [3].

The morphology of martensite in iron-based alloys can appear as laths, plates and lenses [4-11]. Lath martensite shows an internal sub-structure with a high density of dislocations [5,6], while plate martensite is partially [7], or fully [8], internally twinned. Lenticular martensite is composed of an internally twinned central midrib, surrounded by a region with a high dislocation density [9-11] (i.e. slipped martensite).

The formation of lenticular martensite in bulk materials is characterized by strong autocatalytic nucleation [4,12], which results in the observation of bursts [4]. In a burst, a large portion of material is transformed in an instantaneous event [3,4], yielding sudden [13,14] and *ir*reproducible [13] transformation steps. The

underlying autocatalytic nucleation is promoted by the elastic and plastic strains in the surrounding austenite as induced by the forming martensite [15,16].

Regardless of the morphology of martensite, the kinetics of martensitic transformations is historically described as nucleation-controlled [3], with the implicit assumption of instantaneous (i.e. infinitely rapid) growth of martensite. The assumption of instantaneous growth is based on the pioneering works presented in Refs. [17,18], wherein it was established that the duration of a martensite formation event is on the order of a small fraction of a second. Evidently, instantaneous martensite formation in the form of transformation steps (i.e. bursts) [13,14] is indicative of instantaneous growth of martensite.

Nevertheless, the rate of martensite growth depends on the martensite sub-structure [19] and growth is *not* necessarily instantaneous. The review in Ref. [19] yields the conclusion that twinned martensite grows athermally [17,20] at a velocity of about 10^3 m/s (i.e. growth is instantaneous), while slipped martensite grows by thermal activation at a velocity which is proportional to the driving force for martensite formation and in the range of 10^{-6} m/s to 10^{-1} m/s (see Ref. [19]). This implies that the formation of martensite lenses is characterized by athermal instantaneous growth of the midrib upon nucleation, followed by thermally activated (i.e. time dependent) thickening into a lenticular morphology. The thermally activated character of lenticular martensite formation is recently demonstrated in Ref. [21].

In Refs. [13,14,22], time dependent (i.e. isothermal) formation of lenticular martensite at sub-zero Celsius temperature was reported upon continuous cooling after one or multiple sudden transformation steps (i.e. bursts). Interestingly, it was shown that time dependent martensite formation may be characterized by smoothening of the transformation steps into "waves" (i.e. modulated steps), leading to wavy transformation curves. This effect, which was typified *"unusual"* [13] or *"irregular"* [14] and has remained *not* clarified, was observed to be stronger for larger fraction transformed and for a larger tendency for isothermal kinetics [13].

More recently, wavy transformation curves were observed during formation of lenticular martensite at sub-zero Celsius temperature in a high Carbon steel, which was (partially) transformed into martensite during conventional quench to room temperature [23].

The observation of wavy transformation curves is not limited to lenticular martensite formation at sub-zero Celsius temperature [13,14,22,23], but characterizes several solid state reactions in iron-based systems [13,24-31]. All observations are reviewed and rationalized in Ref. [31], where transformations characterized by wavy transformation curves are typified as *"abnormal"* after Refs. [25-28]. The work in Ref. [31] presents for the first time a mechanism to interpret the abnormal formation of lenticular martensite.

According to Ref. [31], on continuous cooling the formation of lenticular martensite starts at M_S and may be characterized by sudden and *ir*reproducible transformation steps (i.e. bursts). In the burst events, midribs form instantaneously. On continued cooling, athermal nucleation is accompanied by thermally activated growth of previously nucleated (thin plate) martensite into lenticular morphology, yielding smoothening of the transformation steps into waves. Modulated controlled multi-step transformation arise as a consequence of the combined effect of autocatalytic nucleation of lenticular martensite and self-induced mechanical stabilization of the austenite. On continuous cooling, autocatalytic nucleation of martensite yields an acceleration of the transformation, which is soon interrupted because of the self-induced mechanical stabilization of the austenite. A new acceleration of the transformation is obtained upon activation of a new population of martensite nuclei on increased undercooling. The mechanism is reproduced several times yielding abnormal transformation behavior.

Nevertheless, experimental evidence of the self-induced mechanical stabilization of austenite is not reported in Ref. [31]. Consequently, the interpretation presented in Ref. [31] remains phenomenological.

The aim of the present work is to contribute to the understanding of time dependent (i.e. isothermal) lenticular martensite formation. In particular, the work is intended to verify whether the evolution of the

state of stress in austenite during martensite formation, which is investigated by X-Ray diffraction, clarifies the observation of abnormal behavior in terms of self-induced mechanical stabilization of the austenite.

Experimental

Material and sample geometry

The alloy investigated was a commercial AISI 52100 steel extruded to a 10mm rod with the composition given in Table 1.

Table 1. Chemical composition (in wt-%) of AISI 52100 as determined by Glow Discharge Optical Emission Spectrometry (GDOES).

Fe	C	Cr	Ni	Mn	Si	Mo	Cu
Bal.	0.96 ±0.02	1.60 ±0.05	0.10 ±0.01	0.28 ±0.04	0.13 ±0.04	0.06 ±0.01	0.15±0.01

Two sample geometries were used: Ø10 mm, 0.33mm-thick disks for X-Ray Diffraction, XRD, investigation and Ø3 mm, 2mm-high cylinders, for Vibrating Sample magnetometry, VSM, investigation.

Heat treatments

The steel was austenitized at 1323 K for 900 s. Oxidation was prevented by sandwiching the samples in-between two 40 × 40 mm^2, 3 mm thick, stainless steel plates. Austenitization was terminated by cooling the samples in oil kept at 413 K and holding them in the oil bath for 180 s. Thereafter, the samples were air cooled and stored at room temperature for about 4 Ms (6-7 weeks). This condition is referred to as the "*initial condition*".

Table 2. List of samples and applied investigation techniques for the different thermal cycles. Samples are named after the temperature of isothermal holding, T_{iso}.

Sample	Technique	T_{iso} [K]
93	XRD, VSM	93
133	XRD, VSM	133
173	XRD, VSM	173
213	XRD, VSM	213
223	VSM	223
233	VSM	233

All samples in the initial condition were subjected to isochronal (i.e at a constant rate) cooling at a rate of 0.5 K/min to a predefined temperature and thereafter held for 7 h at this temperature. After isothermal holding, each sample was isochronally (re)heated at 1.5 K/min. All samples are named after the temperature (in K) of isothermal holding. Table 2 lists all samples and treatments. This heat treatment was carried out in situ, i.e. during VSM and XRD measurements, respectively.

VSM

VSM, was performed with a Lake Shore 7407 VSM, equipped with a Janis SuperTran-VP continuous flow cryostat. Samples were mounted onto a rigid fiber pole using non-magnetic Kapton tape. The degree of transformation was followed by recording the magnetic moment of the sample at saturation; the time

interval was 4 seconds. A magnetic field of 1 Tesla was used to bring the sample at magnetic saturation. Details of quantitative phase analysis are given in appendix A.

XRD

XRD was performed at the synchrotron facility HZB-BESSY II at the experimental stations MagS [32] applying a monochromatic beam (wavelength λ=0.1 nm) focused on a 1 mm round spot. Diffractograms were collected in Bragg-Brentano geometry at four different locations of the sample to enhance grain statistics. Measurement conditions are reported in Table 3. The total recording time for the four diffractograms (i.e. measurement time + alignment time) was about 480 s.

The method applied for quantification of the phase fractions was reported in Ref. [33], and is based on the comparison of the experimentally measured diffraction intensities with those predicted for a powder sample (see Ref. [34]).

Table 3. Measurement conditions for (synchrotron) XRD investigation.

λ [nm]	2θ	step size [2θ]	time per step [s]
0.1	25°-34°	0.04°	0.1
	34°-62°	0.1°	

The lattice strain in austenite was determined assuming a hydrostatic state of stress in austenite and averaging the results over the 111_γ, 200_γ, 220_γ and 311_γ reflections. The hypothesis of hydrostatic state of stress was validated for the sample hereby labeled 93 during previous work presented in Ref. [35]. The lattice strain, ε_γ, was obtained from:

$$\varepsilon_\gamma = \frac{a_\gamma(t,T) - a_\gamma^{ref}(T)}{a_\gamma^{ref}(T)} \tag{1}$$

where $a_\gamma(t,T)$ and $a_\gamma^{ref}(T)$ are the measured and reference lattice parameter of austenite, as a function of temperature, T, and time, t, respectively. The reference condition is taken as:

$$a_\gamma^{ref}(T) = a_\gamma(T_{ref} = 273\ K) \cdot \left(1 + \lambda_\gamma \cdot (T - 273)\right) \tag{2}$$

where λ_γ is the linear expansion coefficient for unconstrained austenite $\lambda_\gamma = 21.3 \cdot 10^{-6} K^{-1}$ [36]. Accordingly, the strains reported are corrected for unconstrained thermal shrink / expansion. Hence, $\varepsilon_\gamma\left(T_{ref} = 273\ K\right) = 0$.

The lattice strain results are presented as averaged values over the four probed sample locations.

Results

Morphology of martensite

The microstructures of the material in the *initial condition* and after cooling 0.5K/min to 93 K, isothermal holding 25.2 ks at 93 K and (re)heating 1.5 K/min to room temperature are given in Figs. 1a and 1b, respectively.

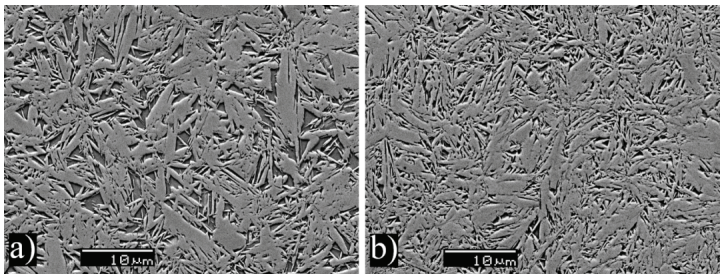

Figure 1. Martensite formation during sub-zero Celsius treatment; back-scatter electron micrographs (electrolytic etching in A-2 solvent by Struers at 30V for 40s on a surface area of 5mm^2). Retained austenite regions appear dark and are surrounded by martensite lenses. a) Initial condition; b) After sub-zero Celsius treatment to 93 K.

The microstructure is dual phase, containing martensite (appearing light grey) and retained austenite (appearing dark). Martensite is of lenticular morphology and its formation progressively partitions the regions of retained austenite. Comparing Figs 1a and 1b, it is concluded that the transformation of austenite to martensite has continued during sub-zero Celsius treatment. As a result, the final microstructure is refined and contains a reduced fraction of retained austenite.

Transformed fraction

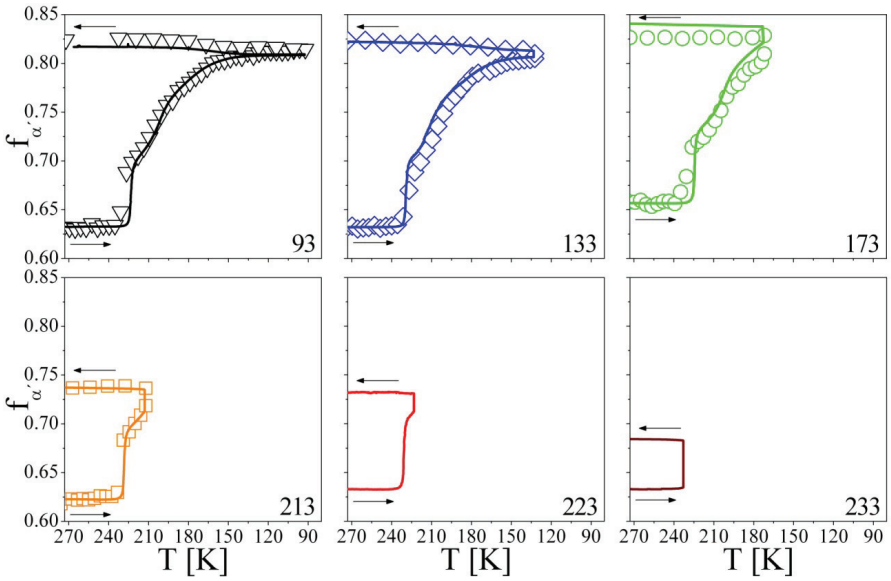

Figure 2. In situ XRD (large open symbols) and magnetometry (continuous lines) investigations of the molar fraction of martensite $f_{\alpha'}$ as a function of temperature T.

The evolution of the molar fraction of martensite, $f_{\alpha'}$, during sub-zero Celsius treatment as obtained in situ with XRD and VSM is shown in Figs. 2 and 3 for the isochronal and isothermal steps, respectively.

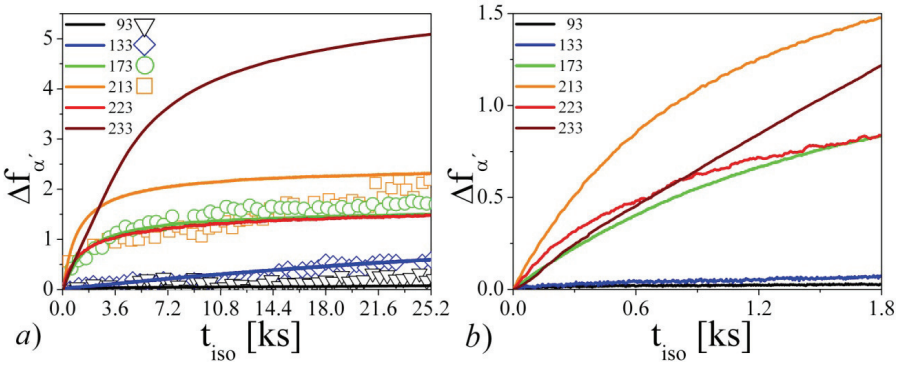

Figure 3. In situ XRD (large open symbols) and magnetometry (continuous lines) investigations of the molar fraction of martensite formed during isothermal holding at the indicated temperatures. $\Delta f_{\alpha'}$ is plotted versus time of isothermal holding t_{iso}: a) all collected data; b) first 1.8 ks of isothermal holding.

An alternative presentation of the VSM data is shown in Fig. 4, where the transformation rate within time intervals of 480 s (i.e. 4 K for the isochronal cooling step) is given as a function of time for both the isochronal cooling step and the isothermal holding step, respectively. The instant of reaching the isothermal holding temperature is taken as zero for scaling the time axis. Consequently, "negative" times are obtained in the isochronal cooling stage.

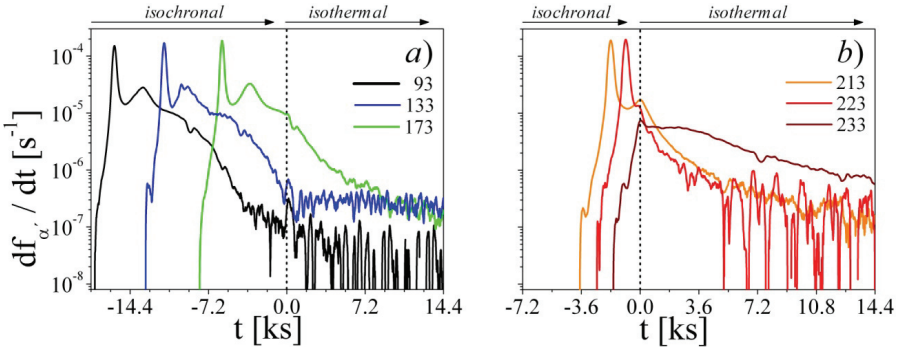

Figure 4. Magnetometry investigation. The rate of martensite formation during continuous cooling followed by isothermal holding $df_{\alpha'}/dt$ is plotted versus time t. Data is presented relatively to the beginning of the isothermal stage where $t = 0$.

In Figs. 2 and 3 it is demonstrated that the fraction of martensite increases in all three stages of the sub-zero Celsius treatment, *i.e.* during cooling (Fig. 2), during isothermal holding (Fig. 3) and during (re)heating (Fig. 2).

Initially, during isochronal cooling from the initial state (Fig. 2), austenite appears stable. At about 240 K, after reaching a certain degree of additional undercooling with respect to the initial condition, the transformation (re)starts at a temperature, $M_{(re)s}$ (=240 K).

A large increase in the martensite content is observed at a few degrees undercooling below $M_{(re)s}$, at say, 235 K. This sudden transformation shows strong similarity with a burst type transformation. It is noted explicitly, that in the present experiments the transformation occurs in a controlled way along with the slow controlled cooling at 0.5 K/min, while bursts are associated with an uncontrolled mechanism (see Ref. [13]).

After the sudden increase in the martensite fraction, on prolonged cooling the transformation path shows a retardation followed by an acceleration of the transformation. This is clearly resolved by the continuous VSM data and confirmed by the independent XRD data. The retardation and acceleration suggests a two-step transformation mechanism, which is abnormal after Refs. [25-28]. Upon further undercooling, the transformation proceeds very slowly and practically comes to a halt for temperatures below, say, 130 K.

Abnormal transformation is more clearly presented in Fig. 4, where in the isochronal stage a maximum is observed in the transformation rate, which is followed by a second maximum. The time difference between the two maxima is approximately 2.6 ks (Fig. 4a).

In the isothermal stage (Fig. 3), martensite formation is observed at all investigated sub-zero Celsius temperatures. For isothermal holding at temperatures up to 213 K the higher is the holding temperature, the faster proceeds the isothermal transformation and the larger is the degree of transformation during isothermal holding. Isothermal martensite formation at 223 K and 233 K, appears atypical. At 223 K, a temperature in between the two maxima of transformation rate observed on isochronal cooling, the isothermal transformation is initially faster than at 213 K, but the total extent of isothermal transformation is smaller. At 233 K, a temperature just below $M_{(re)s}$, but before the "controlled" burst (cf. Fig.2), the isothermal transformation is initially slower than at 223 K (Fig. 3b), but the total extent of isothermal transformation is considerably larger than for all other investigated isothermal transformation temperatures.

The evolution of the transformation rate during the isochronal cooling and isothermal holding steps is more clearly presented in Fig. 4. Fig. 4 shows that the transformation rate remains continuous upon interrupting the isochronal cooling step and that the evolution of the transformation rate on isothermal holding strongly depends on temperature. Upon interrupting the cooling at 133 K and 93 K (Fig. 4a), where the transformation rate is very low, the transformation rate remains almost constant on isothermal holding. For interrupted cooling at 223 K, 213 K (Fig. 4b) and 173 K (Fig. 4a), a sudden deceleration occurs. At 233 K (Fig. 4b), the transformation rate is maintained at a relatively high level during isothermal holding.

On (re)heating after the isothermal stage (Fig. 2), continued martensite formation was observed in samples 93, 133 and 173. No transformation during (re)heating was observed for the samples isothermally held at temperatures higher than 173 K. Martensite formation on (re)heating is observed in the temperature interval 130 K - 210 K with a maximum transformation rate at about 160-170 K.

Evolution of the lattice strain in austenite

The evolution of the (additional) lattice strain introduced in austenite during sub-zero Celsius treatment is shown in Fig. 5. Strain values were evaluated from experimental data with Eqs. (1) and (2).

The (additional) lattice strain appears to be composed of a reversible part and an irreversible part (Fig.5). Initially, during isochronal cooling down to 235 K, a tensile strain is introduced in austenite. During (re)heating in the same temperature range an additional compressive strain is built up, indicating that the

“tensile” strain introduced during cooling is recovered. Also, in the temperature range below 130 K the (additional) tensile strain, is recovered on (re)heating.

An irreversible compressive lattice strain is observed during isochronal cooling in the temperature range 235 K to 130 K and during isothermal holding. This compression is observed along with the martensitic transformation and is retained after (re)heating to room temperature. The retained (additional) compression is the larger the larger the fraction of martensite which has formed during the sub-zero Celsius treatment (cf. Fig. 2).

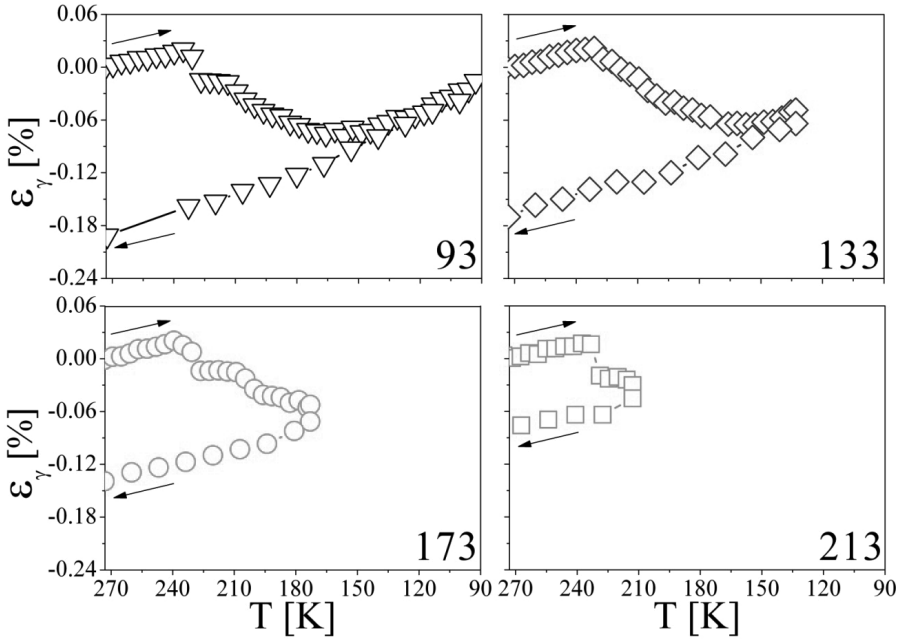

Figure 5. Evolution of lattice strain investigated with in situ XRD investigation. The (additional) lattice strain, relative to the reference condition $\varepsilon_\gamma=0$ at 273K, was corrected for unconstrained thermal expansion / contraction of austenite. ε_γ is presented versus temperature T.

Discussion and interpretation

Evolution of the lattice strain in austenite

In a multi-phases material, the mechanical interaction between the phases during fabrication of a component may result in the generation of residual stresses. These stresses may have thermal origin, as a consequence of different coefficients of thermal expansion of the phases, or may arise as a consequence of phase transformations [37].

The presence of residual stresses yields a change in lattice parameter of the phases which is observable in terms of a lattice strain in an XRD experiment [38]. In the following, the lattice strain in austenite (cf. Fig. 5) are interpreted after Ref. [35].

In the present case, the austenite regions are embedded by martensite (cf. Fig. 1). The constraints imposed on austenite by the surrounding martensite, which in unconstrained condition would experience less thermal shrink/expansion than austenite, leads to an (additional) tensile strain in austenite on cooling. Similarly, on heating additional compression builds up in austenite. This part of the lattice strain has thermal origin and is reversed upon thermal cycling.

On the other hand, martensite formation is associated with a transformation strain which yield a volume expansion of the material. The transformation strain leads to residual compressive strain in austenite which is retained after (re)heating to room temperature. The state of compressive strain measured in the austenite by XRD is a consequence of an hydrostatic pressure (see Ref. [35]) on the austenite which is build up by martensite formation.

Kinetics of the transformation

Athermal nucleation, thermally activated growth

In this section, we discuss an interpretation of the kinetics of the martensite formation in terms of athermal nucleation combined with thermally activated, time dependent, growth of martensite units in line with the recent independent works by Villa et al. [23,31,32], Kim et al. [39], Liu et al. [40] and Löwy et al. [41]. Adopting this interpretation, literature data in Refs. [13,14,22,23] were interpreted consistently in Ref. [31].

It is explicitly mentioned that this interpretation is in conflict with the current opinion that growth of lenticular martensite occurs instantaneously upon nucleation [21,42]. However, as discussed by Brook et al. (see Ref. [13]), instantaneous growth of martensite is *not* compatible with the observation of wavy transformation curves.

The analysis starts with an attempt to quantify the driving force for martensite formation from experimental data, combined with literature data. Through this procedure an explanation is given for abnormal formation of lenticular martensite. Sample 93 is taken as an example.

Driving force for martensite formation

The driving force for the transformation of austenite to martensite, $\Delta G_{\gamma\rightarrow\alpha'}$, is the sum of three energy terms [43-45]: (i) the chemical energy, which results from the relative thermodynamic stability of the austenite and martensite phases and increases with reducing the temperature; (ii) the mechanical energy, which results from the presence of stress fields in austenite and act against the transformation when in terms of an hydrostatic pressure; (iii) the magnetic energy, which results from the presence of magnetic fields and always favors the formation of martensite.

In the present case, the magnetic energy was negligible, as validated by the *quantitative* agreement between VSM and XRD data. The remaining contribution were quantitatively estimated as follows: the chemical energy was estimated from literature data [3,43,46]; the mechanical energy was quantified from the measured (Fig. 5) lattice strain in austenite (see appendix B).

The total driving force was calculated taking $M_{(re)s}(= 240\ K)$ as reference temperature and defining an additional effective driving force ΔG_{eff} as follows:

$$\Delta G_{eff} = -\left(\Delta G_{\gamma\rightarrow\alpha'} - \Delta G_{\gamma\rightarrow\alpha'}\left(M_{(re)s}\right)\right) \tag{3}$$

where $\Delta G_{\gamma\to\alpha'}(M_{(re)s})$ is the driving force for the transformation of austenite to martensite at $M_{(re)s}$ (i.e. it stands $\Delta G_{eff}(M_{(re)s}) = 0$).

The evolution of ΔG_{eff} at $T < 240\ K$ is shown in Fig. 6 together with the separate contributions of the chemical energy, ΔG_{chem}, and mechanical energy, ΔG_{mech}, respectively (see Appendix B for a detailed description of how the energy terms in Fig. 6 were calculated).

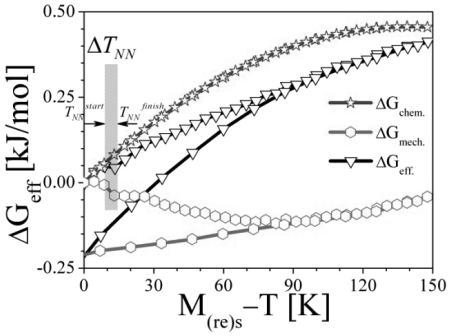

Figure 6. Effective driving force for martensite formation $\Delta G_{eff}(T, f_{\alpha'})$ as a function of undercooling with respect to $M_{(re)s} = 240K$. Within the temperature range ΔT_{NN} the effective driving force first decreases and thereafter regain its maximum value.

As follows from Fig. 6, the effective driving force for martensite formation, ΔG_{eff}, increases monotonously with increasing undercooling, apart from a narrow temperature range, ΔT_{NN}, defined by the temperature where the driving force start decreasing, T_{NN}^{start}, and the temperature where its maximum value is regained, T_{NN}^{finish}, i.e. $\Delta G_{eff}(T_{NN}^{start}) = \Delta G_{eff}(T_{NN}^{finish})$. In Fig. 7, ΔT_{NN} is compared with the transformation rate, df/dt, normalized to its maximum value, df/dt_{MAX}, as derived from the VSM investigation (cf. Fig. 4).

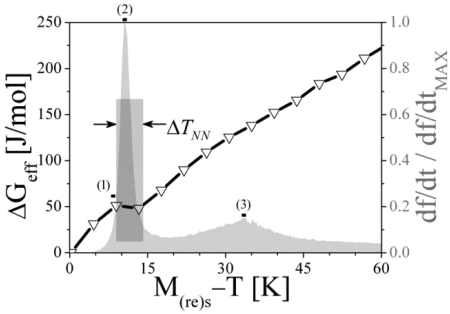

Figure 7. Effective driving force for martensite formation $\Delta G_{eff}(T, f_{\alpha'})$ as a function of undercooling with respect to $M_{(re)s} = 240K$. The right y axis refers to the transformation rate df/dt as normalized to the its maximum value df/dt_{MAX}, which is shown as a grey area.

Fig. 7 shows that ΔT_{NN} coincides with the temperature range wherein the first transformation rate maximum is observed. In correspondence with a sudden acceleration of the transformation, ΔG_{eff} start decreasing (point (1)). For larger undercooling, the transformation rate is observed to reach a maximum (point (2)). The second maximum of the transformation rate is observed only for a larger undercooling beyond ΔT_{NN} (point (3)).

Nucleation and growth of martensite

The potency of a potential site for martensite formation (i.e. an embryo) to be activated and develop a martensite nucleus varies from site to site [47-50]. According to the theory for martensite nucleation due to Kakeshita et al. [43,44], the most potent embryo nucleates martensite instantaneously, i.e. athermally, when (at least) the critical driving force for the transformation is reached.

Independent of the potency distribution, after the first nucleation event, less potent embryos nucleate martensite athermally when their corresponding critical driving force is reached for the first time [47-49]. Applying this concept to Fig. 6, athermal nucleation of martensite during cooling occurs *spontaneously* as long as ΔG_{eff} reached after an increment of the undercooling is larger than ΔG_{eff} at the previous undercooling. Consequently, athermal *spontaneous* nucleation of martensite is not possible in the undercooling region ΔT_{NN}. Also, athermal *spontaneous* nucleation is not possible on isothermal holding and (re)heating.

Athermal nucleation can occur also autocatalytically. Athermal autocatalytic nucleation can be promoted by spontaneous athermal nucleation or by continuous thermally activated growth of martensite units (see for example Ref. [51]).

In relation to growth, (thermally activated) growth of martensite nuclei can occur only, provided that the driving force for the transformation is sufficiently high to overcome the strain energy associated with plate thickening [52-55], which is proportional to the thickness of the martensite units [54], and the energy dissipated during the movement of the interface [52]. Here, it is assumed that the driving force at $M_{(re)s}$ is the minimum driving force necessary to form martensite and that the dissipated energy is constant. Hence, growth of martensite is only possible if $\Delta G_{eff} > 0$ and the maximum allowed dimension for the martensite units increases linearly with ΔG_{eff}.

It follows that autocatalytic nucleation is also possible for $\Delta G_{eff} > 0$ (i.e. on cooling, isothermal holding and (re)heating), but it is expected to be less pronounced in the undercooling region ΔT_{NN}.

In the following, martensite formation as observed in the present investigation is described in accordance with these concepts.

Martensite formation during isochronal cooling

At temperatures just below $M_{(re)s} = 240$ K, martensite starts to nucleate athermally and is able to grow (to a limited extent). Autocatalytic formation of a large number of nuclei requires a certain thickness of the martensite units [51] and is therefore first observed at a few degrees undercooling (i.e. 235 K).

Along with the autocatalytic nucleation, the transformation rate accelerates and the first maximum of the transformation rate is approached (Fig. 4). Simultaneously, compressive stress builds up in austenite such that spontaneous nucleation comes to a halt at T_{NN}^{start} (Figs. 5, and 7). However, as ΔG_{eff} is positive,

growth of (the majority of)[74] the martensite nuclei is not hindered, and continues in the temperature range ΔT_{NN}; hence, martensite formation continues (by both growth and associated autocatalytic nucleation), albeit at a slow rate (Figs. 2 and 7). Consequently, on increasing the undercooling, the effect of the mechanical contribution that counteracts the chemical contribution to the driving force is reduced (Figs. 5 and 6). On continued cooling, the effective driving force regains a value that allows the spontaneous activation of the next population of embryos into nuclei. Moreover, growth of the largest martensite nuclei is regained, significantly contributing to the formation of new nuclei by autocatalysis. Hence, an acceleration of the formation of martensite is observed, which leads to the second maximum in the isochronal transformation curves (Fig. 7). Thereafter, the rate of the martensite formation decelerates continuously (Fig. 4).

In principle, multiple accelerations and decelerations of the overall transformation rate could occur for large amounts of austenite so that the autocatalytic effect can arise repeatedly, yielding wavy transformation curves (i.e. abnormal behavior).

Martensite formation during isothermal holding

Isothermal martensite formation strongly depends on the holding temperature (Figs. 3 and 4). At 233 K (i.e. 7 K undercooling beyond $M_{(re)s}$), the available driving force for martensite formation by growth of athermally developed nuclei is small (Figs. 3 and 4), because this temperature is just below $M_{(re)s}$=240 K. This is reflected as a relatively slow initial isothermal transformation rate as compared to isothermal transformation at other temperatures above 170 K (Figs. 3b). Nevertheless, as suggested by a sustained and approximately constant transformation rate during the first hour of isothermal holding (Fig. 4), substantial nucleation of martensite occurs. Nucleation during isothermal holding results from continuous autocatalytic nucleation of martensite as promoted by thermally activated growth.

At 223 K (i.e. 17 K undercooling beyond $M_{(re)s}$), just after the first maximum of the transformation rate (Fig. 7) athermal spontaneous nucleation is reduced by $\Delta G_{eff} \sim \Delta G_{eff}\left(T_{NN}{}^{start}\right)$. Also, continuous growth of the largest martensite nuclei, and associated strong autocatalytic nucleation, is poor because of a low surplus of ΔG_{eff}. As a result, the extent of martensite formation during isothermal holding at 223 K is limited (Fig. 3a).

At 213 K (i.e. 27 K undercooling beyond $M_{(re)s}$) the athermal spontaneous development of nuclei during cooling is regained (Fig. 7) and these nuclei continue to grow in the isothermal stage. Moreover, continuous growth of the martensite units also contribute to the formation of new nuclei by autocatalysis. However, since the isothermal transformation rate is decreasing continuously, it appears that no significant nucleation occurs during isothermal holding.

Finally, for isothermal transformation at 173 K, 133 K and 93 K, it would be expected that abundant isothermal transformation should be possible, because of the abundance of martensite nuclei and a large driving force for growth (Fig. 6). Nevertheless, the larger the undercooling for isothermal temperatures below 200 K, the smaller is the contribution of isothermal martensite formation. This apparent discrepancy is explained from slow kinetics of thermally activated martensite growth, which not only limits the contribution to the transformation of nuclei formed upon cooling, but also inhibits continuous nucleation by autocatalysis at a significant rate.

[74] Growth is not allowed for the martensite units which already reached the maximum dimension allowed at $\Delta G_{eff}\left(T_{NN}{}^{start}\right)$.

Further indications for thermally activated martensite formation at temperatures below 200 K are observed in Fig. 4.

Upon interruption of isochronal cooling it is observed in Fig.4 that the transformation rate changes continuously. If athermal martensite formation applies (athermal nucleation followed by instantaneous growth) a discontinuity would be expected in the transformation rate upon interrupting the cooling. A continuous transformation rate is only possible if growth of martensite is dominated by time-dependent, thermally activated thickening, as for martensite lenses, rather than by athermal growth, as for twinned martensite.

Thermally activated growth of martensite nuclei is corroborated by the observation of martensite formation during heating from an isothermal holding temperature below 200 K. During heating no new martensite embryos are spontaneously activated but rather existing and autocatalytically generated nuclei grow, provided that sufficient thermal energy is available to activate the rate determining step and that ΔG_{eff} is sufficient to promote further thickening of the martensite lenses.

Abnormal transformations in steel

In the previous paragraph, the abnormal behavior observed during transformation of austenite into lenticular martensite was consistently explained by the role of the self-induced strain energy, arising during autocatalytic martensite formation, on the effective driving force for the transformation.

This interpretation, first introduced in Ref. [31] and hereby validated quantitatively, parallels the description of abnormal martensite formation with the abnormal *massive* transformation of austenite into ferrite as reported in Refs. [25-28]. However, a main difference between the two description is mentioned explicitly in the following.

According to Refs. [25-28], the overall *massive* formation of ferrite is controlled by an energy balance between chemical driving force and strain energy introduced in the system during the transformation.

In the case of martensite, the driving force is known to control the overall martensite formation [46,56-58], but contrary to the case presented in Refs. [25-28] for the *massive* formation of ferrite, this control is believed to result from the number of martensite nuclei per unit volume of austenite as governed by the driving force for the transformation [57,59], rather than from an energy balance.

This concept is corroborated in Fig. 6, where it is observed that the mechanical energy introduced in the system by the formation of lenticular martensite is insufficient to counterbalance the chemical driving force on continued cooling. Evidently, the martensitic transformation in the present case is controlled by the number of martensite nuclei per unit volume of austenite and their dimension as controlled by driving force [54,55] and time available for growth, rather than from an energy balance.

Conclusions

Independent in situ XRD and in situ magnetometry investigations yield quantitatively consistent results on the transformation of austenite to martensite during isochronal cooling, isothermal holding and isochronal (re)heating.

Compressive lattice strains developing in the austenite during martensite formation are largely retained after (re)heating to room temperature.

Abnormal formation of lenticular martensite during isochronal cooling is manifested as several accelerations and decelerations of the transformation rate. This behavior is quantitatively explained from the stabilizing effect of the transformation strain in austenite.

The kinetics of the transformation can be consistently interpreted as the result of a-thermal nucleation followed by thermally activated growth of lenticular martensite.

Acknoledgements

Financial support for the synchrotron measurements by the EU – Transnational Access Program is gratefully acknowledged.

We are indebted E. Dudzik, R. Feyerherm from Helmholtz-Zentrum Berlin and Flemming B. Grumsen from Technical University of Denmark for skillful assistance with the synchrotron XRD experiments.

References

[1] C. Fisher, J.H. Hollomon, D. Turnbull, J. Applied Physics., 19 (1948) 775.
[2] G.V. Kurdjumov, O.P. Maksimova, Dokl. Akad, Nauk SSSR., 61 (1948) 83.
[3] N.N. Thadhani, M.A. Meyers, Progress in Mater. Sci., 30 (1986) 1-37.
[4] G. McDougall, C.M. Wayman, "*Crystallography and Morphology of Ferrous Martensite*" in G.B. Olson, W.S. Owen, "*Martensite*", (OH) , ASM International, 1992.
[5] K. Wasaka, C.M. Wayman, Acta Metal., 29 (1981) 991-1001.
[6] S. Morito, X. Huang, T. Furuhara, T. Maki, N. Hansen, Acta Mater., 54 (2006) 5323-5331.
[7] K. Shimizu, M. Oka, C.M. Wayman, Acta Metall., 18:9 (1970) 1005-1011.
[8] T. Maki, C.M. Wayman, Metall. Trans., A 7:9 (1976) 1511-1518.
[9] H.Y. Lee, H.W. Yen, H.T. Chang, J.R. Yang, Scripta Mater. 62 (2010) 670-673.
[10] M. Unemoto, K. Minoda, I. Tamura, Metallography, 15 (1982) 177-191.
[11] A. Shibata, S. Morito, T. Furuhara, T. Maki, Acta Mater., 57(2009) 483-492.
[12] V. Raghavan, A. R. Entwisle, Iron and Steel Inst. Special Report, 93 (1965) 30
[13] R. Brook, A. R. Entwisle, J. of the Iron and Steel Institute, 203 (1965) 905-912.
[14] A. R. Entwisle, Metall. Trans., 2:9 (1971) 2395-2407.
[15] G.B. Olson, M. Cohen, Metall. Trans. A, 6:4 (1975) 791-795.
[16] S.R. Pati, M. Cohen, Acta Metall., 19 (1971) 1327-1332.
[17] R.F. Bunsham, R.F. Mehl, Trans. AIME. 1953, Vols. 197, pp.1251.
[18] F. Forster, E. Scheil, Naturwissenschaften, 25 (1937), 439-440.
[19] Z. Nishiyama, "*Martensitic Transformation*", New York: Academic Press., 1978.
[20] Yu, Z.Z.; Clapp, P.C., Metal. Trans. A, 20 (1989) 1601-1615.
[21] Shibata, A.; Murakami, T.; Morito, S.; Furuhara, T.; Maki, T., Materials Trans., 49:6 (2008)1242-1248.
[22] C.A.V. Rodrigues, C. Prioul, L. Hyspecka, Metall. Trans. A., 15 (1984) 2193-2203.
[23] M. Villa, M. F. Hansen, K Pantleon, M. A.J. Somers, "*In situ investiation of martensite formation in AISI 52100 bearing steel at sub-zero Celsius temperature*", proceeding of the 2nd Mediterranean conference on heat treatment and surface engineering, Dubrovnik, Croatia, 2013.
[24] K. Tsuzaki, T. Maki, I. Tamura, Scripta Metall. 21 (1987) 1693-1698.
[25] Y. Liu, F. Sommer, E.J. Mittemeijer, Acta Mater., 51 (2003) 507-519.
[26] Y. Liu, F. Sommer, E.J. Mittemeijer, Acta Mater., 52 (2004) 2549-2560.
[27] Y. Liu, F. Sommer, E.J. Mittemeijer, Metall. And Mater. Trans. A, 39 (2008) 2306-2318.
[28] Liu, Y.C.; Sommer, F.; Mittemeijer, E.J., Chinese Sci. Bullettin, 49 (2004) 972-975.
[29] S. Löwy, B. Rheingans, S.R. Meka, E.J. Mittemeijer, Acta Mater., 64 (2014) 93-99.
[30] M. Villa, M.F. Hansen, K. Pantleon, M.A.J. Somers, "*Thermally activated growth of lath martensite in Fe-Ni-Cr-Al precipitation hardenable stainless steel"*, submitted for publication.
[31] M. Villa, K. Pantleon, M. Reich, O. Kessler, M.A.J. Somers, "*Abnormal formation of lath martensite in precipitation hardenable stainless steel"*, submitted for publication.
[32] M. Villa, K. Pantleon and M.A.J. Somers, Scr. Mater. 67 (2012) 621-624.

[33] E. Dudzik, R. Feyerherm, W. Diete, R. Signorato, C. Zilkens, J. Synchr. Rad. 13 (2006) 421-425.
[34] M. Villa, K. Pantleon, M.A.J. Somers, J. All. Comp., 577:1 (2013) S543-S548
[35] ASTM International Standard designation E 975-03, Standard Practice for X-ray Determination of Retained Austenite in Steel with near Random Crystallographic Orientation
[36] M. Villa, K. Pantleon, M.A.J. Somers, "Enhanced Carbide precipitation during tempering of sub-zero Celsius treated AISI 52100 bearing steel", proceedings of the Heat Treat and Surface Engineering Conference and Expo 2013, 2013, Chennai, India.
[37] P.J. Withers, H.K.D.H. Bhadeshia, Mater. Sci. Tech., 17 (2001) 366-375
[38] P.J. Withers, H.K.D.H. Bhadeshia, Mater. Sci. Tech., 17 (2001) 355-365
[39] D. Kim, S-J. Lee, B.C. De Cooman, Metall. and Mater. Trans. A. 43 (2012) 4967-4983.
[40] Y. Liu, L. Zhang, F. Sommer, E.J. Mittemeijer, Metall. Mater. Trans. A, 2012 DOI: 10.1007/S11661-012-1497-6, 51
[41] S. Löwy, B. Rheingans, S.R. Meka, E.J. Mittemeijer, Acta Mater., 64 (2014) 93-99.
[42] R.L. Patterson, G.M. Wayman, Acta mater., 14:3 (1966) 347-369.
[43] T. Kakeshita, K. Kuroiwa, K. Shimizu, T. Ikeda, A. Yamagishi, M.A. Date, Mater. Trans. JIM., 34:5 (1993) 423-428.
[44] T. Kakeshita, T. Saburi, K. Shimizu, Mater. Sci. Eng., A273 (1999) 21-39.
[45] J.R. Patel, M. Cohen, Acta Metall. 1:5 (1953) 531-538.
[46] S.M.C. Van Bohemen, J. Sietsma, Metall. And Mater. Trans, 40A (2009) 1059-1068.
[47] C.L. Magee, Metall. Trans, 2:9 (1971) 2419-2430.
[48] R.E. Cech, D. Turnbull, Transactions of the ASME, 206:2 (1956) 124-132
[49] G.B. Olson, M. Cohen, "*Dislocation theory of martensitic transformations*" in F.R.N. Nabarro. "*Dislocations in Solids" - Vol 7.* Amsterdam, The Netherlands, North Hollande Physics Pubblishing, 1986.
[50] Lin, M.; Olson, G.B.; Cohen, M., Metal. Trans. A., 23 (1982) 2987-2998
[51] Yang, D-Z; Wayman, C.M., Acta Metall., 32 (1984) 949-954
[52] M. Grujicic, G.B. Olson, W.S. Owen, Metall. Trans., 16A (1985) 1713-1722.
[53] G.B. Olson, M. Cohen, Scripta Mater., 9 (1975) 1247-1254.
[54] D. Eshelby, Proc. Roy. Soc. (London) A 241 (1957) 376–396.
[55] T. Maki, S. Shimooka, S. Fujiwara, I. Tamura, Trans. JIM., 16 (1975) 35-41.
[56] Koistinen, D.P.; Marburger, R.E., Acta Metall, 7 (1959) 59-60.
[57] Bhadeshia, H.K.D.H., J. of Mater. Sci., 17 (1982) 383-386.
[58] Koyano, T., Mater. Trans. A, 44:12 (2003) 2541-2544
[59] C.L. Magee, *Phase Transformations*, Metals Park, Ohio: American Society for Metals, 1968
[60] H. Behnken, Ph.D. thesis, RWTH Aachen, 1992.

Appendix A: Quantitative phase analysis for VSM investigations

The quantification of the molar fraction of martensite during sub-zero Celsius treatment, $f_{\alpha'}(t,T)$, expressed as a function of time, t, and temperature, T, is based on the following assumptions:

1. the molar fraction of martensite $f_{\alpha'}(t,T)$ is proportional to the magnetic moment at saturation, $M(t,T)$, corrected for its temperature dependence;
2. no transformation occurs during recording of the baseline;
3. the temperature dependence of the magnetic moment at saturation can be expressed relative to its value at the reference temperature, T_{ref}, and is given by $\frac{M_b(T)}{M_b(T_{ref})}$, where $M_b(T)$ is the magnetic moment at saturation measured at temperature T during recording of the baseline and $M_b(T_{ref})$ is the magnetic moment at saturation measured at T_{ref} during recording of the baseline;
4. the fraction of martensite prior to sub-zero Celsius treatment, $f_{\alpha'_{RS}}$, is known;

5. the saturation magnetization of the sample measured at T_{ref}, prior to sub-zero Celsius treatment,$M(T_{ref})$, is known.

With these assumptions, it can be written:

$$\frac{f_{\alpha'}(t,T)}{f_{\alpha' RS}} = \frac{M(t,T)}{M_b(T)} \cdot \frac{M_b(T_{ref})}{M(T_{ref})} \tag{A1}$$

Hence, $f_{\alpha'}(T,t)$ is given by:

$$f_{\alpha'}(t,T) = f_{\alpha' RS} \cdot \frac{M(t,T)}{M(T_{ref})} \cdot \frac{M_b(T_{ref})}{M_b(T)} \tag{A2}$$

The quantification procedure requires the determination of $f_{\alpha' RS}$ by an independent technique. For this purpose the fraction of martensite as determined by XRD is taken as a reference for samples 93, 133, 173 and 213. The fraction of martensite averaged over samples 93, 133, 173 and 213 is taken as reference condition for samples 223 and 233. The values of $f_{\alpha' RS}$ are collected in table A1.

Table A1. Fraction of martensite taken as reference state $f_{\alpha' RS}$ for VSM quantitative phase analysis.

Sample	233	223	213	173	133	93
$f_{\alpha' RS}$	0.634	0.634	0.625	0.657	0.632	0.633

Baseline recording was performed on sample 93 by measuring a second (identical) cooling cycle (i.e. cooling at a rate of 0.5 K/min followed by (re)heating 1.5 K/min). The baseline on both cooling and (re)heating was assessed by fitting a second order polynomial to the experimental data .

Appendix B Calculation of driving force for martensite formation

In this appendix the driving force for martensite formation will be assessed *quantitatively* omitting the contribution of the magnetic energy and assuming hydrostatic state of stress in the austenite.

Following [43-45], the driving force for the transformation $\Delta G_{\gamma\to\alpha'}$ is written as:

$$\Delta G_{\gamma\to\alpha'} = \Delta G_{chem}(T) + \varepsilon_0(T) \cdot P_\gamma \cdot V_{\alpha'}^m(T) \tag{C1}$$

where $\Delta G_{chem}(T)$ is the chemical driving force, $\varepsilon_0(T) = \frac{V_{\alpha'}^m(T) - V_\gamma^m(T)}{V_\gamma^m(T)}$ is the transformation strain, P_γ is the hydrostatic pressure in austenite and $V_{\alpha'}^m(T)$ and $V_\gamma^m(T)$ are the molar volume of martensite and austenite, respectively.

In the following, $\Delta G_{\gamma\to\alpha'}$ is calculated relative to the driving force at the reference temperature $M_{(re)s} = 240\ K$, $\Delta G_{\gamma\to\alpha'}(M_{(re)s})$, and expressed as an (additional) effective driving force for the transformation, ΔG_{eff}, as:

$$\Delta G_{eff} = -\left(, \Delta G_{\gamma\to\alpha'} - \Delta G_{\gamma\to\alpha'}(M_{(re)s})\right) \tag{C2}$$

It follows:

$$\Delta G_{eff} = \Delta G_{chem}(T) - \Delta G_{chem}(M_{(re)s}) + \varepsilon_0(T) \cdot P_\gamma \cdot V_{\alpha'}^m(T) - \varepsilon_0(M_{(re)s}) \cdot P_\gamma(M_{(re)s}) \cdot V_{\alpha'}^m(M_{(re)s}) \tag{C3}$$

where $\Delta G_{chem}\left(M_{(re)s}\right)$, $\varepsilon_0\left(M_{(re)s}\right)$, $P_\gamma\left(M_{(re)s}\right)$ and $V_\alpha^m\left(M_{(re)s}\right)$ are the chemical driving force, the transformation strain, the hydrostatic pressure on the austenite and the volume fraction of martensite at the reference temperature, respectively.

As shown in Ref. [3,43], the chemical driving force above 250 K is described by a linear temperature dependence with slope 7 J mol^{-1} K^{-1} [46]. In the temperature range 100 to 250 K a quadratic temperature dependence applies. Below100 K the chemical driving force is not further enhanced.

Assuming that the driving force is a continuous function of temperature, the chemical driving force, expressed in J mol^{-1} , is described by the following set of equations:

$$for\ T > 250K: \qquad \Delta G_{chem}(T) = \Delta G_{chem}\left(M_{(re)s}\right) + 7\ \cdot \left(T - M_{(re)s}\right), \tag{C4}$$

$$for\ 100K < T < 250K: \Delta G_{chem}(T) = \Delta G_{chem}\left(M_{(re)s}\right) + 7 \cdot \left(250 - M_{(re)s}\right) - \frac{1}{3} \cdot \Big(875 - 14 \cdot T + 7100 \cdot \mathit{?}2 \tag{C5}$$

$$for\ T < 100K: \qquad \Delta G_{chem}(T) = \Delta G_{chem}\left(M_{(re)s}\right) + 7 \cdot \left(250 - M_{(re)s}\right) - \frac{1575}{3} \tag{C6}$$

where the value of $\Delta G_{chem}\left(M_{(re)s}\right)$ is irrelevant for the quantification of ΔG_{eff}.

The (additional) strain energy contribution to the driving force is given by the lattice strain in austenite calculated from the experimental data obtained by XRD (Fig. 5).

Finally, the elastic lattice strain is converted into elastic stress assuming linear elastic behavior and a bulk modulus of 184 GPa [60].

APPENDIX F

In situ investigation of martensite formation in AISI 52100 bearing steel at sub-zero Celsius temperature

PUBLISHED

M. Villa, M.F. Hansen, K. Pantleon, Marcel A.J. Somers, Proceedings of the 19th IFHTSE Congress, 2011

Work was planned and the results were interpreted by all co-authors. First author performed the experimental activity and wrote the first draft of the manuscript. Comments and suggestions from M.F. Hansen, K. Pantleon and Marcel A.J. Somers were incorporated iteratively in the subsequent versions of the manuscript.

In situ investigation of martensite formation in AISI 52100 bearing steel at sub-zero Celsius temperature

Matteo Villa[1], Mikkel F. Hansen[2], Karen Pantleon[1], Marcel A.J. Somers[1]

Technical University of Denmark, DK 2800 Kongens Lyngby, Denmark
1. Department of Mechanical Engineering;
2. Department of Micro- and Nanotechnology, DTU Nanotech

matv@mek.dtu.dk, mikkel.hansen@nanotech.dtu.dk, kapa@mek.dtu.dk, somers@mek.dtu.dk

Keywords: retained austenite, martensitic transformation, sub-zero Celsius treatment, transformation kinetics, magnetometry

Abstract

Martensite formation in AISI 52100 bearing steel at sub-zero Celsius temperature was investigated with Vibrating Sample Magnetometry. The investigation reports the stabilization of retained austenite in quenched samples during storage at room temperature and reveals the thermally activated nature of the martensitic transformation.
The kinetics of the transformation is interpreted in terms of a-thermal nucleation and thermally activated growth of lenticular martensite.

Introduction

The literature reports beneficial effects of sub-zero Celsius treatments on the mechanical properties of high carbon steel products such as tools, dies and bearings. A complete list of observations and interpretations is reviewed in [1−5].

The transformation of retained austenite into martensite is among the metallurgical reasons for the beneficial effects of sub-zero Celsius treating. High carbon steels may present a partially austenitic, partially martensitic structure upon austenitization and quenching to room temperature. Additional sub-zero Celsius treatment promotes a reduction of the content of retained austenite due to an enhanced driving force for martensite formation.

Retained austenite is generally unwanted in tools, dies and bearings, since its presence reduces the homogeneity of the hardness and, owing to a potential stress- or strain induced transformation of austenite into martensite, the dimensional stability of products in an application. Sub-zero Celsius martensite formation is suggested to modify the tempering response of high carbon steels [6] and has a particularly beneficial effect on the wear performance.

Martensite formation is generally considered to proceed *a-thermally*, i.e., independent on time, implying that the degree of martensite formed is only determined by lowest temperature reached during cooling and develops instantaneously. However, at sub-zero Celsius temperature *thermally activated* martensite formation is a general feature observed in iron-based alloys [7−8]. For AISI 52100 bearing steel, thermally activated martensite formation was previously reported in [6,9−12].

So far, the mechanism behind thermal activation of the martensite formation is unrevealed. Traditionally, thermal activation is interpreted as thermally activated nucleation of martensite [7,13], presuming

instantaneous growth of the developing nuclei to their final size. Recently, the potential role of thermally activated growth was recognized [6,11].

Martensite formation at sub-zero Celsius temperature in carbon steels also depends on the storage time at room temperature before sub-zero treatment. On storage retained austenite is stabilized [14] and martensite formation is (partially) suppressed on subsequent cooling.

The purpose of the present investigation is to study thermally activated martensite formation and achieve insight in the mechanism associated with the stabilization of retained austenite.

Methods

Material and treatments

The alloy investigated is a commercial 100Cr6 steel extruded to a 10mm rod with the composition given in Table 1. Samples were 0.2mm thick disks, 3mm in diameter.

Table 1: Chemical composition (in wt-%) of AISI 52100 as determined by Glow Discharge Optical Emission Spectrometry (GDOES)

Fe	C	Cr	Ni	Mn	Si	Mo	Cu
Bal.	0.96 ±0.02	1.60 ±0.05	0.10 ±0.01	0.28 ±0.04	0.13 ±0.04	0.07 ±0.01	0.15 ±0.01

Austenitization was performed at 1353 K for 60s, followed by quenching in oil at 413 K; the material was kept in the oil bath (martempered) for 20 s and air cooled before storing at room temperature. Protection from oxidation during austenitization was ensured through embedding the samples in 4 layers of 30 µm thick foils of stainless steel Fe-18%Cr-12%Ni-2%Mo. Different sets of samples, S1 to S6, were prepared in independent austenitization batches.

Samples in set 1 were exposed to storage times at room temperature varying from 3 h to 1500 h (10 ks to 3.6 Ms) before the samples were cooled to 123 K at a constant rate (isochronally) of 1.5 K/min.

Samples in sets S2- S6 were stored at room temperature for a minimum of 600 hours (2 Ms), before sub-zero treatment. Samples S2 were isochronally cooled to 123 K applying cooling rates ranging from 0.015 K/min to 40 K/min.

Samples S3 were cooled isochronically applying cooling rates ranging from 0.15 K/min to 75 K/min and subsequently held at 123 K for 16 hours (58ks).

Sample sets S4 and S5 were quenched to 123 K in a nitrogen flow within 30 s. Thereafter, set S4 was isochronally (re)heated to room temperature at heating rates varying from 0.05K/min and 50K/min; set S5 was held at 123 K for 16 hours (58 ks) before (re)heating at 15K/min to room temperature.

Set S6 was quenched to 93 K in nitrogen flow within 35s. Thereafter, the samples were isochronally (re)heated to room temperature applying heating rates ranging from 0.05K/min to 50K/min.

Vibrating Sample Magnetometry, VSM

The samples were subjected to different sub-zero Celsius thermal cycles in a Lake Shore Cryotronics 7407 Vibrating Sample Magnetometer (VSM) equipped with a cryostat. Magnetometry was applied to follow the martensitic transformation in situ. A magnetic field of 1 Tesla was applied to bring the sample to saturation. The temperature was measured in the cryostat close to the sample.

Details on the experimental method and the procedure applied for the quantification of the fractions of austenite and martensite are reported in [11]. As the reference state for the quantification of the fraction transformed the material prior to the sub-zero treatment was taken. In this condition, the sample is dual phase containing lenticular martensite and 29.6% retained austenite as determined with (synchrotron) transmission X-Ray Diffraction; a negligible fraction of primary carbides is also present [6].

The baseline to correct for temperature dependence of the signal was measured using a reference sample cooled 1.5 K/min.

Results and interpretation

Thermal stabilization of austenite, set S1

The formation of martensite during isochronal sub-zero Celsius cooling at 1.5 K/min is reported after storage for various times is shown in Fig.1. Data is presented as the transformation rate $\frac{\Delta f_{\alpha'}}{\Delta T}$ and the fraction of retained austenite f_γ versus absolute temperature T; the inset shows the actual transformation curves.

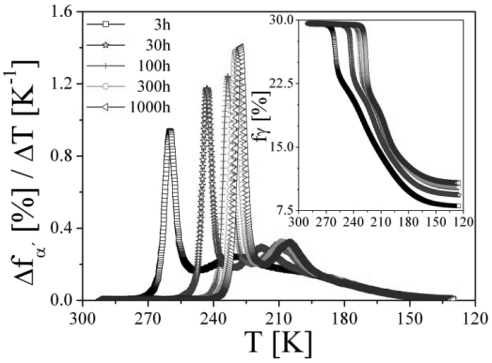

Figure 1. Set S1: transformation rate $\frac{\Delta f_{\alpha'}}{\Delta T}$ as a function of initial storage time at room temperature versus temperature T. Differentiation was done on 4K temperature interval. Inset: fraction of retained austenite f_γ versus temperature T.

As Fig.1 shows austenite is stabilized during storage and a certain undercooling below room temperature is required to continue the transformation. The undercooling necessary for the regaining martensite formation is the larger the longer the storage times.

This austenite stabilization phenomenon is particularly relevant in the first 100 h. The time scale of the stabilization appears compatible with room temperature relaxation of the tetragonal unit cell of previously formed martensite. This relaxation is promoted by the diffusion of carbon atoms to lattice defects [15]. The nature of the stabilization is consequently thermally activated (see [13]).

From the inset in Fig.1 it is observed that the total reduction of retained austenite content during sub-zero Celsius treatment is larger for shorter storage times.

Clearly, the transformation rate in Fig.1 shows two distinct peaks. The peaks appear sharper and closer to each other for the longer storage times at room temperature.

The multi-peak transformation process is defined as abnormal martensite formation, following [11]. In [11], abnormal martensite formation was explained assuming that the kinetics of the transformation as described in terms of a-thermal nucleation and thermally activated growth of lenticular martensite and taking into account the austenite-stabilizing effect of the compressive transformation strain, evoked by the volume expansion on transformation of austenite into martensite.

Transformation during isochronal cooling to 123 K and subsequent isothermal holding, sets S2 and S3

For sets S2 and S3 a minimum storage time of 600 h (2 Ms) was applied to introduce a comparable stabilization of retained austenite among the different samples.

Fig.2 reports martensite formation as a function of cooling rate.

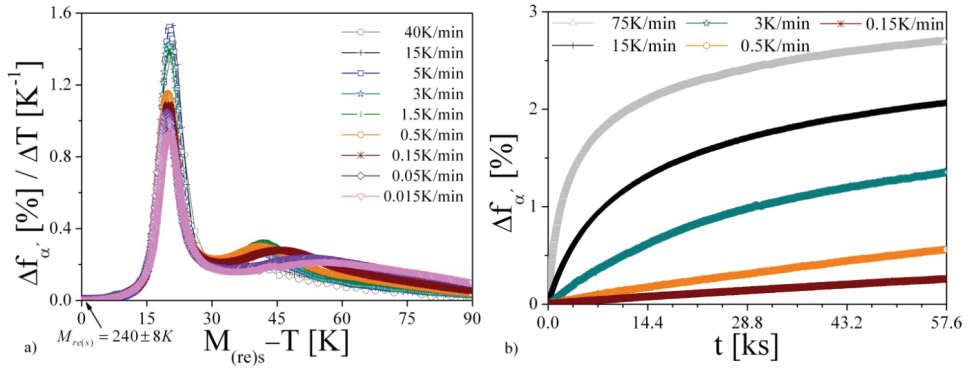

Figure 2. a) Set S2: transformation rate $\frac{\Delta f_{\alpha'}}{\Delta T}$ as a function of cooling rate versus temperature T. Differentiation was done on data averaged over a 4K temperature interval. b) Set S3: isothermal martensite formation at 123 K: $\Delta f_{\alpha'}$ versus time t after isochronal cooling at the indicated rates.

In Fig. 2, isochronal data are plotted in terms of transformation rate, on a logarithmic scale, versus undercooling below the martensite (re)start temperature $M_{(re)s}$=240±8 K. Scattering of $M_{(re)s}$ is appointed to: (i) differences in the stabilization of retained austenite; (ii) experimental error; (iii) a possible effect of the cooling rate on $M_{(re)s}$. The experimental method does not allow concluding on the effect of the cooling rate on $M_{(re)s}$.

The data in Fig.2a show that the martensite formation depends on the undercooling below $M_{(re)s}$ and on the cooling rate. This observation suggests that martensite formation is not a-thermal, but rather thermally activated.

In Fig.2, abnormal behavior is reported (cf. Fig.1). A first transformation peak is observed at about 20 K undercooling independently on the cooling rate; the maximum transformation rate reflected by the first peak appears higher for faster cooling. A second transformation rate maximum is smaller and is closer to $M_{(re)s}$ for faster cooling. The second peak was not observed for the highest cooling rates, i.e. 15 K/min and 40K/min.

Fig.2b shows that martensite formation continues on interrupting the cooling and holding the sample isothermally at 123 K. Evidently, the extent of isothermal transformation depends on the cooling rate applied to reach 123 K and is the larger the faster the cooling rate. Obviously, isothermal martensite formation indicates a thermally activated process.

Thermally activated martensite formation, sets S4, S5 and S6.

For sets S4, S5 and S6, the sub-zero Celsius treatment was started with a quenching step in nitrogen flow. The experimental setup does not allow following in situ martensite formation during quenching. Sets S4 and S5 were quenched to 123 K; set S6 was quenched to 93 K.

The retained austenite content in the sub-zero Celsius quenched material amounts to 15.7±1.0% and 16.0±1.0% for quenching temperatures of 123 K and 93 K, respectively. The content of retained austenite, being 29.6% before sub-zero Celsius treating (Fig 1), is reduced during quenching in nitrogen flow, but it is significantly larger than the content measured in the material subjected to controlled cooling at 1.5 K/min to 123 K (10.5±0.2%, Fig 1). Consequently, the results clearly show that the transformation is (partially) suppressed by the fast cooling in nitrogen flow and that the martensite content is not merely determined by the lowest temperature reached during cooling. Therefore, the observation that the transformation is (partially) suppressed upon fast cooling, or, equivalently that austenite is stabilized during fast cooling, indicates that martensite formation requires thermal activation. On the other hand, the observations do not exclude the presence of an a-thermal component in the transformation process.

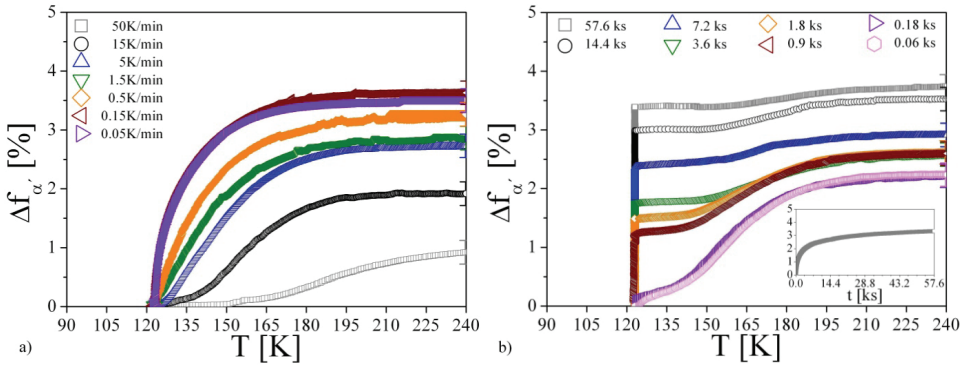

Figure 3. Martensite formation $\Delta f_{\alpha'}$ versus temperature T and time t. a) S4: after quenching to 123 K, as a function of heating rate. b) S5: after quenching to 123 K, as a function of time of isothermal holding at 123K for fixed heating rate of 15K/min. Inset: reports isothermal martensite formation in the sample held for 57.6ks.

In Fig.3 the in situ investigation that followed the quenching step to 123 K (sets S4 and S5) is given. Martensite formation occurs during isochronal (re)heating from 123 K (Figs. 3a and 3b) as well as during isothermal holding (Fig.3b). The development of martensite from austenite during heating is clearly irreconcilable with the classical interpretation of martensite formation as a-thermal and (again) indicates a thermally activated process (either nucleation or growth).

Summarizing, the following observations support thermal activation: (i) time dependent martensite formation on cooling; (ii) suppression of the transformation upon quenching to sub-zero Celsius temperatures; (iii) isothermal transformation; (iv) formation of martensite during heating.

Interestingly, in Fig.3 the possibility to suppress martensite formation upon fast (re)heating is reported. As a matter of fact, if (re)heating is sufficiently slow (<0.5 K/min), the fraction of martensite formed on (re)heating is almost independent on the heating rate and is about 3.6±0.2%. On the other hand, a progressively reduced fraction of martensite forms when the heating rate is increased to 1.5 K/min, 5 K/min, 15 K/min and 50 K/min (Fig. 3a). Similarly, about 3.6±0.2% is the total fraction transformed upon a sufficiently long (>2 hours) isothermal holding at 123 K followed by (re)heating with 15 K/min (Fig. 3b). The total fraction transformed is reduced upon shorter isothermal treatment.

In situ investigation following the quenching step to 93 K is reported in Fig.4a. Data for heating rates in the range 0.05 K/min to 1.5 K/min were selected for determination of the activation energy of the rate determining step(s) for martensite formation during heating [16].

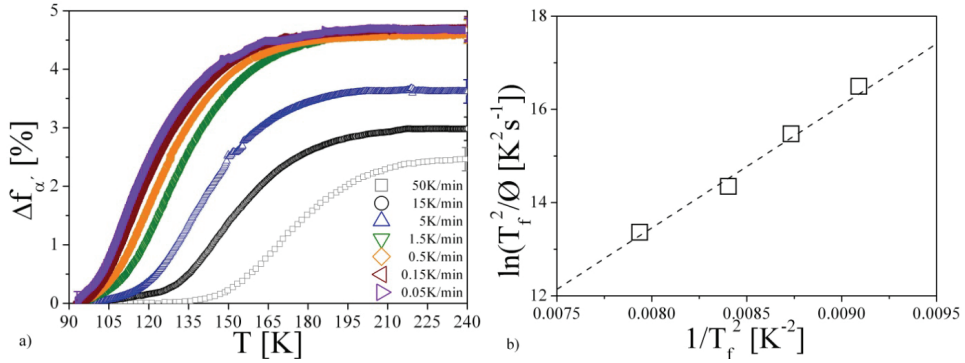

Figure 4. a) Martensite formation versus temperature during isochronal (re)heating; data are collected after quench to 93 K and as a function of the heating rate. b) Plot to obtain the activation energy for the transformation according to the method in [16].

Data in Fig.4 are consistent with data in Fig.3. The martensite formation reaches a saturation level for a sufficiently slow heating rate (<5 K/min), but is reduced for heating rates larger than 1.5 K/min. The maximum fraction transformed upon (re)heating is 4.8±0.2%.

Summarizing, the following observations are reported in Fig.3 and Fig.4 with respect to martensite formation on heating from a sub-zero temperature: (i) partial suppression of martensite formation is possible; (ii) martensite formation is limited to a maximum amount; (iii) the maximum amount appears larger for lower quenching temperatures (cf. fig.3a and 4a).

The activation energy determined for thermally activated martensite formation is 22 kJ/mol. This value is consistent with data reviewed in [7] and may indicate thermally activated dislocation movement as the rate limiting mechanism for the martensitic transformation.

Kinetics of thermally activated martensite formation

n [11], the kinetics of martensite formation is interpreted in terms of a-thermal nucleation followed by thermally activated growth of plate nuclei into lenticular martensite. Moreover, it is assumed that the driving force at $M_{(re)s}$ is the minimum value necessary to form martensite.

As a consequence of these assumptions: (i) nucleation is possible only on cooling; (ii) growth is allowed both during cooling and during (re)heating; (iii) the transformation is never allowed at temperatures

above $M_{(re)s}$. This description is consistent with the data in Figs.2b, 3 and 4. During sub-zero Celsius cooling, a certain number of nuclei forms; the number of formed nuclei depends on the maximum undercooling below $M_{(re)s}$ reached during the thermal cycle and is larger for larger undercooling. Upon cooling, growth is the more suppressed the lower the temperature; hence, suppression is more pronounced for faster cooling. The suppressed transformation reconvenes on isothermal holding or (re)heating, provided enough time is spent at a temperature below $M_{(re)s}$. No transformation can occur at temperatures higher than $M_{(re)s}$.

For the data reported in Fig. 2, the isothermal martensite formation is more pronounced for increased cooling rates, since faster cooling suppresses a larger part of the transformation.

For Figs. 3 and 4, the minimum content of retained austenite in the material is fixed by the quenching temperature (the number of nuclei). The suppressed part of the transformation is defined by the cooling rate, which is also determined by the quenching temperature. Consequently, the quenching temperature fixes the maximum fraction of martensite that can form during isothermal holding and (re)heating. The maximum value is reached only if enough time is spent at temperatures below $M_{(re)s}$ during either a long isothermal holding or a slow isochronal (re)heating. A fast (re)heating hinders growth and the completion of the transformation process.

In connection with the above interpretation, thermally activated martensite formation is controlled by either the movement of dislocation that leads to plastic accommodation of the transformation strain arising upon growth into lenticular morphology, or a not conservative movement of the martensite to austenite interface during growth.

Conclusions

During sub-zero Celsius treatment, a reduction of the content of retained austenite is observed; this reduction is the consequence of a continuation of martensite formation during the thermal cycle at sub-zero Celsius temperature.

After austenitization and standard quenching, retained austenite is stabilized upon room temperature storage. A sub-zero Celsius treatment performed directly after quenching is more effective in reducing the content of retained austenite in the material.

Martensite formation in AISI 52100 at sub-zero Celsius temperature is thermally activated. Martensite can form on cooling, isothermal holding and (re)heating. Martensite formation can be (partially) suppressed upon fast cooling and fast (re)heating.

The kinetics of the transformation is described in terms of a-thermal nucleation and thermally activated growth of lenticular martensite in agreement with previous studies. Nucleation can occur during cooling; growth is allowed at temperatures below the martensite (re)start temperature both on cooling, on isothermal holding and on (re)heating.

The activation energy for thermally activated martensite formation was determined from heating at various heating rates starting at 93 K, and amounts to 22 kJ/mol. This value is compatible with thermally activated dislocation movement.

References

[1] S.S. Gill, H. Singh, R. Singh, J. Singh, Int. J. Adv. Manuf. Technol., 48 (2010) 175-192
[2] S.S. Gill, J. Singh, R. Singh, H. Singh, Int. J. Adv. Manuf. Technol., 54 (2011) 59-82
[3] W. Reitz, J. Pendray, Mater. Manuf. Processes, 16:6 (2001) 829-840
[4] D. N. Collins, Heat treatment of Metals, 3 (1997) 71

[5] D. Das, A.K. Dutta, K.K. Ray, Mat. Sci. Eng., A 527 (2010) 2182-2193
[6] M. Villa, K. Pantleon, M.A.J. Somers, "*Evolution of compressive strains in retained austenite during sub-zero martensite formation and tempering*", submitted for publication
[7] N.N. Thadhani, M.A. Meyers, Progress in Mater. Sci., 30 (1986) 1-37
[8] J.C. Zhao, M.R. Notis, Mat. Sci. Eng., R 15 (1995) 135-208
[9] A. Stojko, M.F. Hansen, J. Slycke, M.A.J. Somers, J. of ASTM Int., 8:4 (2011) 1-9
[10] M. Villa, K. Pantleon and Marcel A.J. Somers, Scripta Mater. 67 (2012) 621-624
[11] M. Villa, K. Pantleon, M.A.J. Somers, "*Abnormal martensite formation during sub-zero treatment of ball bearing steel*", submitted for publication
[12] T.Y. Hsu, C. Yexin, C. Weiye, Metall. Trans., A 18 (1987) 1389-1394
[13] T. Kakeshita, K. Kuroiwa, K. Shimizu, T. Ikeda, A. Yamagishi, M. Date, Mater. Trans. JIM, 34 (1993) 423-428
[14] O.N. Mohanty, Mater. Sci. Eng., B32 (1995) 267-278
[15] L. Cheng, N.M. van der Pers, A. Bottger, Th.H. de Keijser, E.J. Mittemeijer, Metall. Trans. A 22A (1991) 1957–1967
[16] E.J. Mittemeijer, J. Mat. Sci., 27 (1992) 3977-3987

APPENDIX G

Evolution of compressive strains in retained austenite during sub-zero Celsius martensite formation and tempering

PUBLISHED

M. Villa, K. Pantleon, M. A.J. Somers, Acta Mater. 65, (2014) 383-392

Work was planned and the results were interpreted by all co-authors. First author performed the experimental activity and wrote the first draft of the manuscript. Comments and suggestions from K. Pantleon and Marcel A.J. Somers were incorporated iteratively in the subsequent versions of the manuscript.

Available online at www.sciencedirect.com

ScienceDirect

Acta Materialia 65 (2014) 383–392

Acta MATERIALIA

www.elsevier.com/locate/actamat

Evolution of compressive strains in retained austenite during sub-zero Celsius martensite formation and tempering

Matteo Villa *, Karen Pantleon, Marcel A.J. Somers

Technical University of Denmark, Department of Mechanical Engineering, DK 2800 Kongens Lyngby, Denmark

Received 24 October 2013; accepted 1 November 2013
Available online 29 November 2013

Abstract

The development of martensite during sub-zero Celsius treatment of a 1 wt.% C, 1.6 wt.% Cr steel was investigated by in situ and ex situ (synchrotron) X-ray diffraction at the synchrotron facility HZB-BESSY II in order: (i) to quantitatively assess the fractions of retained austenite and martensite; (ii) to measure the evolution of the lattice strain in retained austenite; and (iii) to identify the different stages of tempering. This work shows for the first time that the compressive strains built up in austenite upon martensite formation during sub-zero Celsius treatment are retained after tempering. Furthermore, it is demonstrated that sub-zero Celsius treatment after tempering leads to compressive strain in austenite. Finally, it is reported that no compressive strain builds up in austenite when the martensite formation occurs below a certain critical temperature.

Keywords: Steel; (Synchrotron) X-Ray Diffraction; Retained austenite; Sub-zero Celsius treatment

1. Introduction

Although the basis for understanding the martensitic transformation was established many decades ago [1–4], certain aspects, such as the generation of compressive stress in austenite due to martensite formation at sub-zero Celsius temperatures, were observed [5–7] and recognized only recently [8].

A hydrostatic compressive state of stress stabilizes austenite with respect to its transformation to martensite [9]. Consequently, this characteristic of the transformation indicates the possibility that sub-zero Celsius treatments can be used to reduce the risk of mechanically (i.e. stress and/or strain) induced martensite formation during the working life of steel components.

Generally, in its as-formed state, martensite is a microstructure constituent that is too brittle for practical use [10] and is therefore tempered. On tempering, fine carbide precipitates develop [11,12], which are important for optimizing the mechanical properties of the material. For a sub-zero Celsius treatment to be effective in stabilizing retained austenite, the state of compression in austenite should be maintained after the first stage of tempering, wherein transition carbide precipitations develop. So far the effect of tempering on the state of stress in retained austenite in sub-zero Celsius treated steel has not been investigated. According to Ref. [5], retention of compressive stress in austenite is not possible as the precipitation of carbides is associated with a volume contraction of martensite, which would reduce the pressure on the retained austenite. However, if a relatively low fraction of austenite is present, the austenite will be encapsulated by martensite and, consequently, shrinkage of martensite will impose an additional (hydrostatic) compression on the austenite.

The importance of sub-zero Celsius treatments in improving the performance of high-carbon steels with respect to dimensional stability [13,14], hardness [15–17], wear [17–22] and fatigue [23,24] is well documented, but the mechanisms responsible for these performance

* Corresponding author.
E-mail addresses: matv@mek.dtu.dk, matteo_villa_@hotmail.com (M. Villa).

1359-6454/$36.00 © 2013 Acta Materialia Inc. Published by Elsevier Ltd. All rights reserved.
http://dx.doi.org/10.1016/j.actamat.2013.11.007

improvements are so far largely unknown. As a consequence of this lack of understanding, the scattered data reported in the literature [16] on the improved performance of steel products remains largely unexplained.

The literature is in agreement about two main causes for the improved performance [25]: (i) a reduction of the retained austenite content during sub-zero Celsius treatment; (ii) the development of finer and more numerous transition carbides upon tempering after prolonged holding at a temperature below 195 K, i.e. the sublimation temperature of solid carbon dioxide.

In particular, the sub-zero Celsius austenite-to-martensite transformation was indicated to be the mechanism responsible for both effects [26], and no improvement in the performance of steel products was reported in the absence of continued martensite formation [27]. Accordingly, treatments that stabilize austenite prior to the sub-zero Celsius treatment, such as prolonged storage at room temperature, annealing or tempering [28], should be avoided in order to maximize the effect of sub-zero Celsius treatment [12,17,19,29,30]. On the other hand, annealing prior to sub-zero Celsius treatment can reduce the tendency for microcrack formation in the material during cooling [14,31]. Moreover, austenite stabilization caused by tempering prior to sub-zero Celsius treatment could, in principle, be overcome by a larger undercooling [19].

Presuming that martensite forms athermally, a larger undercooling is equivalent to a larger driving force for martensite formation and, thus, would provide more martensite. Nevertheless, sub-zero Celsius treatment is normally performed at a temperature above the boiling point of liquid nitrogen (i.e. 77 K), and further cooling in boiling helium (i.e. 4 K) was reported not to improve the performance of steel products [32,33].

Finally, sub-zero Celsius treatment has been reported to modify the tempering response, not only by enhancing the formation of precipitation products [21,31,34–39], but also by facilitating the decomposition of retained austenite [14,37] and causing a tendency for overtempering [40].

For a complete list of observations regarding the effects of sub-zero Celsius treatments on high-carbon steels, the reader is referred to Refs. [16,25,41].

In the present work, the effects of the sub-zero Celsius martensite formation on the tempering behavior of an AISI 52100 steel is investigated. The tempering of AISI 52100 steel is discussed following Refs. [42–44], where it was shown to follow the same tempering stages as for unalloyed high-carbon steels [45–47].

2. Experimental

2.1. Material and treatments

2.1.1. Material

The alloy investigated was a commercial AISI 52100 (100Cr6) steel extruded to a 10 mm rod with the composition given in Table 1. This material was chosen because of its high reproducibility and its ability to retain austenite at room temperature after quenching.

The sample geometry for X-ray diffraction (XRD) experiments was 10 mm diameter × 0.2 mm thick disks. In order to record the stages of tempering and associated volume changes, a 10 mm high hollow cylinder with outer and inner diameters of 4.0 and 3.6 mm, respectively, was investigated by dilatometry. Note that the wall thickness of the cylinder is 0.2 mm, i.e. equal to the thickness of the disks.

2.1.2. Austenitization

Samples were austenitized at 1353 K for 60 s, quenched in oil to 413 K and kept in oil for 20 s, after which they were air cooled before storing at room temperature for about 5 Ms. Oxidation during heat treatment was prevented through embedding the samples in four layers of 30 μm thick AISI 316 foil.

2.1.3. Sub-zero Celsius treatment and tempering

One disk in the as-quenched condition, designated D1, was directly heated to the tempering temperature 650 K at 1.5 K min^{-1}. Another disk, D2, was cooled from room temperature to 133 K at 5 K min^{-1} and thereafter heated to 650 K at 1.5 K min^{-1}. Disk D3 was sub-zero Celsius cooled to 133 K at 5 K min^{-1} and thereafter heated at 1.5 K min^{-1} to 300 K only. Disk D4 was first heated to 453 K at 1.5 K min^{-1}, thereafter cooled to 77 K at 5 K min^{-1} and finally heated to 300 K at 1.5 K min^{-1}. Disk D5 was first cooled at 5 K min^{-1} to 133 K, kept at this temperature for 7 h, heated to 453 K at 1.5 K min^{-1} and eventually air cooled to 300 K. A reference sample, designated D0, was maintained in the as-quenched condition. All the thermal cycles are illustrated in Fig. 1.

The hollow cylinder was investigated in a Bähr DIL 805A/D dilatometer. The length change of the sample was measured during isochronal heating at 1.5 K min^{-1} to 650 K for direct comparison with samples D1 and D4.

2.2. Synchrotron X-ray diffraction

Synchrotron XRD was performed at the synchrotron facility HZB-BESSY II at the experimental stations MagS for angular XRD in reflection [48] and EDDI [49] for energy-dispersive XRD in transmission. The measurement conditions are collected in Table 2.

2.2.1. In situ investigation

The in situ investigation was performed at the MagS station maintaining a Bragg–Brentano geometry in reflection mode using a wavelength of 0.1 nm.

All data was obtained based on the 220_γ reflection of austenite and the $200/002_\alpha$ doublet of martensite.

The method applied for quantification of the phase fractions was reported in Ref. [50], and is based on a comparison of the experimentally measured intensities with those predicted for a powder sample [51].

Table 1
Chemical composition (in wt.%) of AISI 52100 as determined by glow discharge optical emission spectrometry.

Fe	C	Cr	Ni	Mn	Si	Mo	Cu
Bal.	0.96 ± 0.02	1.60 ± 0.05	0.10 ± 0.01	0.28 ± 0.04	0.13 ± 0.04	± 0.01	0.15 ± 0.01

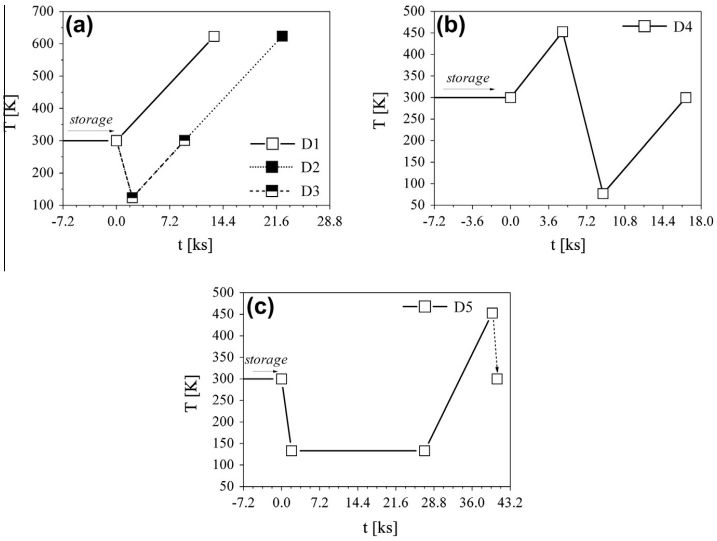

Fig. 1. Thermal cycles: (a) samples D1, D2 and D3; (b) sample D4; (c) sample D5.

Table 2
Measurement conditions for synchrotron X-ray diffraction.

Type of investigation	Sample	λ [nm]	2θ	Step size [2θ]	Time per step [s]
In situ cooling 5 K min^{-1} (MagS)	D1, D2, D4, D5	0.1	37.5°–48°	0.05°	0.25
In situ heating 1.5 K min^{-1} (MagS)	D1, D2, D4, D5		25°–62°		
		Energy range [keV]		Step size [keV]	Acquisition time [s]
Ex situ (EDDI)	D0, D3, D4, D5	0–120	20°	0.08	600

The lattice strain in austenite, ε_γ, was determined from the lattice parameter of austenite in the direction parallel to the scattering vector, i.e. normal to the sample surface, and is expressed as:

$$\varepsilon_\gamma = \frac{a_\gamma^m(T) - a_\gamma^{\mathrm{ref}}(T)}{a_\gamma^{\mathrm{ref}}(T)}, \tag{1}$$

where $a_\gamma^m(T)$ and $a_\gamma^{\mathrm{ref}}(T)$ are the measured and reference lattice spacing of austenite and T is the temperature under consideration. The as-quenched sample stored for 5 Ms. at room temperature was taken as the condition for zero strain. Accordingly, in Eq. (1) $a_\gamma^{\mathrm{ref}}(T)$ is obtained from the $a_\gamma^{\mathrm{ref}}(T)$ (300 K) assuming a linear expansion coefficient for unconstrained austenite equal to $21.3 \times 10^{-6}\,\mathrm{K}^{-1}$ [52]. Hence, all lattice strains given are corrected for unconstrained lattice expansion/contraction.

As was shown in Ref. [8], lattice strains in austenite in AISI 52100 can be interpreted as the result of a mainly hydrostatic state of stress in austenite. The interpretations given in the present work are therefore in terms of a state of hydrostatic stress, as was verified and validated for samples D0 and D3 applying the $\sin^2\psi$ method [53] at the EDDI station.

2.2.2. Ex situ investigation at room temperature

The ex situ investigation was performed at the EDDI station with energy-dispersive XRD in transmission geometry. In energy-dispersive XRD, white radiation is used, the scattering angle is kept constant and the lattice spacing, d(hkl), follows from the position of the reflections in the energy scale [54]:

$$d(hkl) = \frac{hc}{2\sin\theta}\frac{1}{E(hkl)}. \tag{2}$$

Quantitative phase analysis was based on the following relationships:

$$R = m(hkl) \cdot |F_0(hkl)|^2 \cdot e^{(-2M)} \cdot n^{-2} \cdot \mu(E)^{-1} \cdot \left(\frac{hc}{E}\right)^3, \quad (3)$$

$$f_\gamma = \frac{1}{1 + \frac{R_\gamma}{R_{\alpha'}} \cdot \frac{I_{\alpha'}}{I_\gamma}}, \quad (4)$$

$$f_\gamma = 1 - f_{\alpha'}, \quad (5)$$

where R is the theoretical integrated intensity, $m(hkl)$ is the multiplicity factor, $|F_0(hkl)|^2$ is the structure factor, exp^{-2M} is the Debye–Waller factor, n is the number of Fe atoms per unit cell, $\mu(E)^{-1}$ is the energy-dependent absorption factor of pure Fe, h is Planck's constant, c is the speed of light and f is the molar fraction. The subscripts γ and α' refer to austenite and martensite, respectively.

To take the possible presence of crystallographic texture into account, the phase fraction was obtained comparing each reflection of austenite with all the reflections of martensite and averaging the results. The quantification of the molar fraction of retained austenite was performed considering the 220_γ, 311_γ and 420_γ reflections of austenite and the $200/002_\alpha$ and $211/112_{\alpha'}$ doublets of martensite.

3. Results and interpretation

3.1. As-quenched condition: sample D0

The material is dual phase and contains martensite and retained austenite. The presence of a negligible small amount of undissolved primary carbides was detected by electron microscopy. Table 3 reports the results of the ex situ XRD. The content of retained austenite in the as-quenched and stored condition is 29.6%, as measured ex situ by XRD on sample D0 (Table 3).

3.2. Direct tempering vs. fast sub-zero Celsius treatment and tempering: samples D1–D3

The results of the in situ investigation in samples D1 and D2 are reported in Fig. 2. The content of retained austenite after the sub-zero Celsius treatment (sample D3) is reported in Table 3. Dilatometry results are shown in Fig. 3.

3.2.1. Phase transformations during tempering

The initial heating step for sample D1 represents the behavior of the as-quenched material during direct tempering and is identical to the thermal cycle investigated with dilatometry.

During the tempering of sample D1 (Fig. 2a) martensite is observed to lose its tetragonality in the temperature range 360–420 K. Dilatometry indicates that during isochronal heating, the linear expansion rate is about $14.5 \times 10^{-6}K^{-1}$ (Fig. 3). According to Ref. [52], a linear expansion coefficient of this magnitude is consistent with the presence of a minor amount of retained austenite in the material. From 360 K, coinciding with the onset of the loss of martensite's tetragonality in sample D1 (Fig. 2a), thermal expansion of the sample (Fig. 3) is counteracted by a volume reduction, which is ascribed to the precipitation of transition carbides [46]. The development of transition carbides is most pronounced at about 400 K,[1] and is completed at about 460 K. Thereafter, the second stage of tempering occurs, i.e. decomposition of retained austenite, which is associated with a volume expansion in the temperature interval 490–560 K and is counteracted by a volume decrease as a consequence of cementite formation [47,48].

Table 3
Ex situ XRD investigation: content of retained austenite, lattice parameters and integral breadth for the 220_γ and 311_γ reflections in samples D0, D3, D4 and D5.

Sample	Retained austenite [%]	Lattice parameter [nm]	Integral breadth [keV]	
			220_γ	311_γ
D0	29.6	0.3604	0.371	0.415
D3	9.4	0.3597	0.483	0.517
D4	22.8	0.3601		
D5	8.7	0.3599		

Moreover, from comparing the curves for samples D1 and D2 in Fig. 2a it is observed that the tetragonality in martensite is lost in the temperature interval 360–420 K, irrespective of whether or not a prior sub-zero Celsius treatment is carried out.

After sub-zero Celsius treatment the tetragonality of martensite at 300 K is observed to be higher than for the as-quenched and stored sample (see Fig. 2a for sample D2 before and after sub-zero Celsius treatment). The slight increment in the average tetragonality of martensite is explained by the formation of new martensite during the sub-zero Celsius treatment (Fig. 2b). This newly formed martensite has not experienced relaxation (and associated slight loss of tetragonality) during long-term room-temperature storage as for the initial condition. Consequently, the newly formed martensite leads to a larger (average) tetragonality as compared to the initial condition [47]. Martensite formation during the sub-zero Celsius treatment is also confirmed ex situ on sample D3 (Table 3); this sample experienced the same sub-zero Celsius treatment as sample D2.

The second stage of tempering is confirmed by XRD. In sample D1, austenite disappears in the temperature interval 490–560 K, which is consistent with the volume expansion of the sample observed in Fig. 3. The decomposition of retained austenite is observed to commence at a lower temperature when sub-zero Celsius treatment is applied (cf. sample D2 in Fig. 2b). Attempts to verify this observation by a dilatometry cycle including sub-zero Celsius treatment were unsuccessful due to insufficient stability of the dilatometer during and after sub-zero Celsius treatment.

[1] For a thermally activated phase transformation, the temperature at which the fastest transformation rate occurs depends on the heating rate.

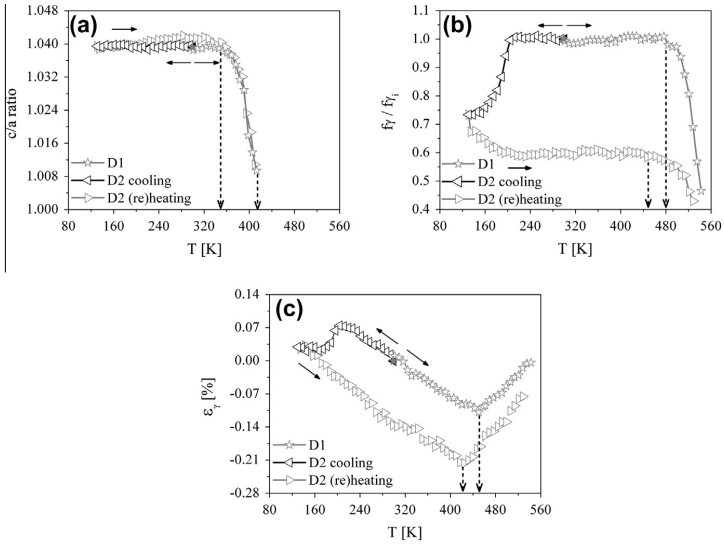

Fig. 2. (a) Tetragonality of martensite (i.e. c/a ratio) vs. temperature T. (b) Molar fraction of retained austenite f_γ normalized to the initial content $f_{\gamma i}$ vs. temperature T. (c) Lattice strain ε_γ for austenite vs. temperature T corrected for expected thermal expansion/contraction; the reference state is represented by the initial condition at 300 K. Starting points are marked as full symbols.

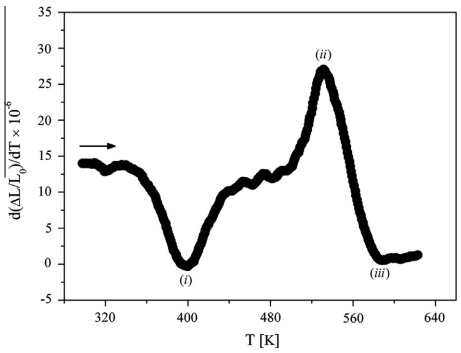

Fig. 3. Relative sample elongation during isochronal heating differentiated with respect to temperature $d(\Delta L/L_0)/dT$ vs. temperature T. Precipitation of secondary carbides and formation of cementite are associated with volume reductions; decomposition of retained austenite induces volume expansion [42,46].

3.2.2. Strain evolution in austenite

The evolution of the lattice strain in austenite during the isochronal heating vs. temperature is reported in Fig. 2c. In sample D1, upon direct heating, constrained thermal expansions of austenite and martensite associated with coherence between the phases introduces a state of compression in austenite, which is the minority phase in the sample. A compensating (additional) state of tension is expected in martensite, albeit with a smaller absolute value than for austenite, because of the higher phase fraction.

An increase in compressive strain due to constrained thermal expansion continues during heating, until a temperature of about 450 K is reached (Fig. 2c). For higher temperatures, the lattice parameter of austenite experiences an expansion that exceeds that due only to thermal effects. The mechanism responsible for this lattice expansion can be of chemical and/or of mechanical origin, implying a carbon enrichment in austenite and/or a gradual relaxation of the hydrostatic state of stress (or a compensating tensile stress).

Van Genderen et al. [55] considered both phenomena to explain a similar observation. Carbon enrichment in austenite resulted from the beginning of the decomposition of retained austenite and yielded the largest effect, while relaxation of compressive stress in austenite during phase transformation was invoked to explain the remaining part of the observed lattice expansion. According to Ref. [55], for a high-carbon steel the precipitation of cementite is kinetically hindered during the decomposition of retained austenite for temperatures below 500 K. Meanwhile ferrite formation, which causes an increase in the average carbon content in austenite, is possible. The increase in lattice parameter of austenite in the temperature range up to 550 K (Fig. 2c) coincides with a faster elongation of the sample (Fig. 3), which can be attributed to the formation of ferrite and cementite. A dominating effect of cementite formation, leading to a deceleration of sample expansion, is for the present case firstly experienced for temperatures higher than 550 K. These observations are consistent with the interpretation in Ref. [55] that supersaturation of austenite with carbon as a consequence of ferrite formation

is the dominating effect at the beginning of the second stage of tempering. Thus, the reduction in compressive strain in austenite is largely composition induced.

Attempts to determine lattice strains in martensite showed that the measured variations in lattice parameter are of the same magnitude as the variation among data for the lattice parameter of the unconstrained phase reported in the literature.

3.2.3. Effect of sub-zero Celsius treatment on strain in austenite

For the sub-zero Celsius treated sample (D2) the reduction in the compressive strain in austenite commences at about 420 K, a temperature well below the 450 K observed for the as-quenched material D1 (Fig. 2c). The reduction in compressive strain is accompanied by a reduction in the content of retained austenite. Consistently, the content of retained austenite also begins to reduce at a lower temperature for the sub-zero Celsius treated sample than for the as-quenched material (Fig. 2b). Evidently, lattice expansion in austenite first occurs after martensite has lost its tetragonality, which is close to completion at 420 K. Hence, lattice expansion in austenite is coupled to the decomposition of austenite and not to the decomposition of martensite. This result demonstrates that the interpretation in Ref. [5], according to which precipitation of carbides in martensite would lead to a relaxation of compressive strain in austenite, is incorrect.

The observation that decomposition of austenite commences at a lower temperature in the sub-zero Celsius treated sample D2 than in sample D1 appears counterintuitive. The higher lattice strain in austenite in D2 as compared to D1 is anticipated to stabilize austenite against the volume expansion that is associated with a transformation of austenite into ferrite and cementite. Following the hypothesis that ferrite is the first phase that nucleates during the decomposition of austenite [55], it is suggested that the reason for retained austenite decomposing at a lower temperature in the sub-zero Celsius treated sample D2 is a consequence of more favorable nucleation sites for ferrite, similar to the enhanced density of defects in austenite due to martensite formation.

A higher density of lattice defects in austenite is consistent with the additional broadening of 220_γ and 311_γ reflections in sample D2 after sub-zero Celsius treatment (cf. Table 3).

3.2.4. Development of strain during sub-zero Celsius treatment

The lattice strain in sample D2 is interpreted in connection with the continuation of the transformation reported in Fig. 2c.

Upon cooling, in the first 70 K where no transformation occurs (Fig. 2b), the coherence between austenite and martensite introduces a state of tension in austenite as a consequence of its larger unconstrained thermal shrinkage as compared to the majority phase, martensite (Fig. 2c).

When the austenite-to-martensite transformation is regained at about 230 K (Fig. 2b), the tension generated in austenite by constrained thermal shrinkage is counteracted by the transformation strain (Fig. 2c), as a result of the volume expansion that accompanies martensite formation. This transformation strain is introduced in the temperature range 230–140 K (Fig. 2c, sample D2 during cooling). At temperatures lower than 140 K the introduced strain is reversible, implying that no transformation strain is introduced in austenite, despite the continued development of martensite. After reheating to room temperature a state of compression remains in austenite.

The observed total compressive strain is a consequence of the volume expansion associated with the austenite-to-martensite transformation, and is therefore the transformation strain [8]. Ex situ XRD transmission measurements (Table 3) confirmed both sub-zero Celsius martensite formation and the build-up of compressive strain in austenite.

3.2.5. Effect of tempering prior to sub-zero Celsius treatment: samples D4 and D5

The effect of different thermal paths on the compressive strain in austenite was further explored with samples D4 and D5. The results of the ex situ XRD investigation are reported in Table 3. The in situ XRD investigations for samples D4 and D5 are collected in Figs. 4 and 5, respectively.

For sample D4, during direct heating to 453 K a continuous increase in the compressive strain in austenite is observed (Fig. 4b). This state of compression is regained on cooling to room temperature, which confirms that the expansion of the austenite lattice as observed in Fig. 2c cannot be a consequence of the precipitation of transition carbides in martensite.

After heating to 453 K, sample D4 was cooled to 77 K and thereafter (re)heated to room temperature. During sub-zero Celsius treatment, austenite appeared stable until about 190 K. Thereafter martensite formation was observed to occur for enhanced undercooling down to 77 K (Fig. 4a). Clearly, martensite also forms upon reheating in the same temperature range at which it developed during cooling. Martensite formation during cooling and during heating induces elastic compression in austenite, as corroborated by XRD transmission measurements (cf. Table 3). The observation that martensite develops on (re)heating cannot be explained by an athermal transformation only and indicates a contribution of thermal activation to the overall transformation.

Interestingly, in spite of a continuation of the transformation, compressive strain in austenite is generated only at temperatures above about 140 K (Fig. 4a,b). This experimental finding indicates that different mechanisms are responsible for the accommodation of the transformation strain at temperatures below and above about 140 K, respectively.

The microstructure of sample D4 at the end of the thermal cycle is shown in Fig. 6. The martensite that developed

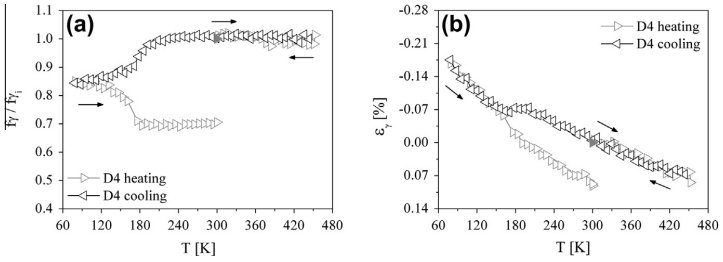

Fig. 4. In situ investigation: sample D4. (a) Fraction of retained austenite f_γ normalized to the initial content $f_{\gamma i}$ vs. temperature T. (b) Lattice strain ε_{33} vs. temperature T determined from the 220γ reflection and corrected for expected thermal expansion/contraction. Starting points are marked as full symbols.

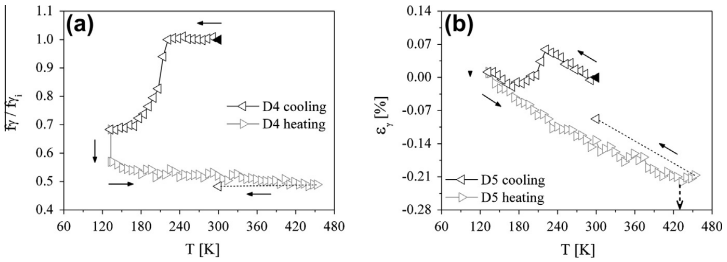

Fig. 5. In situ investigation: Sample D5. (a) Fraction of retained austenite f_γ normalized to the initial content $f_{\gamma i}$ vs. temperature T. (b) Lattice strain ε_γ vs. temperature T determined from the 220γ reflection and corrected for expected thermal expansion/contraction. Starting points are marked as full symbols.

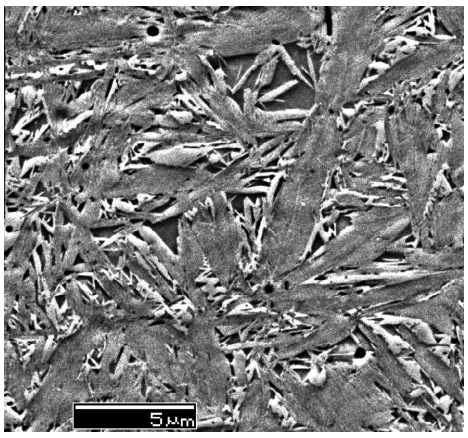

Fig. 6. Microstructure of sample D4 in the final condition. Backscatter electron micrograph; electrolytic etching in Struers A-2 solvent at 30 V for 40 s on a surface area of 5 mm^2: retained austenite regions appear darker and embedded in between the martensitic plates; new martensite is fine and appears lighter than martensite developed prior to sub-zero Celsius treatment.

during the sub-zero Celsius treatment (appearing light in Fig. 6) is relatively fine lenticular martensite as compared to the martensite that was tempered prior to sub-zero Celsius treatment (appearing dark grey in Fig. 6). The aspect ratio of the martensite formed during sub-zero Celsius treatment appears smaller than for the rather thick lenticular form of tempered martensite; even very thin plates are observed.

Sample D5 was sub-zero Celsius treated directly after storage at room temperature. The behavior is comparable with that described for sample D2. During cooling, the transformation (Fig. 5a) contributes to a state of compression in austenite (Fig. 5b). Martensite formation continues during isothermal holding at 133 K (Fig. 5a), but appears not to be associated with additional compression, in agreement with the behavior observed for sample D4 for temperatures below 140 K. The occurrence of martensite formation during isothermal holding is, just like martensite formation during heating, an indication that thermal activation contributes to the overall martensitic transformation.

On reheating to room temperature, compressive transformation strains are retained in austenite (see Fig. 5b and Table 3). A relaxation of compressive strains in austenite appears to be effective from about 420 K (Fig. 5b), in agreement with data reported in Fig. 2c for sample D2.

A direct comparison of samples D4 and D5 shows that a smaller amount of austenite transforms to martensite during sub-zero Celsius cooling after prior tempering, despite the lower sub-zero Celsius temperature reached (see Table 3 and compare Figs. 4a and 5a). Thus, austenite is stabilized by prior tempering. This enhanced stability is particularly evident from the transmission XRD data (Table 3), where the difference in the final content of retained austenite for

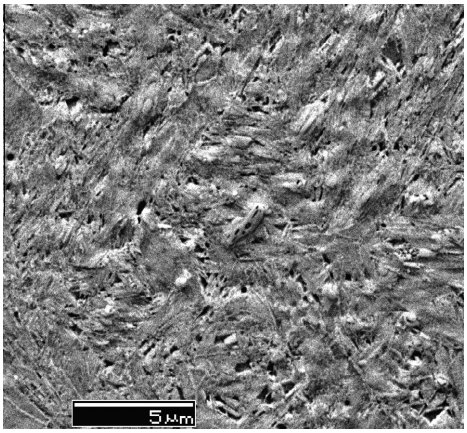

Fig. 7. Microstructure of sample D5 in the final condition. Backscatter electron micrograph; electrolytic etching in Struers A-2 solvent at 30 V for 40 s on a surface area of 5 mm^2: small retained austenite regions appear darker and are embedded in between the martensitic plates. Note that D5 passed the first stage of tempering, while D4 was only heated to room temperature after sub-zero treatment. Nevertheless only negligible thermal decomposition of austenite occurred in D5 (cf. Fig. 5a).

the two samples is significant, such that the directly sub-zero Celsius treated sample (D5) develops more martensite than the pre-tempered sample (D4), despite the larger undercooling for sample D4. The lower content of retained austenite in sample D4 is also readily observed from comparing the microstructures in Figs. 6 and 7.

It is noted that the same result is obtained without the isothermal holding step at 133 K (see Table 3 and compare Figs. 4a and 2b). The lower content of retained austenite in D5 as compared to D4 does not result from the isothermal step for sample D5, but is merely a consequence of prior tempering of sample D4.

4. General discussion

In the literature, a general improvement in the performance of tool steel products by the introduction of a sub-zero Celsius step in their thermal history has been reported. The metallurgical reasons for such improvements are unclear; it is probable that sub-zero Celsius martensite formation is connected with the observed enhancement of mechanical properties. In this paper the martensitic transformation is observed to continue during sub-zero Celsius treatment of a high-carbon steel that contains a relatively large quantity of retained austenite after quenching to room temperature. Martensite forms during cooling, isothermal holding and reheating (Figs. 2b, 4a and 5a). Martensite formation during isothermal holding and on reheating indicates a contribution of thermally activated martensite formation to the overall transformation. Thermally activated martensite formation during heating and isothermal holding at sub-zero Celsius temperature is interpreted as the growth of thin plate martensite that nucleated athermally during cooling into lenticular martensite.

If the as-quenched steel is tempered prior to the sub-zero Celsius treatment, the martensite formation during sub-zero Celsius treatment is less pronounced than in case of sub-zero Celsius treatment directly following storage at room temperature (Table 3).

Martensite formation is accompanied by the introduction of compressive strain in retained austenite, irrespective of whether or not sub-zero Celsius treatment is preceded by tempering. Such compressive transformation strains in austenite build up only when the transformation occurs above about 140 K; below this temperature no transformation strains develop in austenite during martensite formation. Assuming no changes in the chemistry of the phases, compressive strains are the consequence of a state of compressive stress in austenite [8].

A (hydrostatic) compressive state of stress is expected to stabilize austenite, and is retained also after the first stage of tempering (i.e. precipitation of transition carbides) (Figs. 4a and 5a). This new finding suggests that, in addition to a reduction in the content of retained austenite in high-carbon steels, sub-zero Celsius treatments can also be exploited to improve the stability of the remaining austenite regions against transformation. For this purpose, a fast cooling and reheating cycle appears to be sufficient (Fig. 2), while a long isothermal holding at temperatures below 140 K is not effective in building up further compressive stresses in austenite (Fig. 4b).

Fully reversible (thermal) strains are reported during in situ investigation for temperatures below 140 K (Figs. 4b and 5b). This different behavior of austenite during martensite formation is likely to be related to a change in the mechanism of accommodation of the transformation strain at sub-zero Celsius temperature.

It is suggested that below a critical temperature the transformation strain is accommodated in the martensite and not in the retained austenite. This accommodation is suggested to generate additional nucleation sites in martensite for the precipitation of transition carbides during tempering. This interpretation may contribute to understanding the beneficial effect of extended isothermal holding at cryogenic temperature in improving the performance of tool steel products.

Interestingly, while the stability of austenite vs. martensite formation in sub-zero Celsius treated materials is augmented by the build-up of compressive stresses in this phase, its thermal stability against decomposition into ferrite and cementite is reduced by the same treatment (Figs. 2b and 4b). The second stage of tempering (i.e. decomposition of retained austenite) is observed to occur at lower temperatures in sub-zero Celsius treated samples as compared to conventionally quenched samples. This is explained by an increased density of defects in austenite, which favors the decomposition of austenite by easy ferrite nucleation. The last point suggests that tempering after

sub-zero Celsius needs modification and optimization in order to exploit the full potential of sub-zero Celsius treatment.

5. Conclusions

Martensite formation in as-quenched AISI 52100 steel continues during all stages of sub-zero Celsius treatment: cooling, isothermal holding and reheating.

Sub-zero martensite formation is most effective if no tempering is performed prior to the treatment. The development of martensite during isothermal holding and during reheating is interpreted as thermally activated growth of thin plate martensite, which developed athermally during cooling. For transformation temperatures above 140 K compressive transformation strains build up in austenite along the martensite formation. For temperatures below 140 K no transformation strains builds up in austenite. This observation is taken as an indication that martensite accommodates the transformation strain below 140 K, supposedly by internal twinning.

The buildup of compressive strain in retained austenite is the most evident effect of martensite formation during sub-zero Celsius treatment. The compression generated in austenite is retained after the first stage of tempering. Accordingly, sub-zero Celsius treatment could be exploited as an effective method to (mechanically) stabilize retained austenite in steel components against strain-induced martensite formation.

On the other hand, sub-zero Celsius treatment reduces the thermal stability of austenite during tempering. The temperature at which austenite starts to decompose into ferrite and cementite is about 30 K lower than for conventionally quenched material. Consequently, the application of sub-zero Celsius martensite formation necessitates a modified tempering treatment.

Acknowledgements

M. Reich, University of Rostock, is gratefully acknowledged for performing the dilatometry experiment. M.F. Hansen, Technical University of Denmark, is acknowledged for fruitful discussion on sub-zero Celsius martensite formation. Chr. Genzel, M. Klauss, E. Dudzik and R. Feyerherm, Helmholtz Zentrum für Materialien und Energy (HZB), are acknowledged for their support during experiments at the Berlin synchrotron facility HZB-BESSY II. The authors acknowledge the Danish Natural Science Research Council for financial support of part of the work via Danscatt.

References

[1] Bain EC. Am Inst Min Metall Eng – Trans 1924:1299.
[2] Bowles JS, Mackenzie JK. Acta Metall 1954;2:1.
[3] Cech RE, Turnbull D. J Met 1956;8:124–32.
[4] Kulin AS, Cohen M. Am Inst Min Metall Eng – J Met 1950;188:1139–43.
[5] Golovchiner KJa. Phys Metals Metallogr 1974;37:126.
[6] Jershov VM, Oslon NL. Fix Metal 1968;25.
[7] Grindev VN, Trephilov VI. Dokl Akad Nauk SSSR 1957;116:60.
[8] Villa M, Pantleon K, Somers MAJ. Scr Mater 2012;67:621–4.
[9] Patel JR, Cohen M. Acta Metall 1953;1(5):531–8.
[10] Bensely A, Venkatesh S, Mohan Lal D, Nagarajan G, Rajadurai A, Junik K. Mater Sci Eng, A 2008;479:229–35.
[11] Harish S, Bensely A, Mohan Lal D, Rajadurai A, Leneky GB. J Mater Process Technol 2009;209:3351–7.
[12] Vimal AJ, Bensely A, Mohan Lal D, Srinivasan K. Mat Manuf Process 2008;23:369–76.
[13] Senthilkumar D, Rajendran I, Pelizzari M, Siiriainen J. J Mater Process Technol 2011;211:396–401.
[14] Surberg CH, Stratton P, Lingenhöle K. Cryogenics 2008;48:42–7.
[15] Molinari A, Pellizzari M, Gialanella S, Straffellini G, Stiasny KH. J Mater Process Technol 2001;118:350–5.
[16] Das D, Dutta AK, Ray KK. Mater Sci Eng, A 2010;527:2182–93.
[17] Das D, Dutta AK, Ray KK. Wear 2009;266:297–309.
[18] Jaswin MA, Shankar GS, Mohan Lal D. Int J Precision Eng Manuf 2010;11(1):97–105.
[19] Mohal Lal D, Renganarayanan S, Kalanidhi A. Cryogenics 2001;41:149–55.
[20] Bensely A, Prabhakaran A, Mohan Lal D, Nagarajan G. Cryogenics 2006;45:747–54.
[21] Meng F, Tagashira K, Sohma H. Script Metall Mater 1994;31(7):865–8.
[22] Jaswin MA, Mohan Lal D, Rajadurai A. Trib Trans 2011;54:341–50.
[23] Kerscher E, Lang KH. J Phys: Conf Ser 2010;240:01205.
[24] Zhirafar S, Rezeian A, Pugh M. J Mater Process Technol 2007;186:298–303.
[25] Gill SS, Singh J, Singh R, Singh H. Int J Adv Manuf Technol 2011;54:59–82.
[26] Tyshchenko AI, Theisen W, Oppenkowski A, Siebert S, Razumov ON, Skoblik AP, et al. Mater Sci Eng, A 2010;527:7027–39.
[27] Barron RF. Cryogenics 1982;22:409–13.
[28] Mohanty ON. Mater Sci Eng 1995;B32:267–78.
[29] Moore K, Collins DN. Key Eng Mater 1993;86–87:47–54.
[30] Bensely A, Senthilkumar D, Mohan Lal D, Nagarajan G, Rajadurai A. Mater Charact 2007;58:485–91.
[31] Meng F, Tagashira K, Azuma R, Sohma H. ISIJ Int 1994;34:205–10.
[32] Zurecki Z. Air Products and Chemicals, Inc., Pub. No. 330-05-019-GLB; 2005. <http://www.airproducts.com/~/media/Files/PDF/industries/metals-cryogenic-quenching-of-steel-revisited-33005019GLB.pdf>.
[33] Stratton P, Graf M. Cryogenics 2009;49:346–9.
[34] Li S, Deng L, Wu X, Min Y, Wang H. Cryogenics 2010;50:754–8.
[35] Li S, Deng L, Wu X, Wang H, Min Y, Min N. Mater Sci Eng, A 2010;527:7950–4.
[36] Huang JY, Zhu YT, Liao XZ, Beyerlein IJ, Bourke MA, Mitchell TE. Mater Sci Eng, A 2003;339:241–4.
[37] Wierszylloski I, Samolczyk J, Wieczorek S, Andrzejewska E, Marcinkowska A. Def Diff Forum 2008;273–276:731–9.
[38] Das D, Dutta AK, Ray KK. Phil Mag 2009;89(1):55–76.
[39] Das D, Dutta AK, Ray KK. Wear 2009;267:1371–80.
[40] Pellizzari M, Molinari A. Proc. international tooling conference, Turin; 2006. p. 657–9.
[41] Gill SS, Singh H, Singh R, Singh J. Int J Adv Manuf Technol 2010;48:175–92.
[42] Morra PV, Bottger AJ, Mittemeijer EJ. J Thermal Anal Calorimetry 2001;64:905–14.
[43] Perez M, Sidoroff C, Vincent A, Esnouf C. Acta Mater 2009;57:3170–81.
[44] Barrow AT, Kang J-H, Rivera-Diaz-del-Castillo PEJ. Acta Mater 2012;60:2805–10.
[45] Speich GR, Taylor KA. Tempering of ferrous martensites. In: Olson GB, Owen WS, editors. Martensite. Materials Park, OH: ASM International; 1992.

[46] Cheng L, Brakman CM, Korevaar BM, Mittemeijer EJ. Metall Trans A 1988;19A:2415–26.
[47] Cheng L, van der Pers NM, Bottger A, de Keijser ThH, Mittemeijer EJ. Metall Trans A 1991;22A:1957–67.
[48] Dudzik E, Feyerherm R, Diete W, Signorato R, Zilkens C. J Synchr Rad 2006;13:421–5.
[49] Genzel Ch, Denks IA, Gibmeier J, Klaus M, Wagener G. Nucl Instrum Meth Phys Res A 2007;578:23–33.
[50] Villa M, Pantleon K, Somers MAJ. J All Comp; 2013 [in press]. http://dx.doi.org/10.1016/j.jallcom.2011.12.162.
[51] ASTM International Standard designation E 975–03. Standard practice for X-ray determination of retained austenite in steel with near Random Crystallographic Orientation.
[52] Villa M, Pantleon K, Somers MAJ. Enhanced carbide precipitation during tempering of sub-zero Celsius treated AISI 52100 bearing steel. In: Proceedings of the heat treat and surface engineering conference and expo, Chennai; 2013.
[53] Hauk V. Structural and residual stress analysis by non-destructive methods: evaluation – application –assessment. Amsterdam: Elsevier; 1997.
[54] Giessen CB, Gordon GE. Science 1968;159:973–5.
[55] van Genderen MJ, Isac M, Bottger A, Mittemeijer EJ. Metall Trans A 1997;28A:545.

APPENDIX H

Isothermal martensite formation in precipitation hardenable semi-austenitic stainless steel

DRAFT

M. Villa, M.F. Hansen, K. Pantleon, Marcel A.J. Somers

Work was planned and the results were interpreted by all co-authors. First author performed the experimental activity and wrote the first draft of the manuscript. Comments and suggestions from M.F. Hansen, K. Pantleon and Marcel A.J. Somers were incorporated iteratively in the subsequent versions of the manuscript.

Isothermal martensite formation in precipitation hardenable semi-austenitic stainless steel

Matteo Villa[1], Mikkel F. Hansen[2], Karen Pantleon[1], Marcel A.J. Somers[1]

1. Technical University of Denmark, Department of Mechanical Engineering, DK 2800 Kongens Lyngby, Denmark
2. Technical University of Denmark, Department of Micro and Nanotechnology, DTU Nanotech, DK 2800 Kongens Lyngby, Denmark

matv@mek.dtu.dk, mikkel.hansen@nanotech.dtu.dk; kapa@mek.dtu.dk, somers@mek.dtu.dk,

Keywords: isothermal martensite; steels; sub-zero Celsius treatment; (synchrotron) X-Ray Diffraction

Abstract

The austenite to martensite transformation at sub-zero Celsius temperature in precipitation hardenable stainless steel containing 17.3wt%Cr, 7.3wt%Ni, 0.8.wt%Al, was followed in situ with (synchrotron) X-Ray Energy Dispersive Diffraction and Vibrating Sample Magnetometry.
Isothermal martensite formation at sub-zero Celsius temperature is reported.

The precipitation hardenable 17-7 PH stainless steel was first developed and registered during the 40ies of the last century. Its chemical composition is tailored to obtain a partially austenitic, partially martensitic, microstructure after austenitization and cooling to room temperature. Accordingly, 17-7 PH is classified as semi-austenitic precipitation hardenable stainless steel [1].

According to specifications [1], the material is provided solution heat treated (Condition A [1]) or cold rolled (Condition C [1]). Austenitization is performed at 1227±9 K for 600 s followed by air cooling (Condition A-1750 [1]). The full potential in terms of mechanical properties is obtained after complete transformation of the austenite into martensite followed by tempering, as a consequence of a fine precipitation of intermetallic compounds within the martensite [1−3].

Martensite formation can be induced mechanically by metal forming, or applying a sub-zero Celsius treatment [2,3]. Standard specifications [1] indicates sub zero Celsius cooling to 200±9 K, followed by 8 h isothermal holding (Condition R-100 [1]), which is conveniently performed at sublimation temperature of dry ice, i.e. 195 K [2].

Isothermal treatment at sub-zero Celsius temperature suggests the occurrence of isothermal martensite formation, first demonstrated in 1948 for Fe-Ni-Mn alloys [4], and afterwards reported for several materials, among which semi-austenitic stainless steel grades [5−7].

The purpose of this work is to report for the first time experimental evidence of isothermal martensite formation in 17-7 PH commercial steel grade.

The alloy used in the present work is a 17-7 PH, 0.015 mm thick foil, supplied by Goodfellow Cambridge Ltd, in Condition C (i.e. as rolled). The chemical composition of the material is reported in Table 1.

Table 1: Chemical composition of the steel 17-7 PH (in wt%) determined with Energy Dispersive Spectroscopy, EDS. The Carbon content was measured with a LECO-CS230 Carbon analyzer

Fe	C	Cr	Ni	Al	Mn	Si
Bal.	0.09	17.3	7.3	0.8	0.7	0.5

Austenitization of the as-rolled material was performed at 1227 K fo 1800 s and was followed by air cooling to room temperature.

The austenitized material was sub-zero Celsius treated and martensite formation was followed in situ by X-Ray Diffraction, XRD, and Vibrating Sample Magnetometry, VSM.

X-Ray Diffraction, XRD, was performed in transmission at the synchrotron facility HZB-BESSY II, experimental station EDDI [8], which applies energy dispersive XRD [9]. The conditions for the investigation are reported in Table 2.

Table 3. Measurement conditions for synchrotron X-ray diffraction. Initial conditions refer to as-rolled and as quenched material.

Scattering angle (2θ)	acquisition time [s]	Reflection of martensite	Reflection of austenite
20°	900	211_{α}, 220_{α}, 310_{α}, 321_{α}	200_{γ}, 311_{γ}, 220_{γ}, 400_{γ}, 420_{γ}, 422_{γ}

The sample was placed in an insulated chamber of 8 liters capacity, which was filled with pellets of dry ice with a temperature of 188 K. Refill of the pellets was performed every 8 hours, that occurred at the time where the measurement anyway was interrupted due to regular programmed beam shutdown of 300 s to 600 s during injection at the synchrotron facility.

The sample was a 5mm x 25mm strip placed in the middle of the chamber. The sample was isolated from the dry ice with an aluminum net kept 3 away from the sample. The temperature in the surrounding of the sample was monitored with an APPA-55II digital thermometer, placing the thermocouple between the sample and the aluminum net. The temperature during the investigation was measured to be stable (also during refill) in the interval 188-195 K. Two openings in the chamber allowed the passage of the incident and diffracted X-Ray beam.

The X-Ray beam intensity was affected by the presence of dry ice pellets on the incidents and diffracted beam paths, and quantification of the X-Ray absorption during the experiment was not possible since the density of the pellets was observed to change with time. Consequently X-Ray spectra acquired in situ during the transformation process are of qualitative value only.

VSM was applied for quantitative investigation of the evolution of the fraction of martensite and austenite versus time of isothermal holding at different temperatures in the interval 145-225 K.

VSM was performed with a Lake Shore 7407 Cryotronics VSM equipped with a cryostat. Samples were thin disks 3 mm in diameter, 0.15 mm thick, mounted onto rigid fiber pole using non-magnetic Kapton tape. The fiber rod was inserted in pre-cooled cryostat chamber. The time required for thermal stabilization was estimated in 30s by mounting a thermocouple on the fiber rod, whereas 60 s are required to start data acquisition for VSM investigation. Consequently, data refers to the isothermal step only.

A magnetic field of 1 T was used to bring the sample at saturation. The degree of transformation was followed recording the magnetic moment of the sample at saturation every 4 s.

The magnetic moment of the sample was measured as a function of time, and the fraction of martensite $f_{\alpha'}(t)$ was calculated according to $f_{\alpha'}(t) = \frac{M(t)}{M_C}$, where $M(t)$ is the magnetic moment at saturation of the sample, M_C is the magnetic moment of the as rolled material. This relationship assumes that the content of austenite in the as-rolled condition is negligible, as was validated by transmission XRD.

XRD also indicated that the material after austenitization is semi-austenitic.

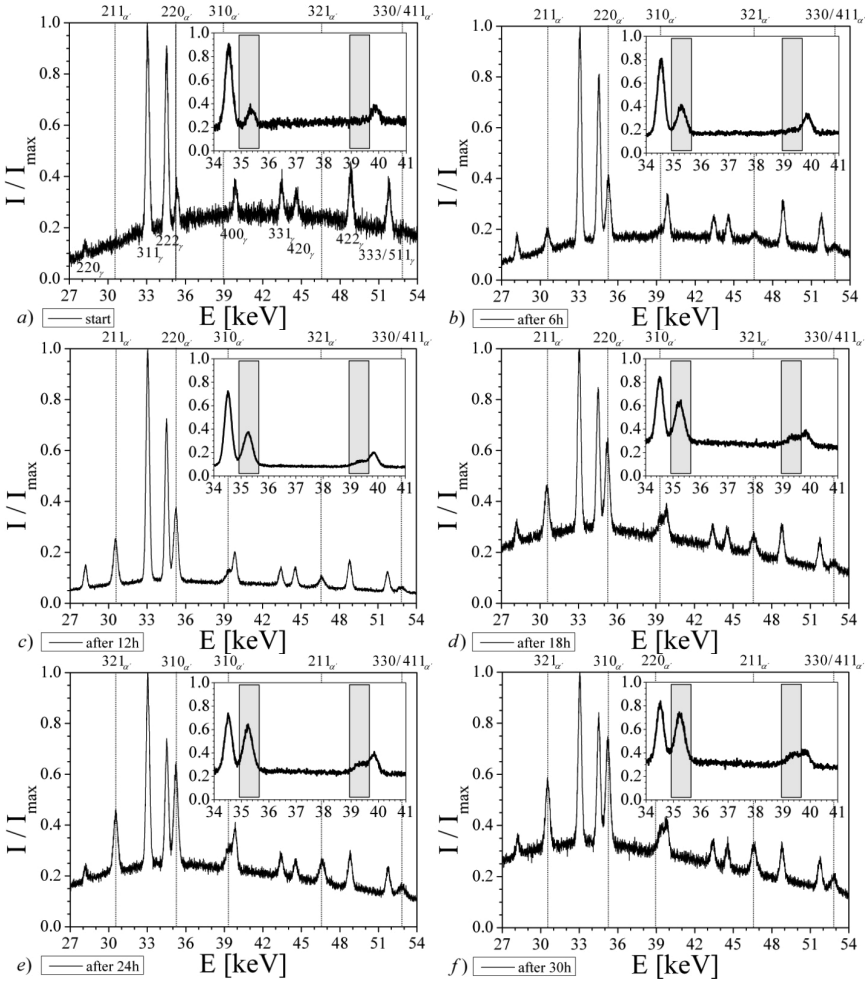

Figure 113. Spectrograms obtained every 6 h of isothermal holding during the in situ investigation at sub-zero Celsius. Intensities are shown normalized to the maximum intensity recorded in the spectrum "I/I_{max}" versus energy "E".

The XRD investigation is presented in Fig. 1. Fig. 1 reports the energy dispersive diffraction spectra obtained every 6 hours time interval as an example of the acquired data during isothermal holding at sub-zero Celsius temperature. Evidently, martensite formation is reported by in situ XRD.

At the beginning of the isothermal holding (Fig.2a), all the reflections of austenite expected in the considered energy interval are observed, while only the $220_{\alpha'}$ reflection of martensite is visible. After 6 hours (Fig.2b), all the reflection of martensite expected in this energy range are reported.

Continuing the isothermal holding, a direct comparison of intensity for different peaks is allowed only for reflection occurring very close in energy: the change in density of the dry ice pellets during time would otherwise affect the result, modifying the dependency on energy of the X-Ray absorption. The comparison between the 222_{γ} reflection of austenite and the $220_{\alpha'}$ reflection of martensite (Fig. 2, enlargements) shows a progressive formation of martensite during time. The same trend is visible comparing the $310_{\alpha'}$ reflection of martensite and the 400_{γ} reflection of austenite (Fig. 2, enlargements).

The VSM investigation is presented in Fig. 2. Fig. 2 reports the transformation curves obtained holding the samples at different temperature for 20 hours under an applied magnetic field of 1T.

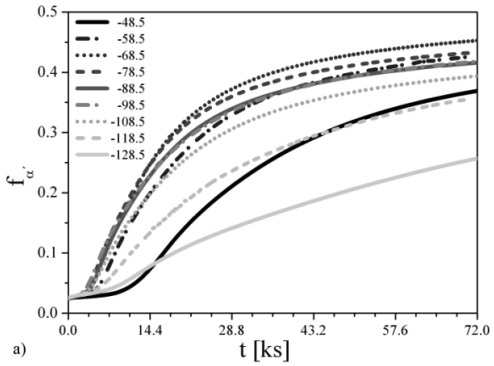

Figure 114. Fraction of martensite "$f_{\alpha'}$" versus time "t" for different temperature of isothermal holding.

Fig. 2 shows that the initial content of martensite equals 2.5±0.1 % and is independent of temperature, suggesting that martensite formation is completely suppressed during cooling.

Thereafter, isothermal martensite formation is observed at all investigated temperature. Isothermal martensite formation is strongly temperature dependent and is particularly pronounced for isothermal holding in the temperature interval 165-215 K.

It is finally observed that, for 8 hours isothermal holing the transformation is maximum for temperatures of 195 and 205 K, in agreement with industrial specification for sub-zero Celsius treatment in Ref. [1].

In conclusion, isothermal martensite formation at sub-zero Celsius temperature in 17-7 PH stainless steel grade is demonstrated, and the metallurgical mechanisms on which the standard refrigeration procedure suggested to maximize the mechanical properties of the material is based, explained.

Mr. Ole West, Technical University of Denmark, Prof. Chr. Genzel and Dr. M. Kaluss, Helmholtz Zentrum für Materialien und Energy (HZB), are acknowledged for their support during experiments at the Berlin synchrotron facility HZB-BESSY II. The authors acknowledge the Danish Natural Science Research Council for financial support of part of the work via Danscatt.

References

[1] "Armco 17-7PH and PH 15-7Mo Stainless Steel and Strip", Arco steel corporation, Middletown, Ohio, 1966
[2] C.J. Slunder, A.F. Hoenie, A.M. Hall, "Thermal and Mechanical Treatment for Precipitation-Hardening Stainless Steel", NASA, Washington, D.C., 1967
[3] D.C. Ludwigson, A.M. Hall, "The Physical Metallurgy of Precipitation-Hardenable Stainless Steel", Defence Metals information center, Report III, 1959
[4] G.V. Kurdyumov, O.P. Maksimova, O kinetike prevrashcheniya austenite v martensit pri nizkikh temperatorakh, Dokl Akad. Nauk SSSR 61 (1948) 83-86
[5] M. Holmquist, J.O. Nilsson, A. Hultin Stigenberg, Scripta Metall. Mater. 33 (1995) 1367
[6] T.D. Kubyshkina, M. Pevzner, Ya. M. Potak, Metal science and Heat treatment of Metals, 2 (1960) 425-430
[7] D. San Martin, K.W.P. Aarts, P.E.J. Rivera-Diaz-del-Castillo, N.H. Van Dijk, E. Bruck, S. van der Zwaag, J. Magnetism and Magnetic Mater. 320 (2008) 1722-1828
[8] Ch. Genzel, I.A. Denks, J. Gibmeier, M. Klaus, G. Wagener. Nuclear Instruments and Methods in Physics Research A 578 (2007) 23–33
[9] C.B. Giessen, G.E. Gordon, *Science.* 1968, Vols. 159, pp. 973 – 975.

APPENDIX I

Thermally activated growth of lath martensite and abnormal martensite formation in Fe-Ni-Cr-Al stainless steel

DRAFT

M. Villa, M.F. Hansen, K. Pantleon, Marcel A.J. Somers

Work was planned and the results were interpreted by all co-authors. First author performed the experimental activity and wrote the first draft of the manuscript. Comments and suggestions from M.F. Hansen, K. Pantleon and Marcel A.J. Somers were incorporated iteratively in the subsequent versions of the manuscript.

Thermally activated growth of lath martensite in Fe-Ni-Cr-Al stainless steel

Matteo Villa[1], Mikkel F. Hansen[2], Karen Pantleon[1], Marcel A.J. Somers[1]

1. Technical University of Denmark, Department of Mechanical Engineering, DK 2800 Kongens Lyngby, Denmark
2. Technical University of Denmark, Department of Micro- and Nanotechnology, DTU Nanotech, DK 2800 Kongens Lyngby, Denmark

matv@mek.dtu.dk, mikkel.hansen@nanotech.dtu.dk; kapa@mek.dtu.dk, somers@mek.dtu.dk,

Keywords: isothermal martensite; steels; sub-zero Celsius treatment; magnetometry

Abstract

The austenite-to-martensite transformation in a partially hardened stainless steel containing 17wt %Cr, 7wt %Ni and 1wt % Al was investigated with Vibrating Sample Magnetometry and Electron Back-Scatter Diffraction.

Magnetometry demonstrated that measurable martensite formation can be suppressed on fast cooling to 77K as well as on subsequent fast heating to 373 K. Surprisingly, martensite formation was observed during moderate heating from 77 K, instead. Electron Back-Scatter Diffraction demonstrated that the morphology of martensite is lath type.

The kinetics of the transformation is interpreted in terms of a-thermal nucleation of lath martensite followed by thermally activated growth. It is anticipated that substantial autocatalytic martensite formation occurs during thermally activated growth.

The observation of several retardations and accelerations of the transformation rate during slow isochronal cooling is interpreted in terms of the contribution of self-induced mechanical stabilization of austenite during martensite formation.

Introduction

Martensite in iron-based alloys can appear as laths, characterized by an internal sub-structure with a high density of dislocations [1,2], or as plates, which are partially [3,4] or fully [5] internally twinned [6]. Regardless of the morphology of martensite, the kinetics of martensite formation is historically described as fully nucleation-controlled [7], with the implicit assumption of instantaneous growth of martensite upon nucleation.

Martensite in iron-based alloys can appear as laths, characterized by an internal sub-structure with a high density of dislocations,[1,2] or as plates, which are partially[3,4] or fully[5] internally twinned[6]. Regardless of the morphology of martensite, the kinetics of martensite formation is historically described as fully nucleation-controlled,[7] with the implicit assumption of instantaneous growth of martensite upon nucleation.

However, growth of lath martensite is not instantaneous, but time-dependent and proceeds at a velocity in the range of 10^{-6} m s^{-1} to 10^{-1} m s^{-1}.[8] In Refs. 9-10 a growth rate for lath martensite formation in the order of 10^{-3} m s^{-1} was reported[9] and a martensite formation event was estimated to last 10^{-3} s.[10] Although these observations are consistent with Ref. 8 (i.e. time-dependent growth), surprisingly they were considered to corroborate nucleation-controlled descriptions.[7]

Time-dependent growth of lath martensite was followed in-situ by microscopical investigations in Ref. 11-15 and it was observed to induce time-dependent (autocatalytic) nucleation of lath martensite.[12,13,15]

After initial nucleation and growth, autocatalytic nucleation is responsible for an acceleration of the transformation.[7,16] Autocatalytic nucleation can occur either within the same austenite grain wherein martensite formation occurs or in neighbouring austenite grains.[17]

In the case of lath martensite, austenite grains are sub-divided by martensite formation at four length scales.[2,18-20] Firstly austenite grains are divided into groups of laths with the same habit plane, so-called packets. Each packet contains several blocks, which are groups of laths with the same (Kurdjumov-Sachs, K-S) orientation relation to austenite. Block boundaries are high-angle boundaries and are either subdivided in sub-blocks of two K-S variants of martensite laths or can contain a single K-S variant. The individual laths represent the smallest level of subdivision.

In Ref. 15, continuous growth of lath martensite was observed to promote autocatalytic nucleation (mainly) within a single block of laths. In Ref. 12,13, continuous growth of lath martensite was observed to promote the generation of variants with another orientation relation with respect to austenite, leading to the formation of new blocks and packets. Finally, in-situ (synchrotron) X-ray diffraction investigations in Ref. 21 suggested that autocatalytic nucleation of lath martensite spreads the transformation over neighbouring austenite grains.

Accordingly, the applicability of fully nucleation-controlled kinetics can be questioned. In Refs. 22-24 time dependent formation of lath martensite was interpreted in terms of thermally-activated, time-dependent, nucleation, while in Refs. 25,26 time-dependent lath martensite formation was described in terms of thermally activated growth of a-thermally formed nuclei.

The purpose of the present work is to contribute to understanding the kinetics of lath martensite formation. For this purpose, a Fe-17Cr-7Ni-1Al (wt-%) stainless steel was chosen. In this steel grade the isothermal transformation of austenite into martensite[27-29] at sub-zero Celsius temperature is industrially exploited.[27,29]

Martensite formation was investigated by magnetometry, which has been demonstrated to be an accurate technique to study the martensitic transformation in iron-based alloys.[22,23,28,30-34]

Magnetometry was supplemented by Electron Back-Scatter Diffraction, which was applied to evaluate the morphology of martensite.

Experimental

Material and heat treatments

The material used in the present work is a 0.15 mm thick foil 17-7 PH (precipitation hardening) stainless steel, which essentially is a Fe-17Cr-7Ni-1Al (wt-%) alloy, in rolled condition (supplied by Goodfellow Cambridge Ltd.) with the chemical composition reported in Table 1.

Table 1: Chemical composition (in wt%) of 17-7 PH steel as determined with Energy Dispersive Spectroscopy, EDS. The carbon content was measured with a LECO-CS230 Carbon analyzer

Fe	C	Cr	Ni	Al	Mn	Si
Bal.	0.09	17.3	7.3	0.8	0.7	0.5

Austenitization of samples prepared from the rolled condition was performed in argon at 1127±10 K for 0.6 ks and was followed by cooling to 423K at an approximate average rate of 20 K min^{-1} in an argon flow. Hereafter the flow was interrupted and the samples were slowly cooled to room temperature in the sealed furnace. The as-quenched material was stored at 295±2 K for about 10 Ms (4 months) prior to magnetometry investigation; this is the controlled temperature in the room where magnetometry was performed.

Two sets of samples were prepared: a first set of three samples I, II and III; a second set of three samples A, B and C.

After room temperature storage, samples I, II and III were heat treated as follows. On installing the sample in the magnetometer the samples were cooled to 290 K for 60 seconds and thereafter kept at room temperature, 295 K, for 180 s. Then, samples (one at a time) were immersed in boiling nitrogen and kept at 77 K for 60 s. From this temperature, the samples were isochronically heated to 290 K at 10 K min^{-1} (sample I), 3 K min^{-1} (sample II) and 0.15 K min^{-1} (sample III). The temperature history is shown in Fig.1a for the first 6 ks.

After room temperature storage and pre-treatment for 60 seconds at 290 K (identical to samples I, II and III) samples A, B and C were treated as follows:

A. immersion in boiling nitrogen for 60 s followed by immersion in boiling water. Thereafter, isochronal cooling from 373 K to 80 K (at 0.1 K min^{-1}) and heating to 290 K (at 10 K min^{-1}) was followed with magnetometry.

B. immersion in boiling water, followed by magnetometry investigation of isochronal cooling from 373 K to 80 K (at 0.1 K min^{-1}) and heating to 290 K (at 10 K min^{-1}).[75]

magnetometry investigation of isochronal cooling from 290 K to 80 K (at 0.1 K min^{-1}) and heating to 290 K (at 10 K min^{-1}).

Vibrating Sample Magnetometry, VSM

Magnetometry was performed with a Lake Shore Cryotronics 7407 vibrating sample magnetometer equipped with a Janis SuperTran-VP continuous flow cryostat. Samples were 3 mm in diameter, 0.15 mm thick disks and were mounted onto a rigid fiber pole using non-magnetic Kapton tape. The degree of transformation was followed by recording the magnetic moment of the sample at saturation. A magnetic field of 1 Tesla was applied to bring the samples to magnetic saturation.

The absolute temperature was verified and validated at the boiling point of liquid nitrogen (i.e. 77 K) and at room temperature (i.e. 295±2 K). During thermal cycling, the temperature relative to the set point was accurate within ±0.5 K.

[75] The quenching steps for sample A and B were performed outside the cryostat chamber. Consequently, the content of martensite in sample A after quenching in boiling nitrogen was not measured.

The molar fraction of martensite $f_{\alpha'}(t,T)$ in the material, as measured versus time, t, and temperature, T, is determined on the basis of the following assumptions:

1. the as-received (i.e. as-rolled) material is fully martensitic, as was validated by transmission X-ray diffraction;[33]
2. the *molar* fraction of martensite is proportional to the magnetic moment at magnetic saturation,[76] corrected for its dependence of temperature;[34]
3. the as-rolled sample remains stable in the temperature interval under investigation.

With these assumptions, $f_{\alpha'}(t,T)$ is given by:

$$f_{\alpha'}(t,T) = M(t,T) / M_{\alpha'}(t,T) \quad (1)$$

where M(t,T)is the magnetic moment at saturation measured in the sample and $M_{\alpha'}(t,T)$ is the magnetic moment at saturation measured in the as-rolled material during recording of the baseline.

Electron backscatter diffraction, EBSD

EBSD, was performed in a dual beam FEG-SEM FEI Helios Nanolab 600 SEM equipped with an EBSD system from EDAX-TSL and a Hikari camera. The measurements were performed with an electron probe current of 11 nA at an acceleration voltage of 18 kV, with a step size of 80nm; data were collected at four different sample locations on an overall surface area of 0.025 mm^2. The OIM TSL 6 software was used for analysis of the EBSD results.

Results and discussion

Thermally activated martensite formation.

In Fig. 1b the molar fraction of martensite, $f_{\alpha'}$, measured by magnetometry is shown as a function of temperature, T, for samples I, II, III.

The initial content of martensite in the samples just before immersion in boiling nitrogen is 15±3% (point 1 in Fig. 1b). Apparently, within experimental accuracy, fast cooling to 77 K does *not* lead to a measurable formation of martensite (point 2 in Fig. 1b - 16±3%). Martensite formation is first observed during subsequent isochronal heating. The occurrence of martensite formation during *heating* is counterintuitive and indicates convincingly that martensite formation cannot be the result of a-thermal nucleation and instantaneous growth of martensite nuclei. The observation can only be understood if martensite formation (i.e. nucleation and/or growth) is thermally activated.

The present set of experiments does *not* give an indication whether thermally activated martensite nucleation or thermally activated growth occurs. A kinetic analysis of the data in Fig.1b taking a 50% transformation as a reference (cf. Ref. 35) yielded an activation energy of 15 kJ mol^{-1}.

[76] Note that Refs. 22, 23, 30, 31 refer to the volume fraction of martensite as determined by magnetometry. This is incorrect; magnetometry provides a measure for the molar fraction of the martensite formed.

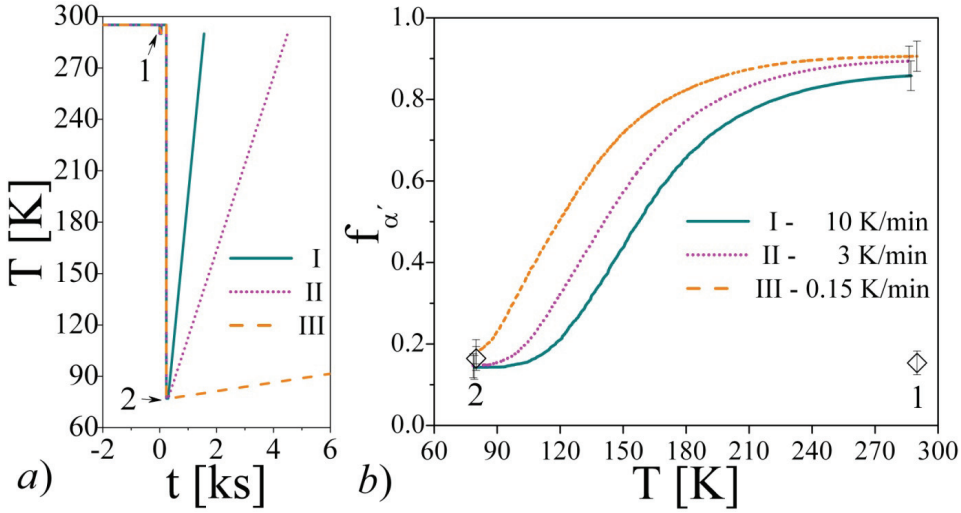

Figure 115. (a) Thermal cycles of samples I, II, and III: all samples were pre-treated at 290 K (point 1) and quenched in boiling nitrogen (point 2). The heating step terminates at 1.56 ks, 4.5 ks and 84.3 ks (out of scale) for sample I, II, and III, respectively. (b) Martensite fraction $f_{\alpha'}$ plotted versus temperature T. Black open symbols, labelled 1 and 2, refer to the average fraction of martensite determined over the different samples after pre-treatment to 290 K and after pre-treatment followed by quench in boiling nitrogen (77 K), respectively. Error bars represent reproducibility of the results according to Ref. 33.

Thermally activated growth of martensite.

The experiments presented in this section are based on the following reasoning. Provided that the transformation is *completely* suppressed on fast cooling followed by fast (re)heating above a threshold temperature were martensite formation is inhibited by thermodynamics, martensite formation during a second, slower, cooling step is:

1. *not* influenced by the initial thermal step, in the case that the kinetics of the transformation is controlled by time-dependent nucleation;
2. strongly influenced by the initial thermal step if the kinetics of the transformation is controlled by time-dependent growth of nuclei that have developed a-thermally during the initial cooling sequence.

Samples A, B and C were heat treated accordingly.

The fractions of martensite measured during the different controlled thermal cycles are collected in Fig. 2a. The transformation rate on controlled cooling in the temperature interval 330 K to 240 K is shown in Fig. 2b.

Martensite formation appears suppressed on fast (re)heating to 373 K, both from 290 K and from 77 K. The slightly higher fraction of martensite at 373 K, (i.e. 19±3%) as compared to point 1 and 2 (i.e. 15±3%) is still within experimental error.

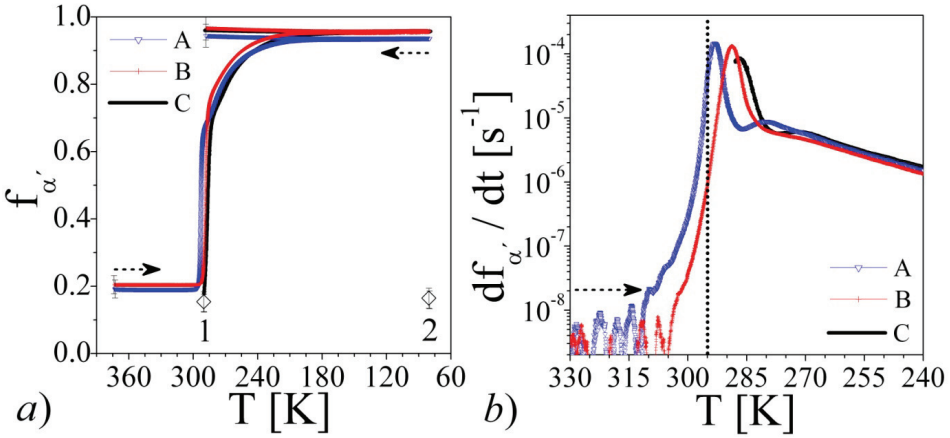

Figure 2. (a) Martensite molar fraction $f_{\alpha'}$ versus temperature T. Black open symbols, labelled 1 and 2, correspond to point 1 and 2 in Fig.1b. c) Transformation rate $f_{\alpha'}/dt$ calculated within 2400 s time intervals (±2 K), versus temperature T; the vertical dotted line marks the long-term storage temperature (295±2 K).

On isochronal cooling, neither sample A nor sample B showed a measurable transformation down to 310 K (Fig. 2b). The criterion for a measurable transformation is taken as $df_{\alpha'}/dt > 2 \cdot 10^{-8}\ s^{-1}$, which is a value safely larger than the noise level (see arrow in Fig 2b).

At 310 K, martensite formation is observed to start slowly in sample A, while martensite formation in sample B is first observed at 304 K. The onset of the transformation in samples A and B at temperatures well-above the long-term storage temperature of 295±2 K after austenitization, cannot be reconciled with a-thermal nucleation; neither can it be a consequence of thermally activated nucleation of martensite.

These results indicate that both the pre-treatment from 295 K to 290 K (sample B) and the additional cooling to 77 K (sample A) have led to the development of martensite nuclei, and that these nuclei are thermally activated to grow in the isochronal cooling stage at a temperature higher than the storage temperature. The instantaneous martensite formation as observed in sample C on cooling from 290 K corroborates that cooling from 295 K to 290 K has indeed led to the development of martensite nuclei.

The observation that measurable martensite formation starts at a higher temperature in sample A than in sample B (Fig. 2), is explained by a faster transformation in sample A, resulting from a larger number of nuclei formed upon cooling to 77 K (sample A) as compared to cooling to 290 K (sample B). During continuous cooling, the transformation rate reaches a maximum at 293 K, 289 K and 287 K for samples A, Band C, respectively. After this maximum, the transformation rate in samples A and C shows a deceleration followed by an acceleration, while for sample B the transformation decelerates monotonically. The occurrence of a deceleration of the transformation followed by a second acceleration is *abnormal* after Refs. 36-39. It is anticipated that abnormal transformation indicates the presence of autocatalytic nucleation.

The results of orientation image microscopy of samples A and B are shown in Figs. 3. A quantitative evaluation of the EBSD results (Fig.4) was obtained for the areas separated by high angle grain boundaries, i.e. a misorientation larger than 15°, which represent blocks in the lath martensite microstructure.

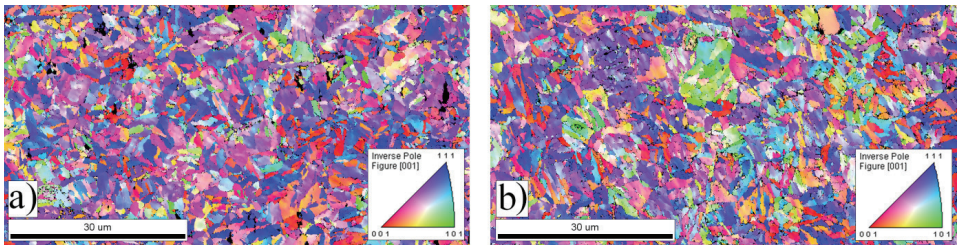

Figure 3. EBSD investigation: orientation image microscopy: a) sample A; b) sample B. The reported orientation images represent 15% of the area investigated by EBSD.

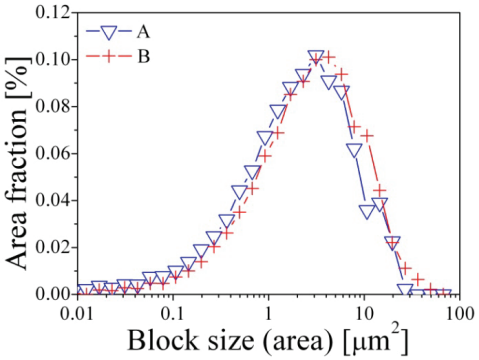

Figure 4. Block size distribution (area) for the samples A and B, respectively. Data refers to an overall surface area of 0.025 mm^{-2} per sample.

Evidently, the quantitative size distribution of martensite regions in samples A and B is identical within experimental accuracy (Fig. 4). This indicates that the higher number of nuclei in sample A as compared to sample B is not reflected in the microstructure after completed transformation. Hence, it has to be concluded that additional nucleation has occurred in sample B during isochronal cooling.

In principle, such nucleation could have taken place purely a-thermally. However, since the largest part of the transformation is accomplished within a very narrow temperature range for all investigated samples (cf. Fig. 2b), it is anticipated that autocatalytic nucleation has contributed substantially to the transformation.

Abnormal martensite formation.

In this section, abnormal martensite formation is discussed in relation to the abnormal *massive* transformation of austenite into ferrite, as described in Refs. 36-39. The latter is introduced first.

At the beginning of the massive transformation, nucleation of ferrite at several locations in the sample is followed by thermally activated growth. The strain energy which is introduced *locally* in the system as a consequence of the volume misfit between ferrite and austenite (i.e. the introduction of shear stresses), promotes autocatalytic nucleation of ferrite in front of the ferrite -austenite interface.[36] Autocatalytic nucleation yields a strong acceleration of the transformation, which comes to a halt when the strain energy introduced in the system by the transformation itself, *averaged* over the entire sample (i.e. the sum of interfacial energies, introduction of crystal defects and build up of hydrostatic pressure in austenite),

equals the chemical driving force. Thereafter, an increment of the driving force upon continuous cooling is necessary to initiate a new (autocatalytic) nucleation event.

In the present case, at 310 K, several (infinitively small) nuclei of lath martensite are present in the material as a consequence of a-thermal nucleation in the first cooling step. The number of nuclei differs for samples A and B and is largest in sample A, because of the significantly lower temperature reached in sample A during cooling (i.e. 77 K versus 290 K).

On cooling below 310 K, martensite starts to grow. Evidently, the driving force at 310 K is sufficient to compensate for the interfacial energy and the elastic and plastic strain energy terms associated with martensite formation and the frictional work accompanying the movement of the austenite/martensite interface.[40,41] For a relatively small transformed fraction, martensite formation introduces shear[21] and tensile dilatational[42] stresses in the surrounding austenite matrix, which exceeds the other energy terms in austenite accompanying martensite formation and *promotes* the driving force for (autocatalytic) martensite formation.

For a relatively large transformed fraction, (retained) austenite regions become encaged by martensite. Then additional martensite formation induces compressive strain energy terms in austenite,[42-44] which *counteracts* the driving force for martensite formation[45-47] (i.e. mechanical stabilization of austenite[8] occurs during martensite formation).

The compressive strain energy in austenite suppresses martensite nucleation and results in a deceleration of the transformation. However, martensite formation does not completely stop, because growth of pre-existing nuclei can still occur.

A new acceleration of the martensite formation occurs when additional undercooling leads to a further increase of the driving force. At this point, provided that there is enough austenite to transform, an increase in the nucleation rate may yield a new acceleration of the transformation, as is observed at 280 K in sample A (and C). The reason that this acceleration is not observed for sample B, could be the lower fraction of untransformed austenite as compared to sample A (and C) at this point.

To summarize, autocatalytic nucleation of martensite is promoted by continuous growth of the martensite areas. The combined effect of autocatalytic nucleation and self-induced mechanical stabilization of austenite yield abnormal transformation, characterized by repeated acceleration and deceleration of the transformation.

Conclusions

Martensite development in a 17-7 PH (i.e. 17wt %Cr, 7wt %Ni and 1wt % Al) stainless steel was investigated with magnetometry and Electron Back-Scatter Diffraction. It was observed that fast cooling to 77 K, well below M_s, and fast heating from below M_s to a temperature well above M_s did not lead to a measurable formation of martensite. Instead martensite develops during controlled cooling from above M_s or controlled heating from a temperature well below M_s (77 K).

The results can be interpreted consistently assuming that a-thermal (mainly autocatalytic) nucleation occurs, followed by thermally activated growth of the martensite nuclei. The activation energy for thermally activated martensite growth was assessed at 15 $kJ.mol^{-1}$.

The observation of abnormal lath martensite formation is reported on continuous cooling. Abnormal transformation is interpreted in terms of self-induced mechanical stabilization of austenite during martensite formation.

References

[1] K. Wakasa, C.M. Wayman, *"Crystallography and Morphology of Ferrous Lath Martensite"*, Acta Metal., 1981, 29, 991-1001.
[2] S. Morito, X. Huang, T. Furuhara, T. Maki, N. Hansen, *"The Morphology and Crystallography of Lath Martensite in Steel"*, Acta Mater., 2006, 54, 5323-5331.
[3] K. Shimizu, M. Oka, C.M. Wayman, *"The association of martensite platelets with austenite stacking faults in an Fe-8Cr-1C alloy"*, Acta Metall., 1970, 18:9, 1005-1011.
[4] A. Shibata, S. Morito, T. Furuhara, T. Maki, *"Substructures of lenticular martensites with different martensite start temperatures in ferrous alloys"*, Acta Mater., 2009, 57:2, 483-492.
[5] T. Maki, C.M. Wayman, *"Substructure of ausformed martensite in Fe-Ni and Fe-Ni-C alloys"*, Metall. Trans., 1976, 7A:9, 1511-1518.
[6] G. Krauss, A.R. Marder, *"The morphology of martensite in iron alloys"*, Metall. Trans., 1971, 9:2, 2343-2357.
[7] N.N. Thadhani, M.A. Meyers, *"Kinetics of isothermal martensitic transformation"*, Progress in Mater. Sci., 1986, 30:1, 1-37.
[8] Z. Nishiyama, "*Martensitic Transformation*", 1978, New York: Academic Press.
[9] K. Takashima, Y. Higoa, S. Nunomura, *"The propagation velocity of the martensitic transformation in 304 stainless steel"*, Philosophical Mag., 1984, 49A:2, 231-241.
[10] F. Foerster, E. Scheil, "*Acoustical study of formation of martensite needles"*, Naturwissenschaften, 1936, 28:9, 245-247.
[11] J.H. Lee, T. Fukuda, T. Kakeshita, *"Isothermal Martensitic Transformation in Sensitized SUS304 Austenitic Stainless Steel at Cryogenic Temperature"*, Mater. Trans., 2009, 50:3 473-478.
[12] D-Z. Yang, C.M. Wayman, *"Slow growth of isothermal lath martensite in an Fe&z.sbnd;21N&z.sbnd;4Mn alloy"*, Acta Metall., 1984, 32:6, 949-954.
[13] T. Kakeshita, K. Kuroiwa, K. Shimizu,T. Ikeda, A. Yamagishi, M. Date, *"Effect of magnetic fields on athermal and isothermal martensitic transformations in Fe-Ni-Mn alloys"*, Mater. Trans. JIM., 1993, 34:5, 415-422.
[14] T. Araki, K. Shibata, K. Asakura, H. Wada, *"Direct observation of the gamma yields alpha prime isothermal martensitic transformation of iron alloys in electron microscope"*, ISIJ., 1975, 15:4, 175-184.
[15] J.M. Marder, A.R. Marder, *"Formation of low Carbon Martensite in Fe-C Alloys"*, ASM Transaction, 1969, 62:1, 1-10.
[16] S.R. Pati, M. Cohen, *"Kinetics of isothermal martensitic transformations in an iron-nickel-manganese alloy"*, Acta Meta., 1971, 19:12, 1327-1332.
[17] P.R. Rios, J.R.C. Guimarães, *"Formal Analysis of Isothermal Martensite Spread"*, Mater. Research, 2008, 11:1, 103-108.
[18] H. Kitahara, R. Ueji, N. Tsuji, Y. Minamino, *"Crystallographic features of lath martensite in low-carbon steel"*, Acta Mater., 2006, 54:5, 1279–1288.
[19] S. Morito, H. Tanaka, R. Konishi, T. Furuhara, T. Maki, *"The morphology and crystallography of lath martensite in Fe-C alloys"*, Acta Mater., 2003, 51:6, 1789–1799.
[20] T. Furuhara, N. Takayama, G. Miyamoto, *"Key Factors in Grain Refinement of Martensite and Bainite"*, Mater. Sci. Forum, 2010, 638-642, 3044-3049.
[21] D. San Martin, E. Jimenez-Melero, J.A. Duffy, V. Honkimaki, S. van der Zwaag, N.H. van Dijk, J. *"Real-time synchrotron X-ray diffraction study on the isothermal martensite transformation of maraging steel in high magnetic fields"*, Appl. Cryst., 2012, 45, 718-757.
[22] D. San Martin, K.W.P Aarts, P.E.J. Rivera-Diaz-del-Castillo, N.H. van Dijk, E. Bruck, S. van der Zwaag, *"Isothermal martensitic transformation in a 12Cr-9Ni-4Mo-2Cu stainless steel in applied magnetic fields"*, J. Magnetism and Magn. Mater., 2008, 320:10, 1720-1728.
[23] D. San Martin, N.H. van Dijk, E. Jimenez-Melero, E. Kampert, U. Zeitler, S. van der Zwaag, *"Real-time martensitic transformation kinetics in maraging steel under high magnetic fields"*, Mat. Sci. Eng., 2010, 527A:20, 5241-5245.

[24] J.R.C. Guimaraes, P.R. Rios, *"Unified model for plate and lath martensite with athermal kinetics"*, Metall. and Mater. Trans., 2010, 41A:8:, 1928-1935.
[25] Y. Liu, L. Zhang, F. Sommer, E.J. Mittemeijer, *"Kinetics of martensite formation in substitutional Fe-Al alloys: Dilatometric analysis"*, Metall. and Mater. Trans., 2013, 44A:3, 1430-1440.
[26] D. Kim, J.G. Speer, B.C. De Cooman, *"Isothermal Transformation of a CMnSi Steel Below the M-S Temperature"*, Metall. and Mater. Trans., 2011, 42A:6, 1575-1585.
[27] D.C. Ludwigson, A.M. Hall, "*The Physical Metallurgy of Precipitation-Hardenable Stainless Steel"*, 1959, Defence Metals information center, Report III.
[28] T.D. Kubyshkina, L.M. Pevzner, Ya. M. Potak, *"The martensitic transformation in stainless steels of the austenitic-martensitic class"*, Metallov. i Term. Obrabotka, 1960, 8:2, 9-17.
[29] C.J. Slunder, A.F. Hoenie, A.M. Hall, "*Thermal and Mechanical Treatment for Precipitation-Hardening Stainless Steel"*, 1967, NASA, Washington, D.C..
[30] L. Zhao, N.H. van Dijk, E. Bruck, J. Sietsma, S. van der Zwaag, *"Magnetic and X-ray diffraction measurements for the determination of retained austenite in TRIP steels"*, Mater. Sci. Eng., 2001, 313A:1-2, 145-152.
[31] M. Radu, J. Valy, A.F. Gourgues, F. Strat, A. Pineau, *"Continuous magnetic method for quantitative monitoring of martensitic transformation in steels containing metastable austenite"*, Scripta Mater., 2005, 52:6, 525-530.
[32] T. Koyano, *"Isothermal martensitic transformation of γ-FeN in a magnetic field"*, Mater. Trans., 2003, 44:12, 2541-2544.
[33] M. Villa, *"Isothermal martensite formation"*, PhD Thesis, Lyngby, Denmark: The Technical University of Denmark, 2013, submitted.
[34] A. Stojko, *"The effect of cryogenic treatment on structural and phase transformations in iron-carbon martensite"*, PhD Thesis; Lyngby, Denmark: The Technical University of Denmark, 2006.
[35] E.J. Mittemeijer, *"Analysis of the kinetics of phase transformations"*, J. of Mater. Sci, 1992, 27:15, 3977-3987.
[36] Y.C. Liu, F. Sommer, E.J. Mittemeijer, *"Abnormal austenite-ferrite transformation behaviour in substitutional Fe-based alloys"*, Acta Mater., 2003, 51:2, 507-519.
[37] Y.C. Liu, F. Sommer, E.J. Mittemeijer, *"Kinetics of the abnormal austenite-ferrite transformation behaviour in substitutional Fe-based alloys"*, Acta Mater., 2004, 52:9, 2549-2560.
[38] Y.C. Liu, F. Sommer, E.J. Mittemeijer, *"Abnormal austenite-ferrite transformation kinetics of ultra-low-nitrogen Fe-N alloy"*, Metall. And Mater. Trans., 2008, 39A:10, 2306-2318.
[39] Y.C. Liu, F. Sommer, E.J. Mittemeijer, *"Abnormal austenite-ferrite transformation behavior in pure iron"*, Chinese Sci. Bullettin, 2004, 49:9, 972-975.
[40] M. Grujicic, G.B. Olson, W.S. Owen, *"Mobility of martensitic interfaces"*, Metall. Trans., 1985, 16A:10, 1713-1722
[41] D. Eshelby, *"The determination of the elastic field of an ellipsoidal inclusion, and related problems"*, Proc. Roy. Soc. (London) A 241 (1957) 376–396
[42] V.M. Yershov, N.L. Oslon, *"Change in linear expansion coefficient of austenite on transformation to martensite"*, Fiz. Met. Metalloved, 1968, 25:5, 874-881
[43] M. Villa, K. Pantleon, M.A.J. Somers, *"Martensitic transformation and stress partitioning in a high-carbon steel"*, Scr. Mater., 2012, 67:6, 621-624.
[44] K. Ja. Golovchiner, *"Changes in the lattice parameter of austenite during martensitic transformation of steel"*, Phys. Metals Metallogr., 1974, 37:2, 126
[45] J.R. Pati, M. Cohen, *"Criterion for the action of applied stress in the martensitic transformation"*, Acta Mater., 1953, 1:5, 531-538
[46] T. Kakeshita, K. Kuroiwa, K. Shimizu, T. Ikeda, A. Yamagishi, M.A. Date, *"A New Model Explainable for Both the Athermal and Isothermal Natures of Martensitic Transformations in Fe-Ni-Mn Alloys"*, Mater. Trans. JIM., 1993, 34:5, 423-428.

[47] T. Kakeshita, T. Saburi, K. Shimizu, *"Effects of hydrostatic pressure and magnetic field on martensitic transformations"*, Mater. Sci. Eng., 1999, A273-275, 21-39.

APPENDIX J

Abnormal formation of lath martensite in stainless steel

DRAFT

M. Villa, K. Pantleon, Marcel A.J. Somers

Work was planned and the results were interpreted by all co-authors. First author performed the experimental activity and wrote the first draft of the manuscript. Comments and suggestions K. Pantleon and Marcel A.J. Somers were incorporated iteratively in the subsequent versions of the manuscript.

Abnormal formation of lath martensite in stainless steel

Matteo Villa[1], Karen Pantleon[1], Marcel A.J. Somers[1]

1. Technical University of Denmark, Department of Mechanical Engineering, DK 2800 Kongens Lyngby, Denmark

matv@mek.dtu.dk, kapa@mek.dtu.dk, somers@mek.dtu.dk,

Keywords: isothermal martensite; steels; transformation kinetics

Abstract

A stainless steel containing 16wt%Cr-5wt%Ni-3wt%Cu was transformed into martensite applying isochronal cooling followed by isothermal holding. The formation of martensite was monitored with dilatometry. A series of controlled retardations and accelerations of the transformation was observed during isochronal cooling for cooling rates ranging from 1.5 K/min to 50 K/min. The cooling rate in the isochronal stage was observed to influence the transformation rate in the isothermal stage. Electron back-scatter diffraction was applied to determine the morphology of the martensite and to investigate the microstructure of the material. No influence of the cooling rate on the scale of the microstructure was observed and the martensite formed was of lath type. The observation of several retardations and accelerations of the transformation during isochronal cooling is interpreted in terms of the combined effect of autocatalytic nucleation of lath martensite and self-induced mechanical stabilization of the austenite.

Introduction

Martensite in iron-based alloys can appear as lath or plate morphology [1-8]. Lath martensite shows an internal sub-structure with a high density of dislocations [2,3], while plate martensite is partially [4-7], or fully [8], internally twinned.

The microstructure of lath martensite is highly hierarchical. Austenite grains are sub-divided by martensite formation at four length scales [2,3,9]. Firstly, austenite grains are divided into groups of laths with the same habit plane, so-called packets. Each packet contains several blocks, which are groups of laths with the same (Kurdjumov-Sachs, K-S) orientation relation to austenite and are subdivided in sub-blocks of one or two K-S variants of martensite laths. Block boundaries are high-angle boundaries, while sub-blocks boundaries are low-angle boundaries. The individual laths represent the smallest level of subdivision. The formation of lath martensite was suggested to be thermally activated [10].

The microstructure of plate martensite, among which martensites of lenticular shape, so called *lenticular martensites* [1,10] does *not* present a hierarchical structure [1,10,11], but the formation of the martensite plates progressively partitions the prior austenite grains [11]. Lenticular martensite is composed of an internally twinned central midrib surrounded by a region with a high dislocation density [5-7] (i.e. slipped martensite). The slipped regions grow by thermal activation [12], while the formation of midribs is believed to proceed athermally [10].

Regardless of the morphology of martensite, martensite formation in iron-based alloys is characterized by strong autocatalytic nucleation, which is promoted by the elastic and plastic strains in the surrounding austenite as induced by the forming martensite [13,14].

Autocatalytic nucleation of lath martensite may occur at all different scales of the microstructure [15-19]. Autocatalytic nucleation was demonstrated within singular blocks and packets [15], inter-packets [16,17] and was suggested to spread the transformation over neighbouring austenite grains [18,19].

Similarly, autocatalytic nucleation of plate martensite may occur within the same prior austenite grain or in neighboring austenite grains [19,20]. Autocatalytic nucleation of plate martensite results in the simultaneous formation of multiple martensite variants [1,10,21] and in bursts [11]. In a burst, a large portion of material is transformed instantaneously in a single event [22], yielding *sudden* [11, 23] and *ir*reproducible [11] transformation steps.

In Refs. [11,23], anomalous observations were reported where the steps appear smoothened into a train of accelerations and decelerations of the transformation. Specifically, solid-state transformations characterized by multiple accelerations and retardations during continuous cooling have been reported [11,23−31] for the transformation of f.c.c. austenite into b.c.c. microstructure constituents in steels, as ferrite [24-27], bainite [28], lath martensite [29-30] and lenticular martensite [11,23,31,32].

A series of controlled multi-step transformations were firstly reported in Ref. [11], where time dependent *wavy* transformation curves were observed during the formation of partially internally twinned plate martensites (i.e. lenticular and butterfly martensites, see Ref. [1]) in several Fe-Ni-C, Fe-Ni-C-Mn and Fe-Ni-C-Cr steels. Reproducible multi-step transformation curves appeared after numerous transformation steps, i.e. bursts. This behaviour was typified as *unusual* for martensite formation and remained *not* clarified.

Later, a similar behaviour now typified as *irregular* [23], was reported in Refs. [23,31], where a controlled time dependent multi-step transformation of austenite into lenticular martensite, occurred after a single large transformation burst in Fe-Ni-C systems. The mechanism responsible for irregular behaviour was not described in Refs. [23,31].

The observation of a controlled multi-step transformation of austenite into lath martensite was first claimed in Ref. [28], where *wavy* transformation curves were reported for the first time from the onset of the transformation of f.c.c. austenite into a b.c.c. product in a Fe-15%Ni iron based alloy. The transformation reported in Ref. [28] was later interpreted as bainitic rather than martensitic [33]. Although it was recognized that *wavy* transformation curves result from the combined effect of an athermal mechanism and a thermally activated mechanism [28], the nature of such mechanisms remained *un*recognized.

The suggestion of a combined effect of an athermal mechanism and a thermally activated mechanism was implemented in Ref. [24], where for the first time a controlled multi-step *massive* transformation of virginal austenite into ferrite was presented and typified as *abnormal*. Ref. [24] deals with Fe-2%Mn and Fe-2%Co iron based alloys.

Following Ref. [24], firstly, ferrite nucleates at several locations in the material and starts to grow. The strain energy which is *locally* introduced in the system because of the volume misfit between ferrite and austenite, promotes autocatalytic nucleation of ferrite in front of the austenite to ferrite interface, yielding an acceleration of the transformation. Thereafter, the sudden formation of a large fraction of ferrite introduces a relevant amount of strain energy in the system which counteracts the chemical driving force; the transformation stops when the *overall* strain energy equals the chemical driving force for the transformation. A new acceleration of the transformation is obtained for an additional increase of the driving force upon further undercooling. Evidently, Ref. [24] indicated the transformation itself as thermally

activated, whereas the athermal character arises from the chemical driving force, which depends on temperature only.

Abnormal lath martensite formation was firstly demonstrated recently in Ref. [29,30], where it is typified as *unusual* and *abnormal*, respectively.

In Ref. [29], a train of transformation rate maxima was reported from virginal austenite on isochronal cooling a Fe-Ni-Co-Mo maraging steel. The transformation curves reported in Ref. [29] resemble the ones presented in Ref. [24-28] and show a dependence of the cooling rate. However, according to Ref. [29], lath martensite formation is practically athermal and abnormal martensite formation is ascribed to the simultaneous formation of lath martensite blocks, within packages, throughout the specimen. The effect of the cooling rate on the kinetics of the transformation remains *not* clarified in Ref. [29].

In Ref. [30], two transformation rate maxima were reported on isochronal cooling a partially hardened Fe-Cr-Ni-Al stainless steel. Alternatively, as a demonstration of a (partially) thermally activated character of the process, martensite formation was suppressed on fast cooling and the transformation process was followed on isochronal heating. In a third experiment, martensite formation was suppressed on both fast cooling and fast (re)heating; abnormal transformation was observed on a second slower cooling. Ref. [30] parallels the controlled multi-step transformation of austenite into lath martensite with the abnormal *massive* transformation of austenite into ferrite [24]. *Abnormal* martensite formation is interpreted in terms of the simultaneous effects of autocatalytic nucleation of martensite and the contribution of self-induced strain energy to the driving force for martensite formation. The contribution of the strain energy is a self-induced mechanical stabilization of the austenite after Ref. [10].

The aim of the present work is to contribute to the understanding of abnormal formation of martensite in iron based alloys.

Experimental

Material and heat treatments

The material investigated in the present study was a commercial precipitation hardenable stainless steel, with chemical composition as given in Table 1, extruded to a rod of 20 mm in diameter. This particular steel grade was chosen because of its known time-dependent kinetics and a martensite start temperature at $M_S = 405\ K$ [34], which is well below the tempering temperature of 755 K [34].

Table 1: Chemical composition of the Fe-Cr-Ni-Cu (17-4 PH) steel determined in wt% with Energy Dispersive Spectroscopy, EDS. The carbon content was measured with a LECO-CS230 carbon analyzer.

Fe	C	Cr	Ni	Si	Mo	Nb	Cu
Bal.	0.06	15.9	4.6	0.5	0.6	0.2	3.2

Martensite formation was investigated with dilatometry. Cylindrical samples 10 mm high, 4 mm in diameter were prepared with the principal direction aligned to the rolling direction. Both full and hollow cylinders, with a wall thickness down to 0.4 mm were investigated.

Dilatometry, involving controlled austenitization and cooling, was performed in a Bähr DIL 805A/D dilatometer. The temperature of the samples was monitored by a thermocouple spot-

welded on the sample surface at half of the sample height. Helium was applied as a cooling gas to guarantee fast heat exchange between sample and environment.

For austenitization, the samples were heated isochronally at 50 K/min to 1323 K and held at this temperature for 1.8 ks. Cooling was performed isochronally at 50 K/min to 413 K, i.e. just above M_S. This cooling stage ensured that all samples experienced identical cooling conditions in the stage where they are austenitic.

(Partial) transformation of austenite to martensite was investigated by isochronal cooling in the temperature range 413 to 333 K at rates ranging from 0.015 to 500 K/min. After isochronal cooling, the samples were kept isothermally at 333 K for 3.6 ks before they were air-cooled to room temperature. Data was collected in a series of one thousand points per thermal step.

Quantitative phase analysis

The quantification of the fraction transformed is based on Ref. [35-37]. Assuming the specific volume as an intrinsic property of the phases and isotropic strain, the measure of the sample elongation, $\frac{dl(t,T)}{l_0}$, gives the fraction of martensite according to the relationships:

$$f_{\alpha'}(t) = \int_0^t \frac{dl(t)}{l_0} \cdot \frac{3}{\varepsilon_0(T)} \cdot dt \quad [1]$$

$$f_{\alpha'}(T) = \int_{T_r}^T \frac{dl(T)}{l} \cdot \frac{3}{\varepsilon_0(T)} \cdot dT \quad [2]$$

for isothermal and isochronal analysis, respectively, with $\frac{dl(T)}{l_0}$ the measured sample strain corrected for thermal effects, T and T_r the actual and reference temperature, t the time and $\varepsilon_0(T)$ the dilatational component of the transformation strain expressed as:

$$\varepsilon_0(T) = \frac{2\cdot\left(a_\alpha(T_r)\cdot\left(1+\int_{T_r}^T \lambda_\alpha(T)dT\right)\right)^3}{\left(a_\gamma(T_r)\cdot\left(1+\int_{T_r}^T \lambda_\gamma(T)dT\right)\right)^3} \quad [3]$$

with $a_\alpha(T_s)$ and $a_\gamma(T_s)$ the lattice parameters of α (i.e. martensite) and γ (i.e. austenite) at T_r, $\lambda_\alpha(T)$ and $\lambda_\gamma(T)$ linear expansion coefficients of α and γ, respectively.
Assuming that the transformation occurs isotropically it is obtained:

$$\varepsilon_0(T) \cong \frac{2\cdot\left(a_\alpha(T_s)^3+3\cdot\int_{T_r}^T \lambda_\alpha(T)dT\right)}{a_\gamma(T_s)^3+3\cdot\int_{T_r}^T \lambda_\gamma(T)dT} \quad [4]$$

Consequently, for the present case, the atomic fraction of martensite $f_{\alpha'}(T,t)$ can be calculated from:

$$f_{\alpha'}(T,t) = \sum_i \left(\frac{3\cdot\left(\frac{l_i-l_{i-1}}{l_0} - f_{\alpha' i-1}\cdot\lambda_{\alpha'}(T)\cdot(T_i-T_{i-1}) - \left(1-f_{\alpha' i-1}\right)\cdot\lambda_\gamma(T)\cdot(T_i-T_{i-1})\right)}{\varepsilon_0(T)_i} \right) \quad [5]$$

where $f_{\alpha'}(T,t)$ is the fraction transformed, $\frac{l_i-l_{i-1}}{l_0}$ is the measured length change per data point, $f_{\alpha' i-1}$ is the fraction transformed calculated for the data point $i-1$, $\lambda_{\alpha'}(T)$ the linear expansion coefficient of martensite, $\lambda_\gamma(T)$ the linear expansion coefficient of austenite, $(T_i - T_{i-1})$ the temperature change per data point and $\varepsilon_0(T)_i$ the transformation strain.

In the calculation of $\varepsilon_0(T)_i$, it was assumed: $a_{\alpha'}(T = 300\ K) = 2.868\ \AA$ and $a_\gamma(T = 300\ K) = 3.596\ \AA$ for martensite and austenite, respectively [38]; linear expansion coefficient of martensite $\lambda_{\alpha'}(T) = 11.8 \cdot 10^{-6}[K^{-1}]$ [39]; linear expansion coefficient of austenite $\lambda_\gamma(T) = (15.2 + 0.0035 \cdot T\ [K]) \cdot 10^{-6}[K^{-1}]$ (extrapolated from the cooling step in the austenitization treatment).

Electron back-scatter diffraction

The samples isochronally cooled at 500 K/min, 15 K/min and 0.015 K/min were investigated with Electron Backscatter Diffraction (EBSD) at a cross section perpendicular to the height direction of the samples. EBSD, was carried out in a FEI Helios Nanolab 600 equipped with an EBSD system from EDAX-TSL and a Hikari camera. The measurements were performed at room temperature with an electron probe current of 5.5 nA at an acceleration voltage of 18 kV. The step size was 150 nm and the investigated area was a square of 150x150 μm^2, i.e. 1000x1000 pixels. The OIM TSL 6.1 software was used to analyze the collected data.

Results

Isochronal martensite formation

Effect of the cooling rate

The dilatometry results obtained on full cylinders are presented in Fig.1. The transformation curves for all isochronal cooling rates are depicted in Fig.1a; selected individual transformation curves and their derivatives are displayed in Fig.1b. Data are presented versus undercooling below the martensite start temperature, M_S. The average M_S determined from the dilatometry investigation is M_S= 409±4 K, which is consistent with literature [34]. No systematic dependence of M_S on the cooling rate was observed.

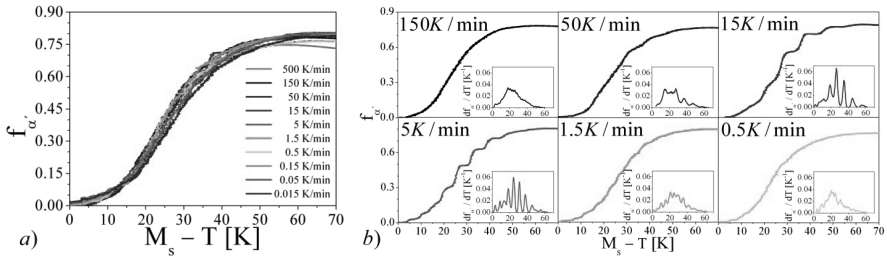

Figure 1. Dilatometry on full cylinders: a) Fraction of martensite $f_{\alpha'}$ versus undercooling, $M_S - T$ $(409 \pm 4\ K)$. b) Fraction of martensite $f_{\alpha'}$ versus the undercooling $M_S - T$ for selected cooling rates of a). For cooling rates in the interval 1.5 to 50 K/min, a multi-step behaviour is observed: the transformation rate shows several retardations and accelerations (insets).

At first sight the transformation curves in Fig.1a show that the cooling rate has no measureable effect on the fraction transformed: the extent of martensite formation is largely driven by the undercooling of the sample with respect to M_S.

On closer inspection, a controlled multi-step transformation behaviour is observed for cooling rates in the range 1.5 to 50 K/min (Fig.1b). For cooling rates up to 15 K/min the transformation steps become more pronounced. For cooling rates faster than 15 K/min the multi-step transformation behaviour becomes less pronounced.

Effect of the sample thickness

In order to verify whether temperature gradients in the samples induced the anomalous multi-step martensitic transformation, a series of hollow cylinders was investigated in a second set of

experiments. The results obtained for hollow cylinders, all isochronally cooled at 15 K /min in the range 413-333K, are collected in Fig.2. The transformation curves for all wall thicknesses are presented in Fig.2a; their derivatives are displayed in Fig.2b.

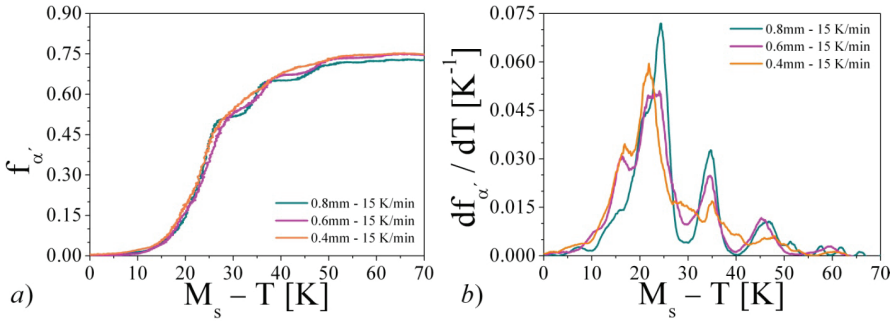

Figure 2. Dilatometry of hollow cylinders with different cylinder wall thickness: a) Fraction of martensite $f_{\alpha'}$ versus undercooling below the martensite start temperature, $M_s - T$; b) transformation rate $f_{\alpha'}/dT$, plotted versus undercooling $M_s - T$.

Fig 2 shows that the controlled multi-step behaviour is reproduced for the hollow cylinders. Evidently, temperature gradients over the sample thickness cannot be held responsible for the anomalous multi-step martensitic transformation. The number of transformation steps appears independent of the sample-wall thickness and the dimensions of the individual steps become smaller for thinner walls (Fig. 2b).

The results indicate that, macroscopically, the undercooling of the sample with respect to M_S is controlling the kinetics. The cooling rate and the sample geometry have a minor, albeit measurable, effect on the transformation kinetics.

Isothermal martensite formation

The progress of the martensite formation upon interrupting the isochronal cooling by isothermal holding at 333 K is shown in Fig.3. The transformation curves for full cylinders cooled to 333 K are collected in Fig.3a; those for hollow cylinders cooled to 333 K at 15K /min are shown in Fig.3b. All data is presented with respect to the product of cooling rate and holding time. It is explicitly mentioned that the temperature on the sample surface is immediately controlled for all samples upon reaching 333 K also for the fastest cooling.

In Fig.3a, up to cooling rates of 15 K/min, i.e. a variation of a factor 1000 in cooling rate, all transformed fractions appear to lie on the same curve. This implies that isothermal transformation is strongly dependent on the cooling rate applied to reach the isothermal temperature. Specifically, it appears that the rate of the isothermal transformation is directly proportional to the cooling rate. For cooling rates faster than 15 K/min, data deviate from this master curve and, instead, more martensite formation is observed in the isothermal stage.

Fig.3b indicates that the isothermal kinetics does *not* depend on the wall thickness. This latter observation excludes the presence of relevant thermal gradients in the hollow cylinders, confirming that the series of accelerations and retardations of the transformation are a genuine

feature of the martensitic transformation in this alloy. Moreover, Fig.3b demonstrates that isothermal martensite formation is similarly a genuine feature of the martensitic transformation.

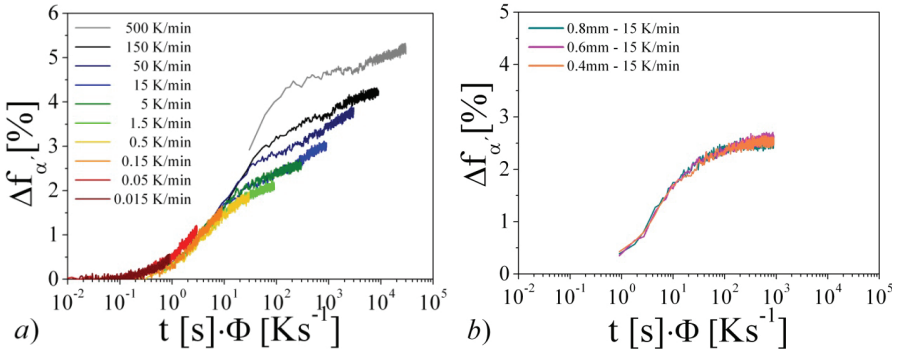

Figure 3. a) Full cylinders: isothermal martensite formation at 333K after isochronal cooling with different cooling rates. The fraction isothermally transformed, $\Delta f_{\alpha'}$, is plotted versus the product of time of isothermal holding, t, and the cooling rate, ϕ (note the logarithmic scale). b) Hollow cylinders: isothermal martensite formation at 333K for different wall thicknesses. The fraction isothermally transformed, $\Delta f_{\alpha'}$, is plotted versus the product of time of isothermal holding, t, (logarithmic scale) and the cooling rate, ϕ.

EBSD

The orientation image maps (OIMs) for the b.c.c. structure as obtained from EBSD are presented in Fig.4: samples cooled 500 K/min in Fig. 4a, 15 K/min in Fig. 4b and 0.015 K/min in Fig. 4c.

In OIMs, blocks of martensite laths appear as regions with an (almost) uniform colour. Packets are observed in forms of groups of parallel blocks. Sub-blocks are observed within single blocks of laths and appear in pairs of similarly coloured regions. Single laths are not resolved in the presentation in Fig.4.

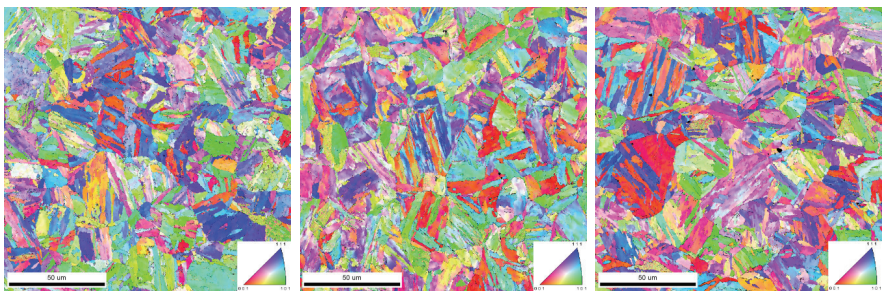

Figure 4. EBSD maps, inverse pole figures for the direction normal to the surface, i.e. the extrusion direction: a) sample cooled at 500 K/min; b) sample cooled 15K/min, c) sample cooled 0.015 K/min.

Apparently, no differences in the average size and shape of grains are revealed from Fig. 4. A quantitative comparison of the scale of the microstructure is presented Fig. 5.

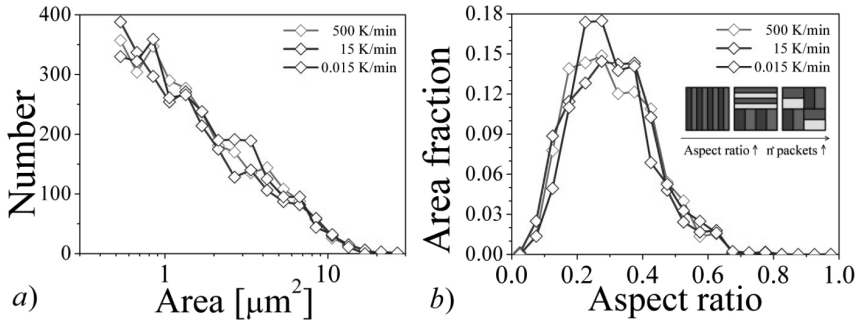

Figure 5. a) Grain size distribution: the number of martensite blocks is plotted versus the area occupied by each block. b) Aspect ratio of the martensite blocks versus area fraction occupied. The inset shows hypothetical microstructure formed by blocks of identical dimensions (area): a sub-division of an austenite grain into packets would imply a larger aspect ratio of the martensite blocks.

Conceiving martensite blocks as regions separated by a mis-orientation angle of at least 15° (high angle boundaries), a size (area) distribution of such regions is given in Fig.5a. Evidently, the size of the martensite blocks is *in*dependent of the cooling rate.

As a consequence of the fact that the number of blocks per unit area is identical between different samples (Fig. 5a) the larger the blocks' aspect ratio (i.e. the thickness to length ratio), the larger would be the dimension of the packets (see inset in Fig. 5b). The aspect ratio of the martensite blocks is presented in Fig. 5b. Evidently, within experimental accuracy also the aspect ratio of the martensite blocks is independent of the cooling rate, as an indication that the dimensions of the martensite packets are independent of the cooling rate.

The size of the sub-blocks is evaluated from the areal density of low angle grain boundaries (i.e. mis-orientation angle between 5 and 15 degrees) which was $2.2 \cdot 10^5$ m^{-1}, $2.1 \cdot 10^5$ m^{-1} and $1.9 \cdot 10^5$ m^{-1} for the samples cooled at 0.015K/min, 15K/min and 500K/min, respectively. This indicates that the cooling rate did not significantly affect the dimensions of the martensite sub-blocks.

Summarizing, the cooling rate does *not* appear to influence the microstructure of the material at the scales resolved by EBSD.

Discussion

Martensite formation in the present investigation

In the following, the present experimental data is discussed to arrive at a consistent description of the transformation mechanism.

Firstly, the present experimental data indicates no systematic dependence of M_S on the cooling rate. This is taken as an indication that the first nucleation event is most likely athermal (i.e. dependent of temperature only). Moreover, (partially) athermal character is demonstrated in Fig. 1a, which shows that the extent of martensite formation is largely driven by the undercooling of the sample with respect to M_S, as an indication that the chemical driving force for the $\gamma \rightarrow \alpha'$ transformation is (macroscopically) controlling the kinetics. On the other hand, martensite formation on isothermal holding demonstrates a (partially) thermally activated character of the transformation.

Thermal activation may arise from thermally activated nucleation and / or thermally activated growth of martensite. It is anticipated that the results in Fig.3 indicate thermally activated *growth* of martensite, which leads to continued nucleation by autocatalysis. In the following, it is demonstrated that athermal, i.e. instantaneous, growth cannot be reconciled with the present data.

According to [39], a martensite embryo can be activated and transform into a martensite nucleus either athermally or thermally activated. For the case of athermal nucleation, the driving force (undercooling) is considered large enough to start the transformation. Thermally activated nucleation occurs after an incubation time, when the driving force (undercooling) necessary for activation of the embryos by athermal nucleation is *not yet* reached. In the present case, martensite formation on continuous cooling is observed to be approximately proportional to the cooling rate. This was demonstrated by the observation that the extent of martensite formation is largely driven by the undercooling of the sample with respect to M_S (Fig.1a), which implies that the rate of martensite nucleation on continuous cooling, as is given by the sum of the athermal and the thermally activated contribution, is similarly proportional to the cooling rate. On interrupting cooling, the contribution of athermal nucleation should cease. Thermally activated nucleation is possible for those embryos which did *not* reach the critical driving force during cooling, or did not have sufficient time to overcome the energy barrier, and occurs at a rate which remains unaltered on interrupted cooling. The observation of a "master curve" for isothermal martensite formation as suggested by Fig.3a indicates that the rate of isothermal martensite formation is proportional to the cooling rate. Assuming athermal growth of lath martensite, this proportionality would be possible only if the contribution of athermal nucleation is nil, which is not the case (see above). Evidently, growth of lath martensite is *not* athermal. More specifically, the proportionality is compatible with *purely* thermally activated growth of lath martensite.

In this respect, the progressive increase of the amount of isothermal martensite for the full cylinders cooled faster than 15K/min is interpreted as the result of a non-uniform temperature distribution in the cylinders. The cooling rates for these samples are so high that the isothermal temperature is *not* attained throughout the sample upon interrupting isochronal cooling. As a consequence of the non-uniform temperature distribution more martensite forms in the isothermal stage than in samples with a uniform temperature distribution.

To summarize, the present experimental data appears consistent with the interpretation of abnormal transformation given in Ref. [30], which considers the combined effect of thermally activated growth of lath martensite and self-induced mechanical stabilization of the austenite to interpret the observation of a train of accelerations and retardations of the transformation on continuous cooling.

Moreover, the interpretation of martensite formation in terms of athermal nucleation and thermally activated growth is compatible with the observation of a final microstructure which is invariant of the cooling rate (Figs. 4 and 5), providing that a strong autocatalytic nucleation of martensite occurs in the specimen and transfers the transformation to several neighboring prior austenite grains.

Transfer of present interpretation to other observations on martensite formation

According to Ref. [9], at M_S, the most favorable variant of lath martensite nucleates athermally at those locations where the lowest local strain energy is introduced. Thereafter, autocatalytic nucleation resulting

in parallel martensite laths within a singular austenite grain develops blocks that grow as long as the driving force is sufficiently large to compensate for the increase in strain energy associated with martensite formation. When the additional strain energy equals the driving force for martensite formation, growth of the martensite blocks stops and the transformation comes to a halt. Further martensite formation requires an increase in driving force which is obtained either upon increased undercooling or upon the reduction of the strain energy through the formation of a new martensite variant, i.e. a new block or packet [9]. This increment in driving force promotes further growth of the pre-existing martensite blocks and may trigger the athermal nucleation of a new population of martensite blocks / packets. When the *local* positive effect of coupled growth of multiple variants ceases, the transformation stops until a point when a new block / packet of laths nucleates and starts growing.

This description can explain a multi-step controlled transformation on the *local* scale and is considered in Ref. [29] to explain the observation of a train of accelerations and retardations of the transformation, assuming that the mechanism is simultaneously reproduced in all austenite grains throughout the specimen.

However, the interpretation given in Ref. [29] cannot explain an effect of the cooling rate on the kinetics of the transformation [29]. Moreover, it does *not* apply to the observation of abnormal transformation on a second cooling step (Ref. [30]) and is limited to martensite with lath morphology (i.e. cannot explain the wavy transformation curves in Refs. [11,23,31,32]). As an alternative explanation, in Ref. [30] it was assumed that the observation of wavy transformation curves is the combined effect of thermally activated growth of lath martensite and self-induced mechanical stabilization of the austenite rather than by the simultaneous formation of blocks in all austenite grains throughout the specimen.

According to Ref. [30], at M_S, lath martensite nucleates athermally at the most favorable locations and starts to grow. Repetitive autocatalytic nucleation of martensite blocks ahead of the advancing martensite front yields an acceleration of the transformation and spreads martensite formation throughout the specimen. The strain energy introduced in austenite as a consequence of martensite formation results in the mechanical stabilization of the austenite, suppressing continued martensite nucleation and yielding a deceleration of the transformation. A new acceleration of the transformation occurs when additional undercooling leads to a further increase of the driving force for martensite formation, which promotes the nucleation of a new population of martensite blocks. This mechanism may repetitively apply on continuous cooling, hence leading to the observation of wavy transformation curves.

Moreover, conceiving the martensite front as extending over several prior austenite grains, the mechanism described in Ref. [30] yields a final microstructure which is invariant of the applied cooling cycle [30]. Under these conditions, time dependent growth does not determine the dimensions of the singular blocks, which are defined by the driving force, but the number of blocks which nucleate autocatalytically ahead of the martensite front per transformation steps.

Finally, adopting an interpretation of abnormal martensite formation in terms of the combined effect of thermally activated growth of martensite and self-induced mechanical stabilization of the austenite, literature data on lenticular martensite formation can be interpreted consistently, as is demonstrated in the following for data in Refs. [11,23,31].

On continuous cooling, the formation of martensite starts at M_S and is characterized by one [23,31] or more [11] bursts, which result in yielding sudden [11, 23] and *ir*reproducible [11] transformation steps. In the burst event, midribs form instantaneously (i.e. athermally). On continued cooling, athermal nucleation is accompanied by continuous thermally activated growth of previously nucleated (thin plate) martensite into a lenticular morphology, leading to the observation of smoothening of the transformation steps into waves. For increased undercooling, growth continues and results in autocatalytic nucleation of martensite, hence in an acceleration of the transformation, which is soon interrupted because of the self-induced mechanical stabilization of the austenite. The mechanism is reproduced several times yielding the observation of wavy transformation curves on continuous cooling [11,23,31].

Conclusions

A train of accelerations and retardations of the transformation on isochronal cooling and a dependence of the isothermal kinetics on the isochronal cooling rate are reported for martensite formation in a Fe-Cr-Ni-Cu alloy of type 17-4 PH steel. This behaviour appears consistent with transformation kinetics controlled by athermal nucleation and thermally activated growth of lath martensite.

In spite of this result, no effect of the cooling rate on the final microstructure was observed. Autocatalytic nucleation of martensite in neighbouring austenite grains, as induced by martensite growth is invoked to explain a final microstructure which is invariant of the applied cooling rate.

The transformation characterized by a train of accelerations and retardations is typified as *abnormal*. Abnormal behavior is interpreted in terms of the combined effect of autocatalytic nucleation of lath martensite and self-induced mechanical stabilization of the austenite.

Acknowledgements

The authors would like to thank S. Löwy and E.J. Mittemeijer from the Max Planck Institute for Intelligent Systems (Stuttgart, Germany) for critical reading of an early version of the manuscript and for stimulating discussion.

References

[1] G. McDougall, C.M. Wayman, "*Crystallography and Morphology of Ferrous Martensite*" in G.B. Olson, W.S. Owen, "*Martensite*", (OH) , ASM International, 1992.
[2] K. Wasaka, C.M. Wayman, Acta Metal., 29 (1981) 991-1001.
[3] S. Morito, X. Huang, T. Furuhara, T. Maki, N. Hansen, Acta Mater., 54 (2006) 5323-5331.
[4] K. Shimizu, M. Oka, C.M. Wayman, Acta Metall., 18:9 (1970) 1005-1011.
[5] H.Y. Lee, H.W. Yen, H.T. Chang, J.R. Yang, Scripta Mater. 62 (2010) 670-673.
[6] M. Unemoto, K. Minoda, I. Tamura, Metallography, 15 (1982) 177-191.
[7] A. Shibata, S. Morito, T. Furuhara, T. Maki, Acta Mater., 57(2009) 483-492.
[8] T. Maki, C.M. Wayman, Metall. Trans., A 7:9 (1976) 1511-1518.
[9] T. Furuhara, N. Takayama, G. Miyamoto, Mater. Sci. Forum, 638-642 (2010) 3044-3049.
[10] Z. Nishiyama, "*Martensitic Transformation*", New York: Academic Press., 1978.
[11] R. Brook, A. R. Entwisle, J. of the Iron and Steel Institute, 203 (1965) 905-912.
[12] A. Shibata, T. Murakami, S. Morito, T. Furuhara, T. Maki, Mater. Trans., 49:6 (2008) 1242-1248.
[13] G.B. Olson, M. Cohen, Metall. Trans. A, 6:4 (1975) 791-795.
[14] S.R. Pati, M. Cohen, Acta Metall., 19 (1971) 1327-1332.
[15] M. Marder, A.R. Marder, ASM Transaction, 62:1 (1969) 1-10.
[16] D-Z. Yang, C.M. Wayman, Acta Metall., 32:6 (1984) 949-954.
[17] T. Kakeshita, K. Kuroiwa, K. Shimizu,T. Ikeda, A. Yamagishi, M. Date, Mater. Trans. JIM. 34:5 (1993) 415-422.
[18] D. San Martin, E. Jimenez-Melero, J.A. Duffy, V. Honkimaki, S. van der Zwaag, N.H. van Dijk, J. Appl. Cryst., 45 (2012) 718-757.
[19] J.R.C.Guimaraes, P.R. Rios, Metall. and Mater. Trans., 41A (2010) 1928-1935.
[20] J.R.C.Guimaraes, P.R. Rios, Mater. Sci., 43 (2008) 5206-5210.
[21] R.L. Patterson, G.M. Wayman, Acta Metal., 14:3 (1966) 347-369.

[22] N.N. Thadhani, M.A. Meyers, Progress in Mater. Sci., 30 (1986) 1-37.
[23] A. R. Entwisle, Metall. Trans., 2:9 (1971) 2395-2407.
[24] Y.C. Liu, F. Sommer, E.J. Mittemeijer, Acta Mater., 51 (2003) 507-519.
[25] Y.C. Liu, F. Sommer, E.J. Mittemeijer, Acta Mater., 52:9 (2004) 2549-2560.
[26] Y.C. Liu, F. Sommer, E.J. Mittemeijer, Chinese Sci. Bullettin, 49:9 (2004) 972-975.
[27] Y.C. Liu, F. Sommer, E.J. Mittemeijer, Metall. and Mater. Trans. A, 39:10 (2008) 2306-2318.
[28] K. Tsuzaki, T. Maki, I. Tamura, Scripta Metall. 21 (1987) 1693-1698.
[29] M. Villa, M.F. Hansen, K. Pantleon, M.A.J. Somers, "*Thermally activated growth of lath martensite and abnormal martensite formation in Fe-Ni-Cr-Al stainless steel"*, submitted for publication.
[30] S. Löwy, B. Rheingans, S.R. Meka, E.J. Mittemeijer, Acta Mater., 64 (2014) 93-99.
[31]
[32] M. Villa, M. F. Hansen, K Pantleon, M. A.J. Somers, "*In situ investiation of martensite formation in AISI 52100 bearing steel at sub-zero Celsius temperature*", proceeding of the 2nd Mediterranean conference on heat treatment and surface engineering, Dubrovnik, Croatia, 2013.
[33] E. A. Wilson, S. P. Allen, and J. Butler, Metal Sci., 16 (1982) 539.
[34] D.C. Ludwigson, A.M. Hall, *The Physical Metallurgy of Precipitation-Hardenable Stainless Steel*, Defence Metals information center, Report III, 1959
[35] H.K.D.H. Bhadeshia, *Worked examples in the Geometry of Crystals.* Second. London : Institute of Materials, 2001. ISBN 0-904357-94-5.
[36] J.Z. Zhao, C. Mesplont, B.C. De Cooman, ISIJ International., 41:5 (2001) 492-497.
[37] Takahashi, M., Bhadeshia, H.K.D.H. J. of Mater. Sci. Letters., 8 (1989) 477-478.
[38] M. Villa, *Isothermal martensite formation*, PhD Thesis, The Technical University of Denmark, Lyngby, submitted for publication
[39] M. Villa, K. Pantleon, Marcel A.J. Somers, "*Enhanced Carbide precipitation during tempering of sub-zero Celsius treated AISI 52100 bearing steel*", proceedings of the Heat Treat and Surface Engineering Conference and Expo 2013, 2013, Chennai, India.
[40] T. Kakeshita, K. Kuroiwa, K. Shimizu, T. Ikeda, A. Yamagishi, M. Date, Mater. Trans. JIM, 34 (1993) 423-428

DTU Mechanical Engineering
Section of Materials Science and Engineering
Technical University of Denmark

Produktionstorvet, Bld. 425
DK- 2800 Kgs. Lyngby
Denmark
Phone (+45) 4525 2205
Fax (+45) 4593 6213
www.mek.dtu.dk
ISBN: 978-87-7475-375-9